An investigation of presynaptic plasticity mechanisms

Thesis submitted for the degree of Doctor of Philosophy in Pharmacology at the University of Oxford

Rudi Tong
New College
November 2019

Declaration

I, Rudi Tong, declare that the work presented in this thesis is entirely my own work except where otherwise indicated (see "Details on statement of authorship" in Appendix). No part of my thesis has been accepted or is currently being submitted for any degree, diploma or certificate or other qualification in this University or elsewhere. Parts of Chapters 6 and 7 have been published (Padamsey et al., 2017a).

Acknowledgements

First and foremost, I would like to thank my two supervisors, Yuki Goda and Nigel Emptage for welcoming me into their labs and for their support, both academically and personally. I would also like to thank Zahid Padamsey for introducing me to the fascinating field of presynaptic plasticity and synaptic computation. His guidance and advise on both, scientific and technical matters were indispensable for the smooth and successful completion of my DPhil project and the maturation of me as a scientist. I would further like to acknowledge people in the Emptage and Goda lab: Peter, for sitting through my long scientific discussions; Carla, for her enthusiasm; Alex and Henry, for making my time in the lab extra fun and enjoyable; Raph and James, for interesting discussions on the theoretical sides of neuroscience; Tom, for his technical guidance and our shared love for ramen; Pete, for endless hours of late night science discussion; Sunita, Ale, Han, Mizuki, Itsuko, Yuko, and Atsushi, for making my time in Japan unforgettable. I would also like to thank the Clarendon Fund, the MRC, the "Studienstiftung des Deutschen Volkes", and RIKEN for their financial support.

Abstract

The regulation of synaptic strength is thought to underlie the complex emergent dynamics of neural networks. The strength of a synapse is determined by its pre- and postsynaptic properties, both of which are under tight regulatory control orchestrated by ongoing neuronal activity. We now have a good understanding of the plasticity rules underlying the regulation of postsynaptic strength. The same set of rules has been imposed onto the regulation of presynaptic strength. However, the operation of pre- and postsynaptic terminals is fundamentally different, both on a mechanistic and functional level. I have therefore systematically investigated the mechanisms underlying presynaptic plasticity at the Schaffer collateral-CA1 synapse under varying conditions of synaptic activity. I have examined three general modes of regulation: (1) synaptic changes dependent on the concerted activity of pre- and postsynaptic neurone (homosynaptic plasticity); (2) changes dependent only on presynaptic activity; (3) changes dependent on postsynaptic activity alone (heterosynaptic plasticity). Using a combination of electrophysiological and optical techniques, I have monitored and manipulated the strengths of single synapses both pre- and postsynaptically, which allowed me to impose certain activity patterns and investigate resulting synaptic modifications. I found that heterosynaptic plasticity along local segments of dendrites is expressed at both synaptic loci and depends on the spatial arrangement of synapses. Pre- and postsynaptic strength changes were weakly correlated and pharmacologically dissociable. Next, I found that glutamate release suppresses both short- and long-term presynaptic function, which required the activation of presynaptic NMDA receptors. Lastly, I found that presynaptic long-term potentiation (LTP) is spike timing-dependent but does not rely on coincidence detection via postsynaptic NMDA receptors. My findings suggest that the presynaptic terminal is functionally distinct, which is reflected in parallel regulatory pathways. I suggest the synapse to be viewed as a two-compartment model, consisting of a presynaptic non-linear transformation followed by postsynaptic linear weighting.

Table of contents

1. Preface

The aim of this thesis is to understand the function and regulation of the presynaptic terminal of central synapses. In particular, I have systematically investigated changes in the stochastic properties of neurotransmitter release under varying conditions of synaptic activity. To do so, I have focused on the Schaffer collateral-CA1 synapse of the hippocampus, at which synaptic plasticity has been extensively studied (Bliss et al., 2007). Although modifications of synaptic strength at the postsynaptic locus are well-documented (Lüscher & Malenka, 2012), work on presynaptic changes, especially with respect to long-term potentiation, has been controversial in the past, in part due to the technical difficulties of accessing the presynaptic locus. With the advancement of optical techniques to study neurotransmitter release, the existence and importance of presynaptic plasticity are now generally accepted. Yet, a common framework for understanding the functional role, and therefore the regulation of presynaptic strength has been lacking. As a consequence, the framework for postsynaptic plasticity, which has substantially advanced our theoretical understanding of synaptic processing and its emerging properties, has been imposed onto the presynaptic terminal. The following question then arises: Are pre- and postsynaptic changes explained by the same set of "rules"? Or alternatively: Are the functional consequences of pre- and postsynaptic changes the same?

One does not have to look far to find that the mode of operation of the pre- and the postsynaptic terminal are fundamentally different. The presynaptic terminal resembles a binomial process, where the incoming signal, in the form of discrete action potentials, is transmitted as discrete packages of quantal events with a certain probability. In contrast, released neurotransmitter bind to postsynaptic receptors and lead to a change in the membrane potential, the magnitude of which is approximately proportional to the number of receptors. The postsynaptic terminal therefore resembles more a linear process. How this difference affects the processing of information at synapses and the rules by which synapses are "optimised" is, however, less clear.

I will briefly introduce the biology of the canonical synapse and its information processing properties, for both pre- and postsynaptic loci. After an introduction to synaptic plasticity, with particular emphasis on differences in pre- and postsynaptic plasticity mechanisms, I present my experimental findings on the long-term regulation of presynaptic strengths before concluding with a discussion on overarching questions raised by the experimental results.

1.1. Why study the presynaptic terminal?

The function of the nervous system is often ascribed to the transmission from sensory to motor. This undoubtedly requires faithful propagation of signals from cell to cell, and studies of peripheral synapses seemed to confirm this notion. For instance, photoreceptor cells in the retina exhibit a constant stream of neurotransmitter release at their ribbon synapses and variations in light level change the amount of neurotransmitters released in a graded manner (Baylor et al., 1979). Similarly, at the neuromuscular junction stimulation of the nerve fibre leads to robust release of vast numbers of neurotransmitter quanta due to the numerous contacts formed by each fibre, enabling robust muscle contraction (del Castillo & Katz, 1954). It is the central synapse where accurate transmission seemed to be amiss, and neurotransmitter release can occur with success rates as low as one out of ten trials. This is puzzling and sparked discussions on whether the noisy synapse is a "bug or a feature" (Smetters & Zador, 1996; Branco & Staras, 2009). We now know that release probability is tightly regulated. For example, different inputs onto layer 4 stellate cells in cat primary visual cortex can be clearly classified on the basis of their presynaptic properties (Stratford et al., 1996). Input-specific presynaptic properties have since been reported in multiple brain areas (Blackman et al., 2013; Markram et al., 1998; Gupta et al., 2000; Koester & Johnston, 2005; Buchanan et al., 2012; Bao et al., 2010; Pouille & Scanziani, 2004). All studies, therefore, suggest an adaptive advantage for "unreliable" transmission. What, then, is the purpose? One way to explore the functional role of presynaptic release probability is to study its regulation: What conditions drive changes in presynaptic strength?

1.2. Experimental strategy for studying the regulation of (pre)synaptic strength

The regulation of synaptic strength is a high-dimensional problem. A multitude of factors have been shown to affect synaptic strength, including neuronal activity, hormonal state, age, and genetic factors (Ho et al., 2011). The interaction between these factors is unclear and likely to be highly complex and non-linear. Here, I have focused solely on synaptic strength regulation by neuronal activity. The underlying assumption is that the regulation of synaptic strength can be phrased as an optimisation problem that depends solely on neuronal activity at the pre- and the postsynaptic neurone. In order to systematically analyse the optimisation function (learning rule), I considered the following linear decomposition (adapted from Zenke & Gerstner, 2017):

$$G(\omega_{ij}, post_i, pre_j) = g_0(\omega_{ij}) + g_1(\omega_{ij}, pre_j) + g_2(\omega_{ij}, post_i) + g_3(\omega_{ij}, post_i, pre_j)$$

where pre and post denote pre- and postsynaptic activity, respectively, and w represents synaptic strength of input j onto neurone i. This leads to four experimental conditions that need to be considered: (1) changes dependent on the concerted activity of pre- and postsynaptic neurone (homosynaptic plasticity); (2) changes dependent only on presynaptic activity; (3) changes dependent on postsynaptic activity alone (heterosynaptic plasticity); and (4) spontaneous fluctuations in synaptic strength. I will present results for cases (1)-(3), with particular emphasis on heterosynaptic plasticity (case 2). Case (4) poses particular technical challenges due to limitations in measuring presynaptic strength, as measurements of Pr necessitate the continuous activation of the presynaptic terminal. This will not be considered in this thesis (for activity-independent postsynaptic plasticity, refer to Yasumatsu et al. 2008).

2. Introduction

2.1. Synaptic strength

2.1.1. What defines presynaptic strength?

Neurotransmitter release is inherently stochastic. The arrival of action potentials (APs) at the presynaptic terminal causes an influx of Ca^{2+} from voltage-gated Ca^{2+}-channels (VGCCs; Llinás et al., 1981; Stanley, 1993), which, in turn, triggers release of neurotransmitter as all-or-none events with a certain release probability (Pr). The release of neurotransmitter is quantised, such that there exists a minimal response amplitude (quantal content, q) that cannot be reduced further (del Castillo & Katz, 1954). Every release event is thus built up as integer multiples of the quantal content. In its simplest form, neurotransmitter release is described by the binomial theorem, in which the mean response to an AP is given by Npq, where N is the number of independent release sites and p is the probability of release at each release site. The basal strength of the presynaptic terminal is therefore uniquely defined by its reliability, p, and the amount of neurotransmitter released, N and q.

The structural correlate for quantised release is found in the vesicular packaging of neurotransmitters. The concentration of neurotransmitter per vesicle, i.e. the quantal content q, although exhibiting substantial variation across vesicles (Bekkers et al., 1990; Liu & Tsien, 1995; Liu et al., 1999; Mainen et al., 1999; Harris & Sultan, 1995; Qu et al., 2009), does not show synapse-specific biases (Harris & Sultan, 1995; Qu et al. 2009) and mainly adjusts to global activity levels in a homeostatic manner (Bekkers et al., 1990; Lau & Murthy, 2012; Hartman et al., 2006; Wilson et al., 2005; De Gois et al., 2005; Erickson et al., 2006), the importance of which has also been questioned (Turrigiano, 2012).

The definition of release sites of central synapses is less clear (Stevens, 2003). Release occurs exclusively at the active zone, a protein-dense region at the presynaptic plasma membrane, directly opposed to the postsynaptic density (Südhof, 2013; Harris &

Weinberg, 2012). Recent super-resolution imaging studies suggest that release sites are formed by protein nanoclusters throughout the active zone, creating hot-spots of Ca^{2+}-channels and the vesicle release machinery (Sakamoto et al., 2018; Tang et al., 2016; Holderith et al., 2012; Miki et al., 2017; Nakamura et al., 2015) and therefore form discrete, stable release sites (Park et al., 2012; Maschi & Klyachko, 2017). Functional studies, however, show that most central synapses release only a single vesicle per AP, even in conditions of high release probability (Chen et al., 2004; Hanse & Gustafsson 2001; Dobrunz & Stevens, 1997; Dobrunz et al., 1997, but see Wadiche & Jahr, 2001; Oertner et al., 2002; Watanabe et al., 2013). To be precise, it was found that the successful release of a vesicle causes a substantial drop of the release probability for subsequent release, which would recover over ~ 5 ms (Stevens & Wang, 1995; Dobrunz et al., 1997; Hjelmstad et al., 1997). This synaptic refractory period (Hjelmstad et al., 1997) therefore suggests that fast synchronous release is strictly univesicular, indicating that the number of release sites does not contribute to the amount of neurotransmitter released (per event), as the majority of central excitatory synapses consist of only a single active zone (Schikorski & Stevens, 1997) contacting a single postsynaptic terminal (but see Woolley et al., 1990; Sorra & Harris, 1993; Harris, 1995; Shepherd & Harris, 1998). Though the universal validity of univesicular release remains unclear, no evidence for multiquantal release could be found in this study (*e.g.* assessed via optical quantal analysis, similar to Oertner et al., 2002). Therefore, presynaptic strength throughout the thesis will refer to the probability of release $Pr \equiv P(x \geq 1)$, where x denotes the number of released quanta, and quantal amplitude (q) is assumed to remain constant.

2.1.2. What determines release probability?

Early studies at the frog neuromuscular junction showed that calcium was necessary for triggering the exocytosis of neurotransmitter vesicles (Katz & Miledi, 1965). By measuring the relationship between extracellular Ca^{2+}-concentration and neurotransmitter release, the action of Ca^{2+} was found to follow a power-law, indicating strong cooperativity, with a Hill coefficient (defined as the quotient logR/log[Ca], where R is a measure for release

and [Ca] the concentration of Ca^{2+}) of approximately 4 (Dodge & Rahamimoff, 1967). This implies that the local, spatiotemporal regulation of Ca^{2+} is crucial in determining Pr. The degree of cooperativity varies between types of presynaptic terminals, ranging from 1-5 (Augustine et al., 1985, Bollmann et al., 2000, Brandt et al., 2005, Thoreson et al., 2004) and has been attributed to differential expression of Ca^{2+}-sensors (*e.g.* synaptotagmins, Yoshihara & Littleton, 2002; Tamura et al., 2007; Xu et al., 2007; Luo & Südhof, 2017; Südhof, 2002; Chen & Jonas, 2017) and modulation of Ca^{2+}-dynamics, *e.g.* via the spatial coupling to VGCCs ("stochastic model" in Dodge & Rahamimoff, 1967; Augustine et al., 2003; Stanley, 2016) or Ca^{2+}-binding proteins (Roberts, 1993).

Next, the definition of Pr predicts an exponential relationship between N and Pr, $Pr = 1-exp(-kN)$, where $k = ln(1-p)$, N is the number of release sites, and p the probability of release at each release site. Indeed, measurements of Pr and the functional readily-releasable pool (RRP) size, the number of vesicles primed for release, are well approximated by a slightly modified exponential function (Dobrunz & Stevens, 1997), which takes into account a partly shared Ca^{2+}-pool between release sites and a non-even distribution of Ca^{2+}-entry across the active zone. Other more direct structural measurements of the RRP or active zone size, which are thought to be proportional to the aforementioned synaptic nanoclusters, report a linear relationship (Branco et al., 2010; Holderith et al., 2012), probably due to the low magnitude of p, which causes the relationship to be well approximated linearly at low values of N. Furthermore, the release probability of individual release sites does not depend on N itself (Sakamoto et al., 2018). Thus, there are two major ways Pr is determined: the number of independent release sites and the dynamics of presynaptic Ca^{2+}-entry, coupling, and binding properties.

2.1.3. What defines postsynaptic strength of glutamatergic synapses?

Postsynaptic strength can be defined as the magnitude of membrane depolarisation upon release of a single quantum of glutamate, which crucially depends on the number and properties of glutamate receptors. The ionotropic α-amino-3-hydroxy-5-methyl-4-

isoxazolepropionic acid receptor (AMPAR), primarily permeable to Na^+ and K^+, comprises a large fraction of postsynaptic depolarisation. Furthermore, the regulation of receptor number, subunit composition, and post-translational modification is thought to underlie most long-term changes of postsynaptic strength (Diering & Huganir, 2018). On the other hand, N-methyl D-aspartate receptors (NMDARs), due to their Ca^{2+}-permeability, play an important role in orchestrating the complex Ca^{2+}-dependent signalling network of the postsynaptic terminal, such as those involved in synaptic plasticity (Lüscher & Malenka, 2012). Furthermore, activation of NMDARs is highly non-linear due to the blockade of the channel pore by Mg^{2+} ions at resting membrane potential, which renders the receptor sensitive to membrane depolarisation (Nowak et al., 1984). Kainate and metabotropic glutamate receptors (mGluRs) also contribute to postsynaptic depolarisation, though, to a lesser extent. The number of receptors crucially depends on the size of the postsynaptic density (PSD), which in turn is determined by the overall spine morphology. Hence, spine volume is found to be positively correlated with PSD area and the number/strength of AMPA receptors (Matsuzaki et al., 2001). Especially mushroom spines, characterised by a thin neck and a bulbous spine head, are thought to represent strong, mature synapses due to higher amounts of AMPA receptors and more complex PSD morphologies (Harris et al., 1992; Matsuzaki et al., 2001). Other classes of spines, such as thin and stubby, contain fewer receptors and are generally more plastic. Spine size is also correlated with the probability of a spine to contain endoplasmic reticulum (ER), ribosomes, and to be contacted by astrocytes (Bourne & Harris, 2008), all signs of postsynaptic strength and synapse maturity.

2.1.4. Firing history-dependent synaptic strength - Short-term plasticity

In addition to the above static view of synaptic strength, the firing history is known to greatly affect transmission efficacy. Studies at the frog neuromuscular junction reported a transient increase or decrease in synaptic efficacy following electrical stimulation (Mallart & Martin, 1967, 1968; Thies, 1965), now referred to as short-term plasticity (STP). Multiple forms of short-term facilitation and depression (and augmentation) have since

been reported at a variety of synapses and the underlying mechanism is thought to be almost exclusively presynaptic (Regehr, 2012; Hennig, 2013; but see receptor desensitisation: Trussell et al., 1993; Neher & Sakaba, 2001; Chen et al., 2002; and receptor saturation: Wadiche & Jahr, 2001). Modulation of presynaptic Ca^{2+}-dynamics is thought to underlie short-term facilitation, either by direct modulation of Ca^{2+}-entry (Lee et al., 2000; DeMaria et al., 2001), Ca^{2+}-buffering (Rozov et al., 2001; Matveev et al., 2004), or accumulation of residual Ca^{2+} (Connor et al., 1986). Short-term depression is mainly attributed to the depletion and slow recovery of synaptic vesicles (Liley & North, 1953; Tsodyks & Markram, 1997). In addition, release sites can inactivate upon successful release (Stevens & Wang, 1995; Dobrunz et al., 1997) and Ca^{2+}-channel modulation has also been suggested to contribute to short-term depression (Catterall & Few, 2008). Importantly, the nature of STP depends on the initial Pr, with low Pr favouring facilitation and high Pr favouring depression (Dobrunz & Stevens, 1997; Tsodyks & Markram, 1997), which can be used as an indirect readout of Pr (see section 2.6.3 "Measuring Pr").

2.1.5. Distribution of synaptic strength

The global distribution of synaptic strengths is tightly regulated and is known to depend on overall network activity (Turrigiano, 2012), dendritic location (Grillo et al., 2018; de Jong et al., 2012; Magee & Cook, 2000; Katz et al., 2009; Menon et al., 2013; Walker et al., 2017), and metabolic state (Harris et al., 2012; Schreiber et al., 2002). Measurements of Pr of neocortical glutamatergic synapses reveal a skewed, continuous distribution with a median around 0.2 (Murthy et al., 1997; Huang & Stevens, 1997; Branco et al., 2008, Branco et al., 2010), which is mirrored in the distribution of active zone size, bouton volume, and the number of docked vesicles (Schikorski & Stevens, 1997; Holderith et al., 2012). Postsynaptic strength is thought to be distributed similarly, according to spine morphology (Harris et al., 1992; Arellano et al., 2007), spine size (Yasumatsu et al., 2008), PSD size (Arellano et al., 2007), or direct functional readouts of the postsynaptic potential (Bekkers & Stevens, 1995). This suggests that pre- and postsynaptic strengths might be matched or balanced. Indeed, ultrastructural parameters of pre- and postsynaptic

strengths are often highly correlated (Holderith et al., 2012; Schikorski & Stevens, 1997), and recent super-resolution studies revealed that nanoclusters of release machinery and postsynaptic neurotransmitter receptors are precisely aligned in a columnar manner (Tang et al., 2016; Biederer et al., 2017). In addition, most synaptic plasticity studies report conjunct changes at both loci, with only few examples of disjunct plasticity (*e.g.* Letellier et al., 2016, 2019). Furthermore, induction of postsynaptic plasticity is followed by slow presynaptic compensation in bouton size (Meyer et al., 2014), release probability (Bayazitov et al., 2007), and nanocolumn alignment (Tang et al., 2016). As a result, this would suggest, that plasticity at both loci should follow the same or similar sets of rules.

2.2. Are the functional consequences of pre- and postsynaptic changes the same?

At this point, a first pass on one of the core questions can be made. Since pre- and postsynaptic strengths are found to be correlated, it would be reasonable to assume their functional impacts to be similar. Postsynaptic modifications translate into a modulation of the postsynaptic potential waveform. The amplitude and kinetics of synaptic potentials determine, how information across synapses is integrated. For instance, rise and decay kinetics dictate the integration time window; the amplitude determines the general impact or weight of a synapse towards the firing non-linearity. The postsynaptic terminal might therefore be particularly sensitive to the local statistics of the membrane potential and correlations across synaptic inputs. Changes in presynaptic strength are qualitatively different. The postsynaptic response to successful presynaptic neurotransmitter release is pretty much constant. The instantaneous impact of a synapse is hence highly non-linearly gated by presynaptic release, resulting in a bimodal response profile. It follows that changes in pre- and postsynaptic strength will have distinct effects on the statistics of postsynaptic membrane potential (Costa et al., 2017). Moreover, presynaptic strength operates largely on the temporal domain of spiking activity: (1) When taking the time average of synaptic activity, presynaptic strength is well-approximated by a linear function; (2) short-term plasticity renders presynaptic strength

especially sensitive to the temporal structure of activity, allowing highly non-linear integration in time. The presynaptic terminal might therefore be particularly sensitive to the temporal structure within individual synaptic inputs. The functional role of unreliable neurotransmission has been extensively discussed in the literature (Harris et al. 2012; Klyachko & Stevens, 2006; Abbott & Regehr, 2004; Goldman, 2004; Thomson, 2003; Zador, 1998; Tsodyks & Markram, 1997; Stevens & Wang, 1994; Moore & Shannon, 1956). Thus, pre- and postsynaptic changes have distinct impact on and are sensitive to distinct parameters of synaptic transmission, which suggests parallel instead of overlapping signalling pathways and learning rules for their regulation, which is in stark contrast to the correlation observed between pre- and postsynaptic strengths in the steady-state. Next, I will consider the long-term regulation of synaptic strengths.

2.3. Synaptic plasticity

Synapses are fundamental for information processing in the brain. It is the synapse that dictates where to and how much information is transmitted. Synapses are not static but constantly evolving in their strength, properties, number, and the identity of their postsynaptic target. This plasticity is thought to be tightly regulated, following some unknown "rule" out of which complex network behaviour emerges. Therefore, the strength and location of a synapse and its regulation are informative of the dynamic processes that take place on the level of the neural network. Conversely, in order to study the regulation of synaptic strength, a basic understanding of the overarching functional goal of the network is also required.

2.3.1. Theoretical frameworks for synaptic plasticity

In arguably the most influential piece of work in the field of synaptic plasticity, Donald Hebb proposed that memory formation requires the modification of synaptic strength to maximise correlations between pre- and postsynaptic neurones (Hebb, 1949). To be precise, Hebb suggested that co-activation of neurones should lead to the strengthening of their connections ("Cells that fire together, wire together"). This naturally leads to the

association of concurrently active inputs, which is thought to play a central role in the formation of memories. In addition, due to the sensitivity of Hebbian-type plasticity to input correlations, it was later shown that neurones will converge towards the principal components of the input distribution (Oja, 1982; Linsker, 1988). In this view, synaptic strength is sensitive to the statistics of the input, and neurones seek to optimally represent the input variance (Barlow, 1959). In recurrent networks, Hebbian plasticity was shown to result in the formation of attractor states, which can be used as a memory storage and recall system (Hopfield, 1982). Similarly, maximisation of information transmission between neurones has been suggested as the central optimisation goal of synapses (Bell & Sejnowski 1995; Linsker, 1992). In this case, synaptic plasticity is thought to increase the efficiency of information transmission by virtue of maximisation of the mutual information between input and output responses (Toyoizumi et al., 2005, 2007; Chechik, 2003) or by minimisation of the conditional entropy, which is interpreted as reducing response variability (Bohte & Mozer, 2007; Pool & Mato, 2011).

These correlation- or information-based frameworks generally assume linear synaptic transmission, often modelled as a multiplicative factor (synaptic weight), and are therefore more suited for understanding postsynaptic plasticity. The effect of the non-linear nature of neurotransmitter release is less well understood. In the early theoretical work by von der Malsburg on correlation theory, synaptic strength was explicitly defined by two variables, differing in their temporal behaviour (von der Malsburg, 1981). A slowly changing synaptic parameter determined the permanent connection strength between two neurones (equivalent to synaptic weight), whereas a fast changing parameter, termed "synaptic modulation", served as a gating mechanism, which was suggested to depend on the degree of signal correlation. This theory extended Hebb's idea of cell assemblies to additionally account for causative input structures, as a step towards solving the binding problem (Friston, 2010). Although correlation theory does not explicitly attribute these parameters to biological substrates, the properties of synaptic modulation are well accounted for by presynaptic STP. The important idea in von der

Malsburg's theory is the treatment of the synapse as a two-compartment model, each with distinct temporal dynamics and therefore distinct sensitivity to neuronal activity. Changes in "synaptic modulation", however, still followed Hebb's idea of correlation-based learning. A fundamentally different view was introduced in studies utilising dynamic synapses in artificial neural networks (Liaw & Berger, 1996; 1999, Maass & Zador, 1999; Natschläger et al., 2001). Dynamic synapses, which incorporate a biologically plausible model of presynaptic STP, were able to extract specific temporal sequence patterns from neuronal input. Similarly, STP allowed for the decomposition of temporal information into a spatial code distributed in a population of neurones (Buonomano & Merzenich, 1995; Buonomano, 2000). The important realisation in these studies, as stated by Liaw and Berger, is the identification of neurotransmitter release as the final output of a neurone, instead of AP firing (Liaw & Berger, 1996). This has important implications on the learning rule, as it predicts that presynaptic plasticity should be sensitive to both success and failure of release, which is in stark contrast to postsynaptic plasticity, especially taking into account the underlying molecular mechanisms. Since the biological parameters underlying the regulation of STP were poorly understood, precise learning rules could not be formulated (Maass & Zador, 1999). A simplification to this problem was offered by limiting modifications to Pr only, which leads to a smooth, predictable trajectory of the short-term behaviour (Tsodyks & Markram, 1997; Markram et al., 1998). It was shown that changes in Pr influence the mode by which information is transferred, transitioning from rate to temporal codes (Tsodyks & Markram, 1997). Therefore, changes in presynaptic strength, as well as their impact, will depend on the temporal firing properties of the presynaptic neurone (Tsodyks et al. 1998; Markram et al., 1998; Fuhrmann et al., 2002; Tsodyks & Markram, 1997; Fortune & Rose, 2001). Recently, the expression locus of synaptic plasticity has been interpreted as an optimisation of the postsynaptic membrane potential statistics (Costa et al., 2017). Here it was suggested that synaptic strength is optimised towards a certain mean and minimal variance of postsynaptic membrane potential. Assuming synaptic transmission to follow binomial statistics, pre- and postsynaptic strength contribute differentially to mean and variance,

hence forming an uneven optimisation landscape.

In summary, conventional models of synaptic transmission do not take into account presynaptic non-linearities. Modification of presynaptic strength does not follow the same logic as postsynaptic plasticity, due to its distinct effects on information transmission. When studying synaptic plasticity, it is therefore important to identify both pre- and postsynaptic contributions and their degree of disjunction.

2.3.2. Stability through homeostatic plasticity

Correlation-based mechanisms (from here on referred to as Hebbian plasticity) are self-reinforcing and tend to result in "run-away" dynamics in which synaptic strengths saturate and hence compromise the network's or neurone's ability to process and store further information (Miller & MacKay, 1994; Abbott & Nelson, 2000). Similarly, maximisation of information tends to only explain the strengthening, but not weakening of synapses, since an increase in activity is always beneficial for information transmission (Toyoizumi et al., 2005; 2007). Even though some learning rules exhibit, under specific circumstances or with slight modifications, stable behaviour (Oja, 1982; Bienenstock et al., 1982; van Rossum et al., 2000; Carpenter & Milenova, 2002; Babadi & Abbott, 2010), it is generally believed that additional homeostatic processes are required (Turrigiano, 2012; Watt & Desai, 2010). Changes in synaptic strength will therefore also depend on homeostatic constraints, which are either intrinsic or dynamically determined by ongoing activity. Homeostasis is also a natural consequence of metabolic constraints on information transmission (Levy & Baxter, 1996; Laughlin et al., 1998; Harris et al., 2012; Toyoizumi et al., 2007), which might be particularly important for explaining the role of presynaptic plasticity (Harris et al., 2012). The proposed triggers for homeostatic plasticity ranges from intracellular Ca^{2+}-levels to competition for energy or maintenance of resources (Turrigiano, 2012; Davis, 2006) and might therefore consist of a complex mix of signals involved in general cellular homeostasis (Frere & Slutsky, 2018). The most commonly studied form of homeostatic plasticity, experimentally, involves global

manipulation of synaptic activity on a comparatively long time scale, which leads to adjustments of synaptic and/or cell intrinsic properties in a compensatory manner, often found to be multiplicative and thus preserving relative differences in synaptic strengths (Turrigiano et al., 1998; extensively reviewed in Turrigiano, 2012). Synaptic changes can occur at both synaptic loci, but what exactly determines the expression locus and the functional consequences of pre- or postsynaptic homeostatic plasticity are unclear. The long time scale required for induction raises further complications as it is in opposition to theoretical implementations, which universally conclude homeostatic mechanisms to require time constants of similar order of magnitude to the destabilising force, i.e. Hebbian plasticity (Zenke & Gerstner, 2017; Chistiakova et al., 2015; Zenke et al., 2013). One potential elegant solution is the direct mechanistic coupling of homeostatic plasticity to the induction of Hebbian plasticity. The most promising point of intersection between the two forms of plasticity is the strong postsynaptic depolarisation, required for all known forms of Hebbian plasticity, and such mechanisms are generally summarised as heterosynaptic plasticity.

Heterosynaptic plasticity is defined as synaptic changes induced solely by postsynaptic activity. This includes several sources of activity, such as postsynaptic APs, dendritic activity, or activity of synapses. In the latter definition, heterosynaptic plasticity refers to changes observed at the non-active synapses. Heterosynaptic plasticity is mainly studied in the context of concurrent induction of homosynaptic plasticity, as a means of establishing cooperation or competition between synapses. Theoretical work on heterosynaptic plasticity is scarce, due to a lack of systematic experimental studies (Zenke & Gerstner, 2017). Heterosynaptic plasticity was shown to be sufficient to counteract the runaway dynamics of Hebbian plasticity and additionally implements synaptic competition (Chistiakova et al. 2015; Zenke et al. 2015; Chen et al. 2013), which is thought to be especially important for development and refinement of sensory cortex (Lo & Poo, 1991; El-Boustani et al., 2018).

In summary, homeostatic concerns predict that plasticity occurs in the absence of

correlated pre- and postsynaptic activity. Synapses change according to shared parameters, indicating substantial cross-talk and break-down of input-specificity of Hebbian plasticity. Global parameters available to each synapse might differ between pre- and postsynaptic terminals, due to the physical and electrical segregation. For instance, postsynaptic membrane potential cannot be directly sensed by the presynaptic terminal and intracellular molecules are not easily shared. It is therefore reasonable to assume that pre- and postsynaptic terminals operate under differing homeostatic baselines.

2.3.3. Local vs. global plasticity

Synaptic plasticity has generally been studied in a global context, neglecting spatial interactions between synaptic inputs (but see Engert & Bonhoeffer, 1997). However, several lines of evidence suggest that synaptic plasticity might be locally implemented . Firstly, synapses are found to be non-uniformly distributed along individual dendritic branches, with an abundance of synapse clusters, of both, functional (Kleindienst et al., 2011; Makino & Malinow, 2011; Takahashi et al., 2012) and anatomical origin (Druckmann et al., 2014; Deguchi et al., 2011). Secondly, dendrites are highly electrically compartmentalised and can act as independent functional units (Branco & Häusser, 2010; Larkum & Nevian, 2008). Thirdly, local dendritic activity, such as dendritic spikes and local protein synthesis, is known to be sufficient to drive synaptic plasticity (Cichon & Gan, 2015; Gambino et al., 2014; Remy & Spruston, 2007). In fact, local synaptic plasticity was shown to substantially increase a neurone's processing capacity (Poirazi & Mel, 2001; Poirazi et al., 2003; Kastellakis et al., 2015). Lastly, homeostatic plasticity has been reported to act locally at individual dendritic branches or individual synapses (Ju et al., 2004; Liu, 2004; Branco et al., 2008; Sutton et al., 2006, 2007; Bourne & Harris, 2011; Hou et al., 2008, but see Ibata et al., 2008) indicating local rather than global organising principles. The functional interpretation of local plasticity further emphasises spatial integration and compartmentalised processing, which leads to predictions of non-random spatial distribution of synaptic inputs (Rabinowitch & Segev, 2008; Mel, 1992).

Throughout the thesis, I have adopted the view of dendritically compartmentalised synaptic inputs and as such, experiments are specifically designed to take this into account.

In summary, theoretical considerations of the functional impact of presynaptic plasticity have been lacking, mainly due to a lack of careful dissection of the expression loci in experimental studies. I will next discuss the experimental conditions required for the induction of synaptic plasticity and their underlying molecular signalling pathways. Are there qualitative differences in the induction of pre- vs postsynaptic plasticity? Do their biochemical pathways follow a similar logic?

2.3.4. Homosynaptic Hebbian plasticity: $g(w_{ij}, pre_j, post_i)$

The most extensively studied form of Hebbian plasticity is NMDAR-dependent plasticity. At the hippocampus Schaffer collateral-CA1 synapse, correlated activity in the form of high-frequency stimulation (tetanus) leads to strong postsynaptic spiking and results in long-term potentiation (LTP) of synaptic strength (Bliss & Lømo, 1973). Conversely, sustained low-frequency stimulation, which mimics uncorrelated, sub-threshold activity, induces long-term depression (LTD, Dudek & Bear, 1992). At moderate stimulation frequencies, the precise timing of pre- and postsynaptic spikes determines the quality of synaptic plasticity (spike-timing dependent plasticity, STDP; Bi & Poo, 1998; Froemke et al., 2006). Causal pairing (presynaptic followed by postsynaptic stimulation) generally leads to LTP and anti-causal pairing induces LTD. The relation to stimulation frequency was investigated by Wittenberg and Wang, who showed that the timing-dependence is strictly linked to stimulation frequency (Wittenberg & Wang, 2006; see also Sjöström et al. 2001; Froemke et al., 2006) and represent the same parameter space. Although not directly shown, these conditions are thought to induce predominantly postsynaptic forms of plasticity, especially in case of the Schaffer collateral-CA1 synapse. The general underlying biological mechanism to sense activity correlations is thought to reside in the voltage-dependent activation of NMDARs (Lüscher & Malenka, 2012), which act as

coincidence detectors of glutamate release and postsynaptic depolarisation. The strength of NMDAR activation is translated into a rise in Ca^{2+}-concentration, which is crucially dependent on the level of postsynaptic depolarisation due to the voltage-dependence of NMDARs. Ca^{2+}, in turn, engages specific kinase (CaMKII) and phosphatase (PP1, calcineurin) pathways to induce LTP or LTD, respectively. Due to the difference in the kinetic properties between kinase and phosphatases, as phosphatases have higher affinity, differences in the temporal dynamics of Ca^{2+}-influx gate the sign of synaptic plasticity. This was elegantly demonstrated by photolytic release of Ca^{2+} in the postsynaptic terminal, which, depending on the pattern of Ca^{2+}-release, can induce either LTP or LTD (Yang et al., 1999). Additionally, a recent study using fluorescent probes of CaMKII and calcineurin activity showed that, whereas CaMKII activity is highly non-linear with respect to the number and frequency of stimulation, calcineurin activity is almost independent of frequency (Fujii et al., 2013), which explains the frequency-dependence of (postsynaptic) plasticity. Downstream signalling pathways of both kinase and phosphatase converge onto the regulation of AMPA receptors, either by direct modulation of channel conductance or by regulating the vesicular trafficking of receptors (Chater & Goda, 2014). Postsynaptic strength is therefore a reflection of the average depolarisation experienced by the active synapse.

The induction of presynaptic Hebbian plasticity has been controversial in the past (Kullmann, 2012). A recent meta-analysis of the literature suggested that the reported discrepancies in presynaptic expression locus could be explained by an independent molecular induction mechanism, which involves the activation of L-type VGCCs instead of NMDARs (Padamsey & Emptage, 2014). The basis of argument relies on the observation that (1) LTP could still be induced when NMDARs were blocked pharmacologically (Grover & Teyler, 1990; Grover, 1998), (2) NMDAR-independent LTP required the activation of L-VGCCs (Kullmann et al., 1992; Huang & Malenka, 1993), (3) L-VGCC-dependent LTP was expressed presynaptically (Stricker et al., 1999) and was pharmacologically dissociable from postsynaptic LTP (Bayazitov et al., 2007). In addition, simultaneous

stimulation of the presynaptic terminal was necessary (Grover, 1998; Grover & Yan, 1999). Induction of presynaptic (Hebbian) plasticity therefore depends on the biophysical properties of L-VGCCs, which has a higher voltage threshold compared to NMDARs and exhibits voltage and Ca^{2+}-dependent inactivation (Lacinová & Hofmann, 2005; Hofmann et al., 1999). This suggests that presynaptic plasticity requires strong, transient depolarisation paired with presynaptic stimulation. Presynaptic strength might therefore more accurately reflect a count metric (or probability when normalised) of high-pass filtered postsynaptic membrane potential.

Most studies have examined presynaptic plasticity under a Hebbian framework, in which synaptic changes are related to the correlation between pre- and postsynaptic spiking activity. As pointed out previously, presynaptic plasticity should be sensitive to the temporal structure of the presynaptic input. Experimentally, this can be simplified by examining presynaptic plasticity with respect to success or failures of release, which is ultimately shaped by the temporal structure due to STP. This has been examined in a recent study from our lab (Padamsey, Tong & Emptage, 2017a), which will be introduced in chapter 7, where I will report some additional observations.

2.3.5. Heterosynaptic plasticity: $g(w_{ij}, post_i)$

The first experimental evidence for heterosynaptic plasticity was provided by studies on synaptic plasticity in the hippocampus CA1 region. Due to the unique anatomy, field stimulation of non-overlapping input fibre bundles was possible. When one input pathway was potentiated, the unstimulated pathway showed marked synaptic depression (Lynch et al., 1977; Dunwiddie & Lynch, 1978). Interestingly, heterosynaptic plasticity was dependent on stimulation frequency and not necessarily compensatory (see also Schuman & Madison, 1994; Scanziani et al., 1996). Subsequent studies confirmed that heterosynaptic depression was long-term (Abraham & Wickens, 1991; Pockett et al., 1990, Abraham et al., 1994) and emphasised the importance of postsynaptic depolarisation, since blockade of inhibitory transmission enhanced

heterosynaptic LTD (hetLTD) and hetLTD could be induced in the absence of presynaptic stimulation by postsynaptic depolarisation via direct current injection (Christofi et al., 1993). Similar findings were reported in cortical neurones, where intracellular tetanisation in the form of repeated bursts of high frequency depolarising pulses induced both, LTP and LTD (Volgushev et al., 1994, 1997, 1999, 2000; Lee et al., 2012; Bannon et al., 2017). These studies also indicated that strong depolarisation acts via a rise in intracellular Ca^{2+} via NMDARs or L-VGCCs (Abraham & Wickens, 1991; Christofi et al., 1993; Balaban et al., 2004). The induction mechanism therefore resembles that of Hebbian plasticity (Yang et al., 1999).

Spatial proximity is a known modulator of heterosynaptic plasticity (White et al., 1990). Unlike early experiments that targeted spatially segregated synapse populations, heterosynaptic plasticity was also found to spread spatially from the site of stimulation. Using local perfusion to spatially isolate synapses for electrophysiological recordings, Engert and Bonhoeffer elegantly showed that the induction of homosynaptic LTP is not input-specific but instead spreads up to 70 µm to neighbouring synapses (Engert & Bonhoeffer, 1997). Similarly, LTP could spread to synapses of neighbouring cells, where it elicited hetLTP (Bonhoeffer et al., 1989; Schuman & Madison, 1994) or compensatory hetLTD (Scanziani et al., 1996).

The development of optical methods to assess synaptic strength allowed for more precise measurements of the spatial spread of synaptic plasticity. Wiegert and Oertner induced homosynaptic LTD using low-frequency stimulation at optically identified synapses and monitored spine morphology over several days (Wiegert & Oertner, 2013). Spines that have experienced LTD but also neighbouring spines within 8-10 µm of the same dendrite were more likely to be eliminated in the following 7 days. The spread was spatially confined, indicating an intracellular diffusible signal. Interestingly, the probability of spine elimination was inversely correlated with Pr. In a related study (Hayama et al., 2013), LTD was induced by anti-causal pairing of local glutamate photolysis at single spines with postsynaptic spiking, which is known to induce LTD

electrophysiologically. Surprisingly, spine shrinkage was only observed if the inhibitory neurotransmitter γ-aminobutyric acid (GABA) was additionally provided. Neighbouring spines up to 15 µm along the dendrite were found to decrease in size, which could be abolished by the application of FK-506, a selective blocker of calcineurin. It was therefore proposed that diffusion of calcineurin along the dendrite caused the spread in LTD. Interestingly, spines undergoing structural LTP were protected from LTD. Similarly, in a recent study it was shown that induction of homosynaptic LTD at hippocampal CA3-CA3 synapses led to local spread of LTD along the dendrite, which reversed into LTP further away (Letellier et al., 2019). Other studies report spatially modulated compensatory changes. In one study, potentiation of groups of spines led to selective shrinkage of spines located within, but not outside the group (Oh et al., 2015). This hetLTD required a critical number of potentiated spines and was very sensitive to spatial proximity (below 3.4 µm), indicating high activation threshold. Again, calcineurin was implicated as the key signalling molecule and its inhibition led to heterosynaptic increase in spine size. In addition, successful induction of LTP was not necessary, since hetLTD persisted under CaMKII inhibition. Similar compensatory effects have been attributed to cadherin/catenin complexes during spine maturation (Bian et al., 2015). Here, the authors propose that spines compete for a limited pool of cadherin/catenin in an activity-dependent manner. Activating subsets of synapses led to specific elimination of neighbouring inactive synapses. Indirect *in vivo* evidence has been observed in visual cortex, where hetLTD is thought to play a role in shifting receptive field properties (El-Boustani et al., 2018), and during motor learning (Lee et al., 2013). Lastly, activity of neighbouring synapses can also modulate subsequent induction of plasticity, referred to as metaplasticity (Abraham, 2008). Induction of homosynaptic LTP at single synapses was shown to reduce the threshold for LTP at neighbouring synapses within 8 µm and up to 10 min post-induction (Harvey & Svoboda, 2007), which was dependent on the diffusion of h-Ras (Harvey et al., 2008) from the potentiated synapse or RhoA and Rac1 (Hedrick et al., 2016). In addition, in protein-synthesis dependent plasticity, heterosynaptic stimulation can both facilitate and compete with subsequent plasticity induction (Fonseca et al., 2004; Govindarajan et

al., 2011), and was shown to be dendritic branch-specific. These studies suggest two non-mutually exclusive models of heterosynaptic interactions: (1) Resource competition and (2) diffusion of signalling molecules.

Signalling molecules, such as small molecule second-messengers or proteins, can diffuse across the spine neck into the dendrite (Nishiyama & Yasuda, 2015). The diffusion time constant ranges from hundreds of milliseconds to several seconds, depending on the biophysical properties of the molecule (Bloodgood & Sabatini, 2005; Murakoshi et al., 2011; Harvey et al., 2008) and is therefore suitable for fast, spatially confined induction of heterosynaptic plasticity. 2-photon fluorescence lifetime imaging microscopy (2pFLIM) has been used to study the spatiotemporal profile of important signalling molecules following stimulation of single synapses. CaMKII activity, which is thought to extend the duration of the Ca^{2+}-signal, was constrained to the stimulated spine (Lee et al., 2009; Fujii et al., 2013). However, downstream effector molecules, such as small GTPases involved in the regulation of actin polymerisation (RhoA, H-Ras, Rac) or calcineurin, were found to diffuse and invade neighbouring spines, with the exception of Cdc42, which remained confined to the stimulation site (Hedrick et al., 2016; Murakoshi et al., 2011; Harvey et al., 2008). The diffusion of these molecules crucially depends on their biochemical properties, such as passive diffusion, activation and inactivation time constants, and are therefore thought to implement specific biochemical computations along the dendrite (Nishiyama & Yasuda, 2015).

Both, resource competition and diffusion of biochemical signals are easily understood in the context of postsynaptic modifications, since parameters directly linked to postsynaptic strength are partially included. Presynaptic changes necessitate some form of retrograde signalling, which could potentially, but not necessarily, add further layers of complexity, and therefore differentiate the biochemical logic of pre- and postsynaptic plasticity. Only few studies have attempted to identify the exact expression locus of heterosynaptic plasticity. For instance, synaptic changes following intracellular tetanisation are thought to be partly expressed presynaptically, potentially via the

retrograde messenger nitric oxide (NO; Volgushev et al., 2000; Bannon et al., 2017). NO was also implicated in intercellular spread of LTP (Schuman & Madison, 1994), but the expression locus was not identified. The main objective in chapters 4 and 5 is therefore to examine the differential contribution of pre- and postsynaptic heterosynaptic plasticity.

2.3.6. Transmitter-induced plasticity: g(wij, prej)

Very little is known about synaptic plasticity that is independent of postsynaptic signalling. All main types of glutamate receptors, Kainate, AMPA, NMDA receptors and mGluRs have been found at the presynaptic terminal, where they serve as autoreceptors and are known to exert both short- and long-term influence on presynaptic strength (Pinheiro & Mulle, 2008). For instance, Kainate receptors are involved in short-term facilitation at Schaffer-collateral synapses onto interneurones (Sun & Dobrunz, 2006), whereas NMDARs facilitate presynaptic release in a frequency-dependent manner at synapses onto CA1 pyramidal cells (McGuinness et al., 2010). In cortical neurones, presynaptic NMDARs are required for the induction of presynaptic LTD (Sjöström et al., 2003), pattern-dependent LTD (which is independent of postsynaptic activity) (Rodríguez-Moreno et al., 2013), and facilitation of release (Berretta & Jones, 1996; Kunz et al., 2013; Buchanan et al., 2012). The exact molecular mechanism is still unclear, however, direct ionotropic action, such as depolarisation (Lauri et al., 2001; Kamiya et al., 2002) or influx of Ca^{2+} (McGuinness et al., 2010; Cochilla & Alford, 1999), regulation of K^{+} -conductances (Cochilla & Alford, 1998), regulation of Ca^{2+}-conductances (Takago et al., 2005; Rusakov et al., 2005), Ca^{2+}-induced Ca^{2+}-release (CICR) from internal stores (Cochilla & Alford, 1998; Duguid & Smart, 2004), and modulation of the release machinery (Blackmer et al., 2001; Van Hook et al., 2017) have all been implicated. In cortical neurones, Mg^{2+}-dependent and independent pathways have been shown to regulate different aspects of release (Abrahamsson et al., 2017). In chapter 6, I will presents experiments that attempt to study the role of glutamate on presynaptic strength, both on long and short timescales.

2.4. Retrograde messengers

An obvious difference between the induction of pre- and postsynaptic Hebbian or heterosynaptic plasticity is the strict requirement of a retrograde messenger in the case of presynaptic plasticity. In the following section, I will give a brief overview of retrograde messengers implicated in presynaptic plasticity. These molecules fulfil, to some extent, the general requirements of a retrograde messenger (O'Dell et al., 1991): (1) postsynaptic locus of synthesis; (2) presynaptic locus of action; (3) disruption of postsynaptic synthesis or presynaptic target blocks retrograde signalling; (4) exogenous application bypasses postsynaptic mechanisms.

2.4.1. Nitric oxide

One of the most frequently studied retrograde messenger is NO. NO is a known signalling molecule in the peripheral nervous system (Rand & Li, 1995; Toda & Okamura, 2003; Toda & Herman, 2005). First identified as "Endothelium-derived relaxing factor" (Palmer et al., 1987; Ignarro et al., 1987), the release of NO was shown to elevate cyclic guanosine monophosphate (cGMP) levels in smooth muscle cells, which leads to their relaxation. Similarly, NO was known to elevate cGMP levels in brain tissues (Arnold et al., 1977; Miki et al., 1977) and NO release was shown to depend on glutamate and Ca^{2+}-influx via NMDARs (Garthwaite et al., 1988; Garthwaite et al., 1989; Bredt & Snyder, 1989; East & Garthwaite, 1991). The gaseous nature and membrane permeability of NO allowing it to diffuse over long distances led to the idea of NO as a potential retrograde messenger.

The majority of NO in the brain is produced by the nitric oxide synthase (NOS) isoform NOS1, also called neuronal NOS (nNOS), by conversion of L-arginine (Huang et al., 1993). nNOS is expressed throughout the brain, but in an uneven pattern (Bredt et al., 1991; Vincent & Kimura, 1992; Rodrigo et al., 1994; Egberongbe et al., 1994; Doyle & Slater, 1997), with high abundance in cerebellum, striatum, and hippocampus. Tonic levels of NO is thought to be regulated by NOS3, or endothelial NOS (eNOS), which is mainly

expressed in endothelial cells (Seidel et al., 1997; Blackshaw et al., 2003; Stanarius et al., 1997) or astrocytes (Lin et al., 2007), and could have a distinct role in synaptic plasticity (Bon & Garthwaite, 2003; Hopper & Garthwaite, 2006). Activation of nNOS is Ca^{2+}-dependent and requires the binding of calmodulin (CaM). Several phosphorylation sites further modulate nNOS catalytic activity, most notably CaMKII-dependent phosphorylation of serine-847 and Akt-dependent phosphorylation of serine-1412, which are thought to be inhibitory and facilitatory, respectively (Garthwaite, 2008). Furthermore, nNOS associates with PSD-95 through its PDZ domain, thus enabling tight coupling to NMDARs. The putative signalling sequence is thought to require Ca^{2+}-influx through NMDARs, activation of CaM and phosphorylation via Akt, which leads to production of NO, inactivation via phosphorylation by CaMKII, and subsequent dephosphorylation for reset (Rameau et al., 2007). These characteristics, combined with fast and far-reaching diffusion, with a diffusion coefficient on the order to 3000-4000 $\mu m^2/s$ and relatively slow intrinsic inactivation rates (Philippides et al., 2000; Schweighofer & Ferriol, 2000; Lancaster, 1994), make NO an ideal spatial signal for strong postsynaptic depolarisation, which can be used for computation in downstream signalling pathways.

Inhibition of NOS or extracellular sequestering of NO has been shown to block tetanus-induced LTP at Schaffer collateral-CA1 synapses (O'Dell et al., 1991, 1994; Schuman & Madison, 1991; Böhme et al., 1991; Haley et al., 1992, 1993; Williams et al., 1993; Boulton et al., 1995; Arancio et al., 1996, Malen & Chapman, 1997; Zhuo et al., 1998; Wilson et al., 1999; Bon & Garthwaite, 2001; but see Gribkoff & Lum-Ragan, 1992; Kato & Zorumski, 1993; Cummings et al., 1994) as well as theta-burst stimulation (TBS) LTP (Johnstone & Raymond, 2011; Musleh et al., 1993). Additionally, direct perfusion or photolytic release of NO is sufficient to induce LTP, but only when paired with concurrent presynaptic stimulation (Zhuo et al., 1993; Malen & Chapman, 1997; Arancio et al., 1996; Bon & Garthwaite, 2001, 2003; Padamsey et al., 2017a). Selective application of NOS inhibitors to the postsynaptic terminal, but not the presynaptic terminal, blocks LTP, indicating a

postsynaptic locus of NO production (O'Dell et al., 1991; Schuman & Madison, 1991). NO scavengers block LTP when applied to either pre- or postsynaptic terminal, but LTP induced by direct perfusion or photolytic release of NO was only blocked by presynaptic or extracellular scavengers (Arancio et al., 1996). This indicates that NO diffuses from the postsynaptic terminal to act at the presynaptic terminal (but see Ko & Kelly, 1999). At the presynaptic terminal, NO activates soluble guanylyl cyclase (sGC, Boulton et al., 1995; Chetkovich et al., 1993), which produces cGMP to enhance presynaptic function via cGMP-dependent protein kinase (PKG, Arancio et al., 1995; Arancio et al., 2001; Wang et al., 2005a). NO-dependent increase in presynaptic strength was attributed to an increase in Pr (Stanton et al., 2005; Johnstone & Raymond, 2011), most likely due to an increased RRP size (Ratnayaka et al., 2012). Additionally, the presynaptic terminal undergoes morphological remodelling following TBS, which was abolished by NOS blockers (Nikonenko et al., 2003). Interestingly, NO also affects the activity-dependent formation and development of spines, and a loss in NO signalling *in vivo* was shown to decrease spine and bouton density and prevent the formation of synapse clusters along dendritic branches (Nikonenko et al., 2013).

NO signalling has also been implicated in other forms of plasticity. In a series of studies, Stanton and colleagues showed that hippocampal homosynaptic LTD induced via LFS requires NMDAR-dependent production of NO to trigger a cGMP signalling cascade in the presynaptic terminal. Downstream signalling was proposed to involve Ca^{2+} release from internal stores, gated by cyclic ADP-ribose and ryanodine receptors, and the activation of presynaptic CaMKII, which ultimately lead to a decrease in Pr (Izumi & Zorumski, 1993; Stanton & Gage, 1996; Stanton et al., 2001, 2003; Gage et al., 1997; Reyes-Harde et al., 1999; Zhang et al., 2006). Heterosynaptic plasticity induced by intracellular tetanisation in cortical pyramidal neurones was reported to depend on retrograde NO signalling. Here, NO seems to modulate the weight-dependency, but not the actual expression, of heterosynaptic LTP and LTD (Volgushev et al., 2000; Lee et al., 2012).

2.4.2. Carbon monoxide

Evidence for retrograde signalling of carbon monoxide (CO) came from early experiments examining the effect of Zinc protoporphyrin IX (ZnPP), which inhibits the enzyme for CO synthesis, heme oxygenase, on hippocampal LTP. ZnPP was able to block tetanus-induced LTP, but not LFS-induced LTD (Zhuo et al., 1993; Stevens & Wang, 1993; Zhuo et al., 1998). Moreover, pairing CO application with weak tetanic stimulation, which in isolation had no long-term effects on synaptic transmission, led to robust LTP. However, in a later study, where heme oxygenase-2, the predominant isoform found in the brain, was genetically knocked-out, no impairment in LTP induction were observed (Poss et al., 1995). Furthermore, ZnPP was still detrimental to LTP induction, indicating the possibility of off-target effects. For instance, ZnPP was shown to inhibit GC (Luo & Vincent, 1994; Serfass & Burstyn, 1998), the main target in NO-dependent LTP. The effects of CO application were attributed to the direct activation of sGC, which binds CO with low affinity (Ma et al., 2007; Friebe et al., 1996). CO as a potential retrograde messenger has therefore fallen out of favour, especially for hippocampal synaptic plasticity.

2.4.3. Endocannabinoids

Endocannabinoids (eCB) comprise another well-studied class of retrograde messengers, due to their prominent role in regulating synaptic transmission (Castillo et al., 2012; Heifets & Castillo, 2009; Kano et al., 2009). Cannabinoid receptors (CB1R & CB2R) are widely expressed in the brain and are activated by a variety of ligands, the best characterised being anandamide (AEA) and 2-arachidonoylglycerol (2-AG). eCB signalling is primarily inhibitory towards synaptic transmission, and is implicated in various forms of LTD, including homosynaptic and heterosynaptic LTD of both inhibitory and excitatory synapses. In the hippocampus, eCB signalling is involved in multiple forms of presynaptic LTD, especially of inhibitory inputs (Lafourcade & Alger, 2008; Kang-Park et al., 2007; Zhu & Lovinger, 2007; Edwards et al., 2008; Wilson & Nicoll, 2001; Chevaleyre & Castillo, 2003; Chevaleyre et al., 2007). At excitatory synapses, eCBs can also induce LTD, but expression

mechanism and locus are less clear (Han et al., 2012; Yasuda et al., 2008; Takahashi & Castillo, 2006). In one case, eCB signalling was reported to decrease heterosynaptic presynaptic excitability, which was dependent on presynaptic PKA (Yasuda et al., 2008). However, Han and colleagues showed that the suppression of excitatory synaptic transmission by eCBs can be abolished by genetic knock-out of astrocytic CB1Rs (Han et al., 2012), consistent with work at neocortical synapses showing retrograde feedback via the release of gliotransmitters (Min & Nevian, 2012). These studies therefore indicate that the eCB system is almost exclusively inhibitory and biochemical computations of neural activity are thus upstream of eCB release.

2.4.4. Brain-derived neurotrophic factor

Neurotrophins are known regulators of synaptic function of both developing and mature neurones, and brain-derived neurotrophic factor (BDNF) is the most extensively studied, due to its prominent role in synaptic plasticity (Leal et al., 2015; Lu et al., 2014; Lu, 2003). BDNF, by activating its receptor TrkB, is known to facilitate the induction of LTP at Schaffer collateral-CA1 synapses, and is sometimes found to be necessary for induction and maintenance of LTP. BDNF is release by both, the pre- and the postsynaptic terminal, and due to the existence of receptors at both terminals, the locus of action is still heavily debated. An early study by Zakharenko and colleagues using selective genetic knock-out of BDNF suggested that the presynaptic enhancement by BDNF is caused by presynaptically but not postsynaptically released BDNF, indicating autocrine signalling (Zakharenko et al., 2003). Additionally, postsynaptic BDNF was shown to act on heterosynaptic postsynaptic TrkB receptors to facilitate spine structural LTP (Hedrick et al., 2016). However, other studies have shown, by pure postsynaptic intervention, that BDNF can act presynaptically to enhance presynaptic function (Magby et al., 2006, Jakawich et al., 2010). Recently, a careful genetic dissection of region-specific knock-out of BDNF and TrkB suggested that the induction of LTP requires anterograde BDNF signalling, whereas retrograde signalling is only necessary for LTP maintenance (Lin et al., 2018). In addition, the authors suggested that presynaptic TrkB receptors are important

for the regulation of basal neurotransmission, since knock-out resulted in global changes in presynaptic strength. Apart from its facilitatory role, pro-BDNF, the precursor peptide of BDNF, has been suggested to mediate LFS NMDAR-dependent LTD through p75NTR receptors (but see Matsumoto et al., 2008). Thus, due to complex signalling mechanisms and technical difficulties, the role of BDNF as a retrograde messenger is still unclear. In general, BDNF, as a counterpart to eCBs, positively reinforces synaptic strength. However, interesting biochemical computations might underlie the processing of pro-BDNF, which can be cleaved upon release into the extracellular space (Pang et al., 2004; Mowla et al., 1999), hence providing context-dependency.

In summary, multiple retrograde messengers act in concert to regulate synaptic strength and their impact might substantially overlap. However, the underlying biochemical logic is likely to differ and is therefore informative of the overall computational goal. Both eCB and BDNF have comparatively uni-directional roles in depression and potentiation, respectively. These mediators are more likely to act downstream of the necessary computation of neuronal activity laid out in the general learning rule. In contrast, NO resembles more a representative messenger of postsynaptic activity, and extends the spatial volume permissive to computation of neuronal activity. Alternative means of retrograde signalling, such as cell-adhesion proteins, would implicate combined processing of pre- and postsynaptic changes. Identification of the retrograde messenger is therefore central in understanding and generalising experimentally derived learning rules.

2.5. Thesis - Pre an postsynaptic plasticity follow distinct rules in their long- and short-term regulation

I will now formulate the guiding hypotheses for this work, which will be split into three parts according to the three cases of regulation alluded to in the introduction.

(1) Chapters 4 and 5 concern the heterosynaptic regulation of synaptic strength, the main focus of this thesis. As pointed out, very little is known about the locus of expression.

Adopting local, spatially modulated heterosynaptic plasticity along individual dendritic compartments as a working model, I have devised an experimental strategy to simultaneously monitor pre- and postsynaptic strength of single synapses in response to purely postsynaptic activity. I sought to answer the questions: Is heterosynaptic plasticity expressed at both loci? Do changes at both loci follow similar spatiotemporal dynamics? How much do their biochemical pathways overlap and at what point do they separate? My working hypothesis states that, due to the differing impact on synaptic transmission, differences in the spatiotemporal dynamics of pre- and postsynaptic strengths should be observable. Molecularly, these differences should be explainable by contrasting signalling via intracellular diffusible factors and retrograde messengers. As such, I suggest a segregation of the biochemical pathways as early as the detection of synaptic activity by postsynaptic neurotransmitter receptors.

(2) In chapter 6, I will present work on transmitter-induced forms of presynaptic regulation. Here, I have studied the potential role of glutamate as an autocrine feedback signal, in the context of both long- and short-term plasticity, following previous and ongoing work in the lab. I have asked the following questions: Does the presynaptic terminal sense single events of glutamate release? How does glutamate release affect Pr? What is the sensor for glutamate? As explained before, theoretical considerations suggests that presynaptic plasticity should be sensitive to success and failure of release. An autocrine effect of glutamate is therefore a potential way of signalling release successes and might play a role in homosynaptic Hebbian plasticity as well. Experiments in this chapter were collectively obtained and analysed by me and Carla Schmidt (appropriately indicated).

(3) In chapter 7, I will present additional observations on recently published work from our lab (Padamsey, Tong & Emptage, 2017a) concerning homosynaptic Hebbian-type presynaptic plasticity. This work focuses on synaptic plasticity that is sensitive to release failures, and is as such independent of glutamate signalling.

2.6. Methodology

2.6.1. Model system: The hippocampus

The synapse of interest is the Schaffer collateral-CA1 synapse of the hippocampus. The hippocampus is an intensively studied brain region, especially in the context of synaptic plasticity, due to its prominent role in the formation of memories, specifically episodic and declarative memory, and the processing of spatial information (Bird & Burgess, 2008; Burgess & O'Keefe, 1996). It is located in the caudal part of the forebrain, extending in a C-shape along the septo-temporal axis, adjacent to its main input from the entorhinal cortex (EC), which in turn receives major inputs from the perirhinal and postrhinal cortex.

The hippocampus is divided into distinct subregions: the dentate gyrus (DG), which mainly receives input from EC; regions CA3, CA2, CA1, which make up the hippocampus

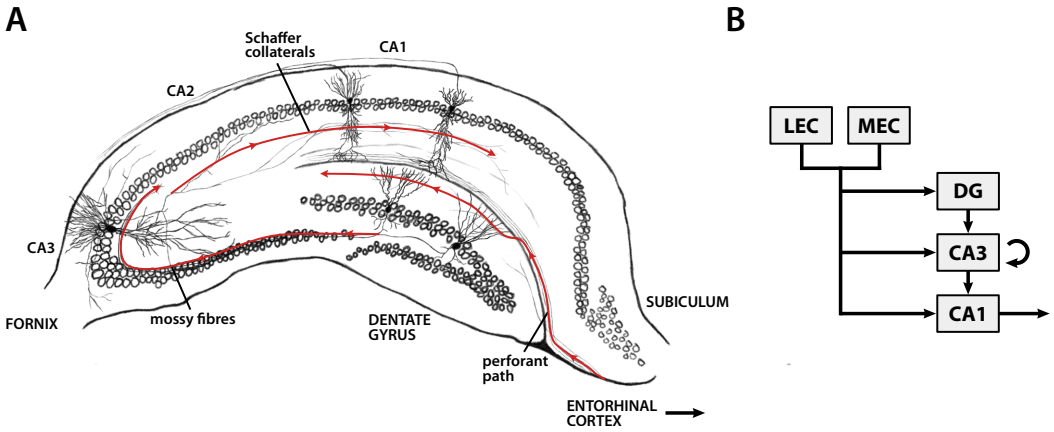

Fig. 2.1: The anatomy and connectivity of the hippocampus. (A) Illustration of a coronal hippocampal section. The hippocampus is sub-divided into dentate gyrus, CA3, CA2, CA1, and the subiculum. Cell bodies of the principal neurones are contained in a single layer. The standard tri-synaptic pathway is shown in red. Input fibres from the entorhinal cortex project into the dentate gyrus along the perforant path. Mossy fibres from the dentate gyrus form synapses onto the proximal apical dendrite of pyramidal neurones in CA3. The output of CA3, the Schaffer collaterals, projects mainly to *stratum radiatum* of CA1. (B) Schematic of the main synaptic connections of the hippocampus. LEC: Lateral entorhinal cortex, MEC: Medial entorhinal cortex, DG: Dentate gyrus.

proper, and the subiculum (Fig. 2.1). Each region is subdivided into three layers. Principal neurones are contained in a single layer, called the granule layer in the DG and *stratum pyramidale* elsewhere, and their dendrites extend into the adjacent deep and superficial layers. Axons from the superficial layers (II & III) of lateral and medial areas of the EC make up the perforant path and project to all subregions of the hippocampus, most prominently to the superficial layer of DG, *stratum moleculare*. Granule cells of the DG, in turn, project via the mossy fibres to the proximal apical dendrite of CA3 pyramidal neurones in *stratum lucidum*. CA3 is often regarded as an autoassociative network due to its extensive recurrent connections, formed throughout its neuropil layers. The output from CA3, the Schaffer collaterals, project to the superficial layer of CA1, *stratum radiatum*, where they form the majority of their synapses onto radial oblique dendrites branching off the main apical trunk (Megías et al., 2001). This tri-synaptic feedforward pathway, EC -> DG -> CA3 -> CA1, is regarded as the standard model of the hippocampus. Additionally, Schaffer collaterals project to the basal dendrites in the deep layer of CA1, *stratum oriens*, which also receives strong multi-quantal inputs from CA2 (Chevaleyre & Siegelbaum, 2010). EC also projects directly onto the apical tuft in *stratum lacunosum moleculare* of both CA3 and CA1 (though the inputs might originate from distinct layers in EC, van Strien et al., 2009). CA1, the main output of the hippocampus, projects to the subiculum and various other brain regions, including prefrontal cortex, amygdala, and feedback connections to the entorhinal and perirhinal cortex (Naber et al., 2001; van Groen & Wyss, 1990, van Strien et al., 2009).

Principal neurones in CA1 are excitatory, glutamatergic pyramidal cells. Morphologically, they are characterised by a long apical dendrite extending orthogonally into the superficial layer. Radial oblique dendrites branch from the proximal part of the apical trunk; the distal tuft receives isolated inputs from the perforant path. A set of extensively branched network of basal dendrites, thought to be highly electrically compartmentalised in pyramidal neurones (Nevian et al., 2007), spans into the deep layer, where it receives inputs from CA3 and CA2 neurones. Distinct interneurone populations

are known to exert inhibition onto certain parts of the principal neurone, further regulating and compartmentalising dendritic processing (Somogyi & Klausberger, 2005; Milstein et al., 2015; Royer et al., 2012).

The Schaffer collateral-CA1 synapse is a typical excitatory, glutamatergic synapse, formed by presynaptic oblong-shaped varicosities, boutons *en passant*, onto dendritic spines. The number of contacts is estimated to lie in a range between 20000 and 30000 per axon, and the number of synapses between pairs of neurones is generally low, thereby exhibiting substantial divergence in the output of CA3 (Shepherd & Harris, 1998). However, ~20% of synaptic contacts are identified as multiple-synapse boutons (MSBs), where a single presynaptic terminal contacts more than one postsynaptic density (Sorra & Harris, 1993, Shepherd & Harris, 1998), suggesting some degree of convergence (Harris, 1995), perhaps of specific microcircuits. Indeed, projections from CA3 to CA1 are non-random and do not seem to follow Peter's rule (Braitenberg & Schüz, 1998), which assumes uniform distribution of synaptic contacts, which should scale linearly with the neuropil surface area. Instead, connectivity seems to depend on neuronal identity (Deguchi et al., 2011) and developmental history (Druckmann et al., 2014), in which neurones that share similar developmental timing are also found to have higher connectivity.

The highly structured organisation of the axonal fibre bundles, especially the relatively isolated Schaffer collaterals extending along *stratum radiatum* of CA1, makes the CA3-CA1 synapse particularly accessible to electrophysiological interrogation. This has led to an extensive literature on the synaptic properties and plasticity of this pathway, making it an ideal model system for the purpose of my thesis.

2.6.2. Organotypic slice cultures

The connectivity of the hippocampus, especially the tri-synaptic pathway of the standard model, is largely contained in the two-dimensional plane across the septotemporal axis, and is therefore well-suited for conducting experiments in acute or organotypic slice

preparations. In this study, due to the heavy reliance on optical methods for measuring and manipulating synaptic strength (see next section), I have, for the most part, used organotypic slice cultures, owing to their excellent optical access. Although organotypic hippocampal slices are well-established (Gogolla et al., 2006; Gähwiler et al., 1997; De Simoni & Yu, 2006; Humpel, 2015), general concerns about the validity and translatability to hippocampal function *in vivo* remain, mainly attributed to the non-natural development of the circuit remote of natural activity patterns and biochemical milieu. I will briefly review studies comparing cellular and synaptic properties of CA1 pyramidal cells between organotypic and acute slice preparations (De Simoni et al., 2003; Gähwiler et al., 1997; Gähwiler, 1988, 1981; Collin et al., 1997; Debanne et al., 1995; Bahr, 1995; Bahr et al., 1995; Muller et al., 1993). The general cytoarchitecture and connectivity of the hippocampus is largely preserved, especially when prepared from slightly older (P5-7) animals, and all connections and cell types have been identified. Due to the denervation of extrahippocampal inputs and the CA1 outputs fibres, minor reorganisation in the connectivity occur, such as supragranular collaterals formed by the mossy fibres and increased recurrent and potentially autaptic innervation in CA1. Preserving parts of the EC can alleviate these aberrations to some extent (Gähwiler et al., 1997). Dendritic morphology is comparable, but dendritic branching is more complex in organotypic slices. Synapse density is reduced by ~ 20%, especially on more distally located dendrites, but spine morphology, i.e. the distribution of spine shape classes, is roughly similar. Since slices are prepared from young animals with still developing hippocampi, synapse maturation occurs throughout the first three weeks in culture. The expression of certain glial and synaptic proteins (such as glutamate receptors, synaptic adhesion proteins, etc.) plateau and stabilise at around 10 days in vitro (DIV), which is mirrored in an attenuation of the steady increase in EPSP amplitude. No differences in protein expression and general bioelectrical properties have been reported (Bahr, 1995). Similarly, paired-pulse facilitation, a common characteristic of this synapse, is robustly observed at DIV10. Around the same time, a substantial increase in the success rate of inducing LTP occurs (from ~ 60% at DIV9 to > 90% at DIV11, Muller et al., 1993) and induction and expression

of long-term plasticity are likely to follow the same rules as found in acute slices (Mellentin et al., 2006). Interestingly, apart from an initial restructuring shortly after explantation, development parallels that *in situ*. A major discrepancy is seen in the increased spontaneous activity, specifically of excitatory synapses, in organotypic slices, which was suggested to result from the increased connectivity due to the two-dimensional anatomical constraints (De Simoni et al., 2003). This hyperconnectivity is especially notable with long culturing time.

To summarise, organotypic slices are in most respects similar to age-matched acute slice preparations and are well-suited for studying synaptic plasticity. They provide good optical access and facilitate pharmacological and genetic interventions. However, increased synaptic activity and connectivity have to be accounted for experimentally (see Methods).

2.6.3. Measuring release probability

The stochastic nature of neurotransmitter release complicates the direct measurement of presynaptic strength. Structurally, bouton size, active zone area, and the size of the RRP are correlated with Pr, and are primarily accessible via ultrastructural analysis, such as electron microscopy (Schikorski & Stevens, 1997; Holderith et al., 2012; Branco et al., 2010) or super-resolution microscopy (Chéreau et al., 2017). More direct measurements of individual release events rely on fluorescent probes that allow direct monitoring of vesicle exocytosis, such as FM-styryl dyes (Betz & Bewick, 1992; Ryan et al., 1993), genetic labelling of synaptic vesicle protein with pH-sensitive GFP (pHluorins, Miesenböck et al., 1998; Granseth et al., 2006; Balaji & Ryan, 2007), or quantum dots (Zhang et al., 2009; Park et al., 2012). These techniques often require preparations with high optical access, such as dissociated cell cultures, and high sensitivity capturing devices to compensate for the low photon yield. FM-dyes have been successfully used to measure Pr in slice preparations (Zakharenko et al., 2001, 2003).

Identification of the presynaptic terminal is often incompatible with methods used to

stimulate and manipulate neuronal activity (such as patch-clamp recordings). Although synaptic pairs can be identified under some circumstances, *e.g.* using paired recordings or fluorescent labelling of pre- and postsynaptic structures, the efficiency of these methods are comparatively low. Instead, purely postsynaptic readouts can be used to estimate Pr.

The use-dependent NMDAR blocker MK-801 can be used to determine presynaptic strength. The rate of decrease of the NMDAR-dependent current with successive stimulation depends crucially on the number of successful release events, and is therefore indicative of Pr (Huang & Stevens, 1997). However, MK-801 block is irreversible and therefore not suitable for repeated measurements.

As mentioned before, Pr depends strongly on the history of AP firing. At most central, glutamatergic synapses, especially the Schaffer collateral-CA1 synapse, two APs elicited in quick succession (> 5 Hz) will lead to facilitation of the second pulse. The magnitude of facilitation depends on the stimulus interval and, more importantly, on basal Pr due to the ceiling effect of uni-quantal release at high Pr. The relative increase in synaptic efficacy, paired-pulse ratio (PPR), is therefore inversely correlated with basal Pr (Dobrunz & Stevens, 1997) and is routinely used as an indirect read-out (Manabe et al., 1993; Debanne et al., 1996). Similarly, trains of action potentials have been used to estimate STP properties of the synapse (Markram & Tsodyks, 1996), which scale predictably with manipulations of Pr (Tsodyks & Markram, 1997).

According to Katz's quantal hypothesis, neurotransmitter release is described by the binomial theorem. The coefficient of variation (CV) of the response amplitude is defined as

$$CV = \frac{\sigma}{\mu} = \sqrt{\frac{1-p}{Np}}$$

where σ is the standard deviation and μ the mean of the response amplitude. CV, or the more frequently used CV^{-2}, is invariant in q (which, in this case, represents the postsynaptic response to a release quantum) and therefore provides a read-out for Pr,

assuming the number of release sites is unaltered. Potential confounds of this measure have been raised, such as the influence of background noise and the requirement of a large sample size (Faber & Korn, 1991; Martin, 1966).

Extracellular electrical stimulation can be fine-tuned by using minimal stimulation strength to isolate a single to few axonal fibres, thus allowing postsynaptic intracellular recording of putative single synapse responses (Raastad et al., 1992; Stevens & Wang, 1995). Combined with statistical models to estimate the uncertainty of the number of fibres stimulated, this technique has been successfully used to study short-term plasticity

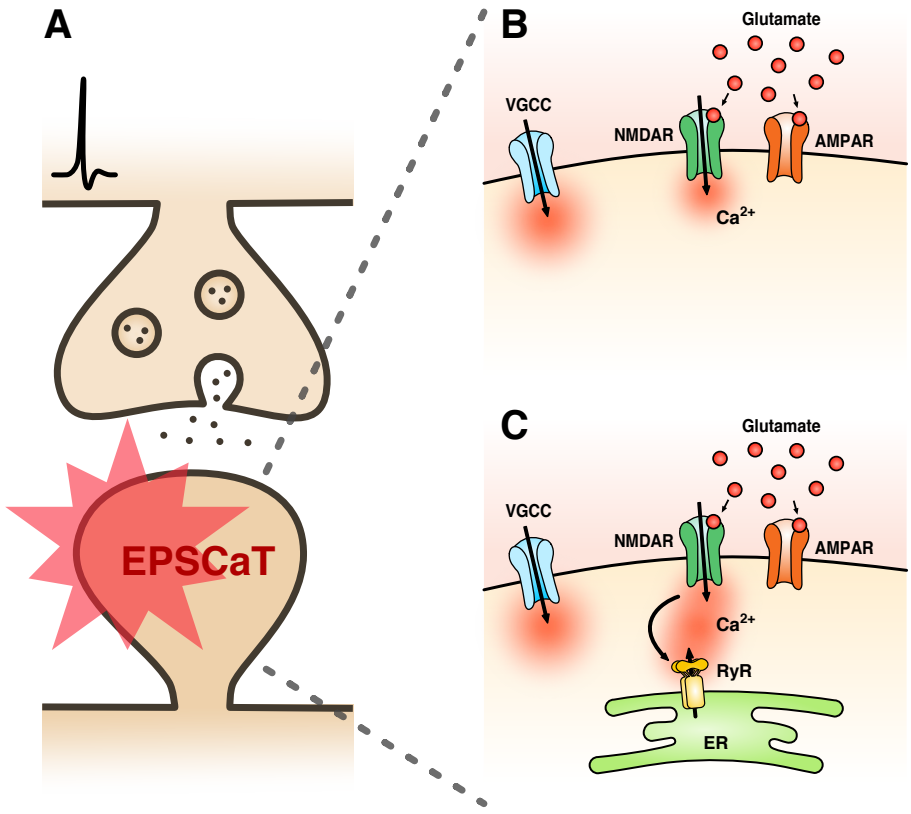

Fig. 2.2: Glutamate release elicits postsynaptic Ca^{2+}-influx. (A) The release of glutamate can be visualised as excitatory postsynaptic Ca^{2+}-transients (EPSCaTs), which allow the direct estimation of release probability. (B) Depolarisation caused by AMPARs leads to the opening of NMDARs and VGCCs and a rapid increase in intracellular Ca^{2+}-concentration. (C) Additional Ca^{2+}-influx can result from Ca^{2+}-induced Ca^{2+}-release from internal stores, mainly via ryanodine receptor-gated stores. Figure adapted from Padamsey et al., 2019.

(Stevens & Wang, 1995; Dobrunz et al., 1997; Dobrunz & Stevens, 1997; Dobrunz & Stevens, 1999) and long-term plasticity of the presynaptic terminal (Malinow & Tsien, 1990; Foster & McNaughton, 1991).

Optical quantal analysis, a robust and direct method of assessing presynaptic strength at optically identified single synapses (Emptage et al., 1999, 2003; Ward et al., 2006; Enoki & Fine, 2009; Oertner et al., 2002; Padamsey et al., 2019), is the main technique used throughout this thesis (Fig. 2.2). Optical quantal analysis relies on the detection of all-or-none synaptic events at single postsynaptic terminals using high-sensitivity reporters of glutamate release. Although genetically encoded glutamate sensors with sufficiently high sensitivity have recently been developed (Marvin et al., 2013; Helassa et al., 2018; Namiki et al., 2007), and successfully used to detect single glutamate quanta and to estimate release probability, high affinity Ca^{2+}-indicators have long been established as reliable reporters of neurotransmitter release at glutamatergic synapses. At most central synapses, glutamate release elicits excitatory postsynaptic calcium transients (EPSCaTs), mainly mediated by Ca^{2+}-influx from NMDARs and VGCCs. Ryanodine receptor-gated Ca^{2+}-induced Ca^{2+}-release from internal stores further amplify the postsynaptic Ca^{2+}-response, however only approximately 10-20% of Schaffer-collateral CA1 synapses contain endoplasmic reticulum (ER; Spacek & Harris, 1997). IP3R-gated stores have also been shown to respond to single glutamate release events, although in a temporally delayed manner (Holbro et al., 2009). EPSCaTs show all characteristics of stochastic neurotransmitter release, such as all-or-none binary events (Emptage et al., 1999), short-term plasticity (Emptage et al., 1999, 2003), similar basal distribution (Ward et al., 2006), and correlation with active zone size (Holderith et al., 2012). In addition, EPSCaT probability scales with pharmacological manipulations known to modify Pr (Emptage et al., 1999; Oertner et al., 2002; Chalifoux & Carter, 2010) and simultaneous electrophysiological recordings show that EPSCaTs coincide with all-or-none unitary EPSPs (Enoki & Fine, 2009). Technical details will be discussed in the Methods and Materials section.

3. Materials and Methods

3.1. Slice preparation

3.1.1. Preparation of organotypic hippocampal slice culture

Organotypic hippocampal slices were prepared from postnatal day P6-7 Wistar rat pups (Harlan UK, Nihon SLC). Rats were sacrificed by cervical dislocation and decapitation and the brain was extracted. The hippocampus of both hemispheres were isolated and cut into 350 µm-thick transverse slices on a McIlwain tissue chopper (Mickle Laboratory Engineering Co. Ltd. and Cavey Laboratory Engineering Co. Ltd.). Dissection of the brain was done in ice-cold Earle's Balanced Salt solution (EBSS)-based dissection buffer, which was modified with 35 mM glucose and 20 mM HEPES and pH-corrected with 5 mM NaOH. For experiments in chapters 4 and 5, 25 mM HEPES was added, instead. Slices were manually curated and slices showing obvious tissue damage or incomplete hippocampal anatomy, which includes an intact dentate gyrus and continuous hippocampus proper, were discarded. 18-24 slices were transferred onto cell culture inserts (0.4 µm pore size, Merk Millipore) and placed in a 6-well plate filled with 1 ml/well of culturing media. Culturing media for experiments in chapter 6 and 7 consisted of 78 % Minimum Essential Medium (MEM, Thermo Fisher Scientific), 20 % horse serum (Thermo Fisher Scientific), 30 mM HEPES, 26 mM glucose, 5.8 mM $NaHCO_3$, 1 mM $CaCl_2$, 2 mM $MgSO_4$, and 2 % B-27 Plus Supplement (Thermo Fisher Scientific). For chapters 4 and 5, culturing media consisted of 50 % MEM, 23 % EBSS, 25 % horse serum, and 36 mM glucose. For the latter preparation, I observed a negative impact of B-27 Supplement (Thermo Fisher Scientific) on slice health and omitted it from the culturing media. 2 % B-27 was still included for experiments in Chapter 4. Culture media was replaced every 2-3 days. Slices were maintained at 37˚C and 5 % CO_2 and used for experiments at DIV10-15.

Slices were transferred by cutting the membrane of the culture insert around the slice and fixated to the recording chamber either using a thin layer of grease (glisseal® HV,

Borer) or by placing a custom made metal frame around the slice. The recording chamber was constantly perfused (1-2 ml/min) with artificial cerebrospinal fluid (aCSF) containing (in mM) 145 NaCl, 2.5 KCl, 16 $NaHCO_3$, 1.2 NaH_2PO_4, 11 glucose, 2-3 $CaCl_2$, and 1-2 $MgCl_2$. For experiments with intensive imaging, 1 mM Trolox (Sigma Aldrich) and 0.2 mM ascorbic acid were additionally included. For electrophysiological recordings, 200 nM NBQX (Abcam) was added to prevent strong recurrent excitation due to hyper-connectivity of the slice. The aCSF was bubbled with 95 % O_2 and 5 % CO_2 and heated to near-physiological temperature (33-35˚C) using a custom made in-line heater.

3.1.2. Preparation of acute hippocampal slices

Acute hippocampal slices were prepared from P14-21 Wistar rats (Harlan UK). Rats were sacrificed by cervical dislocation and decapitation and the brain was extracted and immediately submerged in ice-cold dissection media saturated with 95 % O_2 and 5 % CO_2. Dissection media consisted of (in mM): 65 sucrose, 85 NaCl, 2.5 KCl, 25 $NaHCO_3$, 1.25 NaH_2PO_4, 10 glucose, 7 $MgCl_2$, and 0.2 $CaCl_2$. The cerebellum was manually removed by a coronal cut using a razor blade to create a flat surface, and the brain was glued onto a designated platform of the vibratome (Microm HM 650V, Thermo Scientific). Brains were additionally stabilised by a block of 2 % agar contacting the dorsal surface of the brain. 400 µm coronal slices were cut and the hemispheres were separated and transferred into a recovery chamber containing standard aCSF (in mM: 120 NaCl, 2.5 KCl, 26 $NaHCO_3$, 1.2 NaH_2PO_4, 11 glucose, 1 $MgCl_2$, and 2 $CaCl_2$), which was bubbled with 95 % O_2 and 5 % CO_2. Slices were allowed to recover for 8 min at 37˚C and 60 min at room temperature prior to use. Slices were maintained at room temperature up to 4-5 h.

For experiments, slices were transferred to the recording chamber and secured using a “harp” (Warner Instruments). The recording chamber was constantly perfused (2-3 ml/min) with aCSF and 100 µM picrotoxin (Sigma Aldrich) was added to block inhibitory synaptic transmission. The aCSF was bubbled with 95 % O_2 and 5 % CO_2 and heated to

near-physiological temperature (33-35˚C) using a custom made in-line heater.

3.2. Electrophysiology

3.2.1. Electrophysiological recordings in organotypic slices

Whole-cell patch clamp was established using patch pipettes (prepared using a horizontal micropipette puller, Sutter Instrument Co., or vertical puller, Narishige) filled with standard internal solution, which consisted of (in mM) 135 K-Gluconate, 10 KCl, 10 mM HEPES, 1-2 $MgCl_2$, 2 mM Na_2ATP, and 0.4 Na_3GTP. Data was acquired using an Axoclamp 2B amplifier and WinWCP software (Strathclyde Electrophysiology Software). For experiments in chapters 4 and 5, Clampex (Version 10.7.0.3, Molecular Devices) was used as acquisition software. Current was injected to polarise the resting membrane potential (normally around -60 mV) to -70 mV; cells were clamped at -70 mV in voltage clamp experiments. Access conductance and membrane capacitance were monitored throughout the experiment by injection of brief step currents and recordings were discarded if changes of > 10 % were detected. Moreover, a minimum access conductance of Ga ≥ 30 nS was required for all experiments.

3.2.2. Induction of spike timing-dependent presynaptic LTP

CA1 pyramidal neurones were patched with high-resistance patch-pipettes (6-12 MΩ) in order to minimise dialysis, which has been previously shown to be detrimental to presynaptic LTP (Padamsey et al., 2017a). Recordings were performed in current clamp. A tungsten monopolar stimulation electrode (A-M Systems, Inc.), which was inserted into a glass pipette filled with 150 mM NaCl, was used to stimulate Schaffer collateral axonal fibres. The stimulation electrode was placed in *stratum radiatum* ~ 100 µm away from the neurone. Short current pulses (100 µs, 10-30 µA; Digitimer Ltd.) were used to elicit EPSPs of size 5-10 mV. A stable baseline was established by stimulating at 0.1 Hz and PPR (70 ms inter-pulse interval) was sampled at 0.02 Hz. Due to dialysis, baseline recordings were limited to 5-8 min after whole-cell mode was established. Presynaptic LTP was induced by

pairing presynaptic stimulation with strong postsynaptic depolarisation, generated by current injection (10 ms ramp to maximum current, 20 ms constant current, 30 ms ramp to zero current), 60 times at 5 Hz. The maximum current (2-3 nA) for postsynaptic depolarisation was set to elicit complex spiking, defined as at least 3 APs and the widening of AP waveforms due to the recruitment of Ca^{2+}-spikes. This ensured the activation of L-VGCCs (Padamsey et al., 2017a). Experiments with < 180 AP during LTP induction were discarded. Extracellular stimulation strength was transiently elevated (~ 10 %) during the induction of LTP to minimise potential confounds of small movements of the slice or stimulation electrode. Recordings were made for at least 30 min after the induction and data points were collected at 0.06 Hz. For the last 10 min of the recording, PPRs at 70 ms inter-pulse interval were measured at 0.02 Hz. 50-100 µM AP5 or 20 µM MK-801 were included in the aCSF to prevent the induction of postsynaptic LTP.

3.2.3. Induction of presynaptic LTD

CA1 pyramidal neurones were patched with standard patch-pipettes (3-6 MΩ) and recordings were performed in current clamp. A stable baseline was recorded for 5-10 min at 0.1 Hz and PPRs were measured at 0.02 Hz. Presynaptic LTD was induced by repeated stimulation of short bursts of two pulses at 200 Hz, 60 times at 5 Hz. Single stimulation pulses were used in control experiments. The neurone was hyperpolarised to -90 mV during the induction in order to prevent the generation of somatic or dendritic spikes. In order to block NMDARs, slices were pre-incubated with 100 µM MK-801 (Abcam) for at least 1 h. 20 µM MK-801 was maintained in the aCSF during the experiment. For the inhibition of postsynaptic NMDARs, cells were bolus-loaded with 5 mM MK-801 for 1 min and experiments were commenced after 20 min to ensure proper diffusion (these experiments were kindly provided by Zahid Padamsey). This method blocked postsynaptic NMDARs without affecting L-VGCC function (Padamsey et al., 2017a).

3.2.4. Stimulation of action potential bursts

CA1 pyramidal neurones were patched with standard patch-pipettes (3-6 MΩ) and

recordings were performed in voltage clamp. 1 mM MK-801 was included in the internal solution to block postsynaptic NMDARs. Neurones were stimulated at low frequency (0.06 Hz) for 8-10 min before commencing the experiment to ensure full blockade. Extracellular stimulation consisted of 10 APs at 200 Hz, which elicited strong short-term facilitation. Stimulation was repeated 5-10 times at 0.06 Hz. In order to block presynaptic NMDARs, 50 µM AP5 was either washed in or included in the aCSF from the start and washed out for 10 min to ensure complete exchange of the aCSF.

3.2.5. Analysis of the EPSP slope

Electrophysiological traces were analysed in Clampfit (Version 10.6.2.2, Molecular Devices). The initial slope of the EPSP was used as a readout of synaptic strength, due to the abundance of polysynaptic connections in these slices. The onset of the EPSP was clearly distinguishable from the stimulation artefact as an inflection in the voltage trace ~ 2 ms following stimulation. The slope was calculated for a time window of 2-3 ms. Experiments in which the stimulation artefact overlapped with the onset of the EPSP were discarded. The fractional change in EPSP slope with respect to the baseline was calculated for the last 5 min of the recording. There were no qualitative differences when the EPSP amplitude was used instead.

3.2.6. Analysis of the PPR

The PPR was calculated as

$$PPR = \frac{EPSP_2}{EPSP_1}$$

where $EPSP_1$ and $EPSP_2$ denote the response to the first and second pulse, respectively. The EPSP slope of each pulse was first averaged across trials before the ratio was taken. The mean of ratios is more robust against random fluctuations in the measurements, which have been shown to severely bias PPR calculations towards large values (Kim & Alger, 2001). Changes in PPR were calculated as absolute differences.

3.2.7. Analysis of short-term plasticity

The peak amplitude of the EPSC to each stimulation pulse was used to analyse the short-term plasticity behaviour during 200 Hz burst stimulation. Since consecutive EPSCs overlapped substantially, which masked the peak of the EPSC, maximum amplitude relative to baseline was determined in a time window 2-3 ms preceding the next stimulation artefact. 200 Hz burst stimulation caused strong after-hyperpolarisation. The baseline was therefore manually adjusted by linear interpolation. Peak amplitude was normalised to the first pulse within each experiment. Since experimental conditions were paired, the difference in the short-term facilitation, calculated as fractional change with respect to the first pulse, were determined within experiments before averaging. Similarly, early and late phase behaviour, corresponding to short-term facilitation and depression, respectively, was determined by the slope of the linear regression of pulses 1-4 and 5-10. Goodness of fit was determined by the coefficient of determination and was significant.

3.2.8. Analysis of spike timing-dependent presynaptic LTP

Spike timing was calculated as the time interval between extracellular stimulation and the average onset of the first AP in the complex spike. In order to characterise the relation between spike timing and LTP outcome, a Ricker wavelet was fitted defined as

$$\psi(t) = A(1 - \frac{(t-\mu)^2}{\sigma^2})e^{-\frac{(t-\mu)^2}{2\sigma^2}}$$

where A, μ, and σ were optimised using non-linear least squares methods (SciPy). μ and σ of the fit between spike timing and EPSP change were used to describe PPR changes, and A was adjusted appropriately.

3.2.9. Electrophysiological recordings in acute slices

CA1 pyramidal cells located 50-100 μm below the slice surface were targeted for patch-clamp recordings. For visualisation purposes, 200 μM AlexaFluor 488 (AF488) was

included in the internal solution and cells were bolus-loaded for 5 min. The fluorescence signal was captured on a Leica DMLFSA confocal microscope with a 63x water-immersion objective (NA = 0.9, HCX APO L 63x/0.9 W U-V-I, Leica) using the Leica Confocal Software (Version 2.61). Neurones were stimulated using two monopolar tungsten electrodes placed directly into the tissue. In order to stimulate sets of synapses in close spatial proximity along individual segments of dendrite, stimulation electrodes were positioned within 10-20 µm of a visually-identified segment of dendrite,10-40 µm apart from each other. The position of the stimulation electrode could either be visualised via autofluorescence or as shadows in cases where tissue autofluorescence was strong. After positioning, stimulation electrodes were given 10 min to reach thermal equilibrium in order to minimise spatial drift. Cells were subsequently re-patched with internal solution containing 200 µM AF488. The probability of successful re-patch was > 90 %. Re-patch of the correct cell was confirmed by fluorescence imaging.

3.2.10. Induction of homo- and heterosynaptic plasticity

EPSPs were evoked at 0.06 Hz by 100 µs current pulses (20-80 µA), alternated between the stimulation electrodes. PPR was measured at 0.02 Hz. A stable baseline was recorded for a maximum of 8 min in order to reduce potential confounds due to dialysis. Experiments showing consistent run-up or run-down were discarded. LTP was induced in one pathway (randomly chosen) by pairing stimulation with strong postsynaptic depolarisation via current injection (see "Induction of spike timing-dependent presynaptic LTP"). The unstimulated pathway was kept silent during the induction. EPSPs were recorded for at least 30 min after the induction and PPRs were sampled throughout.

3.2.11. Cross-facilitation test

A cross-facilitation test was used to ensure stimulation of independent pathways (Fig. 3.1). Both stimulation pathways were stimulated sequentially with 70 ms inter-pulse interval followed by stimulation in the reverse order, repeated 10 times. For completely independent pathways, no short-term facilitation of the second pulse should be

detectable. The magnitude of overlap was estimated by comparing the fractional difference in EPSP slope of a given pathway when stimulated as first or second pulse. Significant overlap was rarely observed, which is also evident from the opposing long-term plasticity outcomes and lack of post-tetanic potentiation in the unstimulated pathway.

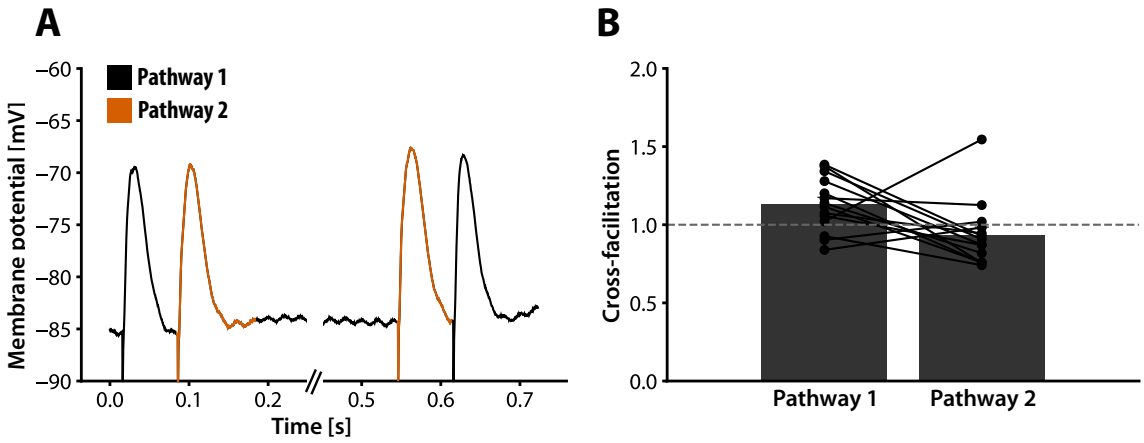

Fig. 3.1: Cross-facilitation test for independent pathways. For acute slice experiments in Chapter 5 (Fig. 5.6), a cross-facilitation test was used to ensure the stimulation of independent pathways. (A) Pathways were stimulated in sequence at inter-pulse interval of 70 ms. An overlap of pathways would lead to significant paired-pulse facilitation. (B) Cross-facilitation of pathways 1 and 2. Independent pathways were assumed when both pathways exhibited a similar degree of cross-facilitation. A slight bias of facilitation and depression of pathway 1 and 2, respectively, was observed, which might be caused by hyperpolarisation following the first pair of pulses, seen in some experiment, which overlapped with the second pulse.

3.3. Fluorescence microscopy

3.3.1. 2-photon imaging of pre- and postsynaptic strengths during clustered structural plasticity

CA1 pyramidal cells were bolus-loaded with 0.5 mM AF594 and 1 mM Oregon Green BAPTA-1 (OGB-1) for 45-60s. OGB-1 was included for optical quantal analysis (see next section). The dyes were given at least 10 min to reach diffusional equilibrium in proximal dendrites and no obvious change in mean fluorescence intensity over time was observed. After identifying a suitable segment of dendrite with linear geometry, which

was largely contained within a single optical plain, presynaptic strength was measured via optical quantal analysis. Afterwards, z-stacks (0.5 µm steps) of the dendrite spanning ~ 35 µm centred on the previously measured spine were taken every 5 min. Images were acquired on a Axio Examiner Z1 (Zeiss) with a 63x 1.0 NA objective (Plan-APOCHROMAT, Zeiss) using commercial software provided by Zeiss (Zen 2009, Version 6.0.0.303). Images were taken at 4x zoom, which leads to a lateral pixel size of 65.9 nm. Both fluorescent dyes were simultaneously excited using a 800 nm 2-photon laser source (Coherent) and emission was separated using bandpass emission filters. At least three baseline images were taken before clustered structural LTP was induced (see below). Structural images were then taken at 1, 5, 10, 20, 30, and 45 min after the induction. Experiments showing elevated Ca^{2+}-levels or outgrowth of filopodia were discarded as these would often proceed to show signs of cell death, such as fragmentation of the dendrite. At the end of the experiment, a z-stack was taken (2 µm steps, 1x zoom), which included the dendrite of interest, the cell body, and the position of the stimulation and puffing electrode.

3.3.2. Optical quantal analysis

For optical quantal analysis, a stimulation electrode (tungsten in glass pipette) was positioned within 5-10 µm of the dendrite of interested (Fig. 3.2A,B). In order to prevent excessive spatial drift, I waited 10 min for the electrode to reach thermal equilibrium and for the surrounding tissue to relax. xt-scans (line scans) covering large fractions of spines were taken at 500 Hz while synapses were stimulated with a paired pulse given at 70 ms inter-pulse interval. The imaging software was synchronised with Clampex software via transistor-transistor logic (TTL) pulses. Stimulation and the initiation of image acquisition were controlled by Clampex, however, due to a random internal lag of the imaging software, the actual timing was extracted *post hoc* from the metadata. Responsive spines were detected as time-locked OGB-1 Ca^{2+}-responses (Fig. 3.2D). Paired pulse stimulation was used to facilitate the detection of low Pr synapses. Three pulses at 70 ms inter-pulse interval were sometimes given to detect very low Pr ($Pr < 0.2$) synapses. In order to prevent potential confounds of AP failures, which will inflate the estimate of release

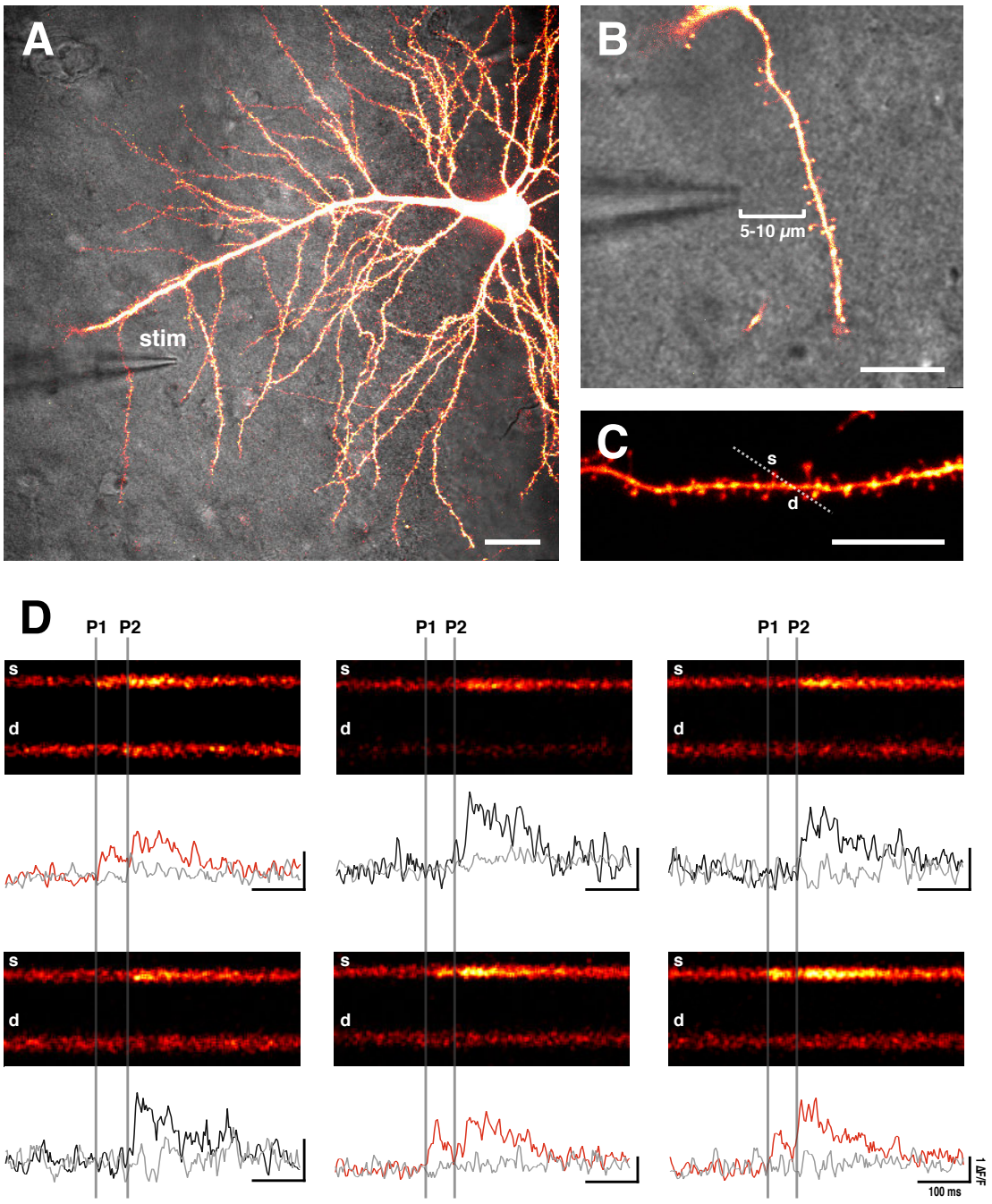

Fig. 3.2: Using optical quantal analysis to measure Pr. (A,B) Example neurone loaded with 1 mM OGB-1 and 0.5 mM AF594. A stimulation electrode (stim) was placed within 5-10 µm of the dendrite of interest. (C) Line scans were taken through the spine (s) and the dendritic branch (d) at 500 Hz. (D) Synapses were stimulated with a paired pulse with 70 ms inter-pulse interval (P1 & P2). Release of glutamate was detected as all-or-none Ca^{2+}-transients following the stimulation. The number of successful release after the first AP was used to calculate Pr (traces shown in red). The nearby dendritic branch showed little to no response (grey traces). Scale bar: 20 µm (A), 10 µm (B,C). Figure adapted from Padamsey et al., 2019.

failures, the stimulation strength was increased until the observed Pr stabilised. For data acquisition, line scans were oriented to capture both, the spine of interest and the dendrite, which allows the detection of local dendritic spikes or back-propagating APs. Before the induction of clustered LTP, optical quantal analysis was limited to 20-25 trials to prevent photodynamic damage. Optical quantal analysis was repeated 30 min after the induction of LTP and 20-30 trials were taken. The stimulation strength was further increased at the end of the experiment and a paired pulse at 5 ms inter-pulse interval was given to ensure that release events could still be detected.

EPSCaTs were analysed in ImageJ (Schindelin et al., 2012; Schneider et al., 2012) and a custom written Python script. Fluorescence signals were background-subtracted and averaged within the spatial dimension and represented as

$$\frac{\Delta F}{F} = \frac{F - F_{baseline}}{F_{baseline}}$$

where $F_{baseline}$ is the average fluorescence intensity prior to stimulation. A custom-written script in ImageJ utilising the Bioformats library (Linkert et al., 2010) was used to extract the metadata of the image file, which included the exact time points of each captured line and the time of stimulation. Synchronisation of the imaging software with Clampex led to short time lags, which caused an inhomogeneous sampling frequency, which was on average 500 Hz. All data shown in the thesis were plotted with respect to the corrected imaging time. Successful release events were manually detected and counted based on a rapid increase in Ca^{2+}-signal following stimulation. All results were cross-validated using an automated analysis script, which detected successful release as an increase in the average Ca^{2+}-signal within 6 ms after stimulation that exceeded two standard deviations above the mean of the baseline. No qualitative difference was found, however, the automated method was not robust against imaging artefacts or unstable baselines. To distinguish successful release events from dendritic or somatic spikes, the peak intensity was required to be at least 50 % larger in the spine compared to the neighbouring dendrite. Alternatively, the onset of EPSCaTs should precede dendritic/somatic spikes,

which can be used for identification. Pr was calculated as the ratio between the number of successful release events and number of trials

$$Pr = \frac{N_{success}}{N_{total}}$$

The sampling error is given by the binomial theorem

$$\sigma = \sqrt{\frac{p(1-p)}{N}}$$

where p is the release probability and N the sampling number. The maximum error occurs at p = 0.5 and N = 20: $\sigma_{max} = 0.11$.

For measuring the Pr for random trains of APs, the line scan was extended to 5 s at 400 Hz. Due to excessive imaging, photodynamic damage was observed more frequently and the number of trials was reduced to 15-20. Random AP trains were generated from a Poisson process with mean frequency of 5 Hz and spike times were sampled from an exponential distribution. The stimulation was triggered using TTL pulses generated by a Raspberry Pi. The output port of the Raspberry Pi, which generates 3.4 V steps, was connected to BNC cables via custom-made adapters to control both stimulation and the recording software. This system allowed stimulation of arbitrary AP patterns.

3.3.3. Glutamate photolysis

Caged glutamate was locally applied during photolysis through a glass pipette coupled to a picospritzer (5-10 psi, Parker Instrumentation). 10 mM MNI-glutamate (Tocris) dissolved in Tyrode's solution (in mM: 58.44 NaCl, 2.5 KCl, 20 HEPES, 30 glucose, 3 $CaCl_2$, 2 $MgCl_2$, pH-adjusted to 7.2 using 5 mM NaOH) was filtered (0.45 µm pore syringe filter, Merk Millipore) and loaded into a glass pipette (3-4 MΩ). The pipette was positioned ~ 10-20 µm from the dendrite of interest. A 2-photon laser source (720 nm) was used for focal photolysis of glutamate. Photolysis was controlled by a custom written script for the imaging software and was synchronised with the electrophysiology via Clampex. Photolysis consisted of 4 ms pulses, and the laser power was adjusted for each experiment to obtain Ca^{2+}-transients similar in size compared to EPSCaTs measured at the

Tab. 3.1: Parameters of cLTP induction and analysis.

Experimental condition	Maximum distance between stimulated spines [µm]	Deviation of the centre of mass [0-1]	Mean pairwise distance of stimulated spines [µm]	Coefficient of variation
cLTP1 (chapter 4)	9.0 ± 0.8	0.13 ± 0.02	3.6 ± 0.3	0.55
CTR no depol.	11.2 ± 1.3	0.13 ± 0.03	4.5 ± 0.5	0.52
AP5	10.5 ± 1.9	0.12 ± 0.03	4.3 ± 0.8	0.47
cLTP2 (chapter 5)	10.2 ± 0.6	0.13 ± 0.01	4.0 ± 0.3	0.51
KN62	9.7 ± 0.6	0.07 ± 0.01	3.9 ± 0.3	0.51
FK-506	8.4 ± 0.7	0.17 ± 0.02	3.2 ± 0.2	0.56
L-NAME	10.2 ± 0.8	0.09 ± 0.02	4.0 ± 0.3	0.52

same cell. An error in the photolysis script caused a spatial misalignment of the photolysis spot during the titration (the position of the uncaging spot did not correctly map from xy-mode to line-scan mode), which might have caused the use of slightly stronger laser power in experiments shown in Chapter 4. The error did not affect the positioning during the actual experiment. For the induction of clustered LTP, laser power was reduced slightly to prevent overexcitation, which would frequently cause excitotoxicity observed as sustained elevated Ca^{2+} in the dendrite. For quasi-synchronous photolysis, the inter-pulse interval was ~ 2.2 ms.

3.3.4. Induction of structural LTP

Clustered structural LTP (cLTP) was induced by quasi-synchronous glutamate photolysis at 5-7 spines paired with postsynaptic depolarisation, 30 times at 0.5 Hz. The postsynaptic neurone was re-patched with internal solution containing 100 µM OGB-1 and 50 µM AF594 to reduce the osmotic pressure of the dye. Photolysis was set up after the GΩ-seal was established and initiated within 10 s of establishing whole-cell mode in order to prevent dialysis. Cells were held at 0 mV in voltage clamp. The average access conductance was Ga = 45.86 ± 2.56 nS. Cells were immediately patched-off after the induction. The maximum distance and mean pairwise distance between stimulated spines are shown in Tab. 3.1 and did not vary across experimental conditions.

3.3.5. Analysis of spine structural changes

Spine size was analysed in ImageJ. The integrated fluorescence of a spine contained in a

rectangular regions of interest (ROI) was used as an estimate of spine size. Integrated fluorescence was measured on the focal plane that resulted in the maximal value. The background fluorescence was subtracted proportionally to the area of the ROI. The re-patch during clustered LTP induction caused a substantial global reduction in the fluorescence intensity. Fluorescence signals were therefore normalised to the mean fluorescence intensity of the underlying dendrite, which was assumed to remain structurally stable. At least three segments of dendrites were average to calculate the mean fluorescence intensity. Spine size changes were calculated as fractional changes with respect to the average size prior to cLTP induction. Spine size changes at the end of the experiment was defined as the average change observed at 30 and 45 min.

All visible spines along the dendrite of interest were analysed. Spines that were only partially visible or those located within 2 µm of the photolysis spot were excluded from the analysis. Spines that show substantial fluctuations (> 25 %) during the baseline were also excluded.

For subgroup analysis of spines, such as distance bins, spine structural changes were averaged within experiments before averaging across experiments. The standard error of the mean (SEM) was therefore calculated for experimental and technical errors rather than internal biological fluctuations. This also prevents uneven weighting of experiments due to differences in the number of analysed spines.

3.3.6. Analysis of the spatial arrangement of spines

A custom written script was used to extract the spatial arrangement of spines from fluorescence images. Structural images of the measured dendrites were first maximum projected to obtain a single reference image. The dendrite was parameterised as a sequence of vectors using the "Line ROI" tool in ImageJ. The position of spines were imported from the ROIs used for the analysis of spine structure and assumed to lie at the centre of the ROI. Spine positions were mapped to the closest point on the parameterised dendrite and the pairwise distance between spines was returned. Distances were then

scaled according to the lateral resolution of the image. Spine neck length and axial distance were omitted.

Distances in the thesis are reported as distance to the centre of mass of the stimulated group of spines. The centre of mass was calculated as the average pairwise distance between the stimulated spine located most laterally and the remaining stimulated spines and it did not deviate substantially from the centre defined by the bounding spines (deviation is measured on a linear scale where 0 defines the real centre and 1 the boundary, Tab. 3.1).

3.3.7. Estimation of initial spine size

Initial spine size was estimated from the basal distribution of fluorescence intensities, since differences in dye concentrations prevent direct comparisons across experiments. The normalised integrated fluorescence values of all spines prior to the induction of cLTP were used to estimate mean and standard deviation of an underlying normal distribution. Spine size s was then normalised as

$$s_{absolute} = \frac{s - \mu}{\sigma}$$

where μ and σ are mean and standard deviation, respectively. Validity of this method can be seen in similar coefficients of variation across experiments (Tab. 3.1), suggesting that the basal spine size distribution is constant. This normalisation also allowed the conversion of fractional spine size change into absolute units (Z-score).

3.3.8. Analysis of bi-directional postsynaptic heterosynaptic plasticity

In order to analyse the bi-directional heterosynaptic regulation of postsynaptic strengths, the distance range of maximal correlation was determined. Specifically, the Pearson correlation coefficient was calculated for spines within an increasing distance range (starting from spines located within 1 µm). The correlation coefficient steadily increased and eventually plateaued. The maximum distance range was defined as the maximum distance with a correlation coefficient within 10 % of the maximum. In order to find the

inversion point, linear regression was performed and the x-axis intercept was determined. The maximum correlation coefficient was found to be highly significant, estimated by randomisation of the data and generation of the empirical null distribution. No qualitative difference was seen when spines were grouped in fixed-sized distance bins.

3.4. Pharmacology

CaMKII was blocked by bath application of 10 µM of the non-competitive inhibitor KN62 (IC_{50} = 0.9 µM, Tocris). Due to its low solubility in water, KN62 was first dissolved in DMSO and subsequently diluted in aCSF heated to 37˚C. In some cases, precipitation was observed in which case the experiment was discarded.

Calcineurin was blocked by bath application of 2 µM FK-506 (IC_{50} = 3 nM, Tocris). Both, KN62 and FK-506 were maintained in the aCSF throughout the experiment.

NO signalling was blocked by either bath application of 100 µM L-NAME (Cayman Chemical), a NOS inhibitor, or intracellular loading of 5 mM carboxy-PTIO (cPTIO, Sigma Aldrich), a NO scavenger. L-NAME was pre-incubated for at least 1 h before the experiment to abolish tonic levels of NO. cPTIO was directly added to the internal solution and cells were bolus-loaded for 45-60 s.

NMDARs were blocked by either bath application of 50-100 µM D-AP5 (Abcam) or 20 µM MK-801 (Abcam). Since MK-801 is an open-channel blocker, slices were pre-incubated for at least 1 h with 100 µM MK-801 to ensure complete blockade of NMDARs. To selectively block pre- or postsynaptic NMDARs, 1 mM MK-801 was directly included in the internal solution and cells were bolus-loaded for 1 min (postsynaptic) or 5 min (presynaptic NMDAR). When NMDAR inhibition was combined with optical quantal analysis, 500 µM AP5 was included in the solution containing 10 mM MNI-glutamate and was locally applied. Successful blockade was verified by measuring the photolysis-evoked Ca^{2+}-transient, which showed significant reduction in peak amplitude, even though a higher

laser power was used for photolysis. The remaining Ca^{2+}-signal originates most likely from other VGCCs (Padamsey et al., 2017a).

3.5. Imaging and analysis of presynaptic action potential-evoked Ca^{2+}-transients

CA3 pyramidal neurones in organotypic hippocampal slices were bolus-loaded with 1 mM OGB-1 for 3-5 min. The dye was given 30-45 min to diffuse into the axon. The axon was structurally identified as a thin process branching off the primary dendrite in *stratum oriens*, lacking dendritic spines, and exhibiting branching at obtuse angles, which is typical for these axons (McGuinness et al., 2010). Presynaptic terminals were found as clear varicosities along the axon, ~ 50-100 µm away from the soma. In order to evoke APs, the neurone was re-patched with internal solution containing 100 µM OGB-1 and 5 ms current steps were used to elicit single APs. The magnitude of the current step was adjusted accordingly. Glutamate was photolytically released at or adjacent to the presynaptic terminal. The strength of the photolysis laser was titrated at the start of the experiment at nearby spines to elicit EPSCaTs of 0.5-1 ΔF/F. Glutamate photolysis was timed to occur 1-5 ms following the AP. 10-15 line scans through the presynaptic terminal were taken for each condition. Experiments showing obvious photodynamic damage, such as swelling or an increase in basal Ca^{2+}-signal, were discarded. 1 µM NBQX was included in the aCSF to prevent the activation of postsynaptic terminals.

For analysis, Ca^{2+}-transients were normalised to the baseline and average across trials. The peak amplitude was then determined by taking the maximum in a 20 ms time window following the onset of the AP.

3.6. Statistics

Non-parametric tests were used for all statistical comparisons if not indicated otherwise. Mann-Whitney U test was used for comparisons of independent means; Wilcoxon signed-rank test was used for dependent means. For multiple comparisons, Kruskal-Wallis H test

was used followed by *post hoc* Dunn's test for pairwise comparisons. Linear correlation was evaluated using the Pearson correlation coefficient if not indicated otherwise. In some cases, the statistical result was further confirmed using bootstrapping. An empirical distribution of the measurement was generated by randomly resampling the data 10000 times and empirical confidence intervals were determined (for alpha = 0.05, the 2.5- and 97.5-percentiles were used). The alternative hypothesis was rejected when it was excluded by the confidence intervals.

All calculations were made using the Numpy and Scipy libraries in Python. For *post hoc* Dunn's test, the scikit-posthocs toolkit was used. Significance is denoted as follows: *$p < 0.05$, **$p < 0.01$. In all tests, alpha = 0.05.

4. Heterosynaptic coordination of pre- and postsynaptic strength along local dendritic segments

4.1. Introduction

Synaptic plasticity is often studied in terms of the concerted activity of pre- and postsynaptic terminals. Synaptic strength therefore depends on the firing correlation between neurones. Synapses must often cooperate, since individual synaptic events are generally not sufficient to reach the firing threshold. This suggests that necessary information for the modification of synaptic strengths is contained in the spatiotemporal pattern of activity impinging onto the postsynaptic neurone and therefore suggests the interaction across synaptic inputs. The scale of interaction depends on the mechanisms of synaptic integration. Evidence of dendritic non-linearities suggest that dendritic branches can form compartmentalised units and locally integrate synaptic inputs (Branco & Häusser, 2010). In particular, electrical signals attenuate when travelling along the dendrite due to a loss of current through the surrounding plasma membrane (Rall, 1959; Spruston, 2008); the strong impedance mismatch at dendritic branch points leads to asymmetric signal propagation, hindering feedback (soma to dendrite) to a lesser extent than feed-forward signalling (dendrite to soma; Ferrante et al., 2013); and the ability to generate regenerative spikes (dendritic spikes) due to the expression of voltage-gated ion channels (Häusser et al., 2000; Johnston et al., 1996), has been shown to lead to non-linear summation of synaptic inputs (Losonczy & Magee, 2006). This raises the question about the minimal operating unit of synaptic plasticity. Specifically, what is the extent to which synaptic plasticity is confined to individual synapses, as originally postulated for Hebbian plasticity? If neighbouring synapses influence synaptic plasticity, how so?

With the advance in optical techniques to interrogate synaptic function, multiple studies have shown that synaptic plasticity is not confined to the stimulated synapse but instead extends spatially to neighbouring synapses independent of activity (Oh et al., 2015; Hayama et al., 2013; Harvey & Svoboda, 2008; Wiegert & Oertner, 2013; Govindarajan et

al., 2011; Hedrick et al., 2016). These observations were based on spine structural changes, a purely postsynaptic readout of synaptic strength. As laid out in the introduction, pre- and postsynaptic plasticity are unlikely to operate through similar mechanisms and rules, due to their distinct functional consequences. I therefore hypothesised that, if heterosynaptic changes occurred at the presynaptic locus, these changes should be distinguishable from their postsynaptic counterpart with respect to spatiotemporal dynamics and underlying biochemical computations. I therefore devised an experimental setup that allowed me to monitor both pre- and postsynaptic strengths of spatially identified synapses following the induction of synaptic plasticity. Using optical readouts of both pre- and postsynaptic strengths, I show that locally coordinated activity leads to heterosynaptic plasticity at both pre- and postsynaptic loci, which depended on spatial proximity to the stimulation site. Pre- and postsynaptic changes did not correlate and followed distinct spatiotemporal dynamics. In particular, postsynaptic heterosynaptic plasticity was bi-directional, exhibiting a Ricker wavelet (or Mexican hat)-shaped profile and was likely mediated by two distinct signalling pathways. Presynaptic heterosynaptic plasticity strongly depended on the initial strength of the synapse and was restricted to weakening only. My findings suggest that pre- and postsynaptic heterosynaptic plasticity are differentially implemented and therefore require parallel signalling pathways.

4.2. Experimental setup

The goal of the following series of experiments was to identify and characterise the expression locus of heterosynaptic plasticity. This required establishing an appropriate experimental paradigm. As laid out in the introduction, strong evidence indicate local spatial organisation of synaptic inputs, especially prominent along individual dendritic segments. The local spatial organisation might be explained by ongoing coordination and communication between synapses, instantiated by synaptic plasticity. Here, I have assumed that local synaptic plasticity is implemented as a tight balance between coordination and competition between synapses. As such, I have experimentally

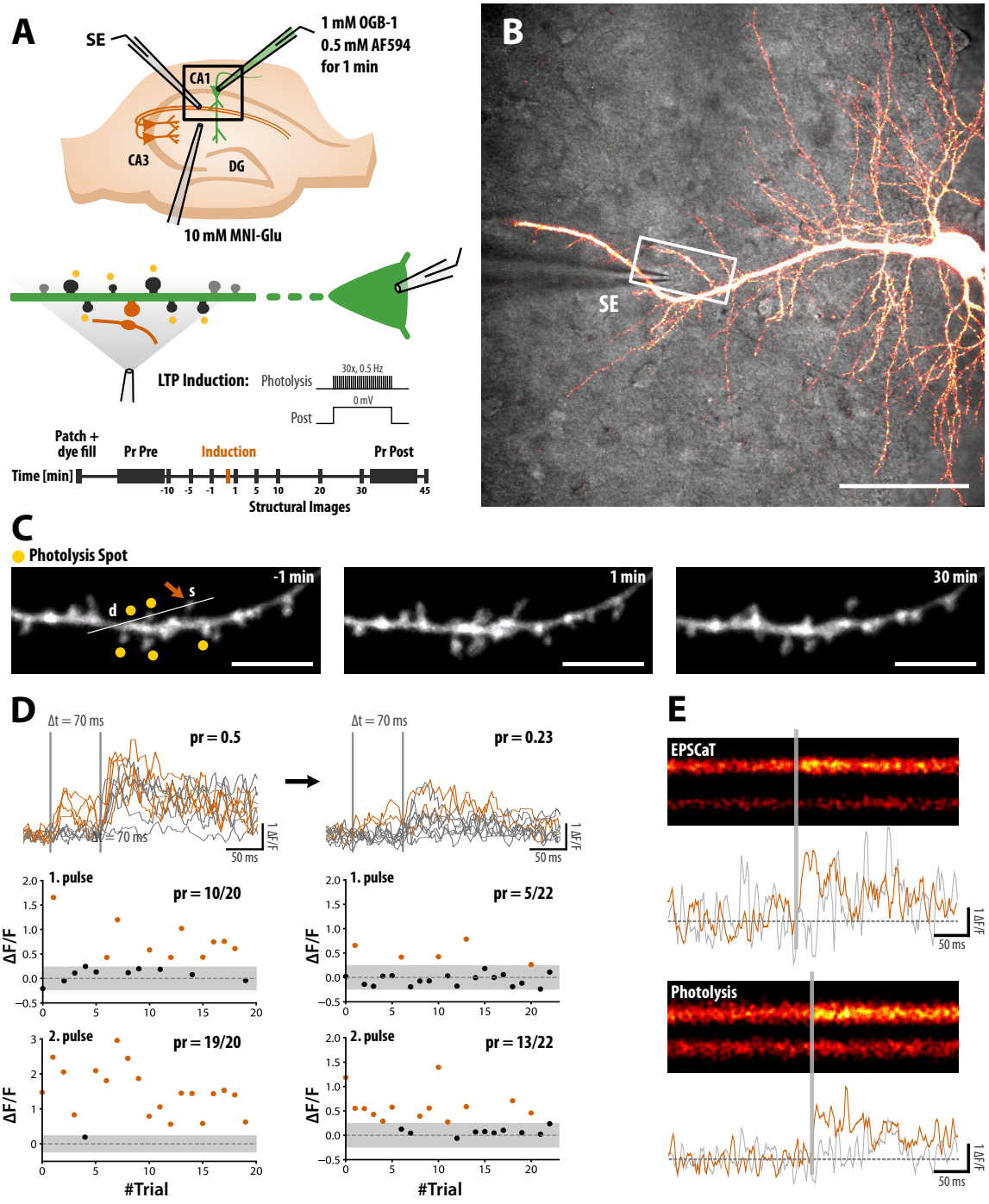

Fig. 4.1: Experimental setup to study pre- and postsynaptic heterosynaptic plasticity. (A) Schematic of the experimental setup (top), cLTP induction protocol (middle), and timeline (bottom). (B) Example neurone filled with 1 mM OGB-1 and 0.5 mM AF594 for 1 min. The white box illustrates the region shown in (C). SE: Stimulation electrode. Scale bar: 20 µm. (C) cLTP was induced via quasi-synchronous photolysis of glutamate at 5-7 spines paired with postsynaptic depolarisation, 30x at 0.5 Hz. An increase in spine size is evident immediately after photolysis. For optical quantal analysis, line scans were taken through the spine of interest (s) and the dendritic branch (d). Scale bar: 10 µm. *Cont'd on next page.*

imposed one of the extremes, strong coordination, with the intent of revealing underlying competitive processes. Utilising the excellent spatiotemporal resolution of 2-photon glutamate photolysis, I emulated the (quasi-)synchronous activation of groups of synapses along a local segment of dendrite. In order to facilitate the expression of plasticity processes, stimulation was paired with strong, cell-wide depolarisation, similar to that observed during CA1 place cell formation *in vivo* (Bittner et al., 2017). Next, means of monitoring pre- and postsynaptic strengths were needed. Because spatial information was of importance, postsynaptic strength was inferred from estimates of spine volume (integrated fluorescence of spines in a single plane, see Methods for details), and presynaptic strength was measured using optical quantal analysis. Figure 4.1 summarises the experimental procedure. I first bolus-loaded a CA1 pyramidal neurone with the Ca^{2+}-indicator OGB-1 (1 mM) and a fluorescent dye (0.5 mM AF594) to visualise fine sub-cellular structures (Fig. 4.1A,B). Next, I placed an extracellular stimulation electrode (tungsten electrode encased in a glass pipette) close to a secondary or tertiary dendrite containing large numbers of spines and measured Pr using optical quantal analysis (Fig. 4.1D). In order to prevent photodynamic damage and photobleaching caused by excessive excitation of the fluorophores, I have limited optical quantal analysis to 20-25 trials. An estimation of the uncertainty in the measured Pr is given by $\sqrt{(p(1-p)/N)}$, where p is the release probability and N the number of trials. The maximum resulting uncertainty is therefore around 0.1 (for $p = 0.5$). Next, I monitored basal spine structure by taking z-stacks at 0.5 µm steps of a ~15 µm long segment of dendrite, centred around the measured synapse, every 5 min until spines appeared structurally stable. The neurone was then re-patched and five to seven dendritic spines adjacent to the measured synapse

Fig. 4.1 cont'd (D) Example of Pr measurements via optical quantal analysis before and after cLTP induction. Top row shows the raw fluorescence traces. Red traces denote successful release to the first AP. Bottom rows show the peak intensity of the response to the first and second pulse. The grey area around 0 ΔF/F corresponds to two standard deviations of the baseline, which was used as detection criteria for automatic analysis. Facilitation of the second pulse was clearly evident as an increase in Pr. (E) Glutamate photolysis was titrated to elicit Ca^{2+}-transients similar in strength compared to EPSCaTs.

were targeted for quasi-synchronous 2-photon glutamate photolysis (30 times at 0.5 Hz) while the cell was clamped to 0 mV via a patch pipette (Fig. 4.1C, E). In order to prevent dialysis of intracellular molecules, which has been shown to be detrimental to structural plasticity (Matsuzaki et al., 2004), stimulation was initiated within 10-20 s after formation of whole-cell patch clamp. In addition, in order to reduce a decrease in dye concentration upon re-patch, small amounts (~ 10 %) of OGB-1 and AF594 were included in the internal solution to minimise the osmotic pressure. I will refer to this process as clustered LTP (cLTP) from hereon. Depolarisation via current injection was found to be more potent in eliciting plasticity events when multiple synapses were stimulated synchronously compared to a reduction in extracellular Mg^{2+}-concentration, which is more commonly used in the context of structural plasticity, which has also been observed in other laboratories (personal correspondence with Karen Zito). The neurone was patched-off immediately after cLTP induction. Presynaptic strength was examined after 30 min by repeating optical quantal analysis (20-30 trials), whereas spine structure was monitored for up to 45 min post-induction.

4.3. Results

4.3.1. Local structural potentiation of groups of spines induces bi-directional postsynaptic heterosynaptic plasticity

Clustered stimulation of spines led to robust structural changes (Fig. 4.2B). As expected, stimulated spines increased rapidly in size (structural LTP) after cLTP induction and remained stable for at least 45 min ($\Delta V_{30\text{-}45min}$ = 38.7 ± 4.5 % of baseline, N = 17). Neighbouring unstimulated spines also transiently increased in size shortly after cLTP induction (ΔV_{10min} = 10.8 ± 4.0 %) before slowly decaying back to baseline by 45 min ($\Delta V_{30\text{-}45min}$ = -1.1 ± 2.2 %, Fig. 4.2B). When postsynaptic depolarisation was prevented by clamping the cell at -70 mV during clustered stimulation, stimulated spines did not increase in size, neither transiently nor in the long-term ($\Delta V_{30\text{-}45min}$ = -4.9 ± 5.9 %, N = 9, Fig. 4.2C, "No depolarisation"). With the lack of depolarisation, neighbouring spines also

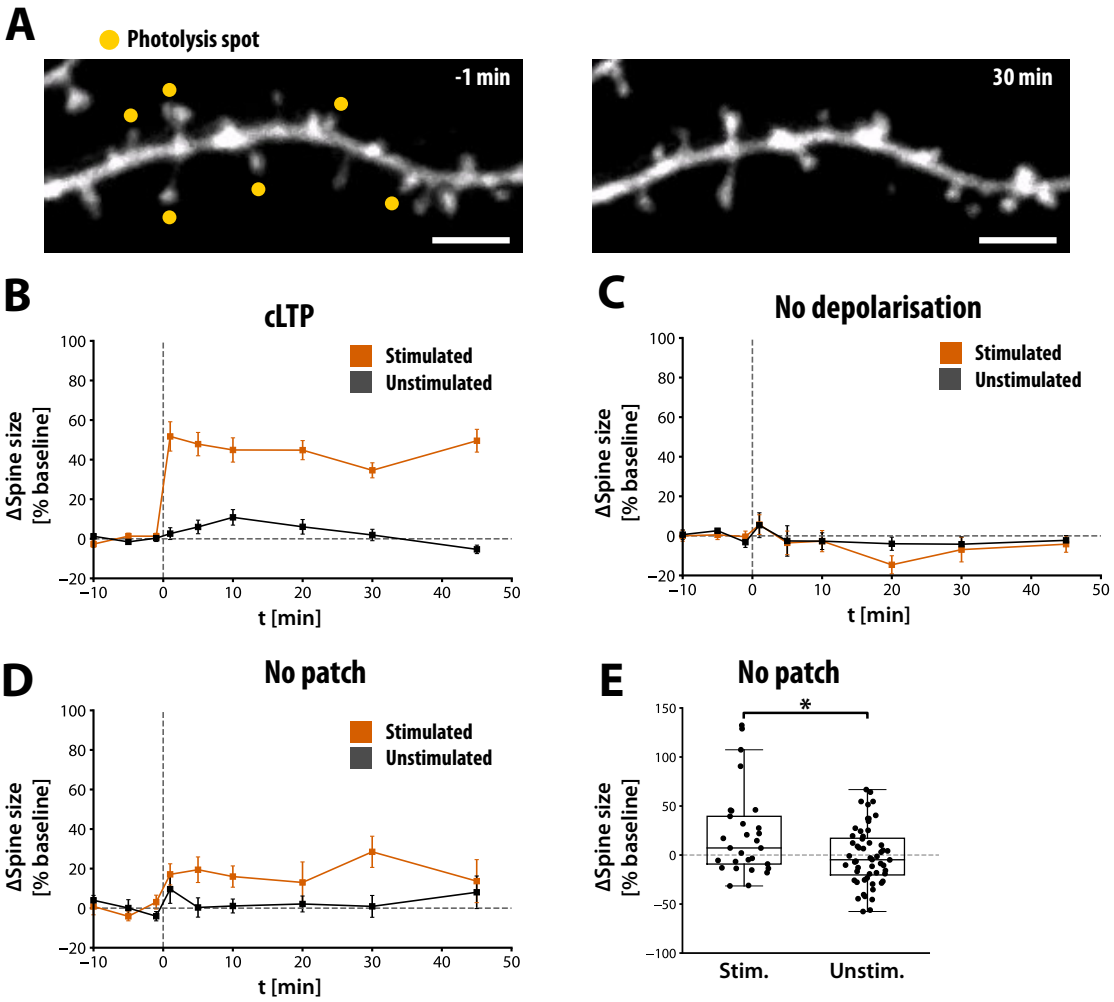

Fig. 4.2: Quasi-synchronous stimulation of clusters of spines leads to robust spine structural LTP. (A) Example of cLTP induction. Structural LTP was induced at six spines via photolysis of glutamate. Long-term structural changes were assessed after 30-45 min. Scale bar: 5 µm. (B) Spine size changes of stimulated and unstimulated spines. cLTP was induced at t = 0 min. Stimulated spines show robust structural LTP ($\Delta V_{30\text{-}45min}$ = 38.7 ± 4.5 %, N = 17), whereas unstimulated spines enlarged transiently (ΔV_{10min} = 10.8 ± 4.0 %, $\Delta V_{30\text{-}45min}$ = -1.1 ± 2.2 %). (C) Postsynaptic depolarisation was prevented by holding the neurone at -70 mV during cLTP induction. Neither stimulated nor unstimulated spines showed substantial structural changes. (D) cLTP was induced without direct depolarisation of the postsynaptic membrane potential (neurones were not re-patched). Stimulated spines showed reduced structural spine LTP (N = 4). (E) Comparison of stimulated and unstimulated spine size change of experiments in (D). The structural increase in spine size of stimulated spine was significant ($p < 0.05$, Mann-Whitney U test). Data points are shown as mean ± SEM.

remained unchanged (ΔV_{10min} = -2.8 ± 4.2 %; $\Delta V_{30\text{-}45min}$ = -3.1 ± 2.9 %). When I omitted any exogenous manipulation of the membrane potential, I could still observe the expression of structural LTP at stimulated spines, however, at lower success rate (Fig. 4.2D,E) suggesting that clustered stimulation was sometimes sufficient on its own to reach significant depolarisation locally. cLTP therefore requires strong depolarisation to trigger events leading to plasticity. A more thorough analysis revealed that only a fraction of stimulated spines in each experiment expressed stable structural LTP (Average fraction of stimulated spines with $\Delta V_{30\text{-}45min}$ > 20 % = 59.5 ± 4.1 %, N = 17). The fraction of potentiated

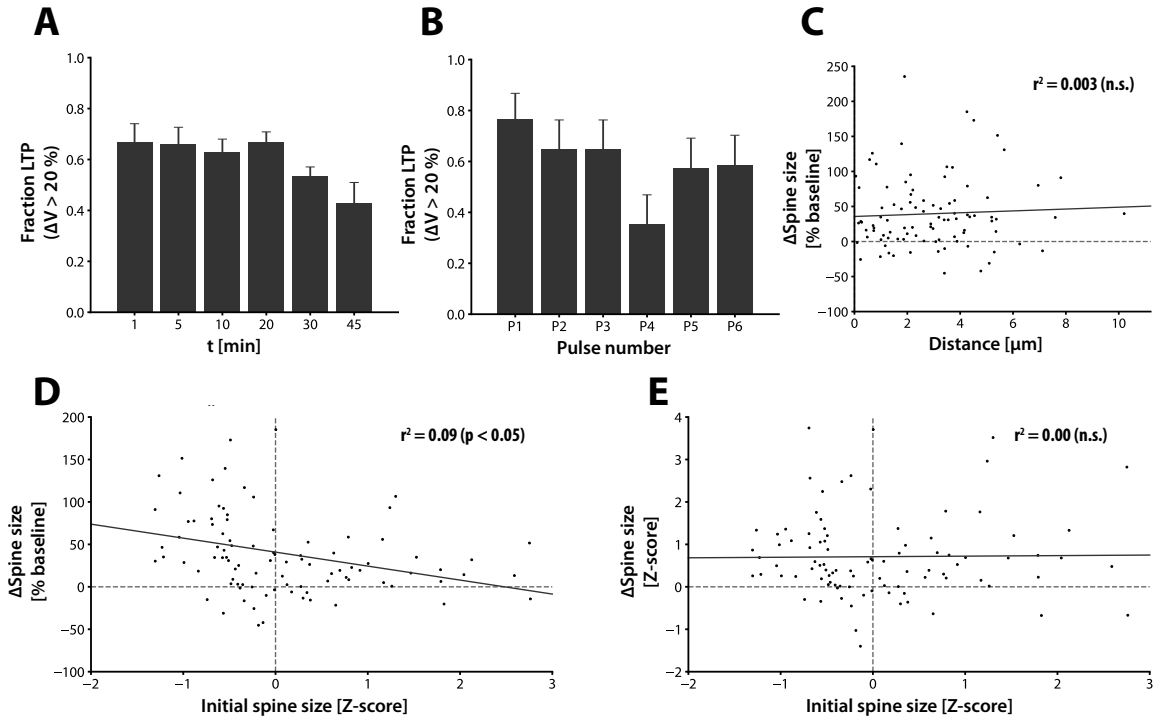

Fig. 4.3: Further analysis of spine structural change of stimulated spines. (A) Fraction of stimulated spines showing > 20 % increase in spine size for different time points after cLTP induction. A decrease can be see for 30-45 min. (B) Fraction of stimulated spines showing > 20 % increase in spine size as a function of photolysis pulse number. The inter-pulse interval was 2.2 ms. A slight decrease can be seen for pulse 4, which was not significant. Data points are shown as mean ± standard deviation given by the binomial distribution. (C) Spine size change in relation to distance. Distance did not affect the magnitude of structural LTP (Pearson r = 0.052, n.s., N = 94 spines). (D) Fractional spine size change in relation to initial spine size. A significant negative correlation was observed (Pearson r = -0.307, $p < 0.01$). (E) Absolute spine size change in relation to initial spine size. Absolute changes were independent of initial spine size (Pearson r = 0.01, n.s.).

spines (ΔV > 20 %) remained constant throughout the first 20 min of the experiment, and decreased afterwards, suggesting failure of LTP maintenance rather than induction as a potential explanation (Fig. 4.3A). It also suggests that LTP is biphasic, with short- and long-term components. Next, stimulation of spines occurred quasi-synchronously, with a delay of 2.2 ms in between, which might render LTP induction sensitive to timing. Accordingly, I found that the fourth pulse was consistently less successful in inducing stable LTP (35.3 ± 11.6 %, Fig. 4.3B), although not reaching statistical significance. LTP was, however, not affected by the spatial arrangement of the spines as measured by their distance to the centre of the stimulated cluster (Pearson r = 0.052, n.s., N = 94, Fig. 4.3C). Lastly, I examined if the initial spine size affects the degree of structural potentiation. Due to methodological challenges, such as the normalisation of spine fluorescence intensity to the local dendritic shaft (see Methods), the absolute spine size could not be easily determined in units that are comparable across experiments. Instead, I have assumed that the relatively high number of spines analysed per experiment (20-30) is a reasonable reflection of the basal distribution of spine sizes. I have further assumed that the basal distribution can be estimated by a normal distribution and does not substantially differ between cells and slices of different age (see Discussion). This allowed me to convert spine fluorescence intensity into units of standard deviation (Z-score). The fractional change in size was significantly correlated with the initial spine size (Pearson r = -0.307, $p < 0.01$, Fig. 4.3D). The correlation was inhomogeneous, with strong modulation for initially small spines and weak modulation for initially large spines, apparent from the "hinge" like or hyperbolic shape in Fig. 4.3D. This renders the absolute change in spine size independent of the initial spine size (Pearson r = 0.01, n.s., Fig. 4.3E).

In order to detect potential spatial modulation of heterosynaptic plasticity, I grouped neighbouring unstimulated spines based on their distance to the stimulated cluster. The general metric I have used, if not indicated otherwise, measures the distance along the dendritic branch between spine and centre of mass of the stimulated cluster. The length of the spine neck was neglected. Spines located within 2 µm of a photolysis spot were

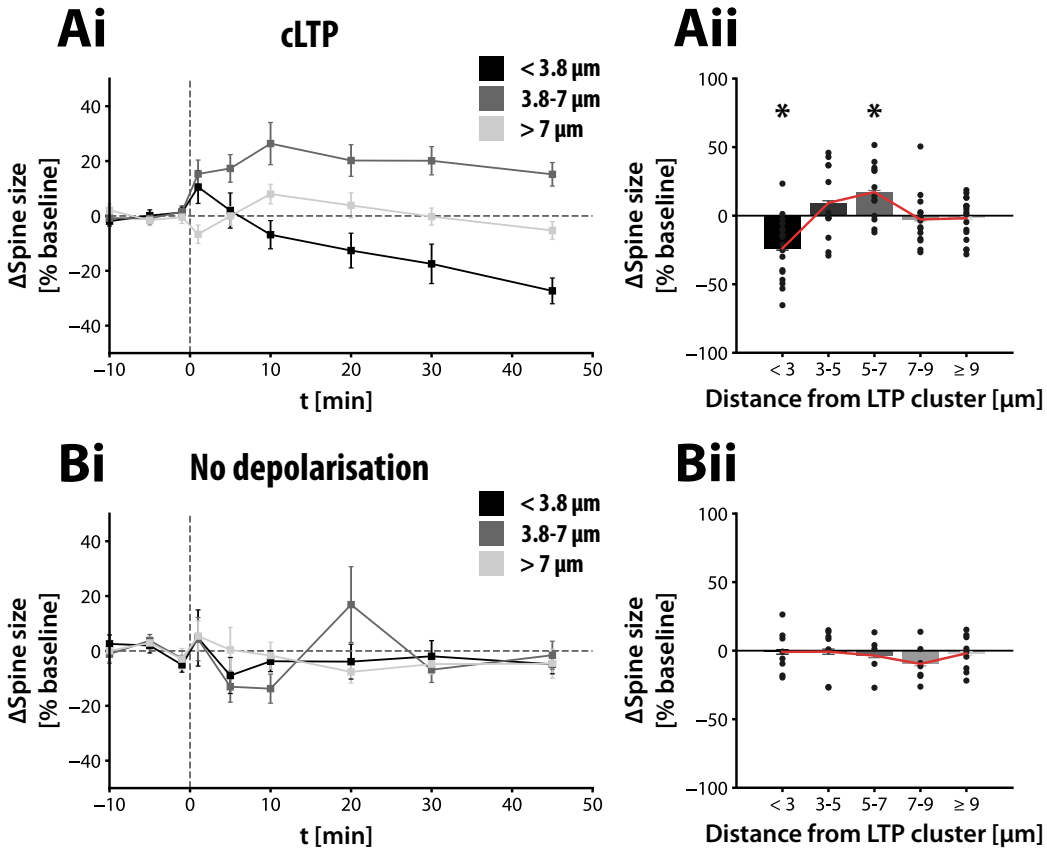

Fig. 4.4: Induction of structural plasticity of groups of spines leads to heterosynaptic bi-directional changes in spine size. (Ai) Spine size changes of unstimulated spines, grouped by distance (< 3.8 µm: $\Delta V_{30\text{-}45min}$ = -23.0 ± 5.3 %; 3.8-7 µm: $\Delta V_{30\text{-}45min}$ = 18.1 ± 4.0 %; > 7 µm: $\Delta V_{30\text{-}45min}$ = -2.3 ± 2.9 %). Spines located close to the stimulated cluster decreased in size. More distal spines showed significant increase in size. (Aii) Persistent spine size change at 30-45 min depends on the distance to the stimulated cluster. Spines within 3 µm and 5-7 µm were significantly different from control experiments shown in (B) (Mann-Whitney U test). Red line emphasises the distance-dependency of the mean spine size change. (B) Same as C but postsynaptic depolarisation was prevented by holding the neurone at -70 mV during cLTP induction. Unstimulated spines showed no long-term changes in size. Data points are shown as mean ± SEM.

omitted from the analysis to avoid potential confounds arising from glutamate spill-over. For analysis, spines were binned according to distance and averaged within experiments to account for uneven sampling across experiments. Unstimulated spines located close to the cluster (< 3.8 µm, see below for identification of distance range) show a substantial decrease in size, which lasted for at least 45 min ($\Delta V_{30\text{-}45min}$ = -23.0 ± 5.3 %, Fig. 4.4Ai). Interestingly, these spines also exhibited the transient increase in size immediately after stimulation. Unexpectedly, spines at a distance of 3.8-7 µm exhibited weak but significant potentiation, which lasted for the duration of the experiment ($\Delta V_{30\text{-}45min}$ = 18.1 ± 4.0 %). Spines located further away only transiently increased in size, reaching a maximum at around 10 min after stimulation and decaying back to baseline by the end of the experiment ($\Delta V_{30\text{-}45min}$ = -2.3 ± 2.9 %). Fig. 4.4Aii summarises the distance-dependent bidirectional regulation of postsynaptic strength, which was absent when postsynaptic depolarisation was omitted (cLTP vs. no depolarisation: $p < 0.05$ for spines located < 3 µm and 5-7 µm, Fig. 4.4B, Mann-Whitney U test). Fig 4.5 presents the distance-size relationship for every unstimulated spine analysed. A clear positive correlation can be seen for spines located within 7 µm. In order to determine the critical distances for bi-directional regulation, I first identified the distance that results in the highest positive correlation (Pearson correlation coefficient) with respect to spine size change. A line was then fitted to find the point of x-axis interception, which was taken as the boundary between proximal and distal spines for all experiments (Fig. 4.5A, dashed red line). Following this procedure, the bi-directional regulation is apparent for spines within 7 µm (Pearson $r_{0\text{-}7µm} = 0.465$, $p < 0.01$) and the inversion point appears to be situated around 3.8 µm. Comparing the cumulative distribution of spines within 3.8 µm with spines > 7 µm away shows that the decrease in spine size manifests itself as a rightward skew of the size distribution ($p < 0.01$, Kolmogorov-Smirnov test, Fig. 4.5C). In contrast, the distribution of spines located within 3.8-7 µm shows a minor translation to the right instead ($p = 0.05$, Kolmogorov-Smirnov test, Fig. 4.5D). Lastly, heterosynaptic spine size changes are not correlated with initial spine size (Fig. 4.5E,F). However, the increase in spine size for spines located 3.8-7 µm away is mainly expressed in small spines (Fig. 4.5E). Examining the

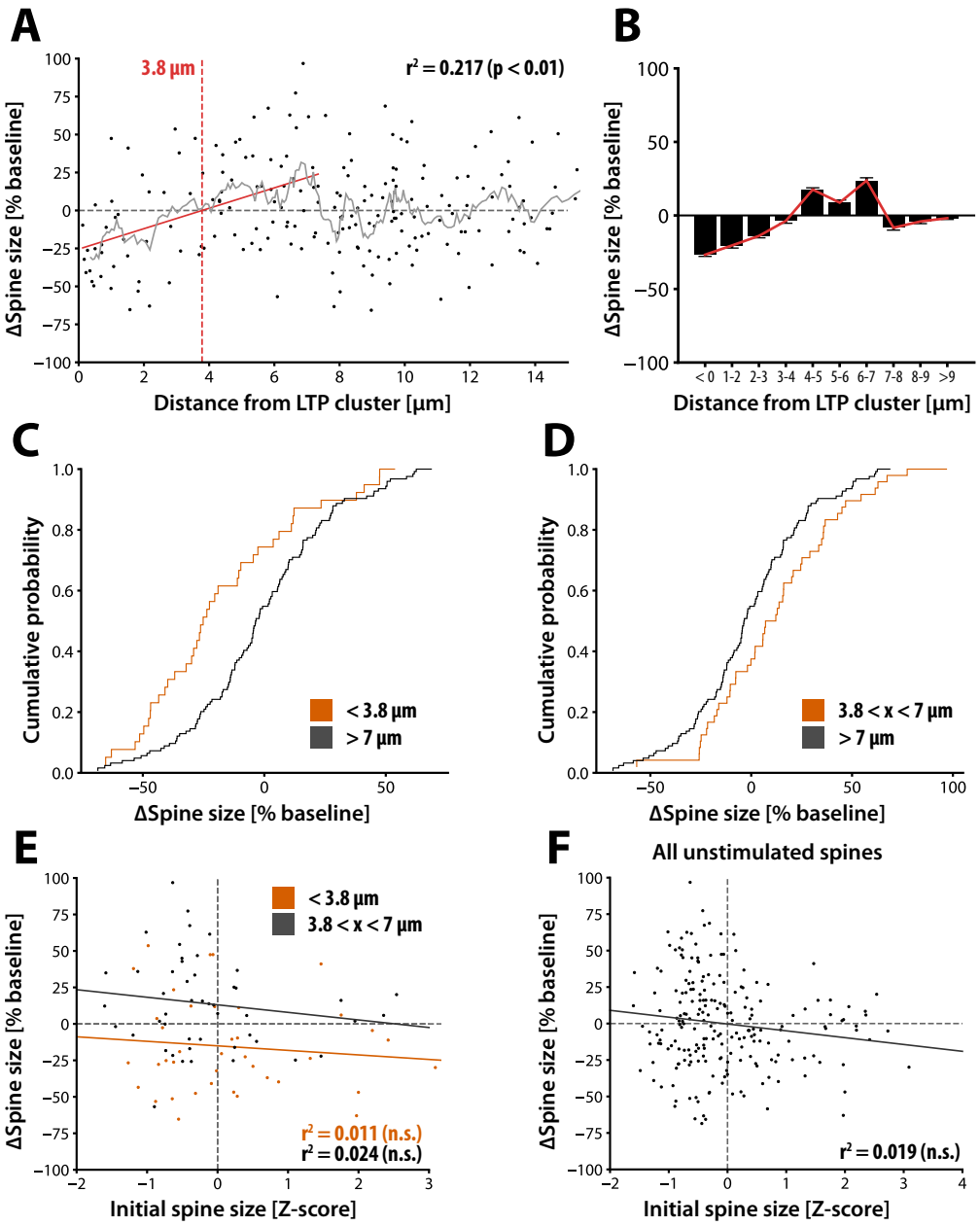

Fig. 4.5: Heterosynaptic spine size change is distance-dependent. (A) Distance and spine size change for all unstimulated spine analysed (N = 199 spines). The strongest correlation between distance and spine size change was found for spines located within 7 µm ($r = 0.465$, $p < 0.01$). The x-axis intercept was 3.8 µm and was used to group spines for further analysis. (B) Spine size changes grouped in 1 µm wide bins. Red line emphasises the mean spine size change. (C) Cumulative distribution of spine size change for proximal and distant spines. A rightward skew of proximal spines can be observed ($p < 0.01$, Kolmogorov-Smirnov test). (D) Cumulative distribution of spine size change for spines 3.8-7 µm away and distant spines. A slight rightward translation can be observed ($p = 0.05$). (E,F) Spine size change in relation to initial spine size. No significant correlation was observed (< 3.8 µm: Pearson $r = 0.105$, $N = 39$; 3.8-7 µm: $r = 0.155$, n.s., $n = 160$; all spines: $r = 0.138$).

relationship between initial and fractional change in spine size for all unstimulated spines clearly shows that small spines are more likely to undergo structural changes in either direction, whereas large spines preferentially shrink (Fig. 4.5F). Accordingly, the distribution of size changes differed significantly between small (Z-score < 0) and large (Z-score > 0) spine ($p < 0.01$, Kolmogorov-Smirnov test). Thus, strong, coordinated stimulation of a group of spines leads to robust shrinkage of spines located close to the stimulated cluster and weak structural potentiation of spines more distally.

4.3.2. Local structural potentiation of groups of spines induces presynaptic heterosynaptic weakening

Next, I have examined presynaptic changes following cLTP. Due to the comparatively low throughput of optical quantal analysis, which generally only allows Pr measurement of a single synapse per experiment, I have focused mainly on synapses located close to the stimulated cluster (synapse located within stimulated cluster in 13/17 experiments and outside in 4/17 experiments). cLTP induction was associated with a decrease in Pr in spatially proximal synapses ($\Delta Pr = -0.27 \pm 0.05$, N = 13, all spines located within 4 µm, Fig. 4.6C,E), whereas synapses located more distally did not change ($\Delta Pr = -0.02 \pm 0.06$, N = 4, all spines located > 4 µm, Fig. 4.6C,E, triangles). Postsynaptic depolarisation alone is known to influence Pr (*e.g.* Branco et al., 2008; Volgushev et al., 1997). To control for this possibility, I repeated the experiment without glutamate photolysis by either locally perfusing aCSF containing no MNI-glutamate or by omitting the photolysis pulse. Postsynaptic depolarisation alone was not sufficient to induce presynaptic weakening ($\Delta Pr = -0.01 \pm 0.03$, N = 18, $p < 0.01$, Kruskal-Wallis H-test with *post hoc* Dunn's test, Fig. 4.6D,E, "no photolysis"). On the other hand, photolysis of large amounts of glutamate might lead to local accumulation and spill-over of glutamate, which could directly activate receptors at nearby synapses. However, holding the neurone at -70 mV during cLTP induction abolished any presynaptic changes ($\Delta Pr = -0.02 \pm 0.06$, N = 11, $p < 0.01$, Kruskal-Wallis H-test with *post hoc* Dunn's test, Fig. 4.6D,E, "no depolarisation"). Thus, presynaptic hetLTD was not caused by prolonged postsynaptic depolarisation and

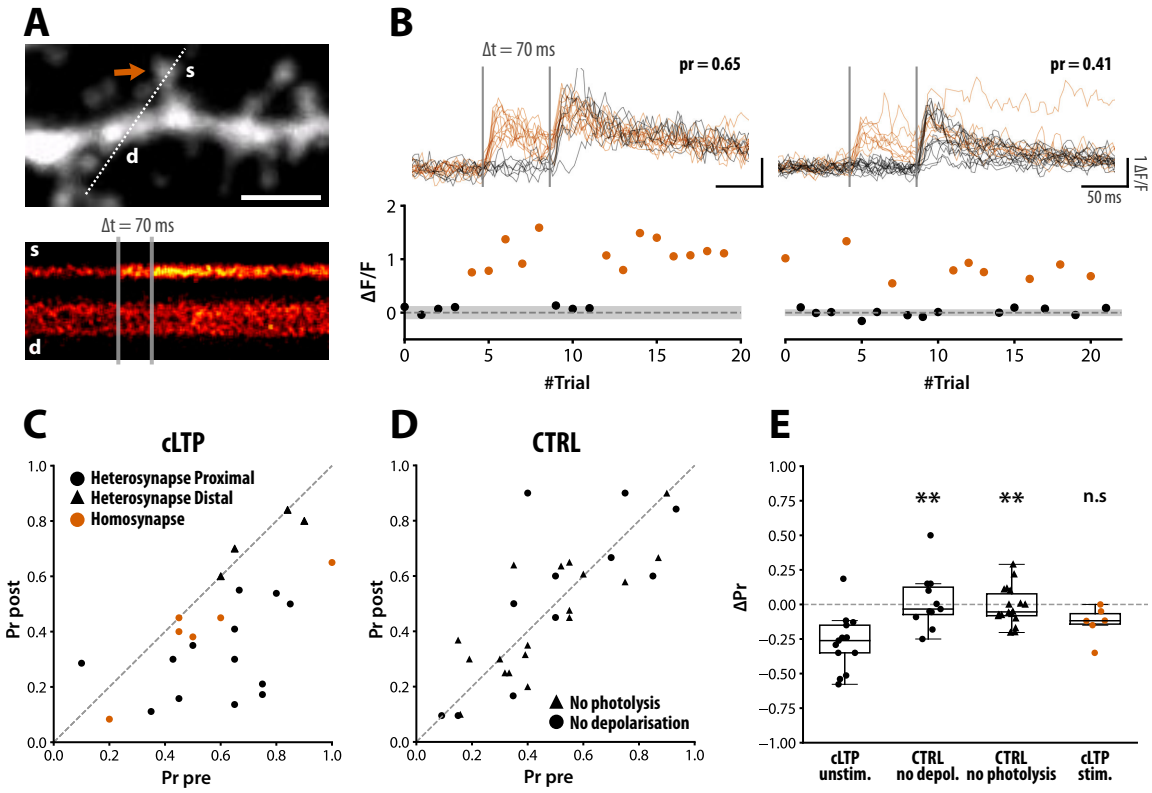

Fig. 4.6: Induction of structural plasticity of groups of spines leads to heterosynaptic presynaptic weakening. (A) Pr was measured using optical quantal analysis. Top: To capture EPSCaTs, line scans were taken through the spine of interest (red arrow, s) and the dendrite (d) while the synapse was stimulated. Bottom: Glutamate release was detected as Ca^{2+}-transients in the spine head (ESPCaTs). (B) Repeated stimulation of synapse results in all-or-none response profile. Top: Raw Ca^{2+}-transients for all trials, before and after the induction of cLTP. Bottom: Peak amplitude of the EPSCaT. The grey area represents 2 standard deviations from the baseline and was used for automated analysis. Failures were clearly distinguishable. 30 min after cLTP induction, a clear increase in release failures was evident (right panel). (C) Summary of Pr changes. Pr before cLTP induction is plotted against Pr 30 min after induction. Pr decreased for synapses located close to the stimulated cluster (< 4 µm, "Heterosynapse Proximal", black spheres) but not in distal synapses (> 4 µm, "Heterosynapse Distal", triangles). Stimulated synapses showed a small decrease in Pr ("Homosynapse", red spheres). (D) No Pr change was observe when omitting glutamate photolysis ("No photolysis", triangles) or postsynaptic depolarisation ("No depolarisation", spheres). (E) Summary of Pr changes (cLTP unstim: ΔPr = -0.27 ± 0.05, N = 13; CTRL no depol.: ΔPr = -0.02 ± 0.06, N = 11; CTRL no photolysis: ΔPr = -0.01 ± 0.03, N = 18). Significance is shown for comparisons with Pr changes at proximal synapses after standard cLTP induction ("cLTP unstim."). Kruskal-Wallis H-test with *post hoc* Dunn's test was used to correct for multiple comparison.

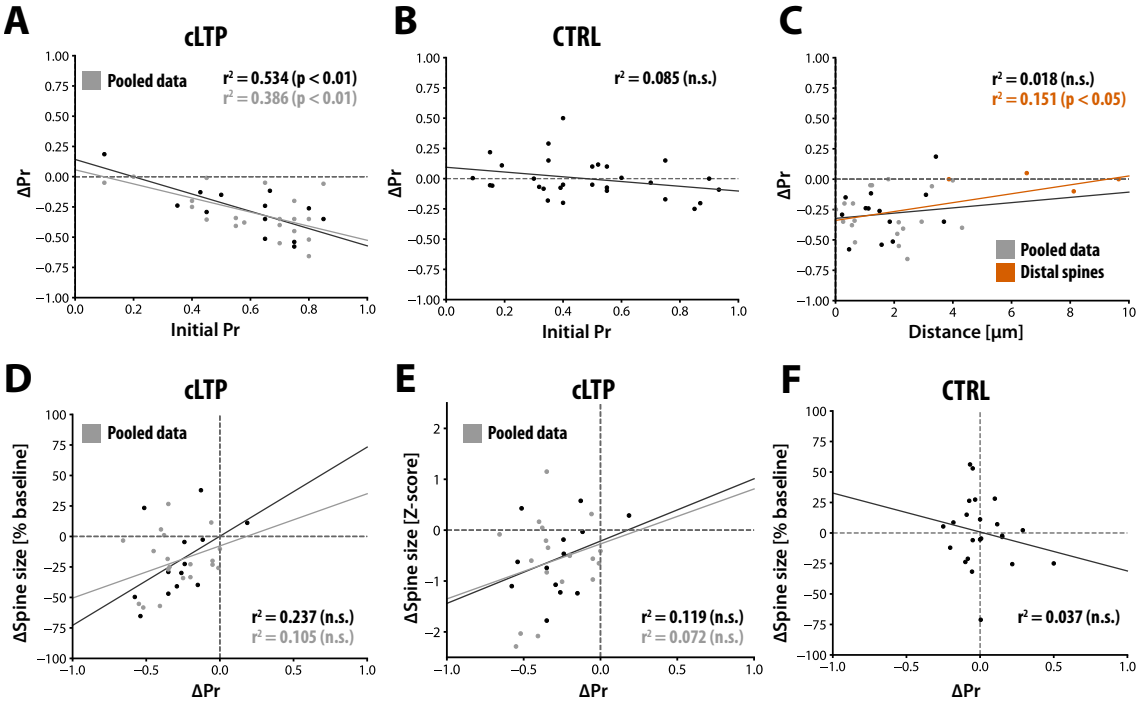

Fig. 4.7: Presynaptic changes depend on the initial Pr but are only weakly correlated with distance and spine size changes. Pooled data points including experiments from Chapter 5 are shown in grey. (A) Pr changes in relation to initial Pr. Initial Pr strongly predicted the magnitude of heterosynaptic presynaptic LTD (Pearson r = -0.731, N = 13, p < 0.01; pooled: r = 0.621, N = 33, p < 0.01). (B) Pr changes in relation to initial Pr for control experiments (omitting photolysis or depolarisation, r = 0.085, N = 29, n.s.). (C) Pr changes in relation to distance. A weak correlation was observed when distal spines (shown in red) were included (pooled: r = 0.134, N = 33, n.s., with distal: r = 0.389, N = 37, p < 0.05). (D) Pr changes in relation to fractional spine size changes. Pre- and postsynaptic changes were only weakly correlated, which was not significant (r = 0.487, N = 13, p = 0.09; pooled: r = 0.324, N = 32, p = 0.07). (E) Pr changes in relation to absolute spine size changes. Absolute spine size changes further deteriorated the correlation (r = 0.345, p = 0.248; pooled: r = 0.268, N = 32, p = 0.138). (F) Pr changes in relation to fractional spine size changes for control conditions (r = -0.192, N = 23, n.s.).

requires the activity of nearby synapses. Lastly, stimulated synapses undergoing structural LTP did not show significant changes in Pr (ΔPr = -0.13 ± 0.04, N = 6, n.s. vs CTR, Fig. 4.6C,E).

The decrease in Pr was strongly negatively correlated with the initial Pr (Pearson r = -0.731, N = 13, p < 0.01, Fig. 4.7A, black data points), which was not observed for the control experiments (Pearson r = 0.085, N = 29, n.s., Fig. 4.7B). Similarly strong correlation was observed in the independent dataset of Chapter 5 (Pearson r for pooled data = 0.621,

N = 33, p < 0.01, Fig. 4.7A, "pooled data"). In fact, the majority of variation could be explained by the initial Pr, especially given that the uncertainty caused by the statistical measurement of Pr is estimated to account for roughly 50 % of the variance observed (see Discussion). Accordingly, no distance-dependency could be observed for synapses in close proximity to the stimulated cluster (Pearson r for pooled data = 0.134, N = 33, n.s., Fig. 4.7C). Taking into account all 17 experiments, induction of presynaptic hetLTD seems to follow all-or-none dynamics dependent on the distance to the stimulated cluster, where the magnitude of change is then given by the initial state of the synapse (Pearson r = 0.389, N = 37, p < 0.05).

4.3.3. Pre- and postsynaptic heterosynaptic plasticity are only weakly correlated

There is a positive correlation between absolute Pr changes and the fractional change in spine size (Pearson r = 0.487, N = 13, p = 0.09, Fig. 4.7D, black spheres), which did not reach statistical significance. This was unexpected given the well-established correlation of pre- and postsynaptic strengths (see chapter 2.1.5). As the relationship between pre- and postsynaptic changes lies at the core of my thesis, I have examined the statistical significance more closely. The magnitude of pre- and postsynaptic changes are difficult to put in relation, since the impact on overall synaptic weight is not known. In particular, it is not immediately evident if the readout of postsynaptic strength, the fractional change in spine fluorescence intensity, behaves similarly (i.e. proportionally) to Pr changes. I therefore calculated the non-parametric, rank-based correlation coefficient, which disregards the absolute values. This leads to a significant correlation, instead (Spearman rho = 0.627, p < 0.05). Non-parametric measures suffer from decreased statistical power and in order to reconcile this result, I have next analysed the correlation in the pooled experiments from Chapter 5. Analysis across the pooled dataset decreased the correlation coefficient and it was no longer statistically significant (Pearson r = 0.324, p = 0.07; Spearman rho = 0.313, p = 0.08, N = 32, Fig. 4.7D). Moreover, the correlation was diminished when absolute spine size changes, in units of the normalised Z-score, were used instead (Pearson r = 0.268, N = 32, p = 0.138, Fig. 4.7E). No significant correlation

between Pr and spine size changes was observed for control experiments (Pearson r = -0.192, N = 23, n.s., Fig. 4.7F).

4.3.4. cLTP induction and maintenance affect pre- and postsynaptic heterosynaptic plasticity differentially

Lastly, the spatial modulation of heterosynaptic changes indicates that the magnitude of stimulation might play an important role, as stimulation strength often correlates with the activity of downstream signalling molecules. The actual stimulation strength is not

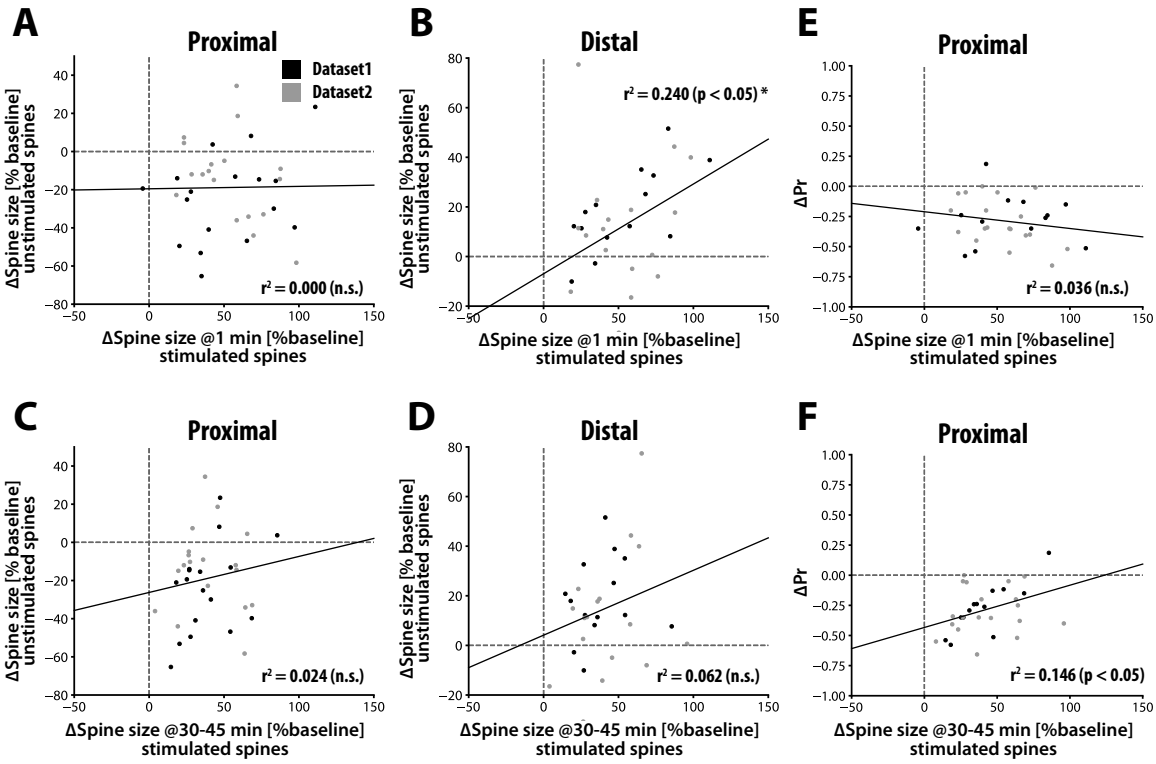

Fig. 4.8: Pre- and postsynaptic heterosynaptic changes depend differentially on transient and persistent spine size changes of stimulated spines. Pooled data points including experiments from Chapter 5 are shown in grey. Coefficient of determination was calculated for pooled data points (A,B,E) Spine size change immediately following cLTP induction of stimulated spines in relation to heterosynaptic postsynaptic changes at proximal (A, r = 0.015, N = 36, n.s.) and distal spines (B, Pearson r = 0.490, N = 36, p < 0.01) and presynaptic changes (E, r = -0.190, N = 32, n.s.). Postsynaptic heterosynaptic LTP showed significant correlation. (C,D,F) Persistent spine size change of stimulated spines in relation to heterosynaptic postsynaptic changes at proximal (C, r = 0.154, p = 0.1) and distal spines (D, r = 0.248, n.s.) and presynaptic changes (F, r = 0.383, p < 0.05). Presynaptic heterosynaptic LTD showed significant correlation.
*The outlier was omitted for calculation of the correlation coefficient.

known in these experiments. I have therefore used the initial size increase immediately after stimulation as an approximate measure of stimulation strength. Pre- and postsynaptic hetLTD at proximal synapses was not significantly correlated with the initial size increase (pooled experiments; presynaptic: Pearson r = -0.190, N = 32, n.s.; postsynaptic: r = 0.015, N = 36, n.s., Fig. 4.8A,E). In contrast, the heterosynaptic structural LTP at spines located more distally (3.8-7 µm for dataset 1; 2.8-6.5 µm for dataset 2, see Suppl. Fig. 9.1) was correlated with the initial size increase, except for a single outlier, which was excluded from this analysis (Pearson r = 0.490, N = 36, $p < 0.01$, Fig. 4.8B). Next, the maintenance of LTP at stimulated spines might be important, especially in the context of resource competition, which is thought to play a crucial role in heterosynaptic interactions (Govindarajan et al., 2011; Fonseca et al., 2004, 2006). Surprisingly, postsynaptic heterosynaptic changes were not correlated with the spine size increase at the end of the experiment (Pearson r = 0.154, p = 0.1; r = 0.248, n.s., proximal and distal spines, respectively, Fig. 4.8C,D). In contrast, presynaptic hetLTD was weakly positively correlated (Pearson r = 0.383, $p < 0.05$, Fig. 4.8F). This is unexpected as it would suggest that presynaptic hetLTD was not compensatory.

4.4. Discussion

I have shown that strong, coordinated activity along local dendritic segments leads to a range of short- and long-lasting modifications of synaptic strength at neighbouring unstimulated synapses. On the postsynaptic side, depending on the distance to the stimulated spine cluster, I have observed the expression of either hetLTP or hetLTD. The presynaptic terminal showed hetLTD at spines close to the stimulated cluster.

4.4.1. What is the most appropriate distance metric?

An important part of my study was to investigate the spatial component underlying heterosynaptic plasticity. This required the use of a distance metric that captures the spatial relationship between the stimulated cluster of spines and unstimulated synapses. There are several valid definitions, such as the average pairwise distance to each

stimulated spine, the distance to the centre of the cluster, the distance to the closest stimulated spine, spines classified as within or outside the cluster, or proximity scores. I have chosen the distance along the dendrite from the centre of mass of the stimulated cluster, which is based on several assumptions. Firstly, I have assumed that interactions between stimulated and unstimulated synapses are spatially restricted to the intracellular space of the dendrite as opposed to the direct unconfined distance between synapses. This implies that diffusion of cytosolic or membrane-bound signalling molecules or propagation of electrical signals along the plasma membrane underlie the observed spatial dynamics. Indeed, induction of spine structural LTP was reported to initiate the intracellular diffusion of a multitude of downstream signalling molecules that have been implicated in the regulation of synaptic strength (Nakahata & Yasuda, 2018; Nishiyama & Yasuda, 2015). These include CaMKII-dependent signalling pathways and various phosphatases, such as calcineurin. Furthermore, local translation in the dendritic shaft is known to generate proteins relevant to synaptic plasticity, such as Arc, PSD-95, GluA1, or CaMKII, in an activity-dependent manner, which are then transported into neighbouring spine heads (Nishiyama & Yasuda, 2015). Protein translation has been shown to be confined to individual dendritic segments (Govindarajan et al., 2011; Sutton et al., 2006). In contrast, various extracellular regulators of synaptic strength are also engaged following the induction of spine structural LTP. For instance, our lab has recently reported that structural LTP requires the exocytosis of lysosomes containing the protease Cathepsin B, which activates extracellular matrix metalloproteinase 9 (MMP-9) by cleaving its inhibitor TIMP1 (Padamsey et al., 2017b). MMP-9, in turn, is known to mediate the remodelling of the extracellular matrix and the cleavage of cell-adhesion molecules, such as neuroligin-neurexin complexes or intercellular adhesion molecule-5 (ICAM-5), which are known modulators of synaptic strength (Peixoto et al., 2012; Conant et al., 2010). Additionally, small molecule transmitters, such as BDNF, eCBs, or NO, which are known to be released following synaptic activity, are thought to act in a volumetric, comparatively spatially unconstrained manner. In order to minimise the potential error introduced by volumetric signalling molecules, I have constrained most of my analysis to

dendrites with minimal curvature. The error introduced is therefore largely due to the neglect of the spine neck length and its angle to the dendritic shaft and assuming an average spine neck length of 0.5 µm (spine neck length ranges from 0-1 µm depending on the type of spine, i.e. stubby vs. thin; Harris et al., 1992) the maximum error would be 1 µm, which lies within the estimated measurement error. However, since the deviations are minimal, this makes it difficult to distinguish between different modes of diffusion by comparing different distance metrics. A pharmacological approach is therefore needed.

Secondly, by using the centre of mass as the reference point, I assumed that stimulated spines contribute equally to the induction of heterosynaptic plasticity and that their contribution decays linearly with distance. Equal contribution of spines is not guaranteed since large spines might contain more signalling molecules that will be activated upon stimulation. Similarly, large spines are more likely to also contain ER, mitochondria, and ribosomes (Bourne & Harris, 2008) and could therefore differ in their signalling properties compared to smaller spines. In fact, it was recently reported that spines containing smooth ER or polyribosomes exhibit enhanced spine structural LTP and promote the formation of synapse clusters (Chirillo et al., 2019). ER has also been strongly implicated in postsynaptic forms of LTD (Holbro et al., 2009; Oh et al. 2015). Smooth ER located at the spine is known to be involved in compartmentalised Ca^{2+}-signalling during synaptic plasticity and the transport and delivery of membrane proteins, such as ion channels. Interestingly, smooth ER has been associated with the actin binding protein synaptopodin (Segal et al., 2010). Synaptopodin has been implicated in the regulation of actin-polymerisation, spine formation, and is required for spine structural LTP (Zhang et al., 2013). It is therefore very likely that the above assumption is false. Without exact knowledge of the parameters related to the contribution of each spine, the extent of the potential error is difficult to estimate. The number of spines containing some form of smooth ER in CA1 pyramidal neurones has been estimated to be ~ 58 %, however, only ~ 10-15 % contain an elaborate spine apparatus (Spacek & Harris, 1997), which is thought to be the predominant form involved in synaptic plasticity. The probability that I have

stimulated at least one spine containing a spine apparatus is therefore > 50 %, and likely to be higher, since large mushroom spines have a higher abundance of smooth ER and are more easily detectable, and thus targeted for stimulation. I found that heterosynaptic spine size changes were not correlated with the fractional change of stimulated spines at the end of the experiment (Fig. 4.8C), suggesting that, on a population level, clusters containing larger number of spines with high propensity to undergo structural enlargement do not significantly influence the outcome of heterosynaptic plasticity. Alternatively, the lack of correlation could indicate homogeneous sampling of spines. There was, however, a positive correlation between the heterosynaptic enlargement and the initial size increase in stimulated spines (Fig. 4.8B), which I have interpreted as an estimate of stimulation strength. In an alternative interpretation, the initial size increase might reflect differences in the molecular composition of the spine.

Using the distance to the centre of mass also assumes that interactions between spines decrease linearly with distance. Assuming that the interaction relies on the diffusion and the strength of the interaction is governed by the amount of signalling molecules, one can easily derive, from the diffusion equation (Langevin equation) that the decay across space is roughly Gaussian (if diffusion is homogenous). This leads to the interesting case in which at short distances, the interaction between synapses is nearly independent of distance, whereas distal spines are well-approximated by a linear interaction. This could explain why Pr changes at proximal synapses were independent of distance (Fig. 4.7C). Conversely, if multiple diffusible signalling molecules interact competitively (and assuming the competition is linear), the diffusion profile at short distances is sharpened as it will take on the shape of a difference of Gaussians function. This could explain the apparent distance-dependency for postsynaptic heterosynaptic weakening at proximal spines (Fig. 4.5A,B). The above analysis additionally assumes that diffusion is fast. If diffusion is slow or highly restricted in space, a more appropriate distance metric might be the minimum distance to a stimulated spine. This, however, does not further explain the variance observe in spine size changes (not shown). Without knowledge of the

underlying diffusible molecules and their diffusion properties, it is difficult to incorporate diffusion into the distance metric. Linear interaction, although not realistic, provides an adequate first order approximation, at least for intermediate distances.

Thirdly, the centre of mass intrinsically normalises for the number of stimulated spines, implying that the relative rather than absolute amount of activated signalling molecules drives synaptic plasticity, which would support a synaptic plasticity rule that is not localised to synapses and information is instead shared and integrated across space. This is, for instance, the case when synaptic plasticity is limited by resources. Any distance metric that takes into account all stimulated spines will introduce normalisation and therefore suffer from the same assumptions. Proximity measures, such as the sum of the inverse distance, could circumvent this problem, since stimulated synapses located further away will have diminishing influence. This, however, requires a good knowledge of how the signalling molecules decay with distance and can lead to significant distortions if it is unknown. Using the sum of inverse distance recapitulates, qualitatively, my results but the distance profile is highly distorted and difficult to analyse or to interpret (not shown). It also does not explain more variance in the data. The potential confounds introduced by this assumption should be negligible, since the number of stimulated spines is similar across experiments. However, a major concern with normalisation is its susceptibility to outliers, such as stimulated spines that are located far away, as the centre of mass weights every stimulated spine equally. I have calculated several parameters to evaluate the degree of a potential confound of outliers. The maximum distance between stimulated spines was similar across experiments and conditions (Tab. 3.1). Within conditions, the maximum distance did not vary substantially, with a standard deviation of ~ 3 µm. Furthermore, the deviation of the centre of mass from the actual centre was low (Tab. 3.1) indicating that stimulated synapses are roughly homogeneously distributed. The mean pairwise distance between stimulated spines was $d_{pairwise,cLTP1} = 3.6 \pm 0.3$ µm, with a standard deviation of ~ 1.0 µm (Tab. 3.1), which means that the majority of stimulated spines were located within 2.6-4.6 µm of each other. I

therefore conclude that the potential confound of normalisation of the number of stimulated spines is negligible given the homogenous sampling.

In summary, the appropriate choice of the distance measure depends on the assumptions about the underlying molecular mechanism. I found that most potential confounds are negligible due to low spatial variation in the stimulation protocol and analysis of mainly straight dendritic morphologies. However, the distance metric does not allow definite conclusions on the mechanism of spatial interaction, such as diffusion.

4.4.2. What is the most appropriate way to measure and compare spine size changes?

I have reported postsynaptic results as fractional spine size changes. This was largely due to experimental constraints. Spine size was estimated by the integrated fluorescence in the image plane that yielded the maximum value. However, since the dye concentration is altered during cLTP induction, due to the use of whole-cell patch clamp, I have normalised fluorescence intensity to the mean fluorescence of the dendritic branch, which I have assumed to remain structurally unchanged. This normalisation was done within experiments, rendering the absolute values incomparable across experiments. To circumvent this limitation, I made the assumption that the basal distribution of spine sizes do not differ between cells and slices and can thus be used as a means of normalisation across experiments. I estimated the population distribution independently for each experiment from mean and variance of measured fluorescence intensity of measurements of all spines before the induction of cLTP, and have therefore assumed an underlying normal distribution. The advantage of estimating a normal distribution is the high accuracy with even low numbers of samples. This allowed me to represent absolute spine size in units of standard deviation, or Z-score. Using this measure, I showed that spine structural LTP leads to a constant increase in spine size independent of initial size (Fig. 4.3E), that postsynaptic heterosynaptic LTD is driven by the intrinsic fluctuation of spine size (see next section), which is more pronounced in larger spines, and that presynaptic changes do not correlate with the absolute change in spine size (Fig. 4.7E).

However, is the underlying distribution of spine sizes normal? As pointed out in the introduction, the distribution of synaptic strengths in general is negatively (rightward) skewed. Indeed, I found that measured spine fluorescence also showed a negative skew, and was significantly different from the normal distribution (Kolmogorov-Smirnov test) and should theoretically be accounted for, for example by using a skew normal distribution. I estimated the magnitude of the potential error by accounting for the skew using a square-root transformation. This results in an absolute error of roughly 6 % of the population standard deviation (i.e. Z-score ± 0.06) and is therefore negligible given the scale of the effect size, which is roughly one order of magnitude larger.

4.4.3. What underlies the spatial dynamics of heterosynaptic postsynaptic plasticity?

The most parsimonious explanation for the distance-dependent bi-directional regulation of postsynaptic strengths is the parallel signalling of two diffusible factors, one exerting potentiation and the other depression. The differences in their effective diffusion properties (diffusion, inactivation constants, and reaction kinetics) could then result in the observed Ricker wavelet shape profile. Evidence for a diffusible potentiating factor can be seen in the transient increase in all unstimulated spines. In Fig. 4.2B, it is apparent that proximal spines increase in size immediately after cLTP induction, which is delayed in very distal (> 7 µm) spines, which could reflect a delay due to diffusion. Next, the probability distribution of spine size changes for proximal and distal spines suggest that potentiation and depression are mechanistically different. Spine size changes under resting conditions are roughly normally distributed, and spines undergo constant morphological changes. The rightward skew in the cumulative distribution of proximal spines shows that the putative depression factor interferes with the basal variance of spine size rather than directly and additively depressing the synapse, which would cause a horizontal translation in the cumulative distribution, as seen in the case of potentiating spines located more distally (Fig. 4.5C,D). This could make postsynaptic hetLTD state-dependent, since the magnitude of depression is governed by the intrinsic fluctuation of the spine. Studies of resting state spine volume dynamics show that the fluctuation (in

absolute units) scales linearly with spine volume (Yasumatsu et al., 2008). This, then, predicts that the absolute change in size during hetLTD should correlate with the initial size. Indeed, I observed a significant negative correlation between the absolute spine size change and initial spine size for spines located within 3.8 µm (Pearson $r = -0.330$, $N = 39$, $p < 0.05$), which was absent in spines located 3.8-7 µm (Pearson $r = 0.015$, $N = 48$, n.s.). Similar results were obtained for an independent dataset (Proximal spines: $r = -0.354$, $N = 35$, $p = 0.05$; Distal spines: $r = -0.224$, $N = 40$, n.s.; Suppl. Fig. 9.1). I therefore conclude, that postsynaptic heterosynaptic plasticity is driven by two opposing, diffusible factors with distinguishable underlying biochemical mechanisms, although this would require further experimental investigation.

4.4.4. What are the properties of heterosynaptic presynaptic plasticity?

Heterosynaptic presynaptic plasticity was observe for synapses located close to the stimulated cluster and was restricted to weakening only. Unlike postsynaptic plasticity, the magnitude of presynaptic LTD was not well predicted by the distance to the stimulated cluster (Fig. 4.7C). Instead, I found that distance serves a permissive role and synapses need to be located within some critical distance of roughly 4 µm. The magnitude of change was, however, strongly negatively correlated with the initial Pr (Fig. 4.7A). In fact, most of the remaining variance in Pr is likely to originate from the measurement itself, which is described by a binomial sampling process. For a given binomial probability p, the variance of p in N observation is given by $p(1-p)/N$. Following the principle of propagation of uncertainty, the expected variance makes up ~ 50 % of the observed variance. The coefficient of determination (r^2) provides a measure of variance explained by the linear regression, which was $r^2 = 0.534$ and $r^2 = 0.386$ for single and pooled datasets, respectively. For control experiments, the measurement error was estimated to account for > 70 % of the observed variance. The remaining variance is probably due to the tendency of high Pr synapses to weaken following sustained stimulation (see chapter 6 for potential mechanism), which is seen as a slight negative correlation (Fig. 4.7B). The initial Pr is therefore the main driver of Pr changes.

Next, I have found that the magnitude or Pr change is correlated with the magnitude in persistent spine size change of stimulated synapses (Fig. 4.8F). This could either mean that presynaptic heterosynaptic plasticity is not compensatory in nature, or that spine structural LTP expression is modulated by presynaptic changes. I therefore predict that in the first case, selective inhibition of spine structural LTP should enhance presynaptic weakening, whereas in the second case, selective inhibition of presynaptic weakening should enhance LTP.

I have also observed slight presynaptic weakening in stimulated spines (Fig. 4.6C). The lack of an increase in Pr following structural LTP is not surprising and is in line with the observation that presynaptic LTP requires concomitant stimulation of the presynaptic terminal (Grover, 1998; Grover & Yan, 1999). The lack of strong presynaptic weakening might indicate that LTP is able to protect synapses from subsequent homeostatic changes. However, the interpretation of any presynaptic changes following photolytic release of glutamate is difficult because it could activate presynaptic receptors in a highly non-physiological context. Additional electrophysiological experiments would therefore be needed to make any conclusive statements.

4.4.5. Do pre- and postsynaptic changes match?

Lastly, I found that pre- and postsynaptic heterosynaptic plasticity were only weakly correlated (Fig. 4.7D,E) however, complete disjunction is unlikely. As pointed out, the magnitude of pre- and postsynaptic changes are difficult to put in relation and is dependent on the assumption and definition of overall synaptic strength. I have therefore used the Spearman correlation coefficient, which is rank-based and does not require direct proportionality between the measured variables. This, however, led to conflicting results when I included a second independent dataset. I have done additional analyses to confirm these observations.

Firstly, both Pearson and Spearman correlation coefficients are not robust against outliers, which can lead to spurious correlations and inflation of the p-value. I have

therefore used bootstrapping to estimate confidence intervals of the correlation coefficient given the specific distribution of my data. Bootstrapping confirmed that the correlation coefficient is not statistically significant under alpha = 0.05 for both, individual and pooled datasets.

Next, I considered the theoretical impact of the measured changes on synaptic strength. The simplest description of synaptic strength is based on a binomial process, where synaptic weight w = Npq. I will assume that N = 1 (see Introduction for rationale). It is easy to see that a relative change in w is equal to the product of relative changes in p and q. Converting ΔPr into the relative change instead further reduced the correlation (Pearson r = 0.285, n.s.; Spearman rho = 0.261, n.s.) similar to comparisons of absolute changes (Fig. 4.7E).

As I have pointed out, the validity of the units used to represent spine size change depends on their relationship to the actual increase in postsynaptic strength as measured for example by an increase in the AMPA receptor conductance. Fractional spine volume change, by direct measurement of spine head diameter, was reported to be linearly correlated with a fractional change in AMPA receptor current (Matsuzaki et al., 2004; Smith et al., 2003; Béïque et al., 2006). The relationship between integrated fluorescence used in this study and actual spine volume is unclear, but it is possible to consider two extreme cases. The resolution of (2-photon) fluorescence microscopy, especially the axial resolution, is not enough to completely resolve spines, which are on the order of 1 µm diameter. Differences in the fluorescence intensity on a single optical plane are therefore not likely to be restricted to changes in area, and could reflect, to some extent, volume changes as well. In one extreme, single plane integrated fluorescence intensity would be directly proportional to spine volume and hence proportional to AMPA receptor current, and a direct comparison with other parameters would therefore be valid. On the other hand, if the fluorescence intensity perfectly reflects the cross-sectional area, the fractional change needs to be corrected by a factor proportional to the square root of the change. This correction would further slightly

deteriorate the observed correlation (Pearson r = 0.293, p = 0.1). Taking together all avenues of analysis, and assuming that the actual relationship lies somewhere between the two bounding cases, I conclude that pre- and postsynaptic heterosynaptic plasticity are not significantly correlated.

This finding agrees with the idea that pre- and postsynaptic strengths are regulated independently due to their distinct functional roles. The reported correlations of basal synaptic strengths might be due to similarities in their regulation at extreme values. For instance, both high Pr synapses and large spines are known to be more likely to undergo synaptic weakening, consistent with my current findings.

4.5. Conclusion

Altogether, I have shown that strong stimulation of groups of synapses leads to the expression of both, pre- and postsynaptic forms of heterosynaptic plasticity. Postsynaptic strength is regulated in a distance-dependent bi-directional manner whereas presynaptic strength of synapses located close to stimulated synapses predominantly weakened. Pre- and postsynaptic changes were only weakly correlated, suggesting the involvement of partly parallel signalling pathways. These signalling pathways spread distinctly in space and do not substantially overlap. Next, I sought to investigate the molecular pathways involved in these heterosynaptic changes.

5. Molecular mechanism of pre- and postsynaptic heterosynaptic plasticity

5.1. Introduction

Virtually all molecular pathways involved in the induction of synaptic plasticity converge onto the activation of Ca^{2+}-dependent kinase/phosphatase signalling pathways (Malenka & Bear, 2004). In particular, activation of CaMKII and calcineurin/PP1 are linked to the expression of LTP and LTD, respectively (Malenka & Bear, 2004). Importantly, differences in the kinetics and spatial distribution of these signalling molecules are thought to implement distinct biochemical computations (Nishiyama & Yasuda, 2015; Fujii et al., 2013). Heterosynaptic plasticity requires the spatial diffusion of signalling molecules. Recent studies show that stimulation of single synapses leads to the activation and diffusion of various signalling molecules involved in mediating LTP and LTD. Specifically, calcineurin has been heavily implicated in the spatial spread of LTD (Oh et al., 2015; Wiegert & Oertner, 2013) and activated calcineurin has been shown to diffuse into neighbouring spines at comparatively high concentration (Fujii et al., 2013). Additionally, heterosynaptic LTD in pyramidal neurones of the visual cortex was shown to require the immediately early gene Arc (El-Boustani et al., 2018), which is a known homeostatic regulator of synaptic plasticity (Shepherd & Bear, 2011). Lastly, competition for cell-adhesion proteins, such as N-Cadherin-β-catenin complexes can lead to local synaptic competition and pruning of inactive spines (Bian et al., 2015). In contrast, the molecular mechanism of a spatial spread in LTP is less well studied. Induction of spine structural LTP was shown to facilitate LTP at neighbouring spines, which required CaMKII-dependent activation of h-Ras, a known regulator of actin dynamics, which is able to diffuse along the dendrite and invade neighbouring spines (Harvey & Svoboda, 2007; Harvey et al., 2008). Similarly, the small GTPases RhoA and Rac1 were also found to invade neighbouring spines following LTP induction, and facilitated subsequent LTP induction (Murakoshi et al., 2011; Hedrick et al., 2016). Apart from diffusional spread of signals, protein synthesis-dependent mechanisms have been suggested (Govindarajan et al.,

2011). These, however, are likely to act on longer time-scales.

Presynaptic heterosynaptic plasticity necessitates a retrograde messenger. This can either be a diffusible molecule that acts directly on the presynaptic terminal or a form of matching driven by concurrent postsynaptic changes. Promising diffusible retrograde messengers include NO, which is strongly implicated in mediating presynaptic LTP, but was also shown to be necessary for heterosynaptic compensatory plasticity at neocortical synapses (Volgushev et al., 2000; Lee et al. 2012), eCBs, which mediate heterosynaptic LTD at inhibitory synapses in the hippocampus (Castillo et al., 2012; Heifets & Castillo, 2009; Kano et al., 2009), and BDNF with its precursor pro-BDNF (Leal et al., 2015; Lu et al., 2014; Lu, 2003). In addition, proteolytic cleavage of postsynaptic cell-adhesion proteins, such as neuroligin-1 has been shown to regulate presynaptic strength (Peixoto et al., 2012). Cleavage of neuroligin-1 leads to a decrease in presynaptic strength, likely via a decrease in Pr, which was due to the destabilisation of presynaptic neurexins. This process was shown to be dependent on NMDARs and MMP-9, both of which are activated during in spine structural LTP. Interestingly, cleavage of neuroligin-1 was not confined to the stimulated synapse, but was also observed at neighbouring synapses, which could lead to novel heterosynaptic interactions.

To tease apart the mechanisms of the bidirectional postsynaptic heterosynaptic plasticity, I have investigated the roles of CaMKII, and calcineurin pharmacologically, both of which are known to be activated rapidly following stimulation. I hypothesised that the bi-directional changes can be explained by the spatial diffusion of two "plasticity factors", one potentiating and the other depressing, dependent on CaMKII and calcineurin signalling, respectively. The observed distance-dependency then arises from differences in the effective diffusion coefficient and the rate of activation of and interaction between these factors. I therefore predicted that selectively blocking one of the factors will (1) facilitate the effect of the opposing factor and (2) reveal the underlying diffusion properties, which should follow distinct dynamics. In addition, it was important to determine if the decrease in presynaptic strength is the result of a parallel signalling

pathway with its own biochemical computation or the consequence of postsynaptic weakening and subsequent "matching" of synaptic strengths. Given the evidence of weak correlation between pre- and postsynaptic changes, I predicted that the respective signalling cascades are pharmacologically dissociable at an early stage. I have next determined the retrograde messenger for presynaptic weakening using pharmacological means. Specifically, I have tested the hypothesis that NO acts as a postsynaptic signal for strong local depolarisation, which can bi-directionally regulate presynaptic strength in a state-dependent manner.

5.2. Results

5.2.1. Pre- and postsynaptic heterosynaptic plasticity requires activation of NMDA receptors

The previous experiments suggest that both, pre- and postsynaptic heterosynaptic plasticity, are triggered by synaptic activity of adjacent synapses. Additionally, concurrent strong postsynaptic depolarisation is necessary, either in the form of cell-wide depolarisation or strong local cooperative synaptic input. This suggests the involvement of a coincident detector for both glutamate release and depolarisation, the best candidate of which is the NMDAR. Moreover, NMDAR-dependent Ca^{2+}-influx is known to initiate various downstream signalling pathways that lead to the heterosynaptic spread of plasticity-related proteins, as well as the synthesis of retrograde messengers, such as NO. To study the involvement of NMDARs, I locally applied the antagonist AP5 in combination with MNI-glutamate (500 µM AP5 + 10 µM MNI-Glutamate, locally perfused) during the induction of cLTP. This transiently blocked NMDARs during cLTP induction while preventing any interference with the detection of EPSCaTs, which are largely dependent on NMDAR-dependent Ca^{2+}-influx (Padamsey et al., 2019). Photolysis-evoked postsynaptic Ca^{2+}-transients were markedly smaller compared to control, even though the laser power was set to the higher end used during vehicle conditions, indicating that NMDARs were sufficiently blocked (Fig. 5.1D). The residual Ca^{2+}-signal is likely due to the

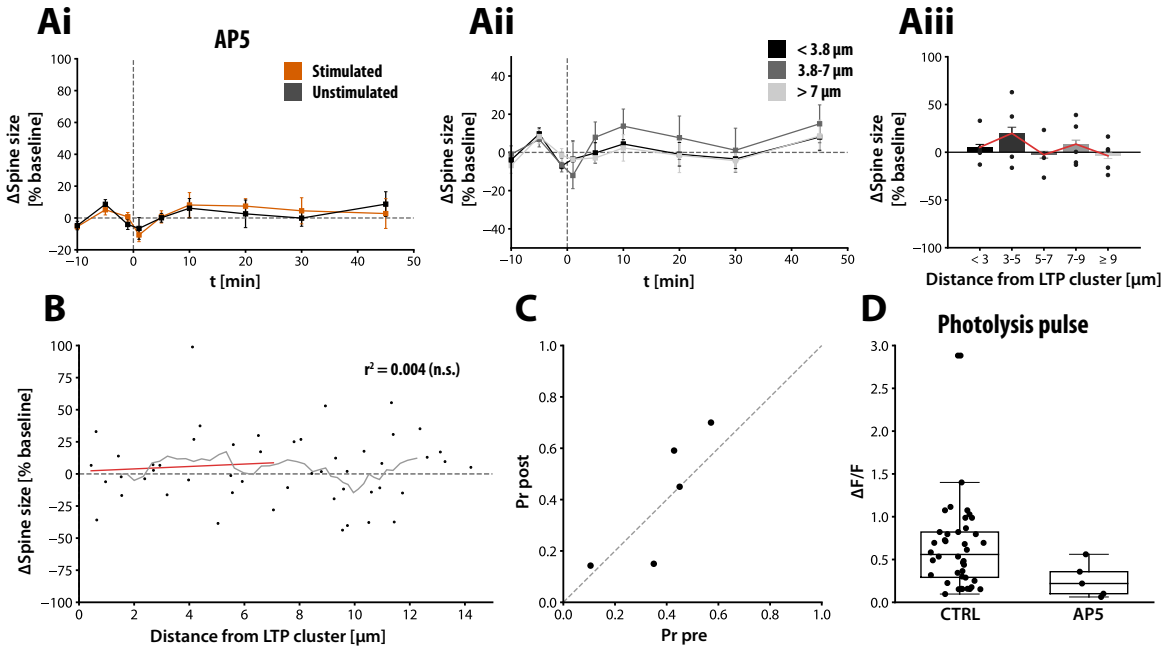

Fig. 5.1: Homo- and heterosynaptic plasticity require activation of NMDA receptors. NMDARs were blocked by locally applying 500 µM AP5 during cLTP induction. (Ai) Spine size changes of stimulated and unstimulated spines. cLTP was induced at t = 0 min. Both, homo- and heterosynaptic spine size changes were abolished ($\Delta V_{30\text{-}45min}$ = 4.4 ± 8.1 %; $\Delta V_{30\text{-}45min}$ = 2.9 ± 5.6 %, respectively, N = 5). (Aii) Spine size changes of unstimulated spines, grouped by distance. (Aiii) Spine size changes of unstimulated spine in 2 µm bins. (B) Spine size changes of all spines analysed shown with respect to distance (Pearson r = 0.063, N = 22 spines, n.s.). (C) Pr of unstimulated synapses located close to the stimulated cluster (< 4 µm). No presynaptic LTD was observed. (D) Local application of AP5 decreased uncaging-evoked spine Ca^{2+}-transients (CTRL: 0.678 ± 0.092 ΔF/F; AP5: 0.239 ± 0.077).

opening of VGCCs (Padamsey et al., 2017a).

Homosynaptic and heterosynaptic structural changes were completely abolished by the application of AP5 (Stimulated: ΔV = 4.4 ± 8.1 %; Unstimulated: 2.9 ± 5.6 %; N = 5, Fig. 5.1A). No bi-directional distance-dependent postsynaptic changes were observed (Fig. 5.1Aiii,B). Likewise, presynaptic strength of neighbouring synapses remained stable after cLTP induction (ΔPr = 0.026 ± 0.056, Fig. 5.1C). Thus, heterosynaptic plasticity requires NMDAR-dependent signalling.

5.2.2. Presynaptic hetLTD requires activation of CaMKII, whereas postsynaptic changes are driven by parallel signalling pathways involving calcineurin and CaMKII

Next, I examined the role of CaMKII and calcineurin. The vehicle control showed similar postsynaptic changes compared to the experiments shown in Chapter 4, with robust homosynaptic structural LTP ($\Delta V_{30\text{-}45min}$ = 42.5 ± 5.1 %, N = 19), transient increase in size of unstimulated spines immediately after induction (ΔV_{10min} = 14.6 ± 3.3 %), and the distance-dependent bi-directional changes (inversion point: 2.8 µm, maximum correlation: 6.5 µm, Suppl. Fig. 9.1; spines < 2.8 µm: $\Delta V_{30\text{-}45min}$ = -15.5 ± 4.7 %; 2.8-6.5 µm: $\Delta V_{30\text{-}45min}$ = 11.4 ± 5.7 %; > 6.5 µm: 5.9 ± 3.1 %; Fig. 5.2A). However, the spread in structural LTP at distant spines was much more pronounced and reached as far as 15 µm from the stimulated cluster. There was no detectable difference in the magnitude of stimulation or fraction of enlarged spines immediately after induction (63.2 ± 4.5 %, n.s.). Most experiments showed robust presynaptic weakening (ΔPr = -0.29 ± 0.04, N = 20, Fig. 5.3A), with similarly strong dependence on the initial Pr (Pearson r = -0.546, $p < 0.05$, Fig. 5.3D) and weak correlation with spine size change (Pearson r = 0.170, n.s., Fig. 5.3G). Bath application of 10 µM KN62, an inhibitor of CaMKII, blocked structural LTP of stimulated spines in 7 out of 10 experiments ($\Delta V_{30\text{-}45min}$ = 6.4 ± 9.2 %, N = 10, $p < 0.01$, Fig. 5.2B). In 3/10 experiments, I observed strong and robust structural LTP contrary to expectations based on the known role of CaMKII. A potential explanation is the low solubility of KN62 in water, which could lead to lower than expected concentrations (see Methods). Unstimulated spines showed no change in size ($\Delta V_{30\text{-}45min}$ = -3.6 ± 2.3 %). When analysed with respect to distance, proximal spines decreased in size as expected, however, the slight enlargement of spines located more distally was completely abolished (< 2.8 µm: $\Delta V_{30\text{-}45min}$ = -10.6 ± 8.2 %; 2.8-6.5 µm: $\Delta V_{30\text{-}45min}$ = -6.9 ± 5.6 %; > 6.5 µm: $\Delta V_{30\text{-}45min}$ = -3.1 ± 3.2 %; Fig. 5.2Biii). Thus, postsynaptic heterosynaptic weakening does not require the maintenance of homosynaptic LTP and appears to be dissociable from the signalling pathway for homosynaptic LTP downstream of the NMDARs. Furthermore, the spread in structural LTP seems to rely on CaMKII-dependent signalling. Presynaptically, the

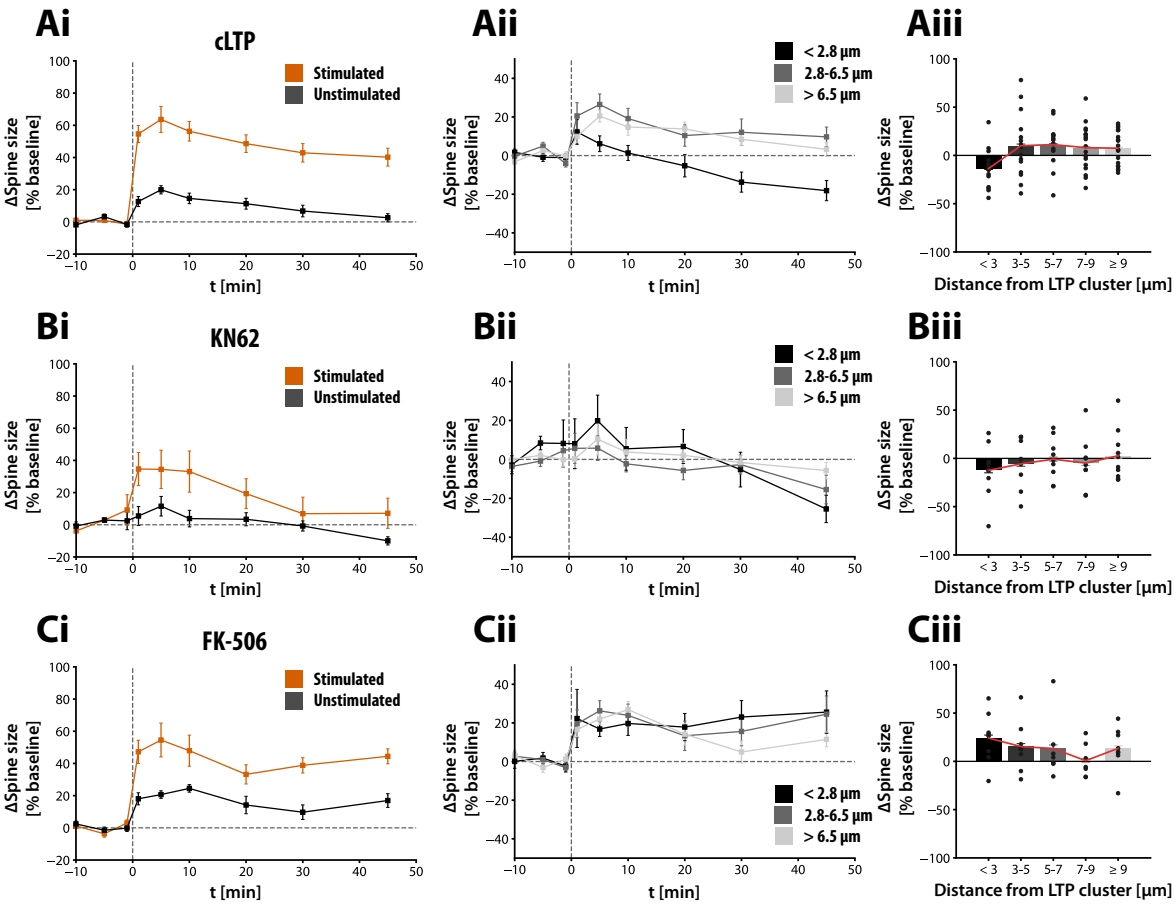

Fig. 5.2: CaMKII is required for postsynaptic heterosynaptic LTP whereas calcineurin is required for postsynaptic heterosynaptic LTD. (Ai) Spine size changes of stimulated and unstimulated spines. Robust persistent spine enlargement of stimulated spines ($\Delta V_{30\text{-}45min}$ = 42.5 ± 5.1 %, N = 19) and transient enlargement of unstimulated spines (ΔV_{10min} = 14.6 ± 3.3 %) were observed. (Aii) Spine size changes of unstimulated spines, grouped by distance (< 2.8 µm: $\Delta V_{30\text{-}45min}$ = -15.5 ± 4.7 %; 2.8-6.5 µm: $\Delta V_{30\text{-}45min}$ = 11.4 ± 5.7 %; > 6.5 µm: 5.9 ± 3.1 %). The distance range for heterosynaptic LTD was found to be shorter (6.5 µm). Robust spine shrinkage of proximal spines was observed, however, the spread of spine enlargement was more substantial compared to experiments in Chapter 4. (Aiii) Spine size changes of unstimulated spine, grouped in 2 µm bins. (Bi-iii) CaMKII signalling was blocked by bath application of 10 µM KN62. The expression of homo- and heterosynaptic LTP but not LTD was abolished (N = 7, stimulated: $\Delta V_{30\text{-}45min}$ = 6.4 ± 9.2 %; < 2.8 µm: $\Delta V_{30\text{-}45min}$ = -10.6 ± 8.2 %; 2.8-6.5 µm: $\Delta V_{30\text{-}45min}$ = -6.9 ± 5.6 %; > 6.5 µm: $\Delta V_{30\text{-}45min}$ = -3.1 ± 3.2 %). (Ci-iii) Calcineurin signalling was blocked via bath application of 2 µM FK-506. Heterosynaptic shrinkage of proximal spines was completely abolished and spine enlargement was observed instead (N = 8, < 2.8 µm: $\Delta V_{30\text{-}45min}$ = 24.7 ± 8.8 %; 2.8-6.5 µm: $\Delta V_{30\text{-}45min}$ = 17.7 ± 8.3 %; > 6.5 µm: $\Delta V_{30\text{-}45min}$ = 6.6 ± 4.9 %). Homosynaptic LTP remained unchanged ($\Delta V_{30\text{-}45min}$ = 40.4 ± 4.3 %, N = 8). Statistical comparisons are shown in Fig. 5.4. Error bars represent SEM.

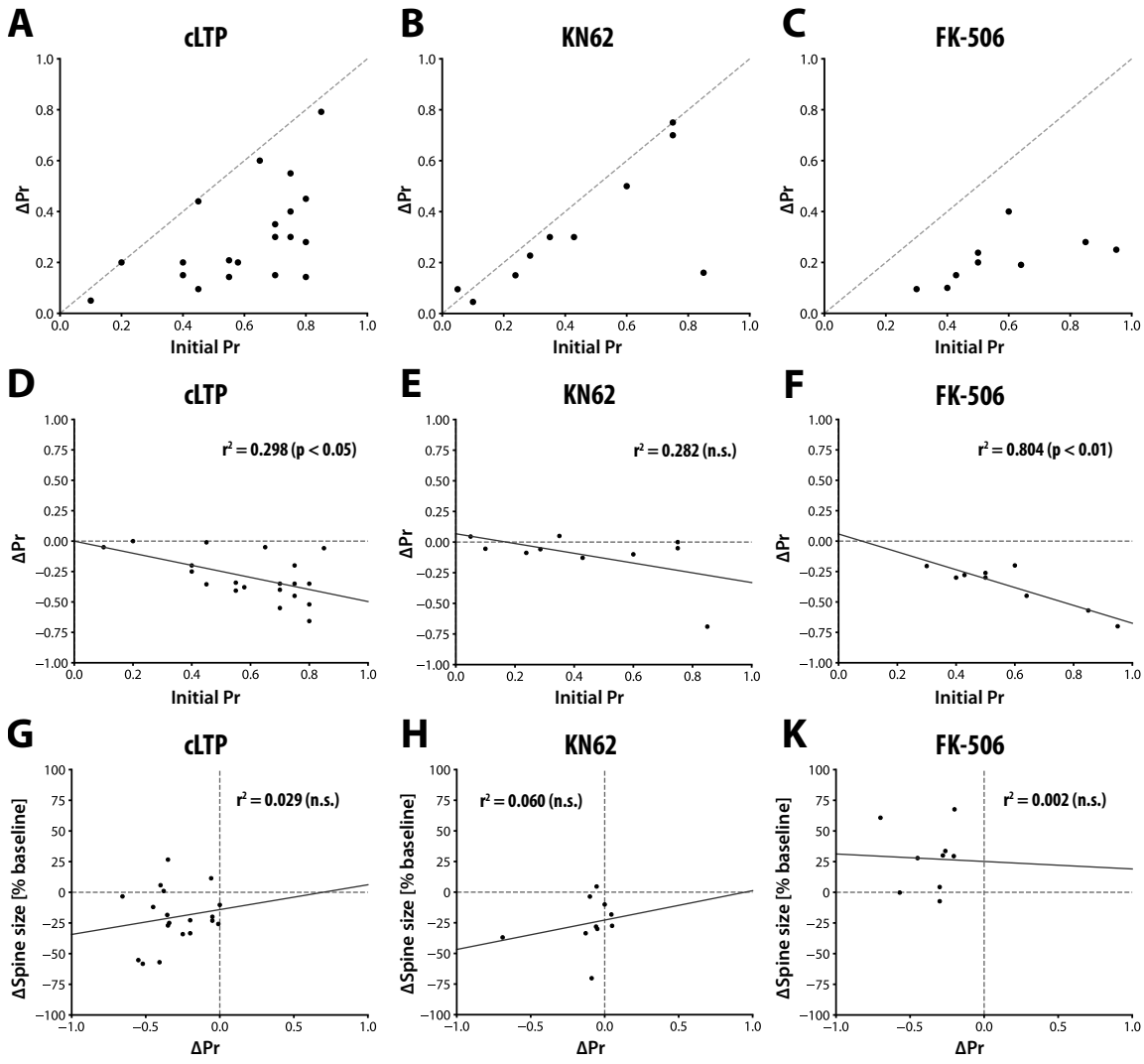

Fig. 5.3: CaMKII, but not calcineurin is required for presynaptic heterosynaptic LTD. (A-C) Pr before and 30 min after the induction of cLTP of unstimulated synapse located close to the stimulated cluster (< 4 µm) of vehicle control experiments (A), experiments with 10 µM KN62 (B), and 2 µM FK-506 (C). CaMKII inhibition abolishes presynaptic weakening. (D-F) Pr changes in relation to initial Pr. Strong correlations were observed for control and FK-506 experiments (cLTP: Pearson r = 0.546, N = 20, $p < 0.05$; KN62: r = -0.531, N = 10, n.s.; FK-506: r = 0.89, N = 9, $p < 0.01$). (G-H) Pr changes in relation to spine size changes. Pre- and postsynaptic changes were not correlated (cLTP: r = 0.170, N = 19, n.s.; KN62: r = 0.245, N = 10, n.s.; FK-506: r = 0.045, N = 9, n.s.).

heterosynaptic decrease in Pr was completely blocked by KN62 (ΔPr = -0.11 ± 0.06, N = 10, all spines located within 3 µm, Fig. 5.3B) except for one outlier. This indicates that presynaptic heterosynaptic LTD requires either the stable expression and maintenance of homosynaptic LTP or a direct involvement of CaMKII. These two options are, of course, not mutually exclusive.

Next, I blocked calcineurin by bath application of 2 µM FK-506 (Fig. 5.2C). Homosynaptic spine structural LTP was expressed in 61.7 ± 4.1 % of stimulated spine and did not differ in magnitude ($\Delta V_{30\text{-}45min}$ = 40.4 ± 4.3 %, N = 8, n.s. vs vehicle). The previously transient enlargement of unstimulated spines was more pronounced (ΔV_{10min} = 24.5 ± 2.3 %, $p < 0.05$) and remained slightly elevated throughout the course of the experiment, although not significant ($\Delta V_{30\text{-}45min}$ = 11.2 ± 4.6 %, n.s.). This increase showed mild distance-dependency, in which proximal spines were slightly more potentiated than distant spines (Pearson r = -0.355, p = 0.07, Fig. 5.2Ciii). FK-506 failed to block presynaptic weakening (ΔPr = -0.36 ± 0.05, N = 9, all spines located within 3 µm, Fig. 5.3C) which speaks against the "matching" hypothesis, in which a postsynaptic change drives an appropriate presynaptic adjustment. Consistently, presynaptic LTP was strongly correlated with the initial Pr (Pearson r = 0.89, $p < 0.01$, Fig. 5.3F), but was completely independent of the magnitude of spine size change (Pearson r = 0.045, n.s., Fig. 5.3K). The overall magnitude of presynaptic changes was not significantly different from the control condition, indicating that presynaptic LTD does not homeostatically compensate for altered postsynaptic plasticity.

The results are summarised in Fig. 5.4 (test for statistical significance additionally includes the dataset of Fig. 5.5 and was corrected for multiple comparison; Kruskal-Wallis H-test with *post hoc* Dunn's test). There is clear pharmacological dissociation between pre- and postsynaptic heterosynaptic plasticity, and these long-term modifications can be expressed and maintained independently. Presynaptic plasticity requires an independent signalling pathway downstream of the NMDAR and the production of a retrograde signal caused directly by the synaptic stimulation. In the postsynaptic case, pharmacological blockade of kinase and phosphatase pathways further consolidate spatial diffusion as the fundamental basis of biochemical computation. As predicted, inhibition of these putative factors facilitated the effect of the opposing factor and revealed underlying diffusive properties. Next, I focused on identifying the retrograde messenger in play.

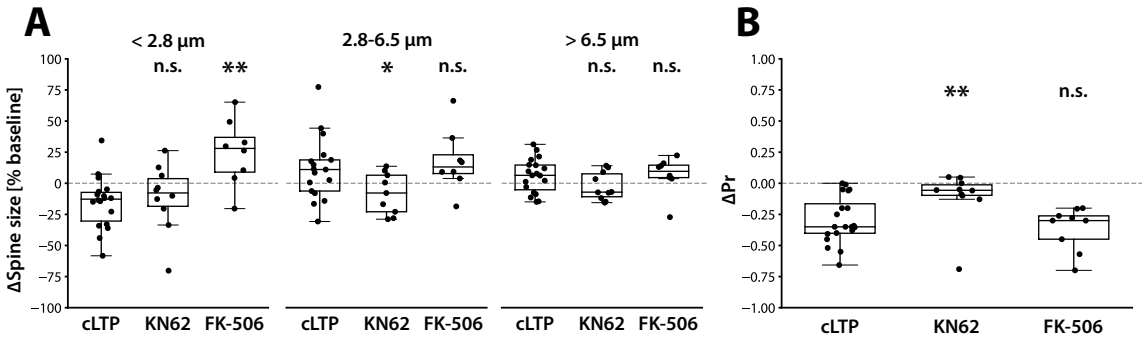

Fig. 5.4: Summary of statistical comparisons. Statistical comparison includes experiments shown in Fig. 5.5. (A) Comparison of heterosynaptic spine size changes for proximal (< 2.8 µm), distal (2.8-6.5 µm), and more distant spines (> 6.5 µm). Inhibition of calcineurin completely abolished spine shrinkage and unmasked persistent enlargement of proximal spines. Inhibition of CaMKII did not affect shrinkage of proximal spines but abolished the spread of spine structural LTP. (B) Comparison of heterosynaptic Pr changes for spine located within 4 µm of the stimulated spine cluster. Inhibition of CaMKII, but not calcineurin completely abolished presynaptic weakening. Data points were compared using Kruskal-Wallis H-test with *post hoc* Dunn's test. Significance indicates comparison with cLTP group.

5.2.3. Nitric oxide is the retrograde messenger for presynaptic heterosynaptic LTD

The experimental paradigm used in this study completely circumvents the activation of the presynaptic terminal and any presynaptic changes therefore necessitate a retrograde messenger. Based on the findings so far, production of the retrograde messenger is likely to depend on NMDAR signalling, interacts with CaMKII signalling either upstream or downstream, and is highly diffusible. Any one of a range of known candidate molecules fulfil these requirements. In particular, NO production and release has been shown to depend on strong local depolarisation (Padamsey et al., 2017a), and NMDAR signalling and CaMKII both modulate and are modulated by NO signalling (Hardingham et al., 2013). NO is also implicated in both, (homosynaptic) presynaptic LTP (Padamsey et al., 2017a) and LTD (Stanton et al., 2003). Here, I hypothesised that strong local activity leads to the production and release of large amounts of NO, which due to its gaseous nature, can diffuse to neighbouring presynaptic terminals to elicit presynaptic weakening.

NO production was blocked by bath application of 100 µM L-NAME, a selective inhibitor of NOS. This completely abolished heterosynaptic presynaptic LTD (ΔPr = -0.02 ± 0.06, N

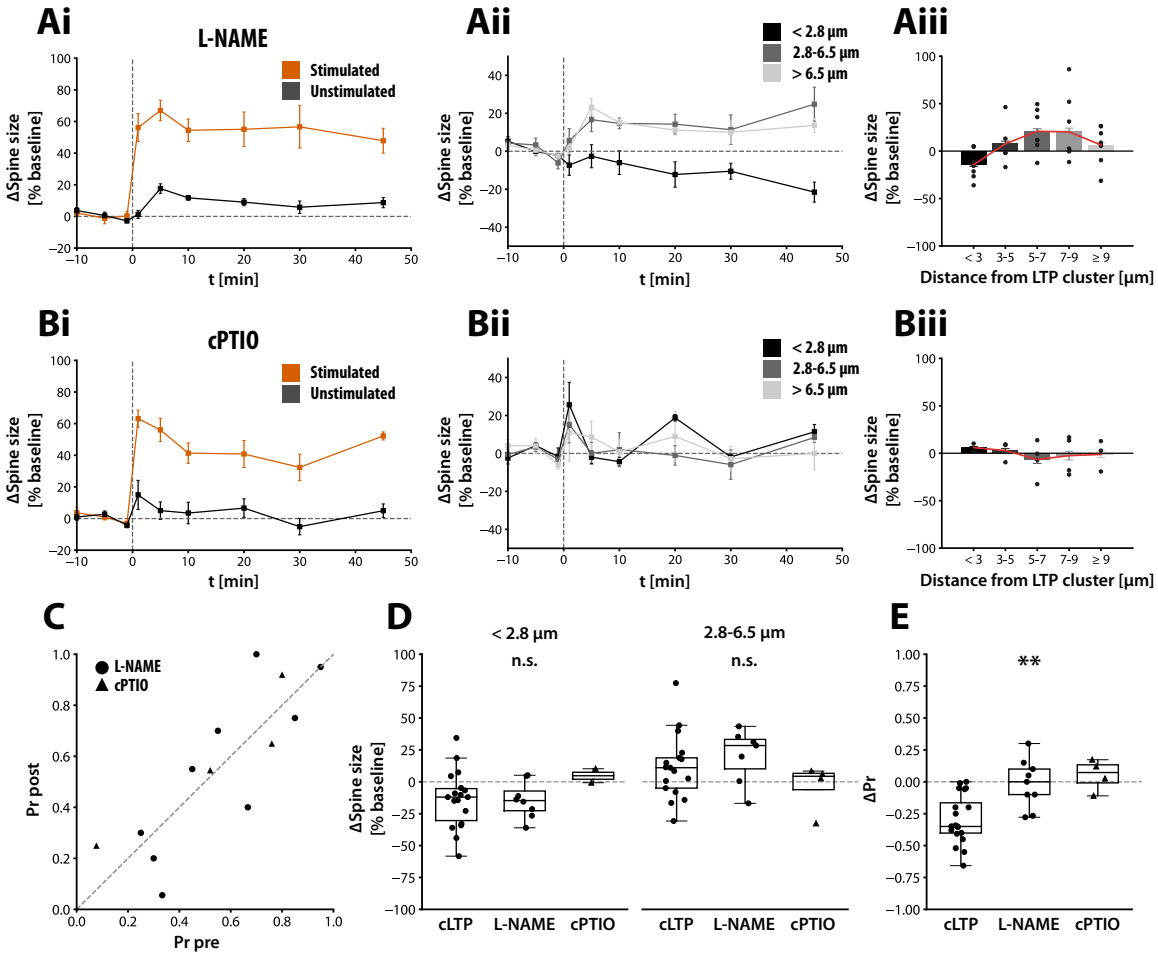

Fig. 5.5: Nitric oxide is the retrograde messenger for heterosynaptic presynaptic weakening. NO signalling was blocked by bath application of 100 µM L-NAME, a NOS inhibitor (A) or postsynaptic intracellular loading of 1 mM cPTIO, a NO scavenger (B). (Ai) Spine size changes of stimulated ($\Delta V_{30\text{-}45min}$ = 53.6 ± 9.5 %, N = 8) and unstimulated spines (ΔV_{10min} = 11.7 ± 1.4 %, $\Delta V_{30\text{-}45min}$ = 7.7 ± 2.7 %). (Aii) Spine size changes of unstimulated spines, grouped by distance (< 2.8 µm: $\Delta V_{30\text{-}45min}$ = -14.3 ± 4.7 %; 2.8-6.5 µm: $\Delta V_{30\text{-}45min}$ = 20.3 ± 6.9 %; > 6.5 µm: 11.7 ± 4.0 %). (Aiii) Spine size changes of unstimulated spine, grouped in 2 µm bins. Inhibition of NO production did not affect spine size changes of either stimulated or unstimulated spines. (Bi-iii) Postsynaptic scavenging of NO did not affect homosynaptic spine structural LTP ($\Delta V_{30\text{-}45min}$ = 39.2 ± 6.2 %, N = 4) but abolished heterosynaptic spine size changes. (C) Pr before and 30 min after the induction cLTP. Both L-NAME (spheres) and cPTIO (triangles) abolished heterosynaptic presynaptic weakening. (D) Summary of spine size changes. Spine size changes were not significantly different when NOS was inhibited. The number of experiments with cPTIO was not sufficient for statistical comparison. (E) Summary of presynaptic changes (cLTP: ΔPr = -0.29 ± 0.04, L-NAME: ΔPr = -0.02 ± 0.06, N = 8, $p < 0.01$, cPTIO: ΔPr =0.05 ± 0.05). L-NAME and cPTIO significantly abolished presynaptic weakening. Error bars represent SEM. Statistical significance was tested using Kruskal-Wallis H-test and *post hoc* Dunn's test and comparisons were done with the cLTP group.

= 8, $p < 0.01$, Fig. 5.5C,E). Similarly, application of the NO scavenger carboxy-PTIO (cPTIO) inside the postsynaptic cell prevented cLTP-induced presynaptic weakening ($\Delta Pr = 0.05 \pm 0.05$, N = 4), suggesting that NO is produced postsynaptically. In contrast, L-NAME did not affect cLTP induction and expression ($\Delta V_{30\text{-}45min} = 53.6 \pm 9.5$ %, N = 8), the transient increase in spine size immediately after induction ($\Delta V_{10min} = 11.7 \pm 1.4$ %), or the distance-dependent bi-directional regulation of spine size (Fig. 5.5A,D). In fact, the fraction of stimulated spines expressing stable structural LTP was significantly larger when NO production was inhibited (77.4 ± 4.5 % of spines with $\Delta V_{30\text{-}45min} > 20$ %, $p < 0.05$ vs. vehicle). Curiously, however, intracellular cPTIO completely blocked the expression of heterosynaptic spine size changes (Fig. 5.5B), the explanation of which is unclear (see Discussion). Taken together, presynaptic heterosynaptic weakening depends on postsynaptic production followed by retrograde diffusion of NO.

5.2.4. Heterosynaptic plasticity via electrical stimulation is expressed presynaptically and requires NO signalling

Experiments so far relied on an exogenous source of glutamate to activate synapses. Although glutamate photolysis was titrated with respect to physiological postsynaptic Ca^{2+}-responses, the spatiotemporal properties of the release mechanism itself might differ substantially. This could lead to potential confounds such as spill-over glutamate and excessive stimulation. Indeed, the strength of the photolysis pulse was purposely adjusted to be marginally lower than the physiological response in order to prevent excitotoxicity, which was sometimes observed as sustained elevation in intracellular Ca^{2+}-concentration following cLTP induction. Moreover, the lack of presynaptic activity at stimulated synapses made it difficult to assess potential presynaptic changes at these synapses. Lastly, although synaptic properties in organotypic slices are thought to be comparable to age-matched acute slices, there are considerable deviations in connectivity, synapse density, and the basal distribution of Pr.

In order to study heterosynaptic plasticity in a more physiological context, I devised an

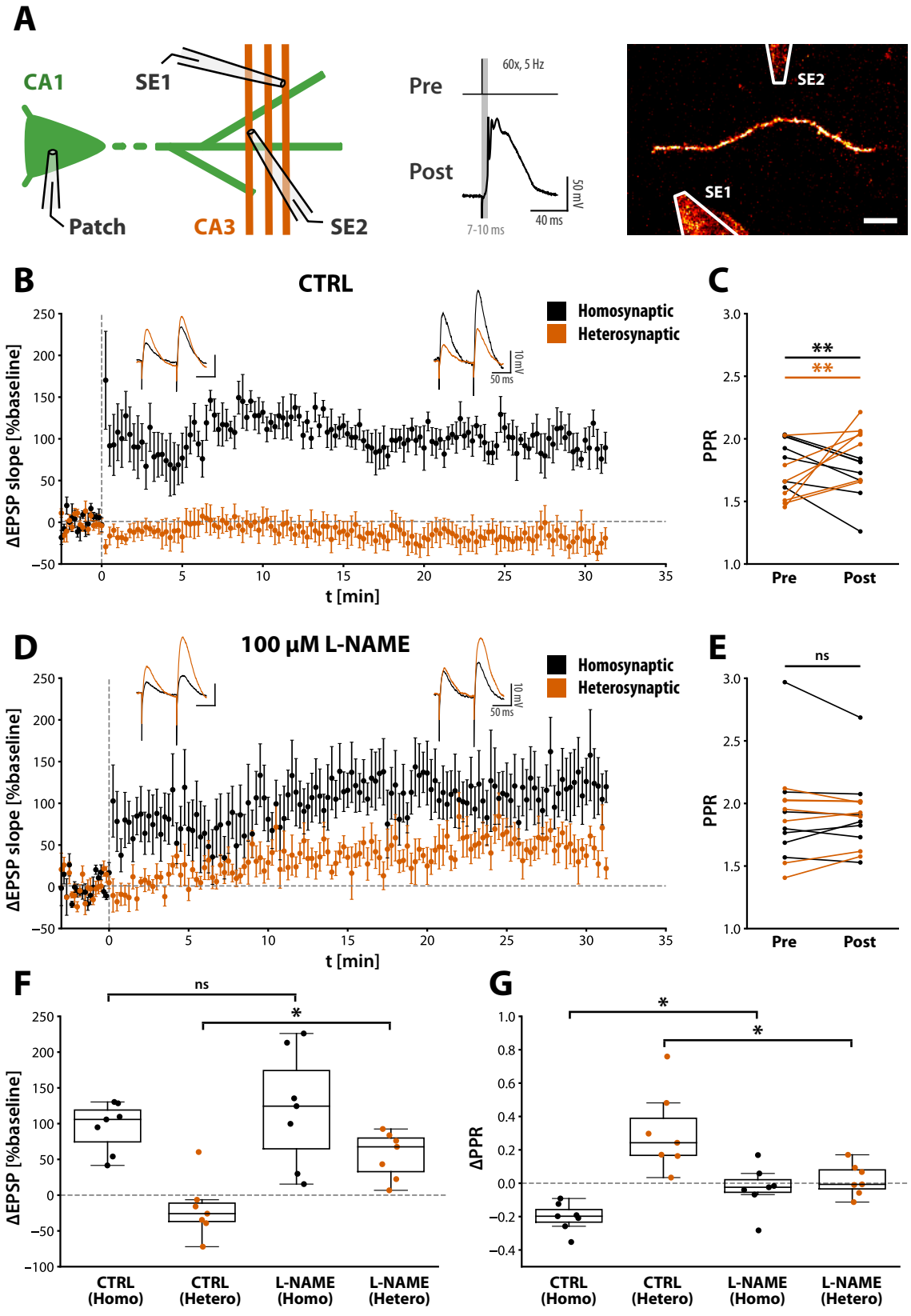

Fig. 5.6: Heterosynaptic LTD in acute hippocampal slices is expressed presynaptically and requires NO signalling. (A) Summary of the experimental setup. *Cont'd on next page.*

electrophysiological paradigm to mimic the optical setup in acute slice preparation, specifically the close spatial proximity of stimulated and unstimulated synapses. Fig. 5.6A shows the experimental setup: Along individual stretches of dendrites, identified by an intracellular fluorescent dye (AF488), I positioned two stimulation electrodes (SE) 10 - 40 µm apart in order to stimulate sets of synapses located close to each other. I used a cross-facilitation test to ensure the stimulation of independent pathways (see Methods 3.2.11.). I induced LTP in one pathway by pairing presynaptic stimulation with strong postsynaptic depolarisation via current injection, which elicited bursts of action potentials, 60 times at 5 Hz, a robust protocol used previously in our lab (Padamsey et al., 2017a). I then examined changes in the unstimulated pathway.

Induction of LTP led to an increase in the EPSP slope of the stimulated pathway (ΔEPSP = 94.9 ± 13.1 %, N = 7, Fig. 5.6B) and a decrease in PPR (ΔPPR = -0.203 ± 0.032, Fig. 5.6C), which was stable for at least 30 min, consistent with our previous findings (Padamsey et al., 2017a). This indicates a presynaptic expression locus. Conversely, the unstimulated pathway showed mild depression of the EPSP with an increase in PPR (ΔEPSP = -19.1 ± 15.4 %, ΔPPR = 0.307 ± 0.092). Heterosynaptic PPR changes were correlated with the

---

Fig. 5.6 cont'd (B) Induction of spike timing-dependent LTP led to long-lasting increase in the EPSP slope of the stimulated pathway ("Homosynaptic") and decrease in the EPSP slope of the unstimulated pathway ("Heterosynaptic"). Example traces illustrate the average EPSP waveform before LTP induction and during the last 5 min of the recording of the stimulated (black) and unstimulated (red) pathway. (C) PPR before and after the induction of LTP. The stimulated pathway showed a significant decrease of the PPR (Wilcoxon signed-rank test). Conversely, the PPR increased in the unstimulated pathway. (D) Bath application of 100 µM L-NAME abolished heterosynaptic LTD, but did not affect the magnitude of homosynaptic LTP. Spread of LTP was unmasked in the unstimulated pathway. (E) PPR changes of both, stimulated and unstimulated pathways, were abolished. (F) Summary of EPSP slope changes. (G) Summary of PPR changes. Statistical significance assessed using Mann-Whitney U test.

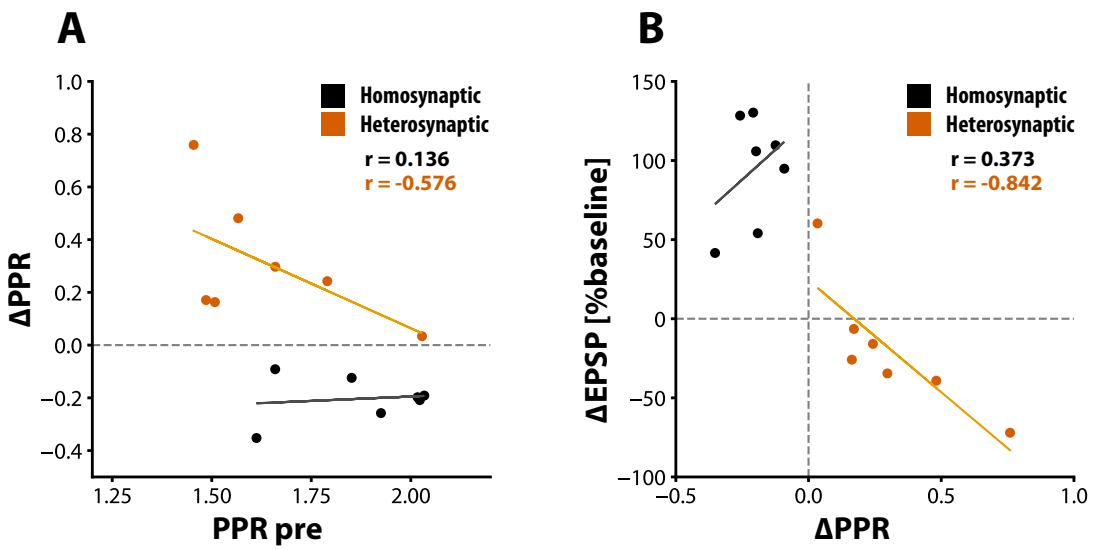

Fig. 5.7: Heterosynaptic plasticity in acute slices is predominantly presynaptic. (A) PPR changes in relation to the initial PPR. PPR changes of the stimulated pathway were independent of the initial PPR (Pearson r = 0.136, N = 7, n.s.). Heterosynaptic PPR changes showed moderate correlation, which was however not significant (r = -0.576, N = 7, n.s.). (B) PPR changes in relation to spine size changes. A strong correlation can be observed between PPR and spine size changes for the unstimulated pathway (r = -0.842, N = 7, $p < 0.05$), but not for the stimulated pathway (r = 0.373, N = 7, n.s.).

initial PPR, although not statistically significant (Pearson r = -0.576, n.s., Fig. 5.7A). Furthermore, the change in PPR was strongly correlated with the fractional change of the EPSP (Pearson r = -0.842, $p < 0.05$, Fig. 5.7B), which suggests that, under this paradigm, electrically induced heterosynaptic plasticity was mainly expressed as a decrease in release probability. In contrast, these correlations were substantially weaker for the homosynaptic pathway (Pearson r = 0.136, r = 0.373, respectively, n.s.), consistent with a concomitant postsynaptic expression locus. Inhibition of NOS via bath application of 100 µM L-NAME abolished the presynaptic changes of homosynaptic LTP (ΔPPR = -0.029 ± 0.052, N = 7, $p < 0.05$, Fig. 5.6E), consistent with recent findings from our lab (Padamsey et al., 2017a, see also Chapter 7), however, it did not affect the increase of the EPSP (ΔEPSP = 120.6 ± 30.7 %, n.s., Fig. 5.6D). The heterosynaptic increase in PPR was completely abolished and a moderately strong and stable potentiation of the EPSP was unmasked (ΔEPSP = 56.0 ± 12.3 %, ΔPPR = 0.020 ± 0.036, $p < 0.05$). NO signalling therefore

orchestrates both potentiation and depression of presynaptic strength in a context-dependent manner.

5.3. Discussion

I have shown, using pharmacological means, that the heterosynaptic bi-directional regulation of postsynaptic strengths depends on competing signalling pathways mediated by calcineurin and CaMKII. I was able to isolate potentiation and depression by inhibition of either calcineurin or CaMKII, respectively. My results also show that inhibition of NO production or diffusion blocks presynaptic heterosynaptic weakening. In addition, presynaptic weakening requires the activation of CaMKII. Blockade of NMDAR function completely abolished all hetero- or homosynaptic changes.

I collected an independent dataset for the vehicle control, which reproduced most findings reported in chapter 4. However, a major difference was the more pronounced spread of spine enlargement, albeit weak in magnitude, which was apparent for most of the observable segment of dendrite. Moreover, unstimulated spines increased in size immediately after cLTP induction and, on average, this increase was stronger than in the previous dataset. There were no significant differences in stimulation strength, the number or spatial arrangement of the stimulated spines, or the fraction of spines expressing stable LTP. The exact cause is therefore unclear. Differences in slice culture conditions or technical improvements might be possible explanations. I saw additional minor differences in the distance range obtained for clustering proximal and distal spines, which was sharper and therefore spanned a shorter distance (however, no qualitative difference was observed when using the distance range from chapter 4). In addition, spine size shrinkage in proximal spines was not distance-dependent (Suppl. Fig. 9.1B), unlike in the first dataset, which might reflect slightly altered experimental conditions, likely differences in glutamate photolysis.

5.3.1. What is the role of CaMKII and calcineurin signalling?

Stimulated synapses

I blocked CaMKII and calcineurin signalling pharmacologically by bath application of KN62 and FK-506, respectively. It is well-established that spine structural LTP requires the activation of CaMKII (Matsuzaki et al., 2004; Lee et al., 2009). Inhibition of CaMKII has been shown to partially or completely block the sustained phase of spine structural LTP (> 30 min), without affecting the initial transient increase (Matsuzaki et al., 2004; Lee et al., 2009). The reported incomplete block of sustained structural enlargement in the literature could be partially due to uncertainties of the concentration of KN62 when dissolved in aqueous solution. 3/10 of my experiments showed unimpaired structural LTP. In some experiments, I could see slight precipitation in the extracellular solution, which might have lowered the drug concentration. These experiments were discarded. Next, in my experiments, CaMKII inhibition diminished the transient and completely blocked the sustained phase of structural LTP (Fig. 5.2Bi). The diminished transient increase might reflect differences in the induction protocol I have used for spine structural LTP. Conventionally, structural LTP is induced in extracellular solution containing low concentration of Mg^{2+} in order to facilitate NMDAR function. This protocol leads to strong transient increase in spine size followed by rapid decay and stabilisation (Matsuzaki et al., 2004). This was not the case in my experiments, in which I directly depolarised the postsynaptic neurone via whole-cell patch clamp instead. Spine size increase was maximal at around 5 min after induction, but did not decay substantially and only slowly towards the end of the experiment. This is consistent with other studies using depolarisation as means of facilitating NMDAR function (Harvey & Svoboda, 2007; Tanaka et al., 2008). The main difference between these induction protocols is the electrochemical drive of Ca^{2+}-influx, which is theoretically stronger in the case of low extracellular Mg^{2+}, as the neurone is more hyperpolarised. Additionally, sustained depolarisation of the postsynaptic neurone via the patch pipette will prevent the initiation of dendritic spiking and can additionally lead to inactivation of voltage-gated

channels, such as L-type VGCCs, which might contribute to the initial increase in spine size. The degree of depolarisation using whole-cell patch clamp depends on the quality of the space clamp, which in turn is determined by the access conductance. The average access conductance during cLTP induction was Ga = 45.86 ± 2.56 nS and the distance of the stimulated cluster from the cell body was roughly 120 ± 10 µm. I have not, however, directly tested the degree of space clamp, for instance by examining the amplitude of electrically evoked EPSCs compared to resting membrane potential. I therefore cannot exclude the contamination of local dendritic spiking.

On the other hand, inhibition of calcineurin is generally thought to enhance LTP (Baumgärtel & Mansuy, 2012). My results show no indication of facilitation, such as differences in the overall magnitude of spine structural LTP or the fraction of spines that remained enlarged by the end of the experiment. This is in line with other studies examining the role of calcineurin in spine structural LTP (Oh et al. 2015; Wiegert & Oertner, 2013; Hayama et al., 2013). Moreover, there is no cross-talk between CaMKII and calcineurin activation, as FK-506 does not affect the magnitude of CaMKII activation (Fujii et al., 2013). A potential explanation could be that calcineurin exerts its inhibitory drive on the threshold for LTP induction rather than directly competing with its expression. Indeed, electrophysiological studies have shown that pharmacological or genetic blockade of calcineurin signalling lowers the threshold for LTP induction (Zeng et al., 2001; Malleret et al., 2001). Consequently, this implies saturation of the intensity of the induction protocol I have used in my study, which agrees with my observation that the protocol is prone to over-excitation leading to excitotoxicity. FK-506 was shown to also increase the baseline activity of CaMKII (Fujii et al., 2013), which could affect the propensity towards plasticity events. Since all measures of spine size in my study were normalised, a difference in the basal condition cannot be easily detected. If, for instance, an increase in basal CaMKII activity raises the mean initial spine size, and assuming that spine size is bounded on both sides, a difference in the variance of the basal distribution should be detectable. Calculating the coefficient of variation, σ/μ, which is scale invariant,

I found no differences across all conditions (Tab. 3.1). This could suggest that the basal spine size distribution might not differ. This would also further justify the normalisation procedure as a means of comparing across experiments.

Blockade of heterosynaptic LTD by FK-506 did not further enhance homosynaptic LTP (Fig. 5.2Ci). This might suggest that the induction of LTP could protect synapses from the depression signal mediated by calcineurin and that the two signalling pathways are not independent from each other. This would require further experimental investigation.

Unstimulated synapses

My results show that the bi-directional heterosynaptic regulation of spine size is regulated by two parallel signalling pathways, which are pharmacologically dissociable via inhibition of CaMKII and calcineurin. The dissociation should, in theory, allow me to make inferences on the underlying molecular mechanisms and diffusion properties. Inhibition of calcineurin revealed a potentiation signal, very likely dependent on molecules downstream of CaMKII, as CaMKII completely abolished heterosynaptic spread of LTP. The potentiation was however not distance-dependent. As discussed in chapter 4, assumptions imposed on by the distance metric strongly affect the biological interpretation. When I used the distance to the closest stimulated spine instead, I found a strong negative correlation between distance and sustained spine size increase (spines located 0-5 µm from closest stimulated spine: Pearson $r = -0.326$, $p < 0.05$, empirical confidence intervals under alpha=0.05 [-0.557, -0.078]). Most parsimoniously, this suggests that the potentiation signal originates from the stimulated spines, diffuses into the dendrite and is rapidly inactivated. This could explain why the distance range of strongest heterosynaptic spine enlargement corresponds to the distance to the edge of the stimulated cluster, as these spines should experience the strongest potentiating signal relative to a depressing signal.

On the other hand, inhibition of CaMKII revealed that the depression signal, which involves calcineurin, is unlikely to be strongly distance-dependent (Fig. 5.2Biii), however,

the low sample number and effect size make it difficult to come to concrete conclusions. Consistent with my previous results, absolute spine size changes of proximal spines, including the stimulated spines, under CaMKII inhibition were negatively correlated with the initial spine size (spine < 6.5 µm: Pearson r = -0.525, N = 93, p < 0.05) unlike the potentiation in FK-506 (Pearson r = -0.066, N = 120, n.s.) again suggesting mechanistic differences and state-dependent LTD. Interestingly, the transient increase in spine size following cLTP induction was still observed under CaMKII inhibition, albeit weaker in magnitude. This could either indicate incomplete CaMKII blockade or a CaMKII independent mechanism. Calcineurin inhibition did not further increase the transient enlargement.

5.3.2. What are the spatiotemporal properties of calcineurin and CaMKII signalling?

The activation of both CaMKII and calcineurin following glutamate photolysis have been studied using Förster resonance energy transfer (FRET) probes (Fujii et al., 2013; Lee et al., 2009; Takao et al., 2005). CaMKII activation is highly supralinear with respect to stimulation frequency and number and spatially restricted to the spine head due to fast inactivation constant (Fujii et al., 2013). Moreover, postsynaptic depolarisation alone can activate a potentially distinct pool of CaMKII in spines via L-VGCCs and the dendritic shaft via mainly non L-type VGCCs (Lee et al., 2009). In contrast, calcineurin activation is sublinear and independent of stimulation frequency and not restricted to the stimulated spine, although a precise quantification of the diffusion properties is lacking. According to the study by Fujii and colleagues, high-frequency (20 Hz) but not low-frequency (5 Hz) stimulation of a single spine led to detectable activated of calcineurin up to 3-4 µm from the stimulation site.

The biochemical signalling network that leads to the activation of calcineurin and CaMKII is highly interwoven as both require the binding of calmodulin. Theoretical studies have shown that competition between CaMKII and calcineurin for calmodulin can lead to bi-phasic activation profiles dominated by either CaMKII or calcineurin (Romano et al., 2017;

Li et al., 2012), and thus the expression of LTP or LTD. Interestingly, studies have shown changes in the sub-cellular localisation of CaMKII and calcineurin following strong stimulation (Penny & Gold, 2018). Under basal, naive conditions, calcineurin is closely anchored to NMDAR Ca^{2+}-microdomains through the interaction with AKAP proteins. Upon stimulation, calcineurin is relocated into the cytoplasm followed by the recruitment of activated CaMKII. Under this framework, spatial proximity to the postsynaptic density might determine the dominating signalling cascade. Moreover, activated calcineurin released into the cytoplasm enables it to diffuse into the dendritic branch and influence neighbouring synapses.

My results suggest that the potentiating signal is CaMKII and NMDAR-dependent and diffuses from the stimulated spines and therefore distinct from the CaMKII subset activated by depolarisation alone. Activation of CaMKII via L-VGCCs can further be excluded due to the quick inactivation of L-VGCC at depolarised membrane potentials. The spatial spread of active calcineurin agrees with the spread in heterosynaptic spine shrinkage in my experiments, which was restricted to 2-3 µm. In addition, the recruitment of activated CaMKII and dissociation of calcineurin from the postsynaptic density might explain the protection of stimulated spines against spine shrinkage. Since CaMKII does not invade the dendritic branch (Fujii et al., 2013; Lee et al., 2009), the diffusible potentiating signal must lie downstream of CaMKII signalling.

5.3.3. What are the downstream signalling pathways engaged by calcineurin and CaMKII?

The role of calcineurin in LTD is well established (Baumgärtel & Mansuy, 2012). Calcineurin was shown to dephosphorylate Ser845 of GluA1, which leads to AMPA receptor internalisation. Furthermore, calcineurin and its downstream target striatal enriched protein phosphatase (STEP) were shown to regulate NMDAR number and subunit composition (Pelkey et al., 2012; Braithwaite et al., 2006). Calcineurin has also been shown to dephosphorylate cofilin, an important regulator of actin polymerisation

(Zhou et al., 2004; Wang et al., 2005b; Kurz et al., 2008; Hayama et al., 2013). Dephosphorylation of cofilin leads to destabilisation of the actin network and ultimately spine shrinkage. Interestingly, this pathway has been implicated in spine loss during epileptic seizure, which could present an exacerbated condition compared to strong coordinated activity (Kurz et al., 2008). Inhibition of cofilin phosphorylation leads to increased spontaneous spine shrinkage (Zhou et al., 2004), which is consistent with my observation of a negative skew in spine size changes of proximal spines. It is therefore likely that heterosynaptic postsynaptic LTD is mediated by calcineurin-dependent dephosphorylation of cofilin and depolymerisation of actin bundles.

The downstream signalling network of CaMKII has been extensively studied and comprises a vast network of substrates. Of particular interest are small GTPases, such as H-Ras, RhoA, and Rac1, which are involved in the regulation of the cytoskeleton and have been reported to diffuse over short distances along the dendrite (Harvey et al., 2008; Oliveira & Yasuda, 2014; Murakoshi et al., 2011; Hedrick et al., 2016). H-Ras, RhoA, and Rac1 are activated by NMDAR and CaMKII-dependent pathways locally at stimulated spines, upon which they diffuse along the dendrite and into neighbouring spines up to 10 µm away. All three GTPases are implicated in heterosynaptic metaplasticity, which leads to facilitated LTP induction (Harvey & Svoboda, 2007; Hedrick et al., 2016). Diffusion properties have been determined as the mean distance travelled before inactivation (length constant L) by measuring inactivation time constant and diffusion constant using FRET-based activity sensors and the decay of photoactivatable GFP, respectively. The length constant of H-Ras was estimated to be $L_{H\text{-}ras}$ = 11 µm, whereas Rho-A and Rac1 were more spatially constrained with L_{RhoA} = 4.5 µm (the length constant for Rac1 was not explicitly stated; diffusion constant is similar to RhoA, whereas inactivation time constant seems slightly larger. It is therefore likely that $L_{RhoA} < L_{Rac1} < L_{H\text{-}ras}$). These differences are thought to arise from the inactivation time constant. My results suggest that the potentiation factor is spatially constrained to ~ 4-5 µm from the closest stimulated spine, which matches the length constant of RhoA and potentially Rac1. The putative signalling

cascade downstream of RhoA activation is thought to involve activation of ROCK and LIM kinase, which in turn leads to phosphorylation of cofilin and assembly of actin bundles (Rex et al., 2009; Murakoshi et al., 2011). However, RhoA activity is also heavily implicated in spine shrinkage and pruning (Ryan et al., 2005; Kang et al., 2009; Fu et al., 2007; Govek et al., 2005). Activation of Rac1 also leads to the phosphorylation of cofilin and stabilisation and polymerisation of actin (Bamburg, 1999; Lai & Ip, 2013) and has been shown to additionally require activation of Ca^{2+}-permeable AMPA receptors (Fortin et al., 2010) and postsynaptic BDNF-TrkB receptors (Hedrick et al., 2016). Taken together, activation of NMDARs and CaMKII leads to diffusion of various small GTPases that converge onto the regulation of the actin cytoskeleton via cofilin. This might lead to the spread in spine enlargement observed in my experiments. Spine shrinkage via calcineurin could be mediated by dephosphorylation of cofilin. Alternatively, calcineurin-dependent AMPA receptor internalisation might cause spine shrinkage.

5.3.4. Comparison with the literature

Heterosynaptic postsynaptic plasticity has been studied in the context of local structural plasticity along dendritic branches (Oh et al., 2015; Harvey & Svoboda, 2007; Harvey et al., 2008; Govindarajan et al., 2011; Wiegert & Oertner 2013; El-Boustani et al., 2018; Bian et al., 2015; Holbro et al., 2009; Hayama et al., 2013; Letellier et al., 2019) and both, compensatory and non-compensatory forms have been reported. The heterosynaptic weakening in my experiments is consistent with the observations by Oh and colleagues. In their study, groups of 6-8 spines were sequentially potentiated using glutamate photolysis, which led to heterosynaptic shrinkage of spines located within the stimulated cluster. No structural change was reported for spines located outside. Spine shrinkage required spines to be located inside the stimulated cluster within 3.4 µm, measured as the average pairwise distance to stimulated spines. Since the mean pairwise distance corresponds to the distance from the centre of mass for spines outside the stimulated cluster, my study has extended the distance analysis for spines located within to reveal a potential fine scale distance-dependency of spine shrinkage (Fig. 4.4B), which was

however absent in the second dataset (Suppl. Fig. 9.1). Oh and colleagues also report a correlation between the magnitude of heterosynaptic spine shrinkage and the number of stably potentiated spines. I did not find any correlation with magnitude or fraction of potentiated spines. Consistent with my findings, spine shrinkage was found to depend on calcineurin and to be independent of CaMKII signalling and inhibition of calcineurin via FK-506 led to the expression of heterosynaptic spine enlargement. Additionally, IP3R, and mGluR signalling were implicated as well. A major discrepancy to my work is the LTP induction protocol. Oh and colleagues induced structural LTP by photolysis of glutamate in low extracellular Mg^{2+} and in the presence of TTX and photolysis was repeated sequentially for each spine. In contrast, spines in my experiments were quasi-synchronously stimulated and paired with postsynaptic depolarisation in the absence of TTX, since a presynaptic readout was necessary. The lack of heterosynaptic spread of LTP that Oh and colleagues report might be due to differences in the activation of CaMKII, which is known to be sensitive to stimulation frequency, whereas calcineurin is sensitive to the number of stimulation pulses (Fujii et al., 2013). With sequential stimulation, the effective stimulation frequency is the frequency of photolysis itself (1-2 Hz). When synchronously stimulated, crosstalk between synapses, for instance via diffusion of Ca^{2+} or direct electrical influence, increases the effective frequency to a maximum of 500 Hz (time between stimulation ~ 2.2 ms). The absence of heterosynaptic weakening during single spine stimulation could be explained by the decreased number of stimulation pulses. Thus, the sign of postsynaptic heterosynaptic plasticity crucially depends on stimulation frequency and number. Interestingly, a recent study reported bi-directional heterosynaptic structural plasticity following the induction of homosynaptic LTD (Letellier et al., 2019). Similar to my findings, proximal spines were found to shrink whereas spines > 10 µm away increased in size. For future work, it would be interesting to systematically vary number and mode of stimulation (sequential vs. simultaneous) in order to untangle the underlying biochemical dynamics.

Both, El-Boustani and colleagues and the study by Govindarajan and colleagues

implicated local translation as a means of heterosynaptic interaction. In one case, shifts in the receptive field of V1 pyramidal neurones were correlated with the potentiation of spines accompanied by weakening of neighbouring spines, which required the immediate early gene Arc. On the other hand, protein-synthesis dependent structural LTP, induced by pairing glutamate photolysis with direct activation of adenylyl cyclase via forskolin, was shown to facilitate subsequent LTP at neighbouring spines, and was dependent on the distance between the spines. In my experiments, protein synthesis dependent mechanisms were unlikely to play an important role due to the short timescale and the lack of direct adenylyl cyclase activation.

Wiegert and Oertner reported that postsynaptic spine elimination was negatively correlated with the release probability, suggesting that high release probability can act protectively, consistent with a recent study on electrophysiological forms of LTD (Sanderson et al., 2018). I have also observed potential cross-talk between pre- and postsynaptic terminals when I inhibited NO production, which enhanced structural LTP at stimulated spines (Fig. 5.5A). This is in line with the observation that presynaptic heterosynaptic weakening is positively correlated with the magnitude of structural LTP of the stimulated cluster (Fig. 4.8F).

Taken together all observations, the most parsimonious biochemical model involves the local diffusion of calcineurin and CaMKII dependent signalling molecules along the dendritic branch (Fig. 5.8). Invasion of calcineurin into neighbouring spines leads to state-dependent spine shrinkage, potentially via dephosphorylation of cofilin or internalisation of AMPARs. CaMKII likely activates small GTPases that can diffuse out of the stimulated synapse. These GTPases can stimulate the polymerisation of actin bundles and lead to spine enlargement. The bi-directional spatiotemporal pattern results from difference in diffusion and kinetic properties of these molecules and their potential competitive interaction. Diffusion of both, calcineurin and CaMKII-dependent signalling molecules is restricted to several µm around the stimulated synapse cluster. Diffusion of CaMKII-dependent signalling molecules is constrained by fast inactivation, whereas

calcineurin possesses a high activation threshold and therefore requires spatiotemporal summation. Potentiation and depression are likely to compete with each other as CaMKII activation protects stimulated synapses from calcineurin-dependent spine shrinkage.

5.3.5. What is the retrograde messenger for presynaptic weakening?

I have shown that the retrograde messenger for presynaptic heterosynaptic LTD is NO. Inhibition of NO production or the addition of NO scavengers completely abolished presynaptic LTD, measured both optically and electrophysiologically. In addition, I found that NMDAR and CaMKII signalling were required.

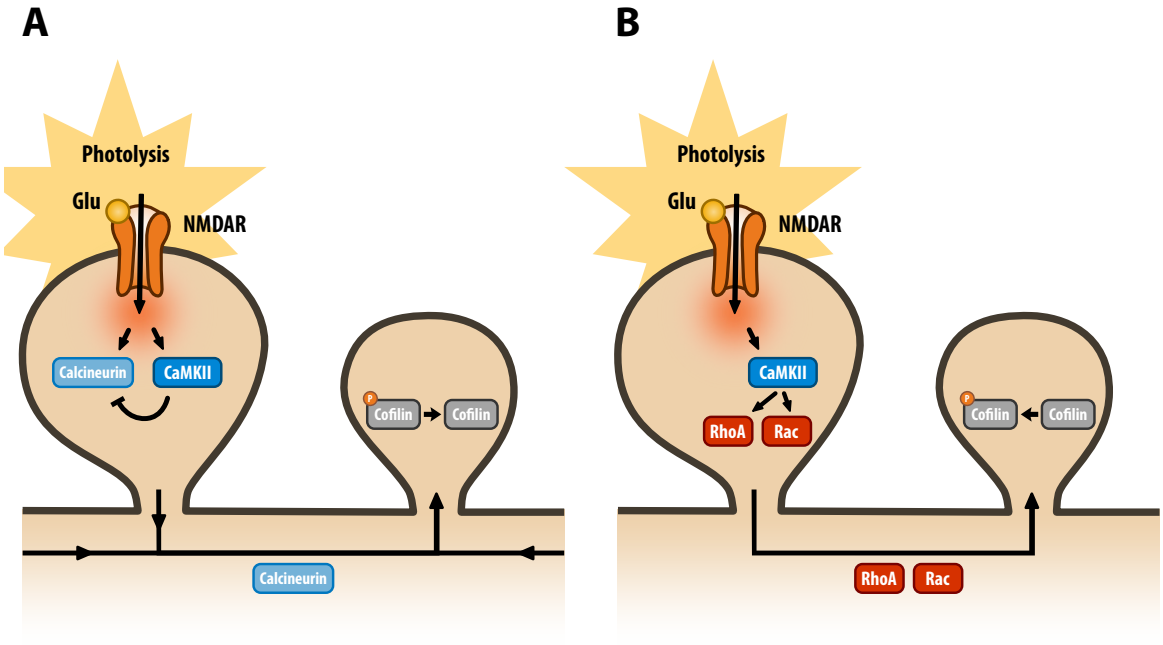

Fig. 5.8: Proposed molecular mechanism of postsynaptic heterosynaptic plasticity along local dendritic segments. (A) Mechanism for heterosynaptic spine shrinkage. Strong stimulation of the postsynaptic terminal leads to NMDAR-dependent Ca^{2+}-influx and the activation of CaMKII and calcineurin. Calcineurin diffuses into the dendritic branch and into neighbouring spines. Accumulation of calcineurin from multiple sources above a certain threshold leads to spine shrinkage, potentially via the dephosphorylation of cofilin resulting in the destabilisation of the actin cytoskeleton. Locally, CaMKII competes with calcineurin signalling and prevents spine shrinkage. (B) Mechanism for heterosynaptic spine enlargement. Activation of CaMKII at stimulated spines activates small GTPases, such as RhoA and Rac. RhoA and Rac diffuse into neighbouring spines where they phosphorylate cofilin inducing actin polymerisation and spine enlargement.

It is well-documented that NMDAR-dependent Ca^{2+}-influx can lead to NO production via nNOS (Garthwaite et al., 1988). nNOS is mainly localised to the PSD (Brenman et al., 1996; Valtschanoff & Weinberg, 2001) due to an interaction with PSD-95 via its PDZ-domain (Rameau et al., 2004) and can be found in ~ 50 % of synapses in developing neurones, including GABAergic synapses (Cserép et al., 2011). The activation of nNOS requires binding of calmodulin, whereas CaMKII-dependent phosphorylation of Ser847 leads to inactivation and decreased NO production. This seems to be at odds with my findings that CaMKII inhibition abolishes presynaptic LTD. A detailed look at the enzymatic cycle of nNOS suggests that phosphorylation of Ser847 might be necessary for the proper regeneration of nNOS (Rameau et al., 2007) and dysregulation could therefore lead to altered spatiotemporal profile and thus lowered NO production following a temporal sequence of activation. Alternatively, NO is able to directly activate CaMKII (Gutierrez et al., 2013; Curran et al., 2014; Coultrap & Bayer, 2014). In this case, CaMKII signalling is downstream and would be located presynaptically. This would require further investigation.

Intracellular sequestering of NO via cPTIO abolished presynaptic LTD and indicates that NO production occurs in the postsynaptic neurone. However, cPTIO also prevented the expression of postsynaptic heterosynaptic spine size changes, which I did not observe when using L-NAME. cPTIO scavenges NO by formation of NO2 and cPTI, however the mechanistic profile is thought to be more elaborate (Pfeiffer et al., 1997). For instance, cPTIO enhances S-nitrosation by peroxynitrites (Pfeiffer et al., 1997). In addition, cPTI can have off-target effects, as seen in a reduction in dopamine uptake (Cao & Reith, 2002). The exact target of cPTI is however unknown. It is therefore possible that the inhibition of postsynaptic heterosynaptic plasticity is due to off-target effects.

The role of NO in heterosynaptic plasticity is not well-studied. Volgushev and colleagues, in a series of studies, have provided evidence for a modulatory role of NO in cortical heterosynaptic plasticity (Volgushev et al., 2000; Lee et al., 2012). They showed that intracellular tetanisation leads to the expression of both, heterosynaptic LTP and LTD, the

direction of which was negatively correlated with presynaptic strength, indirectly measured as PPR. When NO signalling was blocked, this correlation was completely abolished. NO signalling was therefore suggested to play a metaplastic role. In addition, NO was only involved during strong but not weak tetanisation, which was interpreted as a high activation threshold. However, presynaptic changes were not blocked by NO inhibitors. In my study, presynaptic weakening was strongly dependent on the initial Pr, but NO was necessary for the expression of presynaptic changes. This suggest a potential modulatory role of NO, in which a certain threshold of NO is required to initiate presynaptic signalling networks, but the magnitude of change is independent of NO itself. Volgushev and colleagues still observed presynaptic changes when NO signalling was blocked. A potential explanation could be the involvement of distinct pools of nNOS coupled to either NMDARs or L-VGCCs. Intracellular tetanisation does not activate NMDAR and NO is likely produced solely by a L-VGCC dependent mechanism. On the other hand, in my experiment, L-VGCCs are likely inactivated following the prolonged depolarisation during cLTP induction, and the majority of NO should in theory be produced by NMDAR-dependent nNOS. This could also explain why I did not observe heterosynaptic changes with postsynaptic depolarisation alone.

NO has traditionally been studied in the context of presynaptic LTP. Others have reported a role for NO in presynaptic LTD, when paired with LFS (Zhuo et al., 1994, Reyes-Harde et al., 1999; Stanton et al., 2003; Gage et al., 1997). Direct activation of downstream cGMP pathways (paired with inhibition of PKA signalling) mimics NO-dependent LFS-LTD (Stanton et al., 2001), suggesting that this form of LTD can be induced independently of presynaptic activity. Indeed, we have recently shown that photolysis of caged NO dialysed into the postsynaptic neurone leads to the expression of LTD when presynaptic stimulation did not occur in a causal manner (Fig. 5 suppl. 2 in Padamsey et al., 2017a). LTD was accompanied by a mild increase in the PPR. However, application of cPTIO only partly abolished the decrease in EPSP or increase in PPR, indicating either incomplete blockade by cPTIO, or additional off-target effects by the photolysis procedure.

Interestingly, focal photolysis of NO directly at single synapses did not lead to presynaptic weakening (Padamsey et al., 2017a). This could suggest that the trigger for heterosynaptic presynaptic LTD might require a certain threshold amount of NO.

In summary, there is good evidence for NO as a bi-directional regulator of presynaptic strengths. The varied results reported in the literature are likely due to complex spatiotemporal dynamics of NO signalling, as seen in the complex activation cycle of nNOS, and differences in plasticity induction protocols used (Arancio et al., 2001). However, I did not exclude the involvement of other retrograde signalling molecules in my study and both, eCBs or BDNF/proBDNF could act in parallel or in concert to induce presynaptic heterosynaptic LTD.

5.3.6. What is the spatiotemporal profile of NO signalling?

NO is thought to be mainly produced at the synapse. Due to the low molecular weight and high lipid solubility, NO can easily cross the plasma membrane and diffuses rapidly (diffusion constant = 3.3 $\mu m^2 ms^{-1}$) and radially from its origin of production (Garthwaite, 2016). Several studies have simulated the diffusion of NO produced at synapses (Garthwaite, 2016; Philippides et al. 2000; Lancaster, 1994; Schweighofer & Ferriol, 2000; Wood & Garthwaite, 1994). Diffusion of NO is mainly restricted by inactivation mechanisms, which are thought to depend on cytochrome p450 oxidoreductase (Hall & Garthwaite, 2009). Inactivation is rapid but saturable, with a Michaelis constant of Km = 10 nM and therefore suggests a crucial role for spatial and temporal summation of NO release (Hall & Garthwaite, 2006). NO produced at single synapses, which reaches concentrations far below Km of the inactivation mechanism, is thought to exhibit sharp spatial profiles that fall off within 1 µm of the synapse (Garthwaite, 2016) and is therefore unlikely to reach neighbouring synapses. However, at higher concentrations, inactivation saturates resulting in a steady build-up of NO, thus extending the range of NO diffusion.

In my experiments, distance did not predict the magnitude of presynaptic changes. Instead, I observed a sharp drop-off of the success rate of presynaptic heterosynaptic LTD

at ~ 4 µm. This could suggest that the retrograde signal is fully saturated at close range and the sharp drop is caused by the rapid inactivation of the retrograde messenger. Assuming that the signal is produced and released at active synapses, a possible explanation would be the effective increase in diffusivity within the region of stimulated synapses due to a saturation of the inactivation mechanisms caused by excessive amount of released messenger molecules. This spatial profile is in line with simulation studies that include multiple production sources and report a "box-like" profile of NO diffusion (*e.g.* see Fig. 3 in Garthwaite, 2016).

The difference in the diffusion mechanism between NO and the intracellular factors involved in postsynaptic heterosynaptic plasticity, especially differences in their inactivation, gives rise to a potential explanation for the predominantly presynaptic expression locus I observed using electrophysiological techniques (Fig. 5.6). Using electrical stimulation, the location of stimulated synapses cannot be controlled and are therefore randomly situated along the dendrite, which increases the pairwise distance to the stimulated synapses. Since inactivation of NO is sublinear at high enough concentrations, which can be reached by summation of multiple sources, the cooperation between NO producing sources can be extended spatially as long as the pairwise distance does not exceed some critical distance. In Garthwaite's simulation, the critical distance was between 2-4 µm (Garthwaite, 2016), but the exact number strongly depends on the rate of NO production and the precise inactivation mechanism. Therefore, as long as synapses are activated every 2-4 µm, sufficient NO should reach all synapses along the dendrite. In contrast, if the inactivation of intracellular factors is linear (*e.g.* through self-inactivation mechanisms), cooperation between synapses is minimal and activity will scale strongly with distance and therefore deteriorate. When I blocked presynaptic heterosynaptic LTD using L-NAME, I observed the unmasking of an underlying heterosynaptic postsynaptic potentiation. Following the above interpretation, this could be caused by a difference in diffusion constant between calcineurin and CaMKII-dependent pathways, rendering calcineurin more sensitive to

distance.

5.3.7. What are the downstream signalling pathways engaged by NO to regulate presynaptic strength?

The main downstream target of NO is the activation of sGC, which leads to the production of cGMP and activation of PKG. Both, cGMP and PKG have multiple presynaptic targets involved in regulating release probability (Hardingham et al., 2013). The NO-sGC-PKG pathway has been strongly implicated in presynaptic LTP (Arancio et al., 1995, 1996, 2001). PKG was shown to target a range of proteins including direct phosphorylation of Ca^{2+}-channels (Huang et al., 2003; Yang et al., 2007; Jiang et al., 2000), Ca^{2+}-activated K+-channels (Klyachko et al., 2001; Sausbier et al., 2000; Alioua et al., 1998; Fukao et al., 1999), and modulating CICR from internal stores of both ryanodine (Willmott et al., 1996; Dries et al., 2016; Takasago et al., 1991) and IP3R-gated stores (Haug et al., 1999; Murthy & Zhou, 2003; Schlossmann et al., 2000; Ammendola et al., 2001). In addition, PKG regulates neurotransmitter vesicle recycling (Eguchi et al., 2012; Micheva et al., 2001) and the RRP size (Stanton et al., 2003, 2005; Ratnayaka et al., 2012). In addition, cGMP can directly activate cyclic nucleotide-gated channels (CNGs) or hyperpolarisation-activated cyclic nucleotide-modulated channels (HCNs), which are non-selective cation channels and are thought to mainly enhance the release of neurotransmitters (Neitz et al., 2011). At sufficiently high concentrations, NO can also nitrosylate the thiol group of cysteine, a modification which has been detected in various synaptic proteins *in vivo*, although mainly in the context of glutamate receptor regulation (Jaffrey et al., 2001; Huang et al., 2005).

As pointed out above, CaMKII is likely to be downstream of NO signalling due to its known inhibitory role on NO production. CaMKII is expressed at both pre- and postsynaptic terminals (Gorelick et al., 1988; Walaas et al., 1989; Ouimet et al., 1984). Presynaptic CaMKII has been implicated in both potentiation (Ninan & Arancio, 2004; Waxham et al., 1993; Nichols et al., 1990; Lu & Hawkins, 2006) and depression (Stanton & Gage, 1996; Hinds et

al., 2003; Hojjati et al., 2007) of presynaptic strengths (Wang, 2008). Interestingly, the bi-directional regulation profile of CaMKII might be explained by enzymatic and non-enzymatic functions of CaMKII, since blocking kinase activity alone was not enough to abolish its inhibitory effects on presynaptic release (Hojjati et al., 2007). The same study showed that complete KO of presynaptic CaMKII increased the number of docked vesicles, which was not seen with targeted mutations that prevented the autophosphorylation of CaMKII. Next, Stanton and colleagues have proposed a putative model for NO-dependent LTD at Schaffer-collateral CA1 synapses that involves the activation of presynaptic internal stores via PKG, ADPribosyl cyclase, and the RyR, which required concurrent activation of presynaptic CaMKII (Reyes-Harde et al., 1999; Stanton & Gage, 1996; Gage et al., 1997). In their model, CaMKII is activated by VGCCs during LFS, however, activation of CaMKII could also occur via Ca^{2+} originating from RyR-gated stores (Shakiryanova et al., 2011). Accordingly, a recent study showed that hippocampal LFS-LTD is accompanied by CaMKII-dependent phosphorylation of synapsin I, which was blocked when RyRs were desensitised by prior application of ryanodine (Arias-Cavieres et al., 2018).

I therefore suggest two possible signalling pathways for heterosynaptic presynaptic LTD (Fig. 5.9). (1) Coordinated activation of groups of synapses leads to Ca^{2+}-influx through NMDAR, activation of nNOS and production of NO. Spatiotemporal summation of NO allows it to diffuse to the presynaptic terminal of neighbouring synapses, where it activates sGC and potentially CaMKII. cGMP-dependent pathways lead to CICR from RyR-gated stores and increased phosphorylation of synapsin I. This leads to a reduction in Pr. Alternatively, CaMKII activation alone is known to reduce the RRP size independent of synapsin I phosphorylation (Hojjati et al., 2007). (2) In the second case, postsynaptic CaMKII activation would be crucial for modulating the spatiotemporal pattern of nNOS activity in order for NO to reach the presynaptic terminal. At the presynaptic terminal, downstream signalling pathways of NO lead to the decrease in Pr.

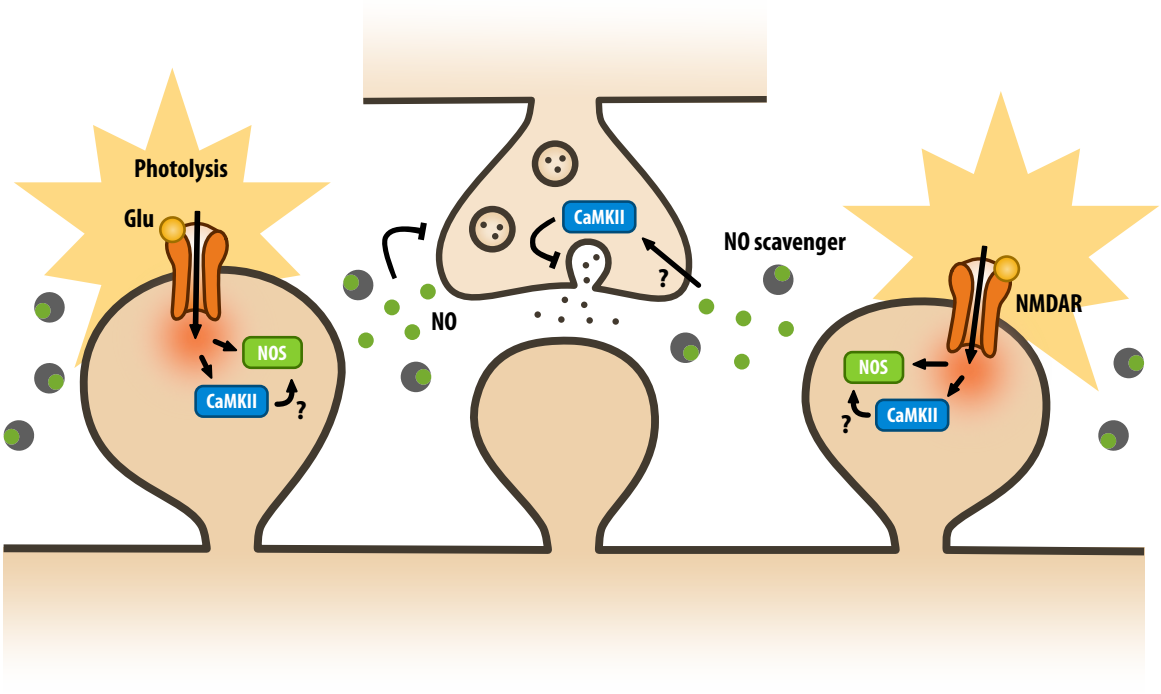

Fig. 5.9: Proposed molecular mechanism of presynaptic heterosynaptic plasticity along local dendritic segments. Strong stimulation of the postsynaptic terminal leads to NMDAR-dependent Ca^{2+}-influx and activation of NOS. Postsynaptic CaMKII potentially modulates NOS function by phosphorylation of Ser847. NO diffuses into the extracellular space and is rapidly inactivated by endogenous scavengers, such as cytochrome p450 oxidoreductase. Saturation of scavengers by prolonged NO release from multiple sources allows NO to reach the presynaptic terminal of neighbouring synapses. At the presynaptic terminal, NO can act either via direct activation of CaMKII or the activation of sGC, production of cGMP, and activation of PKG-dependent signalling pathways. This ultimately leads to a decrease in Pr.

5.4. Conclusion

I have characterised the expression locus of heterosynaptic plasticity along local dendritic segments. Imposing strong coordinated activity led to diverse long-lasting changes in pre- and postsynaptic strength, which were spatially restricted, therefore confirming local organising principles. I have predicted that coordinated activity should reveal underlying competitive processes. For postsynaptic strength, I have observed a reorganisation of synaptic strength in a centre-surround manner. Competition is

therefore spatially restricted and perhaps suggests that dendritic branches can be further subdivided into functional units. Presynaptic changes were compensatory and only weakly correlated with postsynaptic changes. Both pre- and postsynaptic weakening were state-dependent and can be understood as a homeostatic mechanism with a single stable fixed point.

The spatial properties of heterosynaptic plasticity can be understood by the intra- and extracellular diffusion of signalling molecules. Biochemical differences in their diffusion constant, inactivation, scavenging, and competitive interactions result in rich and complex spatial profiles. Intracellular diffusion of calcineurin and potentially CaMKII-activated small GTPases orchestrate postsynaptic plasticity, whereas postsynaptically produced NO acts as a retrograde messenger to engage presynaptic signalling networks, potentially involving presynaptic CaMKII and PKG signalling.

The crosstalk between synapses indicates that neural information processing is not restricted to the synapse but instead distributed over segments of dendrite forming fundamental processing units. The disjunct regulation of pre- and postsynaptic strength emphasises the distinct and partly independent contributions to information processing. This further increases the information processing capacity of individual processing units. Synaptic crosstalk is unlikely to be restricted to the spatial scale studied in my experiments and future work is needed to uncover its full extent.

6. Presynaptic NMDA receptor-dependent short- and long-term plasticity at Schaffer-collateral terminals

6.1. Introduction

Presynaptic (glutamatergic) terminals express a range of glutamate receptors, which sense glutamate release in an autocrine manner to regulate presynaptic strength, both in the short- and long-term (Pinheiro & Mulle, 2008). Presynaptic NMDARs (preNMDAR) have been shown to both facilitate and inhibit neurotransmitter release. For instance, our lab has shown that glutamate release at the Schaffer collateral terminal activates preNMDARs, which leads to an influx of Ca^{2+} and facilitation of subsequent release (McGuinness et al., 2010). Conversely, we have recently reported that activation of preNMDARs prevents the induction of presynaptic LTP and promotes the induction of presynaptic LTD (Padamsey et al., 2017a). This is consistent with findings in neocortical neurones, where preNMDARs modulate spontaneous release (Kunz et al., 2013) and are required for spike-timing dependent LTD (Sjöström et al., 2003; Abrahamsson et al., 2017).

The existence and functional properties of preNMDARs are heavily debated. Multiple studies have provided histological and functional evidence of preNMDARs at neocortical and hippocampal synapses (Padamsey et al., 2017a; McGuinness et al., 2010; Sjöström et al., 2003; Berretta & Jones, 1996; Buchanan et al., 2012; Siegel et al., 1994; Kunz et al., 2013; Abrahamsson et al., 2017), however, direct observation of their activity has been difficult. McGuinness and colleagues observed large AP-evoked Ca^{2+}-transients that correlated with neurotransmitter release events and could be selectively abolished by blocking preNMDARs. Furthermore, photolytic release of glutamate at boutons led to fast Ca^{2+}-transients. Other studies were not able to detect Ca^{2+}-influx in response to glutamate alone, but showed a modulation of AP-dependent Ca^{2+}-influx by preNMDARs, when APs were stimulated at high frequency (Buchanan et al., 2012). On the other hand, Carter and Jahr failed to detect any preNMDAR-dependent Ca^{2+}-influx evoked by glutamate

photolysis at cortical synapses, despite high detection sensitivity (Carter & Jahr, 2016).

Here, we sought to better understand the functional role of preNMDARs at the Schaffer collateral terminal. In the first part, we measured AP-evoked Ca^{2+}-transients in response to photolytic release of single quanta of glutamate. Surprisingly, we found that activation of preNMDARs decreased Ca^{2+}-responses, in a manner dependent on Ca^{2+}-activated K+-channels (SK channels)-dependent sharpening of the AP waveform. These experiments were conducted and analysed in collaboration with Carla Schmidt. In the second part, I provide further electrophysiological evidence for the involvement of preNMDARs in the induction of presynaptic LTD.

6.2. Results

6.2.1. Activation of preNMDARs decreases AP-evoked Ca^{2+}-influx at Schaffer collateral terminals

The goal of the following experiments was to measure the impact of preNMDAR activation on presynaptic Ca^{2+}-influx. The experimental setup is illustrated in Fig. 6.1: CA3 pyramidal cells were bolus-loaded with 1 mM OGB-1 for 3-5 min. The dye was given 30-45 min to reach diffusional equilibrium in the axon. In order to elicit APs, the neurone was re-patched with 100 µM OGB-1 and depolarised via short step pulses of current. Presynaptic terminals were identified structurally as varicosities along axons, ~ 50-100 µm away from the soma and functionally by strong AP-evoked Ca^{2+}-responses relative to neighbouring axon collaterals. AP-evoked Ca^{2+}-responses in boutons were recorded at 400 Hz in the presence or absence of concurrent glutamate photolysis (1 ms pulse paired with local perfusion of 10 mM MNI-glutamate) next to the bouton (Fig. 6.1C, D). Photolysis was timed to occur 1-5 ms after the arrival of the action potential. Photolysis was titrated at nearby spines to elicit EPSCaTs that were similar in magnitude compared to electrical stimulation ($\Delta F/F$ ~ 0.5-1.0). In order to control for potential side effects due to extensive imaging, AP-evoked Ca^{2+}-responses in the absence of local perfusion of MNI-glutamate were recorded both, at the start and the end of the experiment (Fig. 6.1E). We recorded

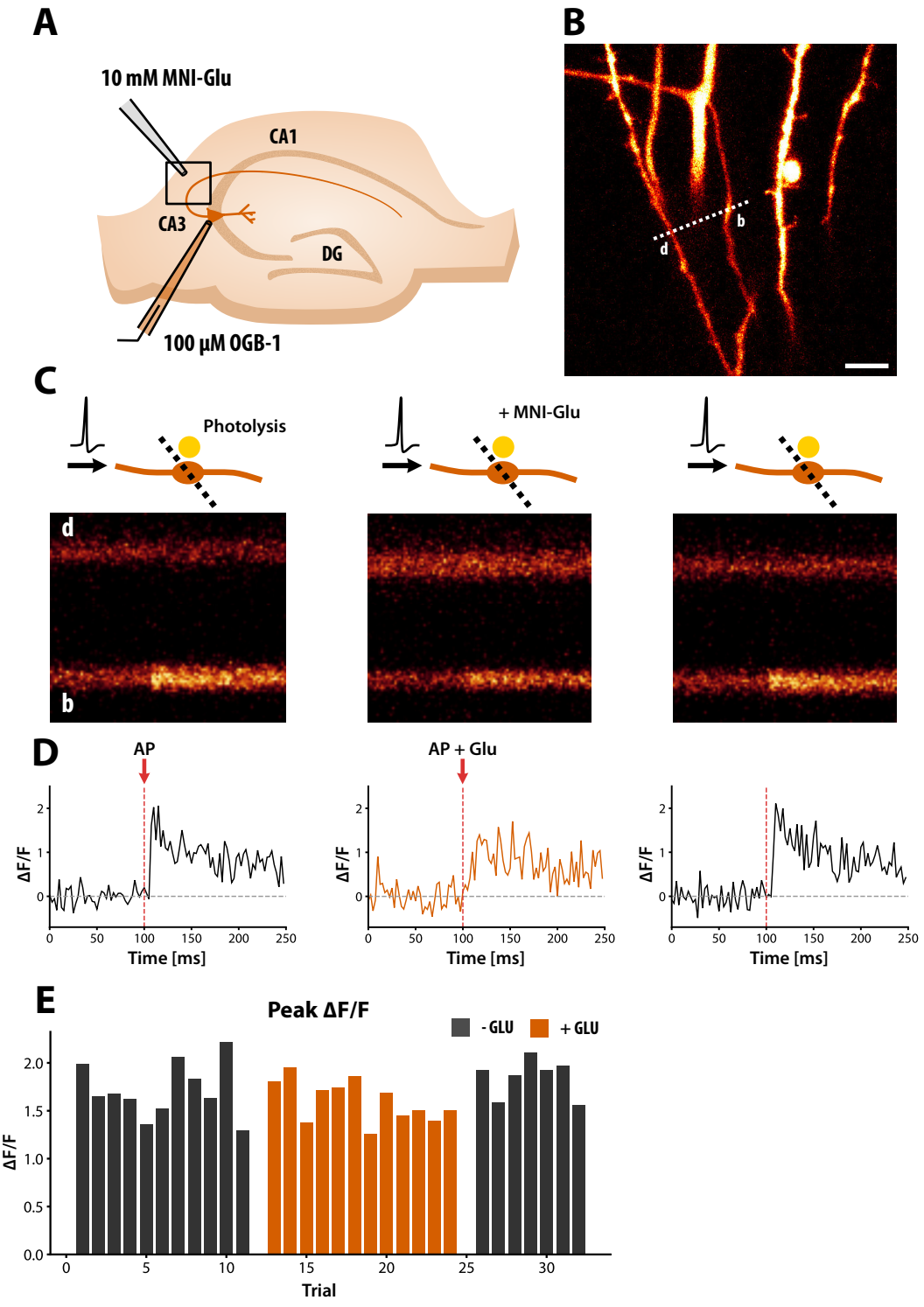

Fig. 6.1: Experimental setup to study the role of preNMDAR in the regulation of presynaptic strength. (A) Schematic of the experimental setup. CA3 pyramidal cells in organotypic slices were bolus loaded with 1 mM OGB-1 for 3-5 min. The cell was then re-patched with 100 µM OGB-1 to elicit APs paired with focal glutamate photolysis at presynaptic terminals in *stratum oriens* of CA3. (B) Example of an axon originating from the trunk of the primary dendrite. A bouton (d) can be clearly identified as varicosities along the axon. Scale bar: 5 µm. *Cont'd on next page.*

10-15 successive trials per condition. Ca^{2+}-responses were averaged within trials and the peak response was compared.

Unexpectedly, the presence of glutamate during AP firing decreased AP-evoked Ca^{2+}-influx in boutons ($\Delta(\Delta F/F) = -0.403 \pm 0.053$, $N = 11$, $p < 0.01$, Wilcoxon signed-rank test, Fig. 6.2). The decrease in Ca^{2+}-influx did not completely recover at the end of the experiment, which suggests either slow recovery or photo-bleaching of the Ca^{2+}-indicator ($\Delta(\Delta F/F) = 0.157 \pm 0.072$, $N = 8$, $p = 0.06$). The decrease in Ca^{2+}-influx occurred immediately with glutamate photolysis and we did not observe a gradual decline with successive trials. We did not observe any difference in the decay kinetics of Ca^{2+}-transients fitted with a single exponential decay ($tau_{CTR} = 204.359 \pm 15.69$ ms, $tau_{GLU} = 221.987 \pm 18.802$ ms, $\Delta tau = 17.627 \pm 8.99$ ms, n.s.). Next, we applied the NMDAR open channel blocker MK-801 (1 mM) intracellularly to selectively block preNMDARs. This significantly reduced the decrease in Ca^{2+}-influx via glutamate photolysis ($\Delta(\Delta F/F) = -0.171 \pm 0.052$, $N = 9$, $p < 0.05$ vs. CTR, Fig. 6.3A,B, Fig. 6.4A), which did not recover at the end of the experiment except for a single outlier (including outlier: $\Delta(\Delta F/F) = 0.111 \pm 0.109$, excluding outlier: $\Delta(\Delta F/F) = 0.022 \pm 0.072$, $N = 9$, n.s. vs. CTR, Fig. 6.4B), suggesting that the remaining decrease in Ca^{2+}-response is due to photobleaching. Thus, preNMDARs are necessary for glutamate photolysis-dependent decrease in AP-evoked Ca^{2+}-transients.

At the postsynaptic terminal, NMDARs are tightly coupled to SK channels, which are activated by NMDAR-dependent Ca^{2+}-influx and lead to hyperpolarisation and rapid deactivation of NMDAR currents (Ngo-Ahn et al., 2005). We therefore wondered if the

---

Fig. 6.1 cont'd (C) Line scans were taken through the bouton at 400 Hz while an AP was elicited via current injection. When paired with glutamate, MNI-glutamate was locally applied and photolysed on or next to the bouton (middle column). The photolysis laser was triggered on every trial to account for off-target effects of the photolysis alone. (D) AP-evoked Ca^{2+}-transients either with (middle) or without glutamate photolysis (left and right). A reduction in peak intensity can be observed. (E) Peak intensities over multiple trials. 10-15 trials per condition were recorded. Black: without glutamate, Red: with glutamate.

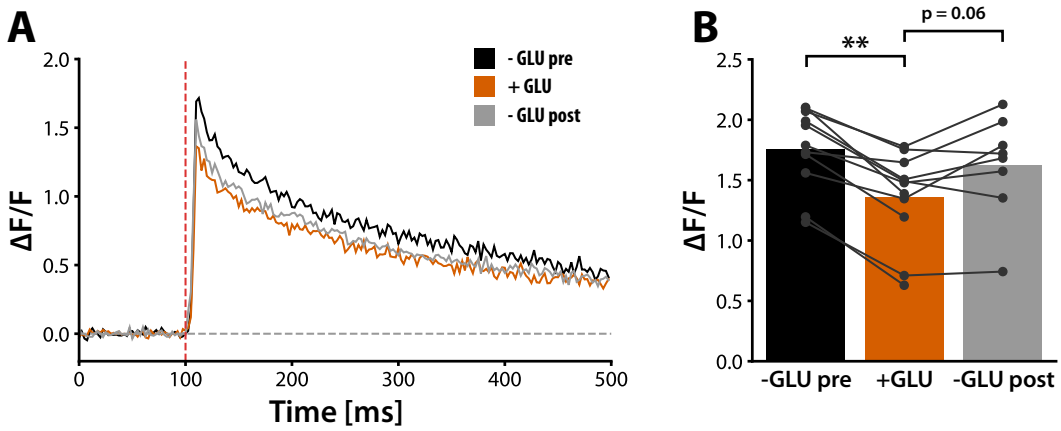

Fig. 6.2: Focal photolysis of glutamate at the presynaptic terminal decreases AP-evoked Ca^{2+}-transients. (A) Averaged AP-evoked Ca^{2+}-transients with (red) or without (black, grey) simultaneous photolysis of glutamate. A clear decrease in the peak intensity can be observed. (B) Summary of data points. Glutamate photolysis led to significant decrease in AP-evoked Ca^{2+}-transients, which only partially recovered (Wilcoxon signed-rank test).

decrease in AP-evoked Ca^{2+} is due to opening of SK channels resulting in the sharpening of the AP waveform. Bath application of the SK channel blocker apamin (1 µM) significantly reduced glutamate photolysis-induced decrease in Ca^{2+}-influx to a similar degree as MK-801 ($\Delta(\Delta F/F) = -0.149 \pm 0.053$, $N = 7$, $p < 0.01$ vs. CTR, Fig. 6.3C,D, Fig. 6.4A). The remaining decrease did not recover at the end of the experiment ($\Delta(\Delta F/F) = -0.143 \pm 0.075$, $N = 5$, n.s. vs. CTR, Fig. 6.4B). Bath application of apamin did not affect the basal magnitude of AP-evoked Ca^{2+}-transients, however, we observed a small decrease in the decay time constant ($tau_{APA} = 169.291 \pm 6.613$, $N = 7$, $p = 0.057$ vs. CTR).

Previous preliminary work from our lab has also ruled out GABA receptors and mGluRs, which, when pharmacologically blocked, did not prevent the decrease in AP-evoked Ca^{2+}-influx (Suppl. Fig. 9.2).

6.2.2. Negative feedback via preNMDARs and SK channels modulates short-term plasticity of bursts of action potentials

We have shown that exogenous application of glutamate during AP firing reduces Ca^{2+}-influx at the presynaptic terminal via activation of preNMDARs and the opening of SK

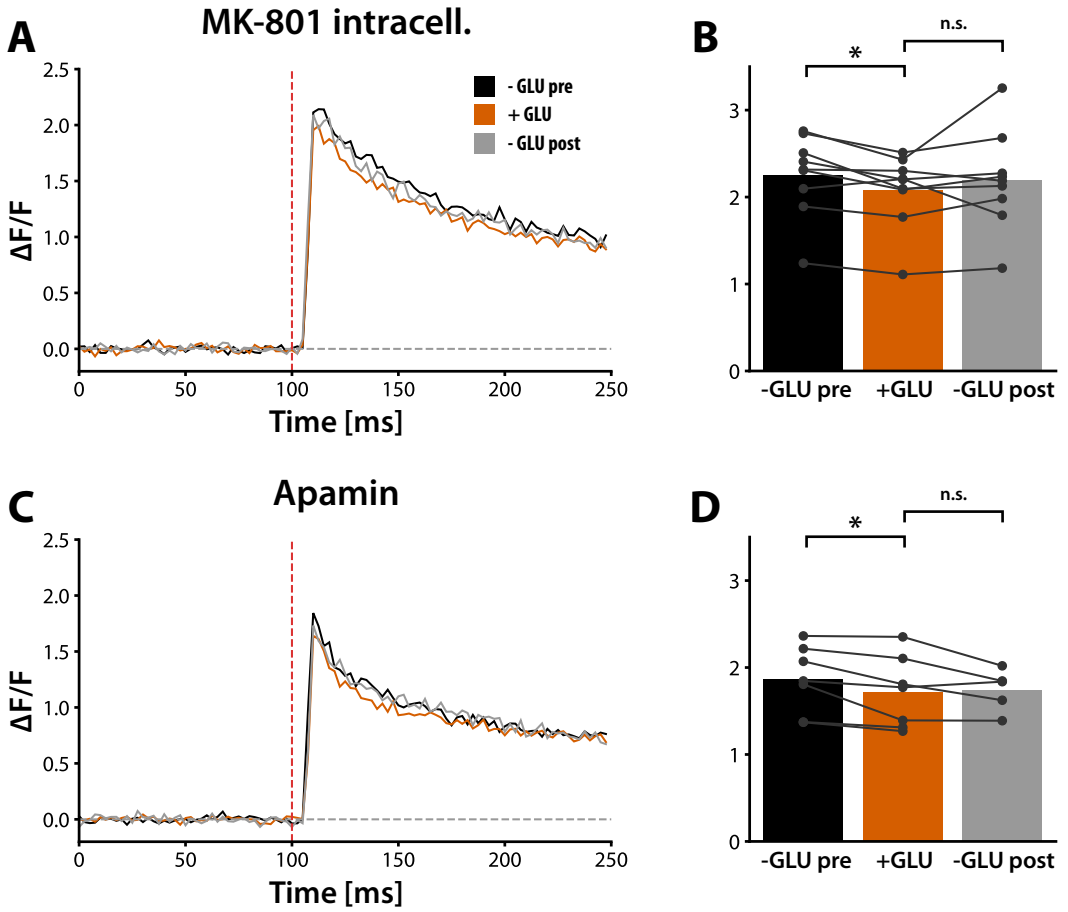

Fig. 6.3: Glutamate-induced decrease in AP-evoked Ca^{2+}-transients requires the activation of presynaptic NMDARs and SK channels. (A) Averaged AP-evoked Ca^{2+}-transients with (red) or without (black, grey) simultaneous photolysis of glutamate in the presence of 1 mM intracellular MK-801 to block preNMDARs. (B) Summary of data points in (A). The decrease in AP-evoked Ca^{2+}-transients was significantly diminished (see Fig. 6.4). (C) Averaged AP-evoked Ca^{2+}-transients with (red) or without (black, grey) simultaneous photolysis of glutamate in the presence of 1 µM apamin to block SK channels. (D) Summary of data points in (C). Statistical significance tested using Wilcoxon signed-rank test.

channels. What are the relevant physiological conditions under which this process occurs? What are the physiological consequences? We hypothesised that the reduced Ca^{2+}-influx might modulate short-term facilitation, which is thought to be mainly driven by residual Ca^{2+} or saturation of Ca^{2+}-buffers and should therefore be sensitive to the magnitude of Ca^{2+}-influx. This would cause short-term plasticity to be dependent on the history of release events (in addition to the frequency of AP firing). Indeed, Dobrunz and colleagues have reported that Pr depends on prior successful release events at

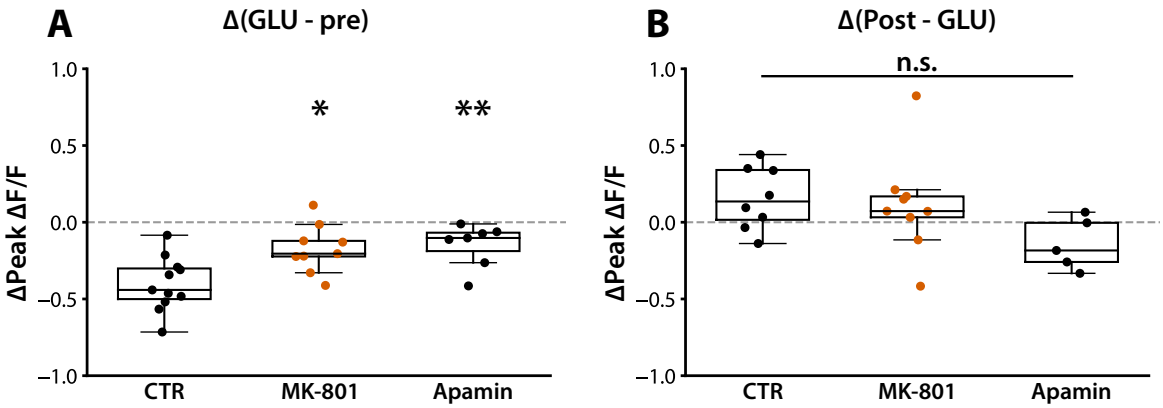

Fig. 6.4: Statistical comparison of pharmacological experiments of glutamate-induced decrease in AP-evoked Ca^{2+}-transients. (A) The difference in the peak amplitude between trials before and during glutamate photolysis is shown for control experiments, experiments with 1 mM intracellular MK-801, and 1 µM apamin. Both, MK-801 and Apamin significantly reduced the decrease in the peak of AP-evoked Ca^{2+}-transients (Kruskal-Wallis H test with *post hoc* Dunn's test). (B) The difference in the peak amplitude between trials after and during glutamate photolysis is shown. No significant differences were detected. Significance is shown in relation to CTR condition.

sufficiently high stimulation frequencies (100-200 Hz, Dobrunz et al., 1997; Stevens & Wang, 1995). We therefore tested if preNMDARs might implement a similar negative feedback signal.

We stimulated Schaffer collateral-CA1 synapses with a train of 10 APs at 200 Hz while recording the postsynaptic current response via whole-cell patch clamp (Fig. 6.5). We then washed on 50 µM AP5 to observe changes in short-term plasticity. In half of the experiments, 50 µM AP5 was included at the start of the experiment and was washed out instead. In order to rule out the contribution of postsynaptic NMDARs, 1 mM MK-801 was included in the patch pipette, and synapses were stimulated at low-frequency (0.06 Hz) for 8-10 min before commencing the experiment. High frequency AP trains elicited strong short-term facilitation, which peaked at the 4-5th pulse followed by a slow decline, indicating the onset of short-term depression. Application of AP5 significantly increased the magnitude of short-term facilitation (N = 9, Fig. 6.5A,B). The difference in facilitation steadily increased for the first 4-5 pulses, after which it plateaued (Fig. 6.5B). This suggests that the increase is due to facilitated short-term potentiation rather than inhibition of

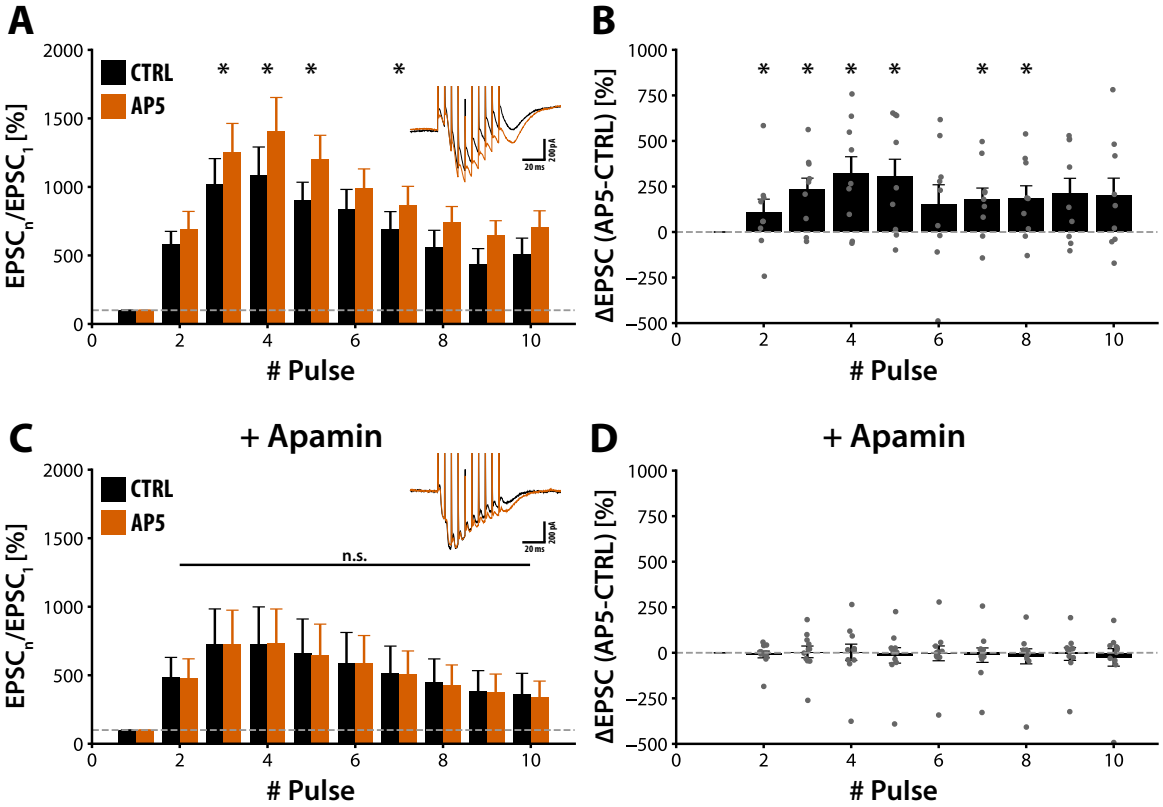

Fig. 6.5: Presynaptic NMDARs suppress short-term facilitation at high stimulation frequency. (A) The average normalised response to burst stimulation of 10 APs at 200 Hz is shown before (black) and after the addition of 50 µM AP5 to block preNMDARs. Application of AP5 significantly increased the magnitude of short-term facilitation at pulses 3-5 (Wilcoxon signed-rank test). (B) The difference in the magnitude of short-term facilitation before and after the addition of AP5 is shown for each experiment. Statistical comparison was done with respect to experiments shown in (C,D) (Mann-Whitney U test). (C) Inhibition of SK channel function occludes AP5-induced increase in short-term facilitation. (D) The difference in the magnitude of short-term facilitation before and after the addition of AP5 in the presence of apamin is shown for each experiment. Error bars represent SEM.

short-term depression. In order to quantify the dynamics of short-term plasticity, we calculated the slope of the first four pulses as a readout of short-term facilitation ("Rise slope") and the slope of the remaining pulses as a readout for short-term depression ("Decay slope", Fig. 6.6A). AP5 significantly increased the rise slope ($N = 9$, $p < 0.05$) without affecting the decay. Short-term plasticity depends strongly on the initial Pr, however, we did not detect a change in the EPSC amplitude of the first pulse (Fig. 6.6Aiii). Our results therefore indicate that preNMDARs modulate short-term plasticity at high frequency by suppressing short-term facilitation.

If the inhibitory effect of preNMDARs is due to the activation of SK channels, inhibition of SK channels should occlude AP5 induced increase in short-term facilitation. We therefore repeated the experiment in the presence of 1 µM apamin. Inhibition of SK channels suppressed both short-term facilitation and depression (Fig. 6.6B), which remained unchanged with the application of AP5 (Fig. 6.5C,D). Apamin did not affect the basal synaptic strength (Fig. 6.6Biii). This effect was specific to high frequency stimulation as preliminary studies from our lab suggest that AP5 had no effect on AP trains given at lower frequencies (unpublished data from the Emptage lab, Suppl. Fig. 9.3). We therefore

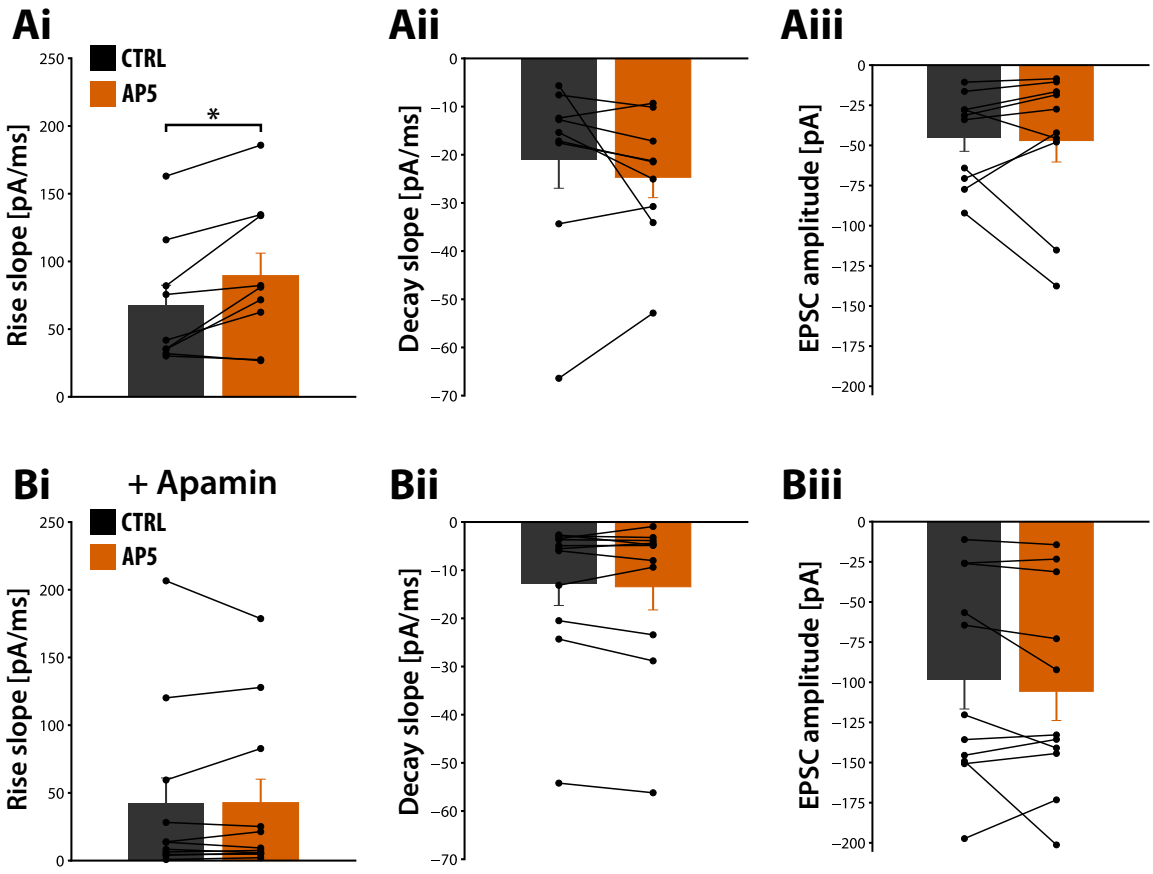

Fig. 6.6: Further analysis of the properties of short-term plasticity. (Ai) The initial phase of short-term facilitation was characterised by the slope of a linear fit of the response to pulses 1-4. AP5 significantly increased the slope (Wilcoxon signed-rank test). (Aii) The slope of a linear fit to responses of pulses 5-10 was used to characterise the degree of short-term depression. No significant difference was found with application of AP5. (Aiii) The EPSC amplitude of the first pulse did not change with the application of AP5. (Bi-iii) No differences in the short-term behaviour of EPSC amplitude after the application of AP5 was observed when SK channels were blocked. Apamin, however, decrease the global magnitude of short-term plasticity.

concluded that glutamate release activates preNMDARs, which leads to the opening of SK channels as a feedback mechanism to reduce the amount of Ca^{2+}-entry and built-up during short-term facilitation.

6.2.3. Excessive glutamate release induces presynaptic LTD via preNMDARs

Previous work from our lab has shown, using optical methods, that glutamate release is inhibitory towards the induction of presynaptic LTP and promotes LTD (Padamsey et al., 2017a). The inhibitory tone was found to require preNMDARs. Here, I have provided further evidence using electrophysiological means.

Excessive release of glutamate that is not correlated with strong postsynaptic depolarisation leads to presynaptic LTD. Repetitive stimulation of high Pr synapses in the absence of postsynaptic depolarisation should therefore induce LTD. I have stimulated Schaffer collateral-CA1 synapses using a paired pulse at 5 ms interval, which, due to paired pulse facilitation, ensures that the majority of synapses will release one quantum of glutamate (Padamsey et al., 2017; Stevens & Wang, 1995). I repeated the stimulation 60 times at 5 Hz and recorded the EPSP for 30 min. In order to prevent strong depolarisation, I hyperpolarised cells to -90 mV during the induction. Paired-pulse stimulation led to marked decrease in the EPSP ($\Delta EPSP_{paired}$ = -59.79 ± 8.79 %, N = 7, $\Delta EPSP_{single}$ = -6.57 ± 9.72 %, N = 5, $p < 0.05$, Fig. 6.7Ai,ii). The decrease in EPSP was accompanied by an increase in the PPR (ΔPPR_{paired} = 0.336 ± 0.043, ΔPPR_{single} = 0.016 ± 0.087, $p < 0.05$, Fig. 6.7Aiii), indicating a presynaptic expression locus. The change in PPR was not significantly correlated with the change in EPSP (Pearson r = -0.625, n.s.), suggesting potential postsynaptic contributions. Next, I blocked NMDARs by bath applying 20 µM MK-801, which decreased the magnitude of LTD induced via paired-pulse ($\Delta EPSP_{MK\text{-}801,\ ex}$ = -31.42 ± 3.61 %, N = 6, Fig. 6.7Bi,ii, "MK-801 extracell.") and completely abolished the increase in PPR ($\Delta PPR_{MK\text{-}801,\ ex}$ = -0.038 ± 0.054, Fig. 6.7Biii). In contrast, including 1 mM MK-801 in the patch pipette also decreased the magnitude of LTD ($\Delta EPSP_{MK\text{-}801,\ in}$ = 26.68 ± 9.53 %, N = 6, Fig. 6.7Bi,ii, "MK-801 intracell."), but did not affect the increase in PPR ($\Delta PPR_{MK\text{-}801,\ in}$ = 0.345

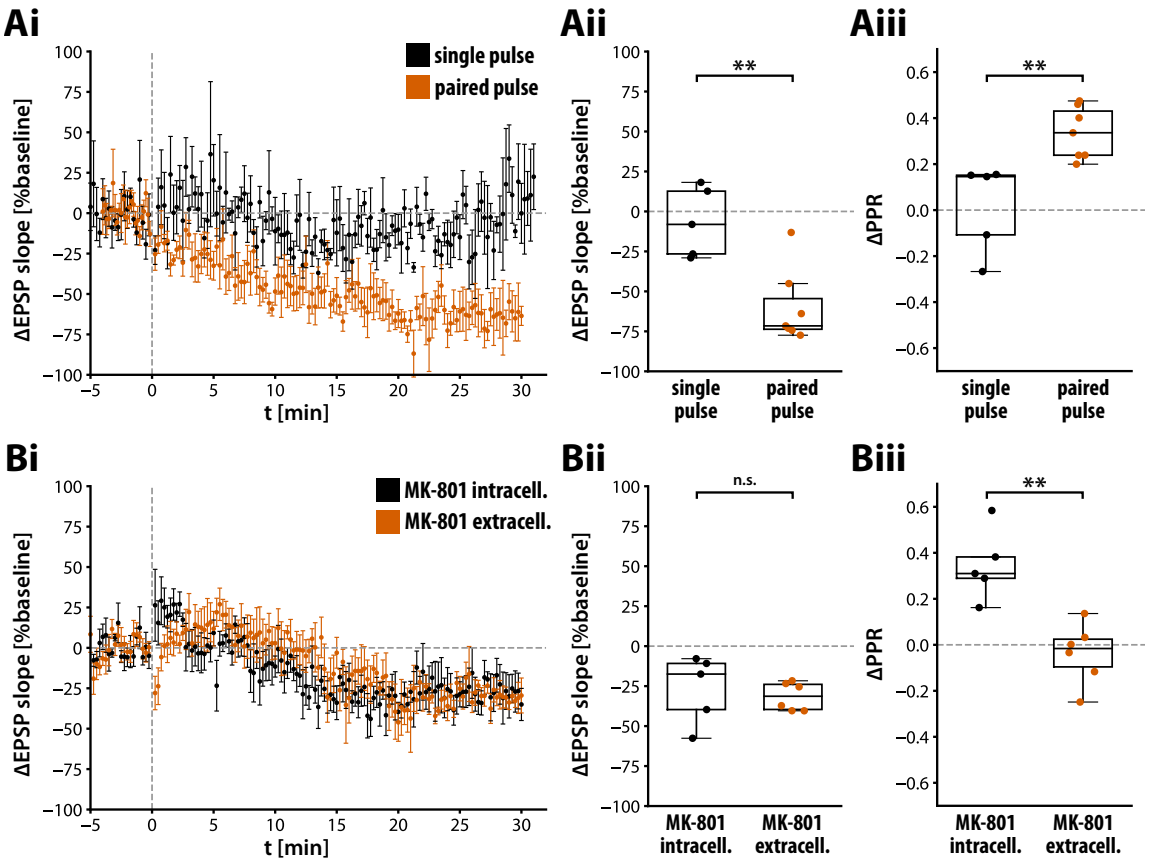

Fig. 6.7: Excessive release of glutamate induces presynaptic NMDAR-dependent presynaptic LTD. (Ai) Presynaptic LTD was induced by burst stimulation of two pulses at 200 Hz, 60 times at 5 Hz ("paired pulse"). The slope of the EPSP showed a long-lasting decrease. Induction using a single pulse ("single pulse") did not cause any changes. (Aii) Summary of EPSP slope changes for all experiments. (Aiii) PPR changes for all experiments. The decrease in EPSP slope after paired pulse stimulation was accompanied by a significant increase in the PPR. (B) The role of preNMDARs was investigated by selectively blocking only postsynaptic receptor ("MK-801 intracell.") or all NMDARs ("MK-801 intracell."). Inhibition of either pre- or postsynaptic NMDARs reduced the magnitude of LTD, however, selective inhibition of postsynaptic NMDARs preserved the increase in the PPR, which was abolished when preNMDARs were additionally blocked. Statistical significance was assessed using Mann-Whitney U test.

± 0.069, Fig. 6.7Biii). The intracellular MK-801 data was kindly provided by Zahid Padamsey. I therefore conclude that excessive glutamate release and activation of preNMDARs leads to the induction of presynaptic LTD.

6.3. Discussion

Here, we have reported novel mechanisms by which preNMDARs regulate presynaptic

strength at the Schaffer collateral-CA1 synapse. Acute activation of preNMDARs leads to the opening of SK channels to reduce AP-evoked Ca^{2+}-influx. This decreases the built-up of Ca^{2+} and suppresses short-term facilitation, which is most apparent during high frequency AP bursts. Successive activation of preNMDARs induces a long-lasting decrease in Pr.

6.3.1. What are the functional properties of preNMDARs?

Our experiments clearly show a presynaptic role of NMDARs and provide further evidence for their expression and functional significance at the presynaptic terminal. However, unlike previous studies (McGuinness et al., 2010; Buchanan et al., 2012), we failed to detect any NMDAR-dependent Ca^{2+}-influx, similar to reports arguing for the absence of preNMDARs (Christie & Jahr, 2008, 2009; Carter & Jahr, 2016). Instead, we observed a decrease in AP-evoked Ca^{2+}-influx, which required preNMDAR signalling.

Our experiments required intensive imaging especially due to high frequency xt-scans and frequent exposure to the photolysis laser. To minimise phototoxicity, we included 200 µM ascorbic acid and 1 mM Trolox in our ACSF, which act as antioxidants. In addition, whenever possible, AP-evoked Ca^{2+}-transients without local perfusion of MNI-glutamate were collected both at the start and the end of the experiment. On average, imaging alone decreased the magnitude of AP-evoked Ca^{2+}-transient by 10-15 % and accounted for ~ 40 % of the decrease due to glutamate photolysis. This is in line with the observation that application of apamin or intracellular MK-801 did not completely abolish the decrease in Ca^{2+}-influx and the residual decrease was similar in magnitude compared to the decrease due to imaging alone (decrease in peak Ca^{2+} fluorescence intensity relative to vehicle control: 42.6 % (MK-801), 36.9 % (apamin)).

Next, photolysis could lead to the release of unphysiological concentrations of glutamate. Photolysis was titrated at the start of each experiment at nearby spines at the same focal depth as the bouton of interest. We adjusted the photolysis laser power so that uncaging elicited EPSCaTs of 0.5-1 ΔF/F, which are comparable in size to electrical

stimulation. The width of the uncaging pulse was larger than the diameter of a synapse. Glutamate photolysis was therefore not restricted to the synaptic cleft and could activate neighbouring synapses as well. Christie and Jahr suggested that activation of nearby postsynaptic terminals could lead to Ca^{2+}-influx via VGCCs in the presynaptic terminal through electrotonic spread (Christie & Jahr, 2008). In order to reduce any postsynaptic influence, we included 1 µM NBQX, which blocks the majority of AMPA and Kainate receptors and prevents postsynaptic depolarisation

Local glutamate photolysis was paired with single APs in order to facilitate the opening of NMDARs. However, some studies have suggested that the duration of depolarisation of single APs is shorter than the time it takes for glutamate to be bound to the receptor and preNMDARs should therefore only be activated at high enough stimulation frequencies (Duguid & Sjöström, 2006; Banerjee et al., 2016). According to McGuinness and colleagues, single AP-evoked release of glutamate can be detected as an increase in Ca^{2+}-entry in the bouton, which depended on preNMDARs (McGuinness et al., 2010). Similarly, preNMDARs have been implicated in regulating spontaneous release (Dore et al., 2017), which occur at much lower frequencies. The involvement of a Mg^{2+}-dependent blockade mechanism is further questioned by our failure of evoking preNMDAR-dependent Ca^{2+}-transient in the absence of extracellular Mg^{2+} (unpublished work of the Emptage lab). It has been suggested that preNMDARs might contain the GluN3A-subunit (Dore et al., 2017), which is insensitive to Mg^{2+} block and has low permeability to Ca^{2+}. Our observations of a potential coupling between preNMDARs and SK channels, however, favours the expression of Ca^{2+}-permeable subunits. Alternatively, NMDARs have been shown to possess additional metabotropic function (Dore et al., 2016; Abrahamsson et al., 2017), however, this is unlikely the case for our observations since preNMDAR function was efficiently blocked by the open channel blocker MK-801. The exact subunit composition of preNMDARs at hippocampal synapses is not well-studied but is generally thought to involve predominantly GluN1/GluN2B subunits (Sjöström et al., 2003), which could depend on the developmental stage of the synapse (Stocca & Vicini, 1998).

One possible explanation for our inability to detect preNMDAR-dependent Ca^{2+}-influx could be that the magnitude of the decrease in VGCC-dependent Ca^{2+} is comparatively larger. However, full blockade of SK channels via apamin did not lead to an increase in Ca^{2+}-influx when paired with glutamate photolysis. However, apamin itself strongly suppressed presynaptic function, such as reduced short-term plasticity, and could lead to cell-wide changes, which could interfere with the Ca^{2+}-influx through NMDARs.

McGuinness and colleagues reported large presynaptic Ca^{2+}-transient that depended on glutamate release and preNMDARs (McGuinness et al., 2010). Although we were able to detect variations in the peak amplitude of AP-evoked Ca^{2+}-transients (*e.g.* Fig. 5.1E), glutamate photolysis did not cause a decrease in variance. This suggests that both phenomena, increase and decrease in presynaptic Ca^{2+}, act in parallel, and their activation mechanism must therefore differ. Whereas the observations of McGuinness and colleagues were based on endogenous release of glutamate, we elicited the decrease in Ca^{2+}-influx via focal glutamate photolysis. Differences in the concentration and spatiotemporal dynamics of glutamate release could therefore be a potential explanation for the discrepancies. For example, glutamate photolysis might engage extrasynaptic NMDARs, which, under physiological conditions, mainly occurs during high-frequency activity, such as AP bursts. Endogenous release of glutamate could also be coupled to co-release of modulators of NMDAR function, such as D-serine or glycine, which have been shown to gate distinct functional outcomes (Mothet et al., 2015).

6.3.2. What are the signalling pathways downstream of preNMDARs?

Our results show that inhibition of SK channels occludes preNMDAR-mediated decrease in presynaptic Ca^{2+}-influx. SK channels can be activated by various Ca^{2+} sources, including P/Q-, R-, L-type channels, and internal Ca^{2+} stores (Adelman et al., 2012). Our finding therefore suggests tight spatial coupling of NMDARs and SK channels leading to microdomain signalling. However, some studies have suggested that postsynaptic SK channels are gated by CaV2.3 instead, which, due to their high activation threshold,

require the additional depolarisation provided by NMDARs (Bloodgood & Sabatini, 2007). CaV2.3 has been reported to be present at the presynaptic terminal (Gasparini et al., 2001), and we cannot exclude their contribution. Interestingly, the indirect coupling of presynaptic SK channels would support the expression of GluN3A-containing preNMDARs.

Prolonged activation of preNMDAR leads to the induction of presynaptic LTD. This is in line with reports on LTD induction at cortical synapses (Sjöström et al., 2003). Interestingly, Rodríguez-Moreno and colleagues have reported a form of "pattern-dependent LTD (p-LTD)" at cortical synapses that is dependent only on presynaptic AP firing pattern and requires the activation of preNMDARs (Rodríguez-Moreno et al., 2013). They further implicated presynaptic calcineurin activation as a potential downstream modulator. Calcineurin is a known modulator of vesicle trafficking (Cousin & Robinson, 2001) and ion channels (Liu et al., 1994). Calcineurin has also been implicated in various forms of presynaptic LTD (Heifets et al., 2008; Andrade-Talavera et al., 2016; Rodríguez-Moreno et al., 2013).

The suggested signalling pathways for short- and long-term plasticity mediated by preNMDARs are shown in Fig. 6.8. Acute activation of preNMDARs open SK channels, either via direct Ca^{2+}-CaM coupling or indirectly via CaV2.3 or CICR. SK channels accelerate repolarisation, which leads to AP sharpening and a decrease in VGCC-dependent Ca^{2+}-influx. Prolonged activation of preNMDARs decreases release probability potentially via CaM and calcineurin.

6.3.3. What is the physiological function of preNMDAR-mediated short-term depression?

Our electrophysiological studies implicated preNMDAR-mediated decrease of AP-evoked Ca^{2+} in inhibition of short-term facilitation, which depended on the history of firing and release events. The opening of SK channels reduced the amount of Ca^{2+}-influx and decreased the built-up of intracellular Ca^{2+}. We reached these conclusion by bath

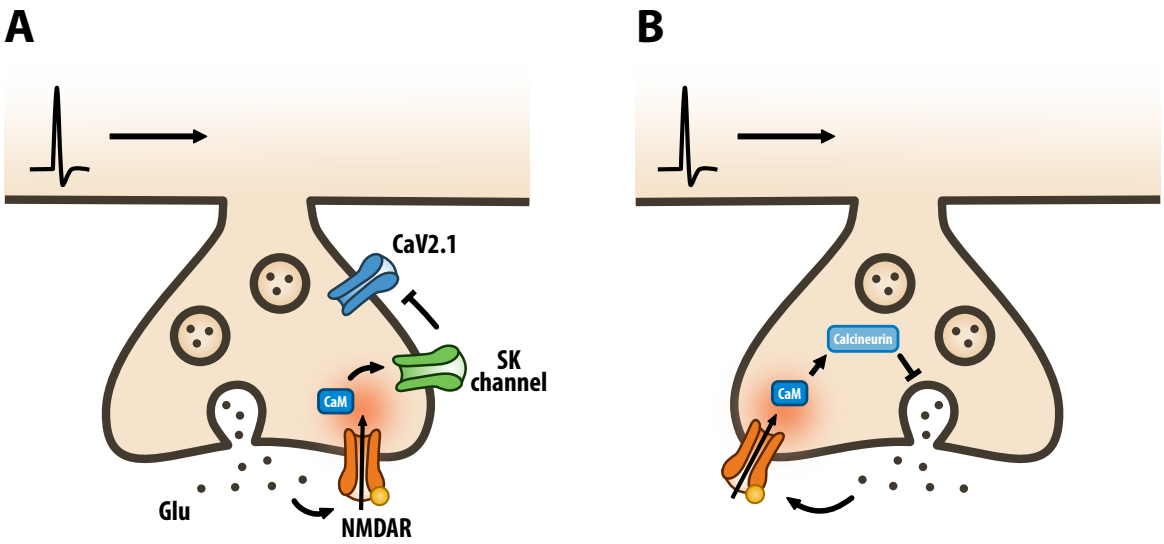

Fig. 6.8: Proposed molecular mechanisms for short- and long-term plasticity mediated by presynaptic NMDARs. (A) Molecular mechanism for preNMDAR-mediated suppression of short-term facilitation. The release of glutamate activates preNMDARs, which causes local Ca^{2+}-influx to activate calmodulin. Calmodulin causes the opening of SK channels, which accelerates the repolarisation of the membrane potential sharpening of the AP waveform. Accelerated closing of CaV2.1 causes a reduction in Ca^{2+}-influx. (B) Molecular mechanism for preNMDAR-mediated LTD. Glutamate release activates preNMDARs, which causes local Ca^{2+}-influx to activate calmodulin. Calmodulin, in turn, activates calcineurin, which has been implicated in presynaptic forms of LTD.

application of AP5 and apamin and observing changes in short-term plasticity following burst stimulation. One confound that we did not account for is a potential impact on polysynaptic connections, which are especially pronounced in organotypic slice cultures. Both, polysynaptic excitatory and inhibitory inputs might contribute significantly to the observed short-term plasticity. Excitatory current were recorded in voltage clamp close to the reversal potential of Cl- channels to minimise inhibitory currents. We were not able to completely block GABA receptors pharmacologically due to the hyperconnectivity in these slices, which led to epileptic discharges and additional experiments will be required to resolve this question.

What could be the physiological role of this type of short-term plasticity? Let's assume that the information transmitted between pre- and postsynaptic neurones is encoded in

the absence or presence of bursts of APs. Encoding information in bursts is advantageous since low release probability would strongly deteriorate information on a spike-by-spike basis, which can be overcome by short-term facilitation induced by high-frequency firing. During the event of an AP burst, the postsynaptic terminal accumulates evidence by temporal summation of neurotransmitter release. With the addition of noise, such as spontaneous baseline AP firing, each neurotransmitter release event can be associated with a reduction in the uncertainty that an event is due to AP bursts rather than noise, which is proportional to the distance between the corresponding probability distributions of firing frequency. A threshold for evidence/certainty (decision boundary) can then be easily implemented by postsynaptic non-linear integration.

The absolute reduction in uncertainty converges towards zero with successive events and this convergence is accelerated by the temporary increase in Pr due to short-term facilitation. Once the evidence surpasses the postsynaptic threshold, any additional evidence is made redundant. I will now additionally assume that synaptic transmission is evolutionary constrained by resource and energy. This renders the redundancy disadvantageous and would promote mechanisms that inhibit neurotransmitter release once enough evidence has been accumulated. This mechanism would be sensitive to both the frequency of firing and the history of release events. I therefore predict the following mode of information transmission at Schaffer collateral-CA1 synapses: In the absence of information transmission, baseline spontaneous activity is minimised by low Pr, which, assuming AP firing to follow a Poisson point process, scales the mean firing frequency linearly. The arrival of a burst of APs causes rapid short-term facilitation, which further exaggerates the frequency difference between burst and noise. Facilitation is promoted as long as no neurotransmitter release has occurred, but hampered otherwise due to diminishing returns on the uncertainty reduction. This can be seen by the steady increase in facilitation of 200 Hz AP bursts caused by bath application of AP5 (Fig 6.5B, pulses 1-5). This also accelerates the decay of Pr after the burst, reduces short-term depression caused by synaptic vesicle depletion, which has much longer recovery time

constants due to slow vesicle replenishment, and shortens the time window between sequential information quanta. Short-term depression that is dependent on the history of release events therefore helps to reduce redundancy in information transfer and minimises metabolic constraints.

6.4. Conclusion

I have shown that preNMDAR act as negative feedback to regulate presynaptic strength. Glutamate release activates preNMDAR, which opens SK channels to decrease Ca^{2+}-entry and attenuates short-term facilitation. This optimises neurotransmitter release during high frequency bursts. Prolonged activation of preNMDARs leads to long-lasting decrease in Pr. In the next section, I will show how this mechanism, combined with presynaptic Hebbian LTP, optimises Pr with respect to mutual information between neurotransmitter release and postsynaptic spiking.

7. Presynaptic Hebbian plasticity is spike-timing dependent

7.1. Introduction

Hebbian plasticity, synaptic strength changes that depend on the correlation between pre- and postsynaptic activity, is the most commonly studied form of synaptic plasticity. In general, activity correlation is thought to be sensed and relayed via the postsynaptic NMDAR, which scales its activation with respect to the membrane depolarisation and concentration of glutamate released (Lüscher & Malenka, 2012). The temporal dynamics of Ca^{2+}-influx through NMDARs and potentially specific subunit compositions have been shown to orchestrate postsynaptic Hebbian plasticity and account for most of the learning rule, such as sensitivity to spike-timing and input frequency (Lüscher & Malenka, 2012). Problems arise when the same framework is imposed onto the presynaptic terminal. Induction of LTP requires activation of NMDARs and therefore the release of glutamate. However, most central synapses release glutamate very infrequently, with a median Pr of 0.2 (Murthy et al., 1997; Huang & Stevens, 1997; Branco et al., 2008, Branco et al., 2010). This raises the questions: Does the presynaptic terminal only "learn" using a fraction of available spiking information? And: How do presynaptically silent synapses induce synaptic plasticity?

Due to the stochastic nature of neurotransmitter release and the predominant presynaptic locus of short-term plasticity (Regehr, 2012), presynaptic strength is especially sensitive to the temporal structure of AP trains. This opens up the possibility that presynaptic strength is adjusted with respect to information contained within the temporal sequence, which is translated into an output sequence of release failures and successes. We therefore postulated that presynaptic plasticity should be sensitive to both, the presence and absence of neurotransmitter. This in turn implies that the activation of postsynaptic receptors, such as NMDARs, cannot be necessary the induction of presynaptic plasticity. Next, successful information transmission only occurs when presynaptic release coincides with a postsynaptic output, such as somatic or local

dendritic spikes. Hence, the simplest learning rule for presynaptic strength would optimise release probability with respect to the probability to encounter a postsynaptic spike: the mutual information between neurotransmitter release and postsynaptic spiking is maximised. We therefore tested the predictions that (1) presynaptic LTP at the Schaffer collateral-CA1 synapse does not require postsynaptic NMDARs and is independent of glutamate, and (2) glutamate is detrimental towards LTP but promotes LTD (Padamsey, Tong & Emptage, 2017a).

In the previous chapter, I have shown evidence for the inhibitory role of glutamate on presynaptic release. This further supported previous work that utilised optical methods (conducted by Zahid Padamsey, Padamsey et al., 2017a). Similarly, we have shown that presynaptic LTP can be induced in the presence of NMDAR blockers as well as complete blockade of glutamate receptors. A hallmark of postsynaptic plasticity is its dependence on spike-timing. I therefore asked if presynaptic LTP is also sensitive to the timing between pre- and postsynaptic activity, and if the spike timing-dependent rules match.

7.2. Results

7.2.1. Presynaptic LTP is spike timing-dependent

Our lab has previously shown that presynaptic LTP can be selectively induced in NMDAR blockade (Padamsey et al., 2017a). Our LTP induction protocol involves causal pairing of presynaptic stimulation and postsynaptic complex spikes, evoked via current injection, repeated 60 times at 5 Hz (Fig. 7.1A). In order to study the role of spike timing, I have varied the time between presynaptic stimulation and the occurrence of the first postsynaptic spike from $\Delta t = 0$ to 20 ms. Previous work has shown that anti-causal pairing fails to induce synaptic changes (Padamsey et al., 2017a). Experiments were conducted at Schaffer collateral-CA1 synapses of organotypic hippocampal slices. Due to the high susceptibility of presynaptic LTP towards dialysis, I have limited the baseline recording to within 8 min from the time of establishing whole-cell patch mode. The magnitude of presynaptic changes was monitored by measuring the PPR before and 30 min after the

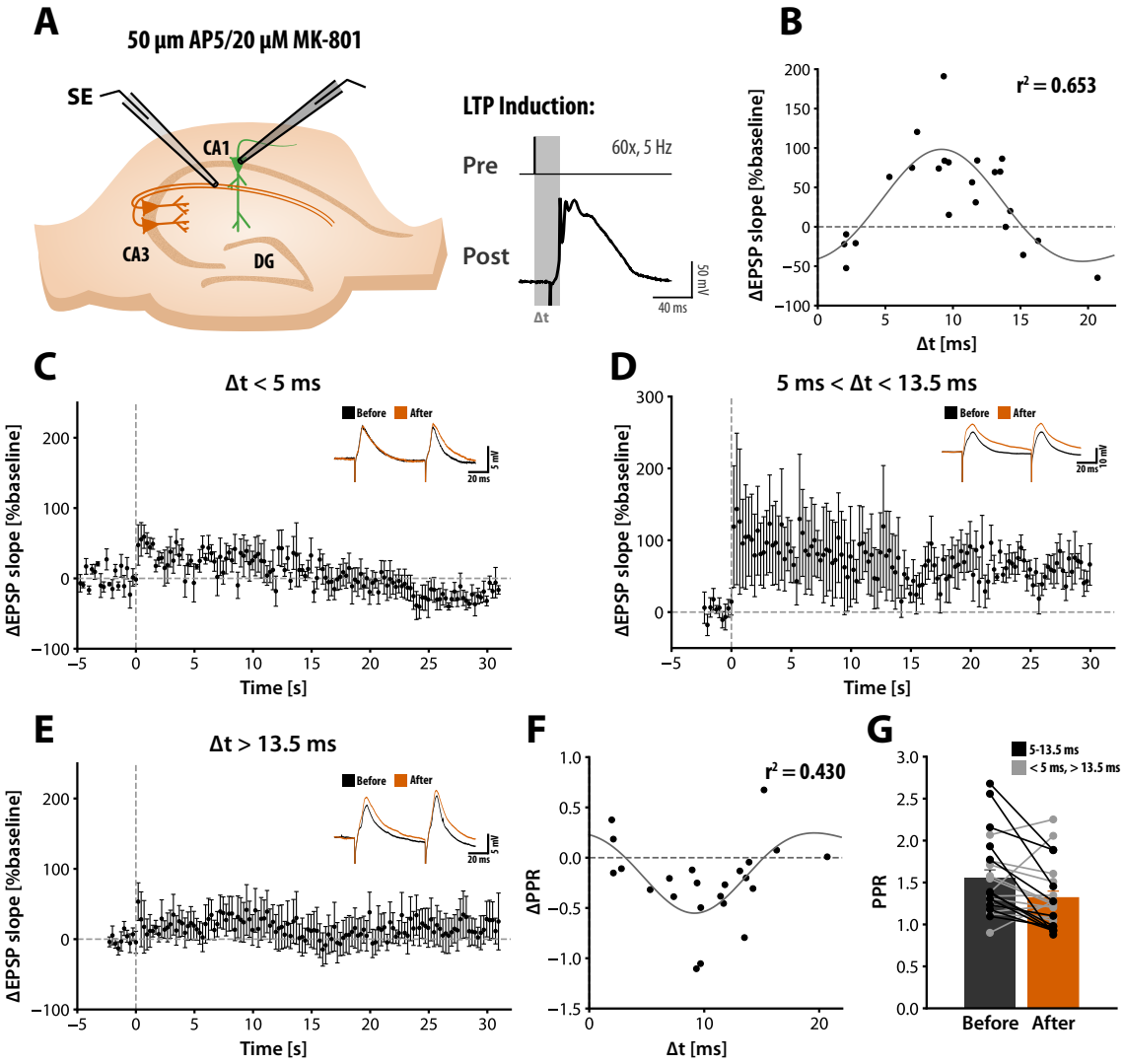

Fig. 7.1: Presynaptic LTP is spike timing-dependent. (A) Schematic of the experimental setup. EPSPs were recorded from Schaffer collateral-CA1 synapses in organotypic slices. Presynaptic LTP was induced by pairing presynaptic stimulation with postsynaptic complex spikes, 60 times at 5 Hz. NMDARs were blocked to prevent the induction of postsynaptic plasticity. (B) The persistent change in the EPSP slope (average of 25-30 min after induction) is shown in relation to the timing between presynaptic stimulation and the first AP in the complex spike. The modulation by spike timing is well described by a Ricker wavelet ($r^2 = 0.653$, N = 23). (C-E) Average EPSP slope change over time for different spike timings. (F) PPR changes in relation to spike timing. PPR changes mirrored that of the EPSP slope. The same wavelet function from (B) was used with adjustments to the normalisation factor to account for the difference in units ($r^2 = 0.430$). (G) PPR before and 30 min after the induction. Successful LTP induction is accompanied by a decrease in the PPR. Error bars represent SEM.

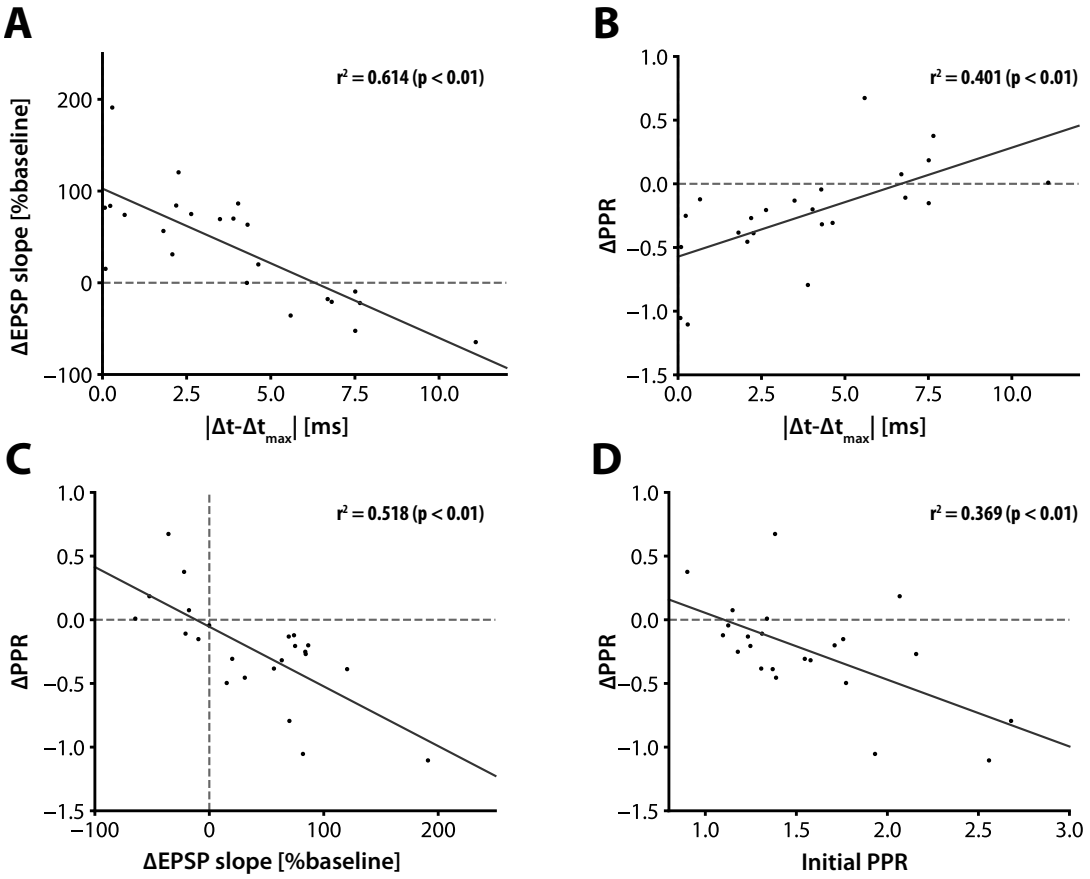

Fig. 7.2: Further analysis of spike timing-dependent presynaptic LTP. (A,B) EPSP slope changes and PPR changes are shown in relation to the absolute time difference from the optimal timing determined in Fig. 7.1B (Δt_{max} = 9.16 ms). The modulation by spike timing is well explained as a linear relationship (Pearson r = -0.784, N = 23, $p < 0.01$; r = 0.633, $p < 0.01$, respectively). (C) Changes in PPR are shown in relation to EPSP slope changes. PPR change was strongly correlated to EPSP slope change (r = -0.719, $p < 0.01$). (D) PPR change in relation to the initial PPR shows moderate correlation (r = -0.607, $p < 0.01$).

induction LTP.

Fig. 7.1B summarises the relationship between spike timing and the fractional change of the initial slope of the EPSP. I observed maximal potentiation when the presynaptic stimulation preceded postsynaptic spiking by ~ 9 ms, and the magnitude of LTP falls off symmetrically for longer and shorter time intervals and is converted into mild LTD. The data was well-explained by a Ricker wavelet ($r^2 = 0.653$, N = 23, $p < 0.01$, Fig. 7.1B) with three degrees-of-freedom (width, horizontal translation, and a normalisation factor), however, the data does not exclude other potential functions (*e.g.* polynomial, Gauss,

etc.). The time interval of maximal LTP determined by the function was Δt_{max} = 9.16 ms. The dependence on spike timing can be further illustrated by a strong linear correlation between the change in EPSP and the absolute time difference from Δt_{max} (Pearson r = -0.798, p < 0.01, Fig. 7.2A). The average trajectory of the EPSP is shown in Fig. 7.1C-E for time intervals Δt < 5 ms, 5 ms < Δt < 13.5 ms, and Δt > 13.5 ms, respectively, chosen arbitrarily based on the spike timing curve. I observed mild short-term potentiation immediately following LTP induction in most cases, which decayed to baseline for short and long Δt. Presynaptic LTP was completely blocked by bath application of the NOS inhibitor L-NAME (100 µM, Fig. 7.3), consistent with previous results (Padamsey et al., 2017a). Unexpectedly, inhibition of NOS led to expression of mild LTD, which was not of presynaptic origin.

Changes in EPSP were strongly correlated with changes in the PPR (Pearson r = -0.719, N = 23, p < 0.01, Fig. 7.2C). Accordingly, PPR changes were similarly dependent on spike timing (Pearson r = 0.617, p < 0.01, Fig. 7.2B) and mirrored that of the EPSP slope (Fig. 7.1F). However, PPR changes were less well explained by the curve obtained from the

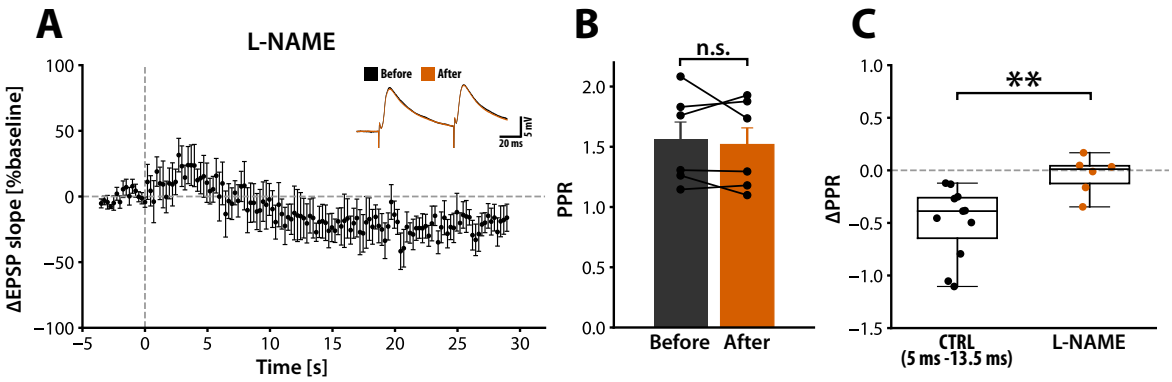

Fig. 7.3: Presynaptic LTP requires NO signalling. (A) NO production was blocked by bath application of 100 µM L-NAME. Shown is the average trace of the EPSP slope. Presynaptic LTP was induced by pairing presynaptic stimulation with postsynaptic complex spikes within 5-13 ms, 60 times at 5 Hz. LTP was completely abolished and mild LTD could be observed. (B) PPR before and 30 min after the induction of LTP. No change in PPR was observed when NO production was inhibited (Wilcoxon signed-rank test). (C) Absolute difference in PPR before and 30 min after the induction of LTP was significantly diminished by L-NAME (Mann-Whitney U test). Error bars represent SEM.

EPSP ($r^2 = 0.430$, $p < 0.01$). I also observed a strong correlation between the initial PPR and changes in PPR (Pearson $r = -0.601$, $p < 0.01$, Fig. 7.2D), indicating that presynaptic plasticity is state-dependent. Initial PPR and spike timing explained the majority of the variance of PPR changes.

7.3. Discussion

I have shown that presynaptic LTP at Schaffer collateral-CA1 synapses is spike timing-dependent and follows approximately a Ricker wavelet-shaped curve. Presynaptic strength changes were indirectly measured using the PPR, which strongly correlated with the EPSP. However, I found that the magnitude of PPR change was comparatively less dependent on spike timing. Absolute PPR changes do not directly translate to Pr changes, since the relationship between PPR and Pr is highly non-linear (Stevens & Wang 1995; Dobrunz & Stevens, 1997). In fact, we found that the relationship between PPR and Pr is approximately exponential ($Pr = a*\exp(-b*PPR) + c$, with constants a, b, c; unpublished work from the Emptage lab). This means that the functional impact of PPR change depends crucially on the initial PPR. Transforming PPR values to $PPR' = \exp(-PPR)$ slightly increased the coefficient of determination of the Ricker wavelet fit ($r^2 = 0.541$). Direct comparison of the magnitude of PPR changes is therefore only valid, if sampling of initial PPRs is homogeneous.

The relationship between spike timing and magnitude of LTP resembles reported spike timing curves in the literature (*e.g.* Wittenberg & Wang, 2006). Wittenberg and Wang reported that pairing of pre- and postsynaptic activity at 5 Hz leads to bi-directional plasticity in the shape of a Ricker wavelet. Consistent with my findings, the maximum potentiation was reported to occur around a time interval of 10 ms. The width of the potentiation window was slightly narrower in my experiments (~ 10 ms compared to 25 ms in Wittenberg & Wang, 2006), however, I did not test time intervals beyond 20 ms or anti-causal pairing. The shape of the spike timing curve is also known to be strongly dependent on the input frequency, which remains to be tested for presynaptic plasticity.

7.3.1. What is the coincidence detector for presynaptic spike timing-dependent LTP?

Spike timing-dependent plasticity requires a coincident detector for pre- and postsynaptic activity. In the case of presynaptic plasticity, spike timing is not sensed by the NMDAR. In fact, the coincident detector is unlikely to involve any kind of glutamate receptor, since presynaptic LTP can be induced in full glutamate receptor blockade (Padamsey et al., 2017a). Whereas postsynaptic plasticity is governed by the coincidence of glutamate release and membrane depolarisation, presynaptic plasticity is sensitive to the timing of the presynaptic AP with respect to strong postsynaptic depolarisation, signalled via the production and release of NO. Where is the coincident detector located? A postsynaptic locus is possible if the production of NO itself is spike timing-dependent, however, we have previously shown that strong depolarisation such as back-propagating AP or local dendritic spikes is sufficient to induce NO release (Padamsey et al., 2017a). Since NO alone is not sufficient to induce presynaptic LTP and requires concomitant presynaptic APs, the coincident detector is likely to be located at the presynaptic terminal and downstream of NO signalling. The putative signalling pathway of NO that leads to an increase in Pr is thought to involve activation of sGC, production of cGMP, activation of PKG, which has been shown to be necessary for presynaptic LTP (Arancio et al., 1995, 1996, 2001). Interestingly, sGC has been shown to be translocated to the plasma membrane, where NO is thought to be enriched due to high solubility, following an elevation in intracellular Ca^{2+}-levels (Zabel et al., 2002). sGC is therefore the prime candidate for implementing coincidence detection as it is activated by NO and is modulated by Ca^{2+}, which is elevated during AP firing (Fig. 7.4).

7.3.2. What is the functional consequence of presynaptic LTP?

We have shown that the presynaptic terminal increases Pr when presynaptic spikes coincide with postsynaptic spiking, and decreases Pr when glutamate is released and that these two processes coexist in parallel (Padamsey et al., 2017a). This learning rule can be summarised as an iterative process of maximisation of mutual information between

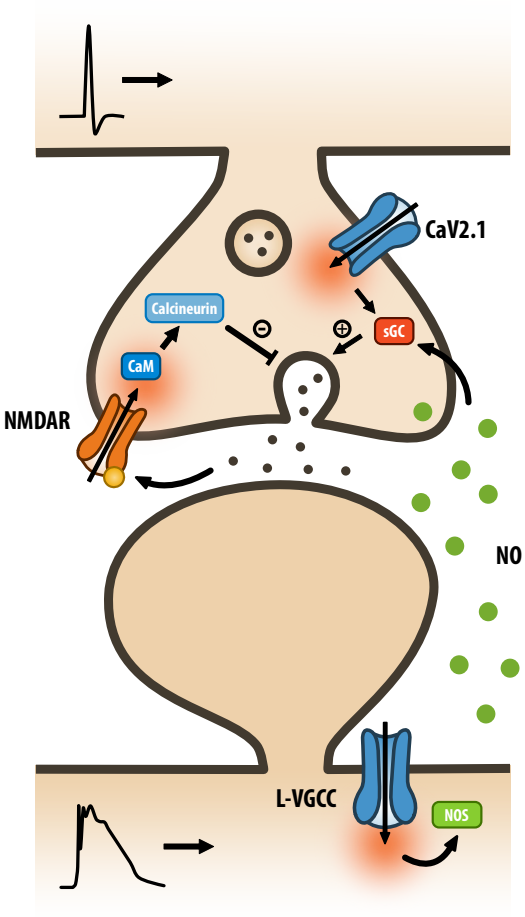

Fig. 7.4: Proposed mechanism for presynaptic plasticity. Presynaptic plasticity consists of two parallel pathways providing positive and negative feedback for adjusting Pr. Glutamate release acts negatively via preNMDARs to decrease Pr as suggested in Chapter 6. Strong postsynaptic depolarisation causes the production and retrograde diffusion of NO, which interacts with sGC to increase Pr. sGC is further modulated by presynaptic Ca^{2+}-levels and is therefore able to process information about spike timing. According to this model, Pr will converge to the conditional probability of postsynaptic spiking given a presynaptic spike. This optimises information transfer across the synapse.

glutamate release and postsynaptic spiking. Mutual information is defined as a reduction in the Shannon entropy MI = H(X) - H(X|Y), where X and Y are random variables. The entropy of the presynaptic terminal is, in its simplest form, solely determined by the Pr and the mean firing frequency. Maximal mutual information is therefore achieved when the conditional probability of postsynaptic spiking given a presynaptic spike matches Pr, Pr = P(postsynaptic spike| presynaptic spike). This can be achieved by a stepwise learning rule that is proportional to the difference $\Delta Pr \propto$ Pr-P(postsynaptic spike| presynaptic

spike), i.e. a prediction error. Spike timing-dependence means that the proportionality factor is variable and adjusts with respect to the temporal contiguity. Molecularly, this is achieved by summation of a positive feedback via NO signalling and a negative feedback via preNMDAR signalling. This learning rule is, however, unstable since postsynaptic spiking probability is positively dependent on the strength of presynaptic inputs, which will lead to run-away dynamics. This can be circumvented if synaptic plasticity is coupled to a supervisory teaching signal. For instance, hippocampal CA1 place cell formation was shown to require coincident input from CA3 and the entorhinal cortex (Bittner et al., 2015, 2017; Milstein et al., 2015; Takahashi & Magee, 2009). Entorhinal inputs onto the distal tuft elicit strong dendritic Ca^{2+}-spikes, which are necessary for the induction of synaptic plasticity. Alternatively, positive and negative feedback signals might be subject to additional non-linear integration, which gates plasticity to occur only when sufficient evidence has been accumulated. Lastly, rapid compensatory mechanisms can counteract run-away dynamics. For instance, in chapters 5 I have reported presynaptic heterosynaptic LTD to also depend on NO. A local increase in synaptic activity will therefore facilitate the induction of hetLTD as well. This effectively restricts an increase in local dendritic depolarisation caused by a local rise in Pr. It will be crucial to test these hypotheses in future work in order to gain a complete understanding of the regulation of Pr.

8. General Discussion

8.1. Are the functional consequences of pre- and postsynaptic plasticity the same?

One of the main guiding questions throughout my thesis concerns the distinct functional consequences of pre- and postsynaptic plasticity. This question is difficult to address without proper knowledge of how information is encoded in the brain, however, certain theoretical considerations can be made.

1. The impact of presynaptic plasticity crucially depends on the temporal structure of the input

Synaptic modifications can be understood as an optimisation of the impact of a synapse on neuronal output. Impact can be quantified in various ways, such as the probability of eliciting postsynaptic spiking or more generally the maximisation of mutual information. These models often consider information on a spike-by-spike basis. This leads to learning rules in which the gradient of the synaptic impact with respect to pre- and postsynaptic strength (defined as release probability and neurotransmitter receptor conductance, respectively) is monotonous, i.e. an increase in synaptic strength always leads to an increase in "synaptic impact". However, it is well-established that neuronal information is encoded in the temporal structure of APs, either as the frequency of firing (rate codes), the inter-spike interval (spike timing codes) or the temporal correlation across inputs (population codes). This necessitates a description of synaptic strength with respect to temporal properties of the inputs.

Both, pre- and postsynaptic mechanisms can influence the temporal structure of inputs. Postsynaptically, the EPSP waveform, especially its decay properties, crucially determines the temporal integration window of synaptic inputs (Branco et al., 2016; König et al., 1996; Shadlen et al., 1994). The decay of the EPSP is determined by the expression pattern of voltage-gated ion channels, which contribute to the repolarisation of the membrane

potential and the biophysical properties of the neurotransmitter receptor, which are determined by their subunit composition and auxiliary proteins (Diering & Huganir, 2018; Greger et al., 2017). Additionally, tightly coupled inhibitory inputs are also able to set the integration time window (Isaacson & Scanziani, 2011). Changes to the integration time window affect the precision of spike timing codes and population codes on the order of milliseconds and set the superlinearity of rate codes. Plasticity of the EPSP decay is, however, not well studied. For instance, postsynaptic plasticity is known to involve the trafficking, insertion and removal of AMPA receptor subunits (Lüscher & Malenka, 2012), which therefore confer different levels of synapse stability. In addition, NMDARs are known to undergo changes to their subunit composition, and due to their comparatively slow channel kinetics, can majorly influence the decay constant of the EPSP (Hunt & Castillo, 2012). However, using the definition of postsynaptic strength as the (maximum) receptor conductance, and the evidence for AMPA receptor insertion/removal following LTP/LTD, i.e. a change in receptor number, the general form of postsynaptic plasticity is invariant towards temporal aspects of the input.

I therefore suggest that optimisation of temporal information requires presynaptic mechanisms (Buonomano, 2000). Presynaptic short-term plasticity is strongly dependent on the history of firing, especially the frequency, but also recent release events (Chapter 6; Dobrunz et al., 1997; Stevens & Wang, 1995). These processes are able to integrate spiking activity over tens to hundreds of milliseconds and, in the case of augmentation, several seconds, vastly exceeding most postsynaptic time scales (but see Branco et al., 2016). Moreover, the variety of semi-independent processes that underlie short-term plasticity, such as Ca^{2+}-entry dynamics, Ca^{2+}-buffering, the RRP, and vesicle recycling, would theoretically allow the presynaptic terminal to adapt to more complex temporal structures. Importantly, release probability is a strong determinant of the short-term behaviour of a synapse and changes to release probability will inevitably affect short-term presynaptic plasticity. The previous argument can also be reversed: changes to short-term plasticity are reflected, and experimentally observed as changes to Pr. In fact,

the interpretation of experimentally determined Pr is questionable, as it often assumes the synapse to be in a naive, inactive state. For instance, I have measured Pr by sequentially sampling neurotransmitter release at very low frequencies (0.06 Hz), a frequency far below the average baseline firing rate under physiological conditions (~ 1 Hz, Wilson & McNaughton, 1993). Fig. 8.1 exemplifies this notion. I stimulated Schaffer collateral-CA1 synapses using a random AP train generated from a Poisson process with average frequency of 5 Hz. Repetition of the AP train allowed me to use optical quantal analysis to calculate the effective release probability of each AP. The "naive" Pr of the synapse shown in Fig. 8.1C is around Pr = 0.32 ± 0.11 (first AP), however, during the stimulation, Pr varies between 0.11 to a maximum of 0.89 due to short-term plasticity,

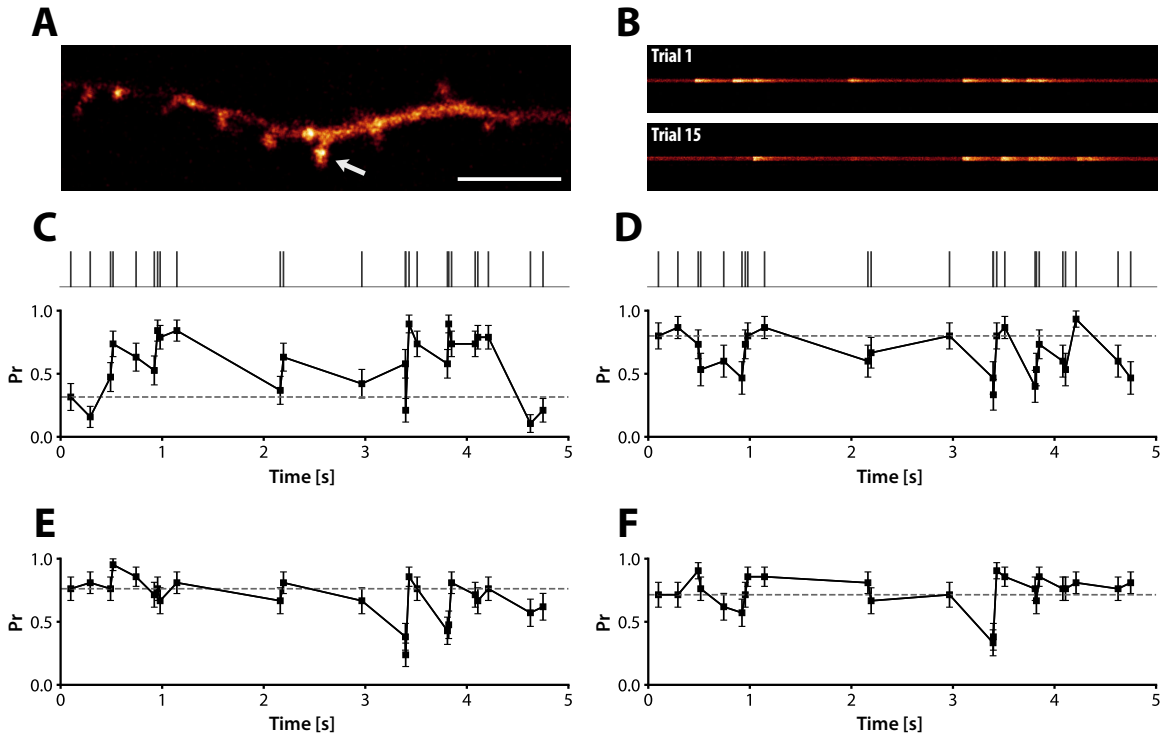

Fig. 8.1: Release probability during complex AP trains. (A) Example image of a spine targeted for optical quantal analysis (white arrow). Scale bar: 5 µm. (B) Example EPSCaTs traces. Traces show raw fluorescence responses of the synapse presented in (C). The basal Pr = 0.32 ± 0.11. (C-F) Estimated Pr for each pulse of a randomly generated AP train. The timing of stimulation is shown at the top in (C,D) and was generated from a Poisson process at 5 Hz. Shown are four synapses from four different slices. The same stimulus train was used in each experiment. Pr follows a complex, but partly predictable trajectory. Error bars represent standard deviation from the estimated binomial distribution.

even at long inter-pulse intervals. I have repeated the same AP train at synapses of substantially higher Pr (Fig. 8.1D-F). Although these synapses exhibit similar trajectories of the effective Pr, some minor qualitative differences can be seen (such as the response to the first six-seven pulses). I cannot make precise quantitative statements due to the low sample number, however, the complexity of the Pr trajectory and variability between synapses provide further evidence that presynaptic strength cannot be defined on a spike-by-spike basis. Similar observations were previously reported by Dobrunz and Stevens, who used minimal stimulation of physiological AP trains (Dobrunz & Stevens, 1999). These experiments, thus, open up a view in which presynaptic strength is adjusted to emphasise or suppress certain temporal motifs in the AP train, a strategy that has been previously suggested for artificial neural networks employing dynamic synapses (Liaw & Berger, 1996; Natschläger et al., 2001; Maass & Zador, 1999). However, the underlying learning rules and biological implementations are unclear.

The role of presynaptic strength in decoding temporal properties of the input can be simplified when assuming that information is transmitted as rate codes, i.e. the average frequency of firing. Short-term facilitation and depression are known to act as frequency filters and therefore non-linearly transform the frequency power spectrum of the input. For instance, Klyachko and Stevens reported that Schaffer collateral-CA1 synapses act as high-pass filter, selectively accentuating frequencies above a characteristic "transition frequency" due to short-term facilitation ($f_{transition}$ ~ 7 Hz, Klyachko & Stevens, 2006). This is mirrored by low-pass properties of inhibitory inputs due to short-term depression ($f_{transition}$ ~ 5.6 Hz, Klyachko & Stevens, 2006). This leads to improvement of the signal-to-noise ratio of information encoded at high frequencies. Following this idea, changes in Pr of synapses with predominant short-term facilitation or depression can be interpreted as sliding the characteristic transition frequency thus creating a sigmoid-shaped non-linearity. For instance, highly reliable or informative inputs could possess high Pr, which leads to low transition frequency and therefore an open filter through which information transmission is unhindered. Conversely, synapses with low Pr require the accumulation of

temporal evidence (in the form of high frequency spiking activity) in order to transmit. This leads to the effective sharpening of the response properties of the neurone (such as receptive field properties), which can be independently adjusted between each synaptic pair.

In an alternative interpretation, presynaptic short-term plasticity could act to transform inputs into a common format as to reduce weighting biases of postsynaptic integration. This could be important when presynaptic inputs originate from distinct populations that differ in their dynamic firing range. For example, Pr was found to be normalised along individual segments of dendrites and was sensitive to the number of synaptic contacts made by the same axon (Branco et al., 2008). At the mossy fibre-CA3 synapse, the magnitude of postsynaptic depolarisation is normalised with respect to the number of APs, independent of frequency (Chamberland et al., 2018). The authors found that the size of the sixth AP given in a burst of varying frequencies was constant. The mossy fibre bouton therefore acts as a preprocessing unit, accumulating temporal evidence, and transmitting a normalised response when evidence was sufficient. The authors have implicated weak coupling between Ca^{2+}-channels and docked neurotransmitter vesicles as a potential mechanism. Similarly, presynaptic Hebbian plasticity at layer 2/3 cortical synapses was shown to normalise inputs with respect to their quantal parameters (Hardingham et al., 2007), since the magnitude and direction of synaptic plasticity were strongly correlated with the initial presynaptic strength. Lastly, a recent study showed that presynaptic short-term plasticity is modulated along branches of dendrites to counteract the electrotonic attenuation, which is more pronounced at distal inputs (Grillo et al., 2018).

Release probability is known to affect the preferred mode of information transmission of a synapse. Markram and Tsodyks have shown that the degree of short-term depression at cortical synapses determines whether the input frequency or the time derivative of the frequency is being transmitted (Tsodyks & Markam, 1997; Tsodyks et al., 1998; Markram et al., 1998). Similarly, Abbott and colleagues showed that short-term depression can lead

to the transmission of relative rather than absolute frequency differences (Abbott et al., 1997). In line with these findings, spike timing codes should be more optimally transmitted at high Pr synapses whereas rate codes should generally prefer low Pr synapses due to the suppression imposed by vesicle depletion and short-term depression at high Pr. Following this line of argument, regulation of Pr cannot be strictly monotonous.

In chapters 6 and 7, we have provided evidence for a new learning rule of presynaptic plasticity (Padamsey et al., 2017a). Presynaptic LTP requires coincident pre- and postsynaptic spiking activity. Release of glutamate, however, negatively impacts on Pr and induces presynaptic LTD. This learning rule intrinsically incorporates and optimises Pr with respect to knowledge about the temporal structure of presynaptic firing. For instance, if burst firing is informative between a given pair of neurones, presynaptic bursts will be followed by, in the optimal case, a single postsynaptic response. For high Pr synapses, excessive glutamate will be released during the AP burst, and LTD will predominate. A steady-state is only reached when Pr matches the conditional probability of postsynaptic spiking given a single presynaptic AP, which, in the optimal case, equates to $P(\text{postsynaptic spike}|\text{presynaptic AP}) = 1/N_{burst}$, where N_{burst} is the average number of AP in the presynaptic burst. This is due to the fact that at steady-state every release event, on average, will be followed by strong postsynaptic depolarisation, which will provide the necessary positive feedback via NO signalling to compensate for glutamate-mediated LTD. Under this framework, robustness of information transmission can be trivially implemented by setting $Pr > P(\text{postsynaptic spike}|\text{presynaptic AP})$, for instance by differentially weighting the positive and negative feedback signals of NO and glutamate, respectively. Conversely, if information is encoded by each spike, such as in the case of spike timing codes, $P(\text{postsynaptic spike}|\text{presynaptic AP}) = 1$, which will be mirrored by the Pr.

Next, I have shown that strong local coordinated activity leads to heterosynaptic presynaptic weakening. As heterosynaptic plasticity is often viewed under a homeostatic

framework, the most parsimonious interpretation is an increase in the characteristic transition frequency of these synapses. This reduces background low frequency activity without compromising potential informative high frequency inputs. I have also provided evidence that presynaptic heterosynaptic weakening is highly thresholded by the diffusion properties of NO, which is dominated by the inactivation dynamics of NO. This might prevent excessive silencing of inputs which could impair beneficial properties of background activity, such as stochastic resonance.

2. The impact of presynaptic plasticity is independent of postsynaptic non-linear integration

Cooperativity is a hallmark of synaptic plasticity and information transmission in neural networks. As single synaptic inputs are rarely sufficient to elicit non-linear spiking activity, inputs need to be coordinated and integrated across synapses. However, with increasing number of integrated synaptic inputs or input strength, which drive the postsynaptic membrane potential closer to non-linearity threshold, the postsynaptic strength of individual synapses becomes negligible and input correlations become predominant. This means that the impact of postsynaptic plasticity is strictly dependent on the average postsynaptic membrane potential. For example, if the membrane potential is close to the non-linearity threshold, small decreases in postsynaptic strength are less effective in reducing a synapse's contribution to postsynaptic spiking. Similarly, if a synapse is correlated with strong inputs, which by themselves are sufficient to drive spiking, changes to the postsynaptic strength will have minimal impact. This, of course, is crucial for the formation of associative memories, however, it is also the main contributor to the instability of Hebbian plasticity, which cannot be easily alleviated by postsynaptic mechanisms. The impact of presynaptic release probability is binary and completely independent of the postsynaptic non-linearity. A reduction in Pr will lead to a reduction of a synapse's contribution by the same amount from the point of view of the synapse, irrespective of the average membrane potential and postsynaptic excitability. Pr also serves as a natural metaplastic switch for postsynaptic plasticity, which is crucially dependent on the activation of NMDARs, i.e. the release of glutamate.

The above considerations might be important for the interpretation of compensatory heterosynaptic pre- and postsynaptic plasticity. For example, the local potentiation of groups of synapses could lead to locally increased excitability due to elevated membrane potential. This will facilitate plasticity induction at neighbouring synapses, the degree of which scales with the input correlation with the potentiated group of synapses. In order to prevent these run-away dynamics, homeostatic mechanisms are needed. Homeostatic compensation of postsynaptic strength might not be sufficient, since postsynaptic spiking will be largely driven cooperatively. Presynaptic compensation, however, would be more effective since it directly impacts on the input correlation and therefore reduces the degree of cooperativity. A special case of this situation is supervised or reinforcement learning. For example, cerebellar climbing fibres are necessary to induce complex spiking in Purkinje neurones to induce synaptic plasticity (Konnerth et al., 1992). Similarly, formation of place cells in hippocampus CA1 requires concomitant input of the perforant path, which induce large dendritic depolarisation and drive synaptic plasticity at Schaffer collateral-CA1 synapses in vivo (Bittner et al., 2017). These learning rules are locally independent of postsynaptic depolarisation. Therefore, spatial coordination and competition would necessitate presynaptic mechanisms.

3. Pre- and postsynaptic strengths possess distinct metabolic footprints

Neural circuits have evolved under strict energy constraints (Aiello, 1997). The main source of energy consumption of neurones is thought to reside in their synapses and the generation of APs (Harris et al., 2012). Maintenance of the postsynaptic membrane potential is thought to comprise half of the synaptic energy and, at glutamatergic synapses, is equally contributed to by NMDA and non-NMDARs. A recent study using fluorescent probes to measure ATP consumption revealed that vesicle endocytosis encompasses the main energetic burden at the presynaptic terminal (Rangaraju et al., 2014). The metabolic constraints on presynaptic plasticity are therefore likely to be more stringent as Pr will affect both pre- and postsynaptic energy consumption (excluding the energy cost of APs), whereas postsynaptic AMPA receptors account for only 40 % of

synaptic energy (Harris et al., 2012), which is likely an overestimate given the recent study of the presynaptic terminal (Rangaraju et al., 2014). It therefore follows that the induction and expression of presynaptic LTP should be more strongly regulated compared to postsynaptic LTP. This is consistent with the requirement of L-VGCCs for presynaptic LTP, which have high activation threshold. Additionally, excessive and redundant glutamate release should be inhibitory, which I have shown to be the case in both, long- and short-term plasticity. This could also explain why I did not detect heterosynaptic presynaptic strengthening, unlike in the postsynaptic case.

In summary, synaptic strength cannot be treated as a single multiplicative weight factor $w = pq$, which is frequently employed in theoretical treatments of the synapse. It has to be realised that the output of a neurone is determined by the release of neurotransmitter rather than the generation of AP trains, since computations at the presynaptic terminal can significantly distort temporal properties and transmit only certain aspects of the original AP train. This is further reflected in the impact of presynaptic strength on the mode of information transfer. Postsynaptic learning rules need to be revised as postsynaptic plasticity, which crucially depends on neurotransmitter release to activate corresponding receptors, does not optimise with respect to presynaptic APs but rather neurotransmitter release. This would predict that two synapses experiencing the same pre- and postsynaptic spiking activity, but differing in their presynaptic properties should also lead to different plasticity outcomes. This remains to be investigated. Lastly, pre- and postsynaptic terminals have evolved under distinct metabolic constraints, which might underlie differences in the biological implementation of their respective plasticity processes.

8.2. Are pre- and postsynaptic changes explained by the same set of rules?

The functional differences outlined above predict that the learning rules for pre- and postsynaptic plasticity are likely to differ. We have shown that presynaptic Hebbian

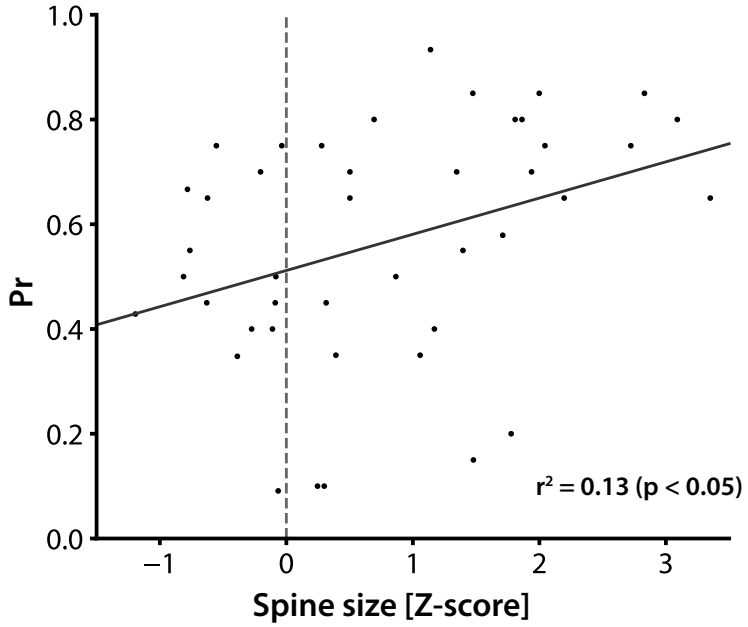

Fig. 8.2: Pre- and postsynaptic strengths were only weakly correlated. The initial spine size is shown in relation to the estimated Pr. Data was pooled from experiments (without pharmacological interventions) of both Chapters 4 and 5. The correlation was weak (Pearson r = 0.36, N = 43, $p < 0.05$).

plasticity is independent of glutamate and requires a molecularly separate mechanism for coincident detection, which is likely localised at the presynaptic terminal. Heterosynaptically, both pre- and postsynaptic strength weaken at proximal synapses, whereas I only observed postsynaptic strengthening at distal synapses. I was able to dissociate the underlying signalling pathways as early as the activation of downstream targets of NMDAR signalling, indicating parallel biochemical computations. Differences in biochemical computation, both spatially and temporally, might explain differences across experimental conditions, such as optically vs. electrophysiologically induced cLTP. Heterosynaptic changes were weakly correlated. This correlation represents the functional overlap.

Apart from their functional differences, the activity experienced by pre- and postsynaptic terminals differs, as the presynaptic terminal has access to the complete input AP train. Therefore, even if the computational rules by which pre- and postsynaptic strengths are optimised are the same, such as maximisation of mutual information, the outcome would

still differ (unless Pr = 1).

How can these results be reconciled with the strong basal correlation between pre- and postsynaptic strengths that suggests a precise matching? As discussed before, presynaptic non-linear computations can be linearised when neural activity is averaged across time. Therefore, the correlation of pre- and postsynaptic strength found in studies of populations of synapses might reflect the regulation of synaptic strength on long time scales at which the functional dissociation is minimal. Fine scale differences of pre- and postsynaptic strengths might therefore be sufficient to account for the functional roles outline above. In addition, synaptic strength regulation on shorter time scales, such as those involved in modulating network dynamics, might present a more pronounced mismatch. Lastly, large scale measurements of presynaptic strength requires indirect methods, such as anatomical markers, and might not capture the full extent of the variability of presynaptic strength. In my experiments, the correlation between the initial spine size and release probability was weak (Pearson $r = 0.36$, $p < 0.05$, Fig. 8.2).

8.3. Towards a two-compartment model of the synapse

Considering the available experimental evidence and theoretical work, I propose that the synapse should be functionally interpreted as a two-compartment model (Fig. 8.3). Similar to the two-compartment model of synaptic integration (Branco & Häusser, 2010), the dissociation of pre- and postsynaptic compartments will increase the computational power of the neural network as it effectively increases the number of non-linear operations of the system. These additional non-linearities, however, do not operate on the integration of synaptic input, but rather diversify the output of a neurone, and is not equivalent to an increase in processing layers in neural networks. The consequences on the performance of neural networks are therefore difficult to judge. Presynaptic terminals of a single neurone might project the output spike train onto feature axes representing different aspects of temporal information and create a decomposition of the spike train. This would facilitate the downstream network to utilise temporal information, allow for

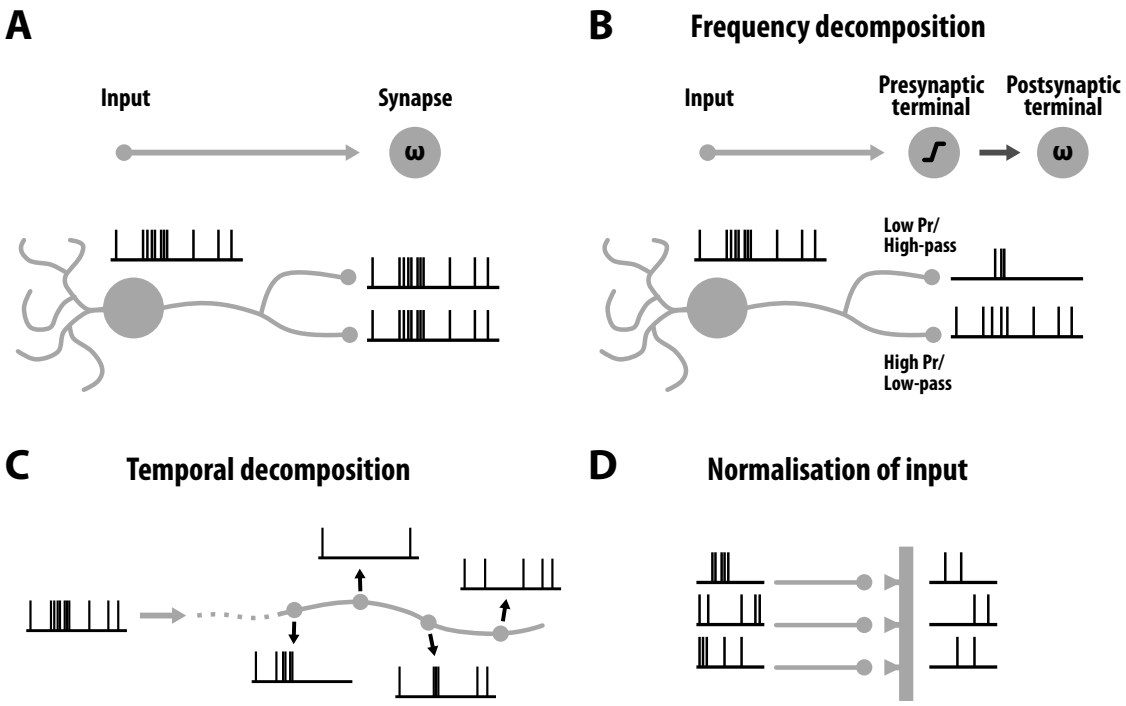

Fig. 8.3: Two-compartment model of the synapse. (A) The conventional single-compartment model views the synapse as a linear operation, which scales the input multiplicatively by its weight, w. (B) In the two-compartment model, the pre- and postsynaptic terminals fulfil distinct functional roles. The presynaptic terminal acts as a non-linear temporal filter, such as a frequency filter. Low Pr synapses will preferentially transmit AP bursts, whereas high Pr synapses support spike timing codes. The postsynaptic terminal inherits the function of the single-compartment model. (C) More generally, presynaptic terminals along the axon can be viewed as a decomposition of input spike trains into distinct temporal features. This, for example, allows neurones to multiplex their output responses. (D) Presynaptic non-linear transformation could also act to normalise inputs and therefore facilitate postsynaptic integration.

multiplexing of information in the output AP train, context-dependent gating of the downstream network, and simplification of postsynaptic integration as a linear integrator.

9. References

Abbott, L.F. & Nelson, S.B. 2000. Synaptic plasticity: taming the beast. *Nature neuroscience*, 3: 1178–1183.

Abbott, L.F. & Regehr, W.G. 2004. Synaptic computation. *Nature*, 431(7010): 796–803.

Abbott, L.F., Varela, J.A., Sen, K. & Nelson, S.B. 1997. Synaptic depression and cortical gain control. *Science*, 275(5297): 220–224.

Abraham, W.C. 2008. Metaplasticity: tuning synapses and networks for plasticity. *Nature reviews. Neuroscience*, 9(5): 387–387.

Abraham, W.C. & Wickens, J.R. 1991. Heterosynaptic long-term depression is facilitated by blockade of inhibition in area CA1 of the hippocampus. *Brain research*, 546(2): 336–340.

Abraham, W.C., Christie, B.R., Logan, B., Lawlor, P. & Dragunow, M. 1994. Immediate early gene expression associated with the persistence of heterosynaptic long-term depression in the hippocampus. *Proceedings of the National Academy of Sciences*, 91(21): 10049–10053.

Abrahamsson, T., Chou, C.Y.C., Li, S.Y., Mancino, A., Costa, R.P., Brock, J.A., Nuro, E., Buchanan, K.A., Elgar, D., Blackman, A.V., Tudor-Jones, A., Oyrer, J., Farmer, W.T., Murai, K.K. & Sjöström, P.J. 2017. Differential Regulation of Evoked and Spontaneous Release by Presynaptic NMDA Receptors. *Neuron*, 96(4): 839–855.

Adelman, J.P., Maylie, J. & Sah, P. 2012. Small-Conductance Ca2+-Activated K+ Channels: Form and Function. *Annual Review of Physiology*, 74(1): 245–269.

Aiello, L.C. 1997. Brains and guts in human evolution: The Expensive Tissue Hypothesis. *Brazilian Journal of Genetics*, 20(1): 141–148.

Alioua, A., Tanaka, Y., Wallner, M., Hofmann, F., Ruth, P., Meera, P. & Toro, L. 1998. The large conductance, voltage-dependent, and calcium-sensitive K+ channel, Hslo, is a target of cGMP-dependent protein kinase phosphorylation in vivo. *The Journal of biological chemistry*, 273(49): 32950–32956.

Ammendola, A., Geiselhöringer, A., Hofmann, F. & Schlossmann, J. 2001. Molecular determinants of the interaction between the inositol 1,4,5-trisphosphate receptor-associated cGMP kinase substrate (IRAG) and cGMP kinase Ibeta. *The Journal of biological chemistry*, 276(26): 24153–24159.

Andrade-Talavera, Y., Duque-Feria, P., Paulsen, O. & Rodríguez-Moreno, A. 2016. Presynaptic Spike Timing-Dependent Long-Term Depression in the Mouse Hippocampus. *Cerebral cortex (New York, N.Y. : 1991)*, 26(8): 3637–3654.

Arancio, O., Antonova, I., Gambaryan, S., Lohmann, S.M., Wood, J.S., Lawrence, D.S. & Hawkins, R.D. 2001. Presynaptic role of cGMP-dependent protein kinase during long-lasting potentiation. *The Journal of neuroscience*, 21(1): 143–149.

Arancio, O., Kandel, E.R. & Hawkins, R.D. 1995. Activity-dependent long-term enhancement of transmitter release by presynaptic 3',5'-cyclic GMP in cultured hippocampal neurons. *Nature*, 376(6535): 74–80.

Arancio, O., Kiebler, M., Lee, C.J., Lev-Ram, V., Tsien, R.Y., Kandel, E.R. & Hawkins, R.D. 1996.

Nitric oxide acts directly in the presynaptic neuron to produce long-term potentiation in cultured hippocampal neurons. *Cell*, 87(6): 1025–1035.

Arellano, J.I., Benavides-Piccione, R., DeFelipe, J. & Yuste, R. 2007. Ultrastructure of dendritic spines: correlation between synaptic and spine morphologies. *Frontiers in neuroscience*, 1(1): 131–143.

Arias-Cavieres, A., Barrientos, G.C., Sánchez, G., Elgueta, C., Muñoz, P. & Hidalgo, C. 2018. Ryanodine Receptor-Mediated Calcium Release Has a Key Role in Hippocampal LTD Induction. *Frontiers in cellular neuroscience*, 12: 403.

Arnold, W.P., Mittal, C.K., Katsuki, S. & Murad, F. 1977. Nitric oxide activates guanylate cyclase and increases guanosine 3':5'-cyclic monophosphate levels in various tissue preparations. *Proceedings of the National Academy of Sciences*, 74(8): 3203–3207.

Augustine, G.J., Charlton, M.P. & Smith, S.J. 1985. Calcium entry and transmitter release at voltage-clamped nerve terminals of squid. *The Journal of physiology*, 367(1): 163–181.

Augustine, G.J., Santamaria, F. & Tanaka, K. 2003. Local calcium signaling in neurons. *Neuron*, 40(2): 331–346.

Babadi, B. & Abbott, L.F. 2010. Intrinsic stability of temporally shifted spike-timing dependent plasticity. L. J. Graham, ed. *PLoS computational biology*, 6(11): e1000961.

Bahr, B.A. 1995. Long-term hippocampal slices: a model system for investigating synaptic mechanisms and pathologic processes. *Journal of neuroscience research*, 42(3): 294–305.

Bahr, B.A., Kessler, M., Rivera, S., Vanderklish, P.W., Hall, R.A., Mutneja, M.S., Gall, C. & Hoffman, K.B. 1995. Stable maintenance of glutamate receptors and other synaptic components in long-term hippocampal slices. *Hippocampus*, 5(5): 425–439.

Balaban, P., Chistiakova, M., Malyshev, A. & Volgushev, M. 2004. Dependence of calcium influx in neocortical cells on temporal structure of depolarization, number of spikes, and blockade of NMDA receptors. *Journal of neuroscience research*, 76(4): 481–487.

Balaji, J. & Ryan, T.A. 2007. Single-vesicle imaging reveals that synaptic vesicle exocytosis and endocytosis are coupled by a single stochastic mode. *Proceedings of the National Academy of Sciences of the United States of America*, 104(51): 20576–20581.

Bamburg, J.R. 1999. Proteins of the ADF/cofilin family: essential regulators of actin dynamics. *Annual review of cell and developmental biology*, 15(1): 185–230.

Banerjee, A., Larsen, R.S., Philpot, B.D. & Paulsen, O. 2016. Roles of Presynaptic NMDA Receptors in Neurotransmission and Plasticity. *Trends in Neurosciences*, 39(1): 26–39.

Bannon, N.M., Chistiakova, M., Chen, J.-Y., Bazhenov, M. & Volgushev, M. 2017. Adenosine Shifts Plasticity Regimes between Associative and Homeostatic by Modulating Heterosynaptic Changes. *The Journal of neuroscience*, 37(6): 1439–1452.

Bao, J., Reim, K. & Sakaba, T. 2010. Target-Dependent Feedforward Inhibition Mediated by Short-Term Synaptic Plasticity in the Cerebellum. *Journal of Neuroscience*, 30(24): 8171–8179.

Barlow, H.B. 1959. Sensory mechanisms, the reduction of redundancy, and intelligence. *NPL Symposium on the Mechanization of Thought Process.*, 10: 535–539.

Baumgärtel, K. & Mansuy, I.M. 2012. Neural functions of calcineurin in synaptic plasticity and memory. *Learning & memory (Cold Spring Harbor, N.Y.)*, 19(9): 375–384.

Bayazitov, I.T., Richardson, R.J., Fricke, R.G. & Zakharenko, S.S. 2007. Slow presynaptic and fast postsynaptic components of compound long-term potentiation. *The Journal of neuroscience*, 27(43): 11510–11521.

Baylor, D.A., Lamb, T.D. & Yau, K.W. 1979. The membrane current of single rod outer segments. The Journal of physiology, 288: 589–611.

Bekkers, J.M. & Stevens, C.F. 1995. Quantal analysis of EPSCs recorded from small numbers of synapses in hippocampal cultures. *Journal of Neurophysiology*, 73(3): 1145–1156.

Bekkers, J.M., Richerson, G.B. & Stevens, C.F. 1990. Origin of variability in quantal size in cultured hippocampal neurons and hippocampal slices. *Proceedings of the National Academy of Sciences*, 87(14): 5359–5362.

Bell, A.J. & Sejnowski, T.J. 1995. An information-maximization approach to blind separation and blind deconvolution. *Neural computation*, 7(6): 1129–1159.

Berretta, N. & Jones, R.S. 1996. Tonic facilitation of glutamate release by presynaptic N-methyl-D-aspartate autoreceptors in the entorhinal cortex. *Neuroscience*, 75(2): 339–344.

Betz, W.J. & Bewick, G.S. 1992. Optical analysis of synaptic vesicle recycling at the frog neuromuscular junction. *Science*, 255(5041): 200–203.

Béïque, J.-C., Lin, D.-T., Kang, M.-G., Aizawa, H., Takamiya, K. & Huganir, R.L. 2006. Synapse-specific regulation of AMPA receptor function by PSD-95. *Proceedings of the National Academy of Sciences*, 103(51): 19535–19540.

Bi, G.-Q. & Poo, M.-M. 1998. Synaptic Modifications in Cultured Hippocampal Neurons: Dependence on Spike Timing, Synaptic Strength, and Postsynaptic Cell Type. *The Journal of neuroscience : the official journal of the Society for Neuroscience*, 18(24): 10464–10472.

Bian, W.-J., Miao, W.-Y., He, S.-J., Qiu, Z. & Yu, X. 2015. Coordinated Spine Pruning and Maturation Mediated by Inter-Spine Competition for Cadherin/Catenin Complexes. *Cell*, 162(4): 808–822.

Biederer, T., Kaeser, P.S. & Blanpied, T.A. 2017. Transcellular Nanoalignment of Synaptic Function. *Neuron*, 96(3): 680–696.

Bienenstock, E.L., Cooper, L.N. & Munro, P.W. 1982. Theory for the development of neuron selectivity: orientation specificity and binocular interaction in visual cortex. *Journal of Neuroscience*, 2(1): 32–48.

Bird, C.M. & Burgess, N. 2008. The hippocampus and memory: insights from spatial processing. *Nature reviews. Neuroscience*, 9(3): 182–194.

Bittner, K.C., Grienberger, C., Vaidya, S.P., Milstein, A.D., Macklin, J.J., Suh, J., Tonegawa, S. & Magee, J.C. 2015. Conjunctive input processing drives feature selectivity in hippocampal CA1 neurons. *Nature neuroscience*, 18(8): 1133–1142.

Bittner, K.C., Milstein, A.D., Grienberger, C., Romani, S. & Magee, J.C. 2017. Behavioral time scale synaptic plasticity underlies CA1 place fields. *Science*, 357(6355): 1033–

1036.

Blackman, A.V., Abrahamsson, T., Costa, R.P., Lalanne, T. & Sjöström, P.J. 2013. Target-cell-specific short-term plasticity in local circuits. *Frontiers in synaptic neuroscience*, 5.

Blackmer, T., Larsen, E.C., Takahashi, M., Martin, T.F., Alford, S. & Hamm, H.E. 2001. G protein betagamma subunit-mediated presynaptic inhibition: regulation of exocytotic fusion downstream of Ca2+ entry. *Science*, 292(5515): 293–297.

Blackshaw, S., Eliasson, M.J.L., Sawa, A., Watkins, C.C., Krug, D., Gupta, A., Arai, T., Ferrante, R.J. & Snyder, S.H. 2003. Species, strain and developmental variations in hippocampal neuronal and endothelial nitric oxide synthase clarify discrepancies in nitric oxide-dependent synaptic plasticity. *Neuroscience*, 119(4): 979–990.

Bliss, T.V. & Lomo, T. 1973. Long-lasting potentiation of synaptic transmission in the dentate area of the anaesthetized rabbit following stimulation of the perforant path. *The Journal of physiology*, 232(2): 331–356.

Bliss, T.V., Collingridge, G.L. & Morris, R.G.M. Synaptic Plasticity in the Hippocampus. In Andersen, P., Morris, R., Amaral, D., Bliss, T. & John, O. 2007. *The Hippocampus Book*. New York: Oxford Univ Press., 343-474

Bloodgood, B.L. & Sabatini, B.L. 2005. Neuronal activity regulates diffusion across the neck of dendritic spines. *Science*, 310(5749): 866–869.

Bloodgood, B.L. & Sabatini, B.L. 2007. Nonlinear Regulation of Unitary Synaptic Signals by CaV2.3 Voltage-Sensitive Calcium Channels Located in Dendritic Spines. *Neuron*, 53(2): 249–260.

Bohte, S.M. & Mozer, M.C. 2007. Reducing the variability of neural responses: a computational theory of spike-timing-dependent plasticity. *Neural computation*, 19(2): 371–403.

Bollmann, J.H., Sakmann, B. & Borst, J.G. 2000. Calcium sensitivity of glutamate release in a calyx-type terminal. *Science*, 289(5481): 953–957.

Bon, C.L. & Garthwaite, J. 2001. Exogenous nitric oxide causes potentiation of hippocampal synaptic transmission during low-frequency stimulation via the endogenous nitric oxide-cGMP pathway. *The European journal of neuroscience*, 14(4): 585–594.

Bon, C.L.M. & Garthwaite, J. 2003. On the role of nitric oxide in hippocampal long-term potentiation. *The Journal of neuroscience*, 23(5): 1941–1948.

Bonhoeffer, T., Staiger, V. & Aertsen, A. 1989. Synaptic plasticity in rat hippocampal slice cultures: local 'Hebbian' conjunction of pre- and postsynaptic stimulation leads to distributed synaptic enhancement. *Proceedings of the National Academy of Sciences*, 86(20): 8113–8117.

Boulton, C.L., Southam, E. & Garthwaite, J. 1995. Nitric oxide-dependent long-term potentiation is blocked by a specific inhibitor of soluble guanylyl cyclase. *Neuroscience*, 69(3): 699–703.

Bourne, J.N. & Harris, K.M. 2008. Balancing structure and function at hippocampal dendritic spines. *Annual Review of Neuroscience*, 31(1): 47–67.

Bourne, J.N. & Harris, K.M. 2011. Coordination of size and number of excitatory and

inhibitory synapses results in a balanced structural plasticity along mature hippocampal CA1 dendrites during LTP. *Hippocampus*, 21(4): 354–373.

Böhme, G.A., Bon, C., Stutzmann, J.M., Doble, A. & Blanchard, J.C. 1991. Possible involvement of nitric oxide in long-term potentiation. *European journal of pharmacology*, 199(3): 379–381.

Braitenberg, V. & Schüz, A. 1998. Cortex: Statistics and Geometry of Neuronal Connectivity. Springer Verlag

Braithwaite, S.P., Adkisson, M., Leung, J., Nava, A., Masterson, B., Urfer, R., Oksenberg, D. & Nikolich, K. 2006. Regulation of NMDA receptor trafficking and function by striatal-enriched tyrosine phosphatase (STEP). *The European journal of neuroscience*, 23(11): 2847–2856.

Branco, T. & Häusser, M. 2010. The single dendritic branch as a fundamental functional unit in the nervous system. *Current Opinion in Neurobiology*, 20(4): 494–502.

Branco, T. & Staras, K. 2009. The probability of neurotransmitter release: variability and feedback control at single synapses. *Nature reviews. Neuroscience*, 10(5): 373–383.

Branco, T., Marra, V. & Staras, K. 2010. Examining size-strength relationships at hippocampal synapses using an ultrastructural measurement of synaptic release probability. *Journal of structural biology*, 172(2): 203–210.

Branco, T., Staras, K., Darcy, K.J. & Goda, Y. 2008. Local dendritic activity sets release probability at hippocampal synapses. *Neuron*, 59(3): 475–485.

Branco, T., Tozer, A., Magnus, C.J., Sugino, K., Tanaka, S., Lee, A.K., Wood, J.N. & Sternson, S.M. 2016. Near-Perfect Synaptic Integration by Nav1.7 in Hypothalamic Neurons Regulates Body Weight. *Cell*, 165(7): 1749–1761.

Brandt, A., Khimich, D. & Moser, T. 2005. Few CaV1.3 channels regulate the exocytosis of a synaptic vesicle at the hair cell ribbon synapse. *The Journal of neuroscience*, 25(50): 11577–11585.

Bredt, D.S. & Snyder, S.H. 1989. Nitric oxide mediates glutamate-linked enhancement of cGMP levels in the cerebellum. *Proceedings of the National Academy of Sciences*, 86(22): 9030–9033.

Bredt, D.S., Glatt, C.E., Hwang, P.M., Fotuhi, M., Dawson, T.M. & Snyder, S.H. 1991. Nitric oxide synthase protein and mRNA are discretely localized in neuronal populations of the mammalian CNS together with NADPH diaphorase. *Neuron*, 7(4): 615–624.

Brenman, J.E., Christopherson, K.S., Craven, S.E., McGee, A.W. & Bredt, D.S. 1996. Cloning and characterization of postsynaptic density 93, a nitric oxide synthase interacting protein. *Journal of Neuroscience*, 16(23): 7407–7415.

Buchanan, K.A., Blackman, A.V., Moreau, A.W., Elgar, D., Costa, R.P., Lalanne, T., Tudor Jones, A.A., Oyrer, J. & Sjöström, P.J. 2012. Target-specific expression of presynaptic NMDA receptors in neocortical microcircuits. *Neuron*, 75(3): 451–466.

Buonomano, D.V. 2000. Decoding temporal information: A model based on short-term synaptic plasticity. *The Journal of neuroscience*, 20(3): 1129–1141.

Buonomano, D.V. & Merzenich, M.M. 1995. Temporal information transformed into a spatial code by a neural network with realistic properties. *Science*, 267(5200): 1028–

1030.

Burgess, N. & O'Keefe, J. 1996. Neuronal computations underlying the firing of place cells and their role in navigation. *Hippocampus*, 6(6): 749–762.

Cao, B.-J. & Reith, M.E.A. 2002. Nitric oxide scavenger carboxy-PTIO potentiates the inhibition of dopamine uptake by nitric oxide donors. *European journal of pharmacology*, 448(1): 27–30.

Carpenter, G.A. & Milenova, B.L. 2002. Redistribution of synaptic efficacy supports stable pattern learning in neural networks. *Neural computation*, 14(4): 873–888.

Carter, B.C. & Jahr, C.E. 2016. Postsynaptic, not presynaptic NMDA receptors are required for spike-timing-dependent LTD induction. *Nature neuroscience*, 19(9): 1218–1224.

Castillo, P.E., Younts, T.J., Chávez, A.E. & Hashimotodani, Y. 2012. Endocannabinoid signaling and synaptic function. *Neuron*, 76(1): 70–81.

Catterall, W.A. & Few, A.P. 2008. Calcium channel regulation and presynaptic plasticity. *Neuron*, 59(6): 882–901.

Chalifoux, J.R. & Carter, A.G. 2010. GABAB receptors modulate NMDA receptor calcium signals in dendritic spines. *Neuron*, 66(1): 101–113.

Chamberland, S., Timofeeva, Y., Evstratova, A., Volynski, K. & Tóth, K. 2018. Action potential counting at giant mossy fiber terminals gates information transfer in the hippocampus. *Proceedings of the National Academy of Sciences of the United States of America*, 9: 201720659.

Chater, T.E. & Goda, Y. 2014. The role of AMPA receptors in postsynaptic mechanisms of synaptic plasticity. *Frontiers in cellular neuroscience*, 8: 4598.

Chechik, G. 2003. Spike-Timing-Dependent Plasticity and Relevant Mutual Information Maximization. *Neural computation*, 15(7): 1481–1510.

Chen, C. & Jonas, P. 2017. Synaptotagmins: That's Why So Many. *Neuron*, 94(4): 694–696.

Chen, C., Blitz, D.M. & Regehr, W.G. 2002. Contributions of receptor desensitization and saturation to plasticity at the retinogeniculate synapse. *Neuron*, 33(5): 779–788.

Chen, G., Harata, N.C. & Tsien, R.W. 2004. Paired-pulse depression of unitary quantal amplitude at single hippocampal synapses. *Proceedings of the National Academy of Sciences*, 101(4): 1063–1068.

Chen, J.-Y., Lonjers, P., Lee, C., Chistiakova, M., Volgushev, M. & Bazhenov, M. 2013. Heterosynaptic plasticity prevents runaway synaptic dynamics. *The Journal of neuroscience*, 33(40): 15915–15929.

Chetkovich, D.M., Klann, E. & Sweatt, J.D. 1993. Nitric oxide synthase-independent long-term potentiation in area CA1 of hippocampus. *Neuroreport*, 4(7): 919–922.

Chevaleyre, V. & Castillo, P.E. 2003. Heterosynaptic LTD of hippocampal GABAergic synapses: a novel role of endocannabinoids in regulating excitability. *Neuron*, 38(3): 461–472.

Chevaleyre, V. & Siegelbaum, S.A. 2010. Strong CA2 pyramidal neuron synapses define a powerful disynaptic cortico-hippocampal loop. *Neuron*, 66(4): 560–572.

Chevaleyre, V., Heifets, B.D., Kaeser, P.S., Südhof, T.C., Purpura, D.P. & Castillo, P.E. 2007. Endocannabinoid-mediated long-term plasticity requires cAMP/PKA signaling and RIM1alpha. *Neuron*, 54(5): 801–812.

Chéreau, R., Saraceno, G.E., Angibaud, J., Cattaert, D. & Nägerl, U.V. 2017. Superresolution imaging reveals activity-dependent plasticity of axon morphology linked to changes in action potential conduction velocity. *Proceedings of the National Academy of Sciences of the United States of America*, 114(6): 1401–1406.

Chirillo, M.A., Waters, M.S., Lindsey, L.F., Bourne, J.N. & Harris, K.M. 2019. Local resources of polyribosomes and SER promote synapse enlargement and spine clustering after long-term potentiation in adult rat hippocampus. *Scientific reports*, 9(1): 3861.

Chistiakova, M., Bannon, N.M., Chen, J.-Y., Bazhenov, M. & Volgushev, M. 2015. Homeostatic role of heterosynaptic plasticity: models and experiments. *Frontiers in Computational Neuroscience*, 9: 89.

Christie, J.M. & Jahr, C.E. 2008. Dendritic NMDA receptors activate axonal calcium channels. *Neuron*, 60(2): 298–307.

Christie, J.M. & Jahr, C.E. 2009. Selective expression of ligand-gated ion channels in L5 pyramidal cell axons. *The Journal of neuroscience*, 29(37): 11441–11450.

Christofi, G., Nowicky, A.V., Bolsover, S.R. & Bindman, L.J. 1993. The postsynaptic induction of nonassociative long-term depression of excitatory synaptic transmission in rat hippocampal slices. *Journal of Neurophysiology*, 69(1): 219–229.

Cichon, J. & Gan, W.-B. 2015. Branch-specific dendritic Ca 2+ spikes cause persistent synaptic plasticity. *Nature*, 520(7546): 180–185.

Cochilla, A.J. & Alford, S. 1998. Metabotropic glutamate receptor-mediated control of neurotransmitter release. *Neuron*, 20(5): 1007–1016.

Cochilla, A.J. & Alford, S. 1999. NMDA receptor-mediated control of presynaptic calcium and neurotransmitter release. *Journal of Neuroscience*, 19(1): 193–205.

Collin, C., Miyaguchi, K. & Segal, M. 1997. Dendritic spine density and LTP induction in cultured hippocampal slices. *Journal of Neurophysiology*, 77(3): 1614–1623.

Conant, K., Wang, Y., Szklarczyk, A., Dudak, A., Mattson, M.P. & Lim, S.T. 2010. Matrix metalloproteinase-dependent shedding of intercellular adhesion molecule-5 occurs with long-term potentiation. *Neuroscience*, 166(2): 508–521.

Connor, J.A., Kretz, R. & Shapiro, E. 1986. Calcium levels measured in a presynaptic neurone of Aplysia under conditions that modulate transmitter release. *The Journal of physiology*, 375(1): 625–642.

Costa, R.P., Padamsey, Z., D'Amour, J.A., Emptage, N.J., Froemke, R.C. & Vogels, T.P. 2017. Synaptic Transmission Optimization Predicts Expression Loci of Long-Term Plasticity. *Neuron*, 96(1): 177–189.e7.

Coultrap, S.J. & Bayer, K.U. 2014. Nitric oxide induces Ca2+-independent activity of the Ca2+/calmodulin-dependent protein kinase II (CaMKII). *The Journal of biological chemistry*, 289(28): 19458–19465.

Cousin, M.A. & Robinson, P.J. 2001. The dephosphins: dephosphorylation by calcineurin triggers synaptic vesicle endocytosis. *Trends in Neurosciences*, 24(11): 659–665.

Cserép, C., Szonyi, A., Veres, J.M., Németh, B., Szabadits, E., de Vente, J., Hájos, N., Freund, T.F. & Nyiri, G. 2011. Nitric oxide signaling modulates synaptic transmission during early postnatal development. *Cerebral cortex (New York, N.Y. : 1991)*, 21(9): 2065–2074.

Cummings, J.A., Nicola, S.M. & Malenka, R.C. 1994. Induction in the rat hippocampus of long-term potentiation (LTP) and long-term depression (LTD) in the presence of a nitric oxide synthase inhibitor. *Neuroscience letters*, 176(1): 110–114.

Curran, J., Tang, L., Roof, S.R., Velmurugan, S., Millard, A., Shonts, S., Wang, H., Santiago, D., Ahmad, U., Perryman, M., Bers, D.M., Mohler, P.J., Ziolo, M.T. & Shannon, T.R. 2014. Nitric oxide-dependent activation of CaMKII increases diastolic sarcoplasmic reticulum calcium release in cardiac myocytes in response to adrenergic stimulation. N. Beard, ed. *PloS one*, 9(2): e87495.

Davis, G.W. 2006. Homeostatic Control of Neural Activity: From Phenomenology to Molecular Design. *Annual Review of Neuroscience*, 29: 307–323.

De Gois, S., Schäfer, M.K.-H., Defamie, N., Chen, C., Ricci, A., Weihe, E., Varoqui, H. & Erickson, J.D. 2005. Homeostatic scaling of vesicular glutamate and GABA transporter expression in rat neocortical circuits. *The Journal of neuroscience*, 25(31): 7121–7133.

de Jong, A.P.H., Schmitz, S.K., Toonen, R.F.G. & Verhage, M. 2012. Dendritic position is a major determinant of presynaptic strength. *The Journal of cell biology*, 197(2): 327–337.

De Simoni, A. & Yu, L.M.Y. 2006. Preparation of organotypic hippocampal slice cultures: interface method. *Nature protocols*, 1(3): 1439–1445.

De Simoni, A., Griesinger, C.B. & Edwards, F.A. 2003. Development of rat CA1 neurones in acute versus organotypic slices: role of experience in synaptic morphology and activity. *The Journal of physiology*, 550(Pt 1): 135–147.

Debanne, D., Guérineau, N.C., Gähwiler, B.H. & Thompson, S.M. 1996. Paired-pulse facilitation and depression at unitary synapses in rat hippocampus: quantal fluctuation affects subsequent release. *The Journal of physiology*, 491 (Pt 1)(1): 163–176.

Debanne, D., Guérineau, N.C., Gähwiler, B.H. & Thompson, S.M. 1995. Physiology and pharmacology of unitary synaptic connections between pairs of cells in areas CA3 and CA1 of rat hippocampal slice cultures. *Journal of Neurophysiology*, 73(3): 1282–1294.

Deguchi, Y., Donato, F., Galimberti, I., Cabuy, E. & Caroni, P. 2011. Temporally matched subpopulations of selectively interconnected principal neurons in the hippocampus. *Nature neuroscience*, 14(4): 495–504.

del CASTILLO, J. & KATZ, B. 1954. Quantal components of the end-plate potential. *The Journal of physiology*, 124(3): 560–573.

DeMaria, C.D., Soong, T.W., Alseikhan, B.A., Alvania, R.S. & Yue, D.T. 2001. Calmodulin bifurcates the local Ca2+ signal that modulates P/Q-type Ca2+ channels. *Nature*, 411(6836): 484–489.

Diering, G.H. & Huganir, R.L. 2018. The AMPA Receptor Code of Synaptic Plasticity. *Neuron*, 100(2): 314–329.

Dobrunz, L.E. & Stevens, C.F. 1997. Heterogeneity of release probability, facilitation, and depletion at central synapses. *Neuron*, 18(6): 995–1008.

Dobrunz, L.E. & Stevens, C.F. 1999. Response of hippocampal synapses to natural stimulation patterns. *Neuron*, 22(1): 157–166.

Dobrunz, L.E., Huang, E.P. & Stevens, C.F. 1997. Very short-term plasticity in hippocampal synapses. *Proceedings of the National Academy of Sciences*, 94(26): 14843–14847.

Dodge, F.A. & Rahamimoff, R. 1967. Co-operative action a calcium ions in transmitter release at the neuromuscular junction. *The Journal of physiology*, 193(2): 419–432.

Dore, K., Aow, J. & Malinow, R. 2016. The Emergence of NMDA Receptor Metabotropic Function: Insights from Imaging. *Frontiers in synaptic neuroscience*, 8.

Dore, K., Stein, I.S., Brock, J.A., Castillo, P.E., Zito, K. & Sjöström, P.J. 2017. Unconventional NMDA Receptor Signaling. *The Journal of neuroscience : the official journal of the Society for Neuroscience*, 37(45): 10800–10807.

Doyle, C.A. & Slater, P. 1997. Localization of neuronal and endothelial nitric oxide synthase isoforms in human hippocampus. *Neuroscience*, 76(2): 387–395.

Dries, E., Santiago, D.J., Johnson, D.M., Gilbert, G., Holemans, P., Korte, S.M., Roderick, H.L. & Sipido, K.R. 2016. Calcium/calmodulin-dependent kinase II and nitric oxide synthase 1-dependent modulation of ryanodine receptors during β-adrenergic stimulation is restricted to the dyadic cleft. *The Journal of physiology*, 594(20): 5923–5939.

Druckmann, S., Feng, L., Lee, B., Yook, C., Zhao, T., Magee, J.C. & Kim, J. 2014. Structured synaptic connectivity between hippocampal regions. *Neuron*, 81(3): 629–640.

Dudek, S.M. & Bear, M.F. 1992. Homosynaptic long-term depression in area CAl of hippocampus and effects of N-methyl-D-aspartate receptor blockade. *Proceedings of the National Academy of Sciences of the United States of America*: 1–5.

Duguid, I. & Sjöström, P.J. 2006. Novel presynaptic mechanisms for coincidence detection in synaptic plasticity. *Current Opinion in Neurobiology*, 16(3): 312–322.

Duguid, I.C. & Smart, T.G. 2004. Retrograde activation of presynaptic NMDA receptors enhances GABA release at cerebellar interneuron-Purkinje cell synapses. *Nature neuroscience*, 7(5): 525–533.

Dunwiddie, T. & Lynch, G. 1978. Long-term potentiation and depression of synaptic responses in the rat hippocampus: localization and frequency dependency. *The Journal of physiology*, 276: 353–367.

East, S.J. & Garthwaite, J. 1991. NMDA receptor activation in rat hippocampus induces cyclic GMP formation through the L-arginine-nitric oxide pathway. *Neuroscience letters*, 123(1): 17–19.

Edwards, D.A., Zhang, L. & Alger, B.E. 2008. Metaplastic control of the endocannabinoid system at inhibitory synapses in hippocampus. *Proceedings of the National Academy of Sciences of the United States of America*, 105(23): 8142–8147.

Egberongbe, Y.I., Gentleman, S.M., Falkai, P., Bogerts, B., Polak, J.M. & Roberts, G.W. 1994. The distribution of nitric oxide synthase immunoreactivity in the human brain. *Neuroscience*, 59(3): 561–578.

Eguchi, K., Nakanishi, S., Takagi, H., Taoufiq, Z. & Takahashi, T. 2012. Maturation of a PKG-dependent retrograde mechanism for exoendocytic coupling of synaptic vesicles. *Neuron*, 74(3): 517–529.

El-Boustani, S., Ip, J.P.K., Breton-Provencher, V., Knott, G.W., Okuno, H., Bito, H. & Sur, M. 2018. Locally coordinated synaptic plasticity of visual cortex neurons in vivo. *Science*, 360(6395): 1349–1354.

Emptage, N., Bliss, T.V. & Fine, A. 1999. Single synaptic events evoke NMDA receptor-mediated release of calcium from internal stores in hippocampal dendritic spines. *Neuron*, 22(1): 115–124.

Emptage, N.J., Reid, C.A., Fine, A. & Bliss, T.V.P. 2003. Optical quantal analysis reveals a presynaptic component of LTP at hippocampal Schaffer-associational synapses. *Neuron*, 38(5): 797–804.

Engert, F. & Bonhoeffer, T. 1997. Synapse specificity of long-term potentiation breaks down at short distances. *Nature*, 388(6639): 279–284.

Enoki, R., Hu, Y.-L., Hamilton, D. & Fine, A. 2009. Expression of long-term plasticity at individual synapses in hippocampus is graded, bidirectional, and mainly presynaptic: optical quantal analysis. *Neuron*, 62(2): 242–253.

Erickson, J.D., De Gois, S., Varoqui, H., Schäfer, M.K.-H. & Weihe, E. 2006. Activity-dependent regulation of vesicular glutamate and GABA transporters: a means to scale quantal size. *Neurochemistry international*, 48(6-7): 643–649.

Faber, D.S. & Korn, H. 1991. Applicability of the coefficient of variation method for analyzing synaptic plasticity. *Biophysical journal*, 60(5): 1288–1294.

Ferrante, M., Migliore, M. & Ascoli, G.A. 2013. Functional impact of dendritic branch-point morphology. *The Journal of neuroscience* , 33(5): 2156–2165.

Fonseca, R., Nägerl, U.V., Morris, R.G.M. & Bonhoeffer, T. 2004. Competing for memory: hippocampal LTP under regimes of reduced protein synthesis. *Neuron*, 44(6): 1011–1020.

Fonseca, R., Vabulas, R.M., Hartl, F.U., Bonhoeffer, T. & Nägerl, U.V. 2006. A balance of protein synthesis and proteasome-dependent degradation determines the maintenance of LTP. *Neuron*, 52(2): 239–245.

Fortin, D.A., Davare, M.A., Srivastava, T., Brady, J.D., Nygaard, S., Derkach, V.A. & Soderling, T.R. 2010. Long-term potentiation-dependent spine enlargement requires synaptic Ca2+-permeable AMPA receptors recruited by CaM-kinase I. *The Journal of neuroscience*, 30(35): 11565–11575.

Fortune, E.S. & Rose, G.J. 2001. Short-term synaptic plasticity as a temporal filter. *Trends in Neurosciences*, 24(7): 381–385.

Foster, T.C. & McNaughton, B.L. 1991. Long-term enhancement of CA1 synaptic transmission is due to increased quantal size, not quantal content. *Hippocampus*, 1(1): 79–91.

Frere, S. & Slutsky, I. 2018. Alzheimer's Disease: From Firing Instability to Homeostasis Network Collapse. *Neuron*, 97(1): 32–58.

Friebe, A., Schultz, G. & Koesling, D. 1996. Sensitizing soluble guanylyl cyclase to become

a highly CO-sensitive enzyme. *The EMBO journal*, 15(24): 6863–6868.

Friston, K. 2010. The free-energy principle: a unified brain theory? *Nature reviews. Neuroscience*, 11(2): 127–138.

Froemke, R.C., Tsay, I.A., Raad, M., Long, J.D. & Dan, Y. 2006. Contribution of individual spikes in burst-induced long-term synaptic modification. *Journal of Neurophysiology*, 95(3): 1620–1629.

Fu, W.-Y., Chen, Y., Sahin, M., Zhao, X.-S., Shi, L., Bikoff, J.B., Lai, K.-O., Yung, W.-H., Fu, A.K.Y., Greenberg, M.E. & Ip, N.Y. 2007. Cdk5 regulates EphA4-mediated dendritic spine retraction through an ephexin1-dependent mechanism. *Nature neuroscience*, 10(1): 67–76.

Fuhrmann, G., Segev, I., Markram, H. & Tsodyks, M. 2002. Coding of temporal information by activity-dependent synapses. *Journal of Neurophysiology*, 87(1): 140–148.

Fujii, H., Inoue, M., Okuno, H., Sano, Y., Takemoto-Kimura, S., Kitamura, K., Kano, M. & Bito, H. 2013. Nonlinear decoding and asymmetric representation of neuronal input information by CaMKIIα and calcineurin. *Cell reports*, 3(4): 978–987.

Fukao, M., Mason, H.S., Britton, F.C., Kenyon, J.L., Horowitz, B. & Keef, K.D. 1999. Cyclic GMP-dependent protein kinase activates cloned BKCa channels expressed in mammalian cells by direct phosphorylation at serine 1072. *The Journal of biological chemistry*, 274(16): 10927–10935.

Gage, A.T., Reyes, M. & Stanton, P.K. 1997. Nitric-oxide-guanylyl-cyclase-dependent and -independent components of multiple forms of long-term synaptic depression. *Hippocampus*, 7(3): 286–295.

Gambino, F., Pagès, S., Kehayas, V., Baptista, D., Tatti, R., Carleton, A. & Holtmaat, A. 2014. Sensory-evoked LTP driven by dendritic plateau potentials in vivo. *Nature*, 515(7525): 116–119.

Garthwaite, J. 2008. Concepts of neural nitric oxide-mediated transmission. *The European journal of neuroscience*, 27(11): 2783–2802.

Garthwaite, J. 2016. From synaptically localized to volume transmission by nitric oxide. *The Journal of physiology*, 594(1): 9–18.

Garthwaite, J., Charles, S.L. & Chess-Williams, R. 1988. Endothelium-derived relaxing factor release on activation of NMDA receptors suggests role as intercellular messenger in the brain. *Nature*, 336(6197): 385–388.

Garthwaite, J., Garthwaite, G., Palmer, R.M. & Moncada, S. 1989. NMDA receptor activation induces nitric oxide synthesis from arginine in rat brain slices. *European journal of pharmacology*, 172(4-5): 413–416.

Gasparini, S., Kasyanov, A.M., Pietrobon, D., Voronin, L.L. & Cherubini, E. 2001. Presynaptic R-Type Calcium Channels Contribute to Fast Excitatory Synaptic Transmission in the Rat Hippocampus. *Journal of Neuroscience*, 21(22): 8715–8721.

Gähwiler, B.H. 1988. Organotypic cultures of neural tissue. *Trends in Neurosciences*, 11(11): 484–489.

Gähwiler, B.H. 1981. Organotypic monolayer cultures of nervous tissue. *Journal of neuroscience methods*, 4(4): 329–342.

Gähwiler, B.H., Capogna, M., Debanne, D., McKinney, R.A. & Thompson, S.M. 1997. Organotypic slice cultures: a technique has come of age. *Trends in Neurosciences*, 20(10): 471–477.

Gogolla, N., Galimberti, I., DePaola, V. & Caroni, P. 2006. Preparation of organotypic hippocampal slice cultures for long-term live imaging. *Nature protocols*, 1(3): 1165–1171.

Goldman, M.S. 2004. Enhancement of information transmission efficiency by synaptic failures. *Neural computation*, 16(6): 1137–1162.

Gorelick, F.S., Wang, J.K., Lai, Y., Nairn, A.C. & Greengard, P. 1988. Autophosphorylation and activation of Ca2+/calmodulin-dependent protein kinase II in intact nerve terminals. *The Journal of biological chemistry*, 263(33): 17209–17212.

Govek, E.-E., Newey, S.E. & Van Aelst, L. 2005. The role of the Rho GTPases in neuronal development. *Genes & development*, 19(1): 1–49.

Govindarajan, A., Israely, I., Huang, S.-Y. & Tonegawa, S. 2011. The dendritic branch is the preferred integrative unit for protein synthesis-dependent LTP. *Neuron*, 69(1): 132–146.

Granseth, B., Odermatt, B., Royle, S.J. & Lagnado, L. 2006. Clathrin-mediated endocytosis is the dominant mechanism of vesicle retrieval at hippocampal synapses. *Neuron*, 51(6): 773–786.

Greger, I.H., Watson, J.F. & Cull-Candy, S.G. 2017. Structural and Functional Architecture of AMPA-Type Glutamate Receptors and Their Auxiliary Proteins. *Neuron*, 94(4): 713–730.

Gribkoff, V.K. & Lum-Ragan, J.T. 1992. Evidence for nitric oxide synthase inhibitor-sensitive and insensitive hippocampal synaptic potentiation. *Journal of Neurophysiology*, 68(2): 639–642.

Grillo, F.W., Neves, G., Walker, A., Vizcay-Barrena, G., Fleck, R.A., Branco, T. & Burrone, J. 2018. A Distance-Dependent Distribution of Presynaptic Boutons Tunes Frequency-Dependent Dendritic Integration. *Neuron*, 99: 1–8.

Grover, L.M. 1998. Evidence for Postsynaptic Induction and Expression of NMDA Receptor Independent LTP. *Journal of Neurophysiology*, 79(3): 1167–1182.

Grover, L.M. & Teyler, T.J. 1990. Two components of long-term potentiation induced by different patterns of afferent activation. *Nature*, 347(6292): 477–479.

Grover, L.M. & Yan, C. 1999. Evidence for Involvement of Group II/III Metabotropic Glutamate Receptors in NMDA Receptor–Independent Long-Term Potentiation in Area CA1 of Rat Hippocampus. *Journal of Neurophysiology*, 82(6): 2956–2969.

Gupta, A., Wang, Y. & Markram, H. 2000. Organizing Principles for a Diversity of GABAergic Interneurons and Synapses in the Neocortex. *Science*, 287(5451): 273–278.

Gutierrez, D.A., Fernandez-Tenorio, M., Ogrodnik, J. & Niggli, E. 2013. NO-dependent CaMKII activation during β-adrenergic stimulation of cardiac muscle. *Cardiovascular research*, 100(3): 392–401.

Haley, J.E., Malen, P.L. & Chapman, P.F. 1993. Nitric oxide synthase inhibitors block long-

term potentiation induced by weak but not strong tetanic stimulation at physiological brain temperatures in rat hippocampal slices. *Neuroscience letters*, 160(1): 85–88.

Haley, J.E., Wilcox, G.L. & Chapman, P.F. 1992. The role of nitric oxide in hippocampal long-term potentiation. *Neuron*, 8(2): 211–216.

Hall, C.N. & Garthwaite, J. 2006. Inactivation of nitric oxide by rat cerebellar slices. *The Journal of physiology*, 577(Pt 2): 549–567.

Hall, C.N. & Garthwaite, J. 2009. What is the real physiological NO concentration in vivo? *Nitric oxide : biology and chemistry*, 21(2): 92–103.

Han, J., Kesner, P., Metna-Laurent, M., Duan, T., Xu, L., Georges, F., Koehl, M., Abrous, D.N., Mendizabal-Zubiaga, J., Grandes, P., Liu, Q., Bai, G., Wang, W., Xiong, L., Ren, W., Marsicano, G. & Zhang, X. 2012. Acute cannabinoids impair working memory through astroglial CB1 receptor modulation of hippocampal LTD. *Cell*, 148(5): 1039–1050.

Hanse, E. & Gustafsson, B. 2001. Quantal variability at glutamatergic synapses in area CA1 of the rat neonatal hippocampus. *The Journal of physiology*, 531(Pt 2): 467–480.

Hardingham, N., Dachtler, J. & Fox, K. 2013. The role of nitric oxide in pre-synaptic plasticity and homeostasis. *Frontiers in cellular neuroscience*, 7: 190.

Hardingham, N.R., Hardingham, G.E., Fox, K.D. & Jack, J.J.B. 2007. Presynaptic efficacy directs normalization of synaptic strength in layer 2/3 rat neocortex after paired activity. *Journal of Neurophysiology*, 97(4): 2965–2975.

Harris, J.J., Jolivet, R. & Attwell, D. 2012. Synaptic energy use and supply. *Neuron*, 75(5): 762–777.

Harris, K.M. 1995. How multiple-synapse boutons could preserve input specificity during an interneuronal spread of LTP. *Trends in Neurosciences*, 18(8): 365–369.

Harris, K.M. & Sultan, P. 1995. Variation in the number, location and size of synaptic vesicles provides an anatomical basis for the nonuniform probability of release at hippocampal CA1 synapses. *Neuropharmacology*, 34(11): 1387–1395.

Harris, K.M. & Weinberg, R.J. 2012. Ultrastructure of synapses in the mammalian brain. *Cold Spring Harbor perspectives in biology*, 4(5).

Harris, K.M., Jensen, F.E. & Tsao, B. 1992. Three-dimensional structure of dendritic spines and synapses in rat hippocampus (CA1) at postnatal day 15 and adult ages: implications for the maturation of synaptic physiology and long-term potentiation. *Journal of Neuroscience*, 12(7): 2685–2705.

Hartman, K.N., Pal, S.K., Burrone, J. & Murthy, V.N. 2006. Activity-dependent regulation of inhibitory synaptic transmission in hippocampal neurons. *Nature neuroscience*, 9(5): 642–649.

Harvey, C.D. & Svoboda, K. 2007. Locally dynamic synaptic learning rules in pyramidal neuron dendrites. *Nature*, 450(7173): 1195–1200.

Harvey, C.D., Yasuda, R., Zhong, H. & Svoboda, K. 2008. The spread of Ras activity triggered by activation of a single dendritic spine. *Science*, 321(5885): 136–140.

Haug, L.S., Jensen, V., Hvalby, O., Walaas, S.I. & Ostvold, A.C. 1999. Phosphorylation of the inositol 1,4,5-trisphosphate receptor by cyclic nucleotide-dependent kinases in vitro and in rat cerebellar slices in situ. *The Journal of biological chemistry*, 274(11): 7467–7473.

Hayama, T., Noguchi, J., Watanabe, S., Takahashi, N., Hayashi-Takagi, A., Ellis-Davies, G.C.R., Matsuzaki, M. & Kasai, H. 2013. GABA promotes the competitive selection of dendritic spines by controlling local Ca2+ signaling. *Nature neuroscience*, 16(10): 1409–1416.

Häusser, M., Spruston, N. & Stuart, G.J. 2000. Diversity and dynamics of dendritic signaling. *Science*, 290(5492): 739–744.

Hebb, D.O. 1949. *The organization of behavior: a neuropsychological theory*. New York: John Wiley & Sons, Inc.

Hedrick, N.G., Harward, S.C., Hall, C.E., Murakoshi, H., McNamara, J.O. & Yasuda, R. 2016. Rho GTPase complementation underlies BDNF-dependent homo- and heterosynaptic plasticity. *Nature*, 538(7623): 104–108.

Heifets, B.D. & Castillo, P.E. 2009. Endocannabinoid signaling and long-term synaptic plasticity. *Annual Review of Physiology*, 71(1): 283–306.

Heifets, B.D., Chevaleyre, V. & Castillo, P.E. 2008. Interneuron activity controls endocannabinoid-mediated presynaptic plasticity through calcineurin. *Proceedings of the National Academy of Sciences of the United States of America*, 105(29): 10250–10255.

Helassa, N., Dürst, C.D., Coates, C., Kerruth, S., Arif, U., Schulze, C., Wiegert, J.S., Geeves, M., Oertner, T.G. & Török, K. 2018. Ultrafast glutamate sensors resolve high-frequency release at Schaffer collateral synapses. *Proceedings of the National Academy of Sciences of the United States of America*, 115(21): 5594–5599.

Hennig, M.H. 2013. Theoretical models of synaptic short term plasticity. *Frontiers in Computational Neuroscience*, 7.

Hinds, H.L., Goussakov, I., Nakazawa, K., Tonegawa, S. & Bolshakov, V.Y. 2003. Essential function of alpha-calcium/calmodulin-dependent protein kinase II in neurotransmitter release at a glutamatergic central synapse. *Proceedings of the National Academy of Sciences*, 100(7): 4275–4280.

Hjelmstad, G.O., Nicoll, R.A. & Malenka, R.C. 1997. Synaptic refractory period provides a measure of probability of release in the hippocampus. *Neuron*, 19(6): 1309–1318.

Ho, V.M., Lee, J.-A. & Martin, K.C. 2011. The cell biology of synaptic plasticity. *Science*, 334(6056): 623–628.

Hofmann, F., Lacinová, L. & Klugbauer, N. 1999. Voltage-dependent calcium channels: From structure to function. In *Reviews of Physiology, Biochemistry and Pharmacology*. Reviews of Physiology, Biochemistry and Pharmacology. Springer, Berlin, Heidelberg: 33–87.

Hojjati, M.R., van Woerden, G.M., Tyler, W.J., Giese, K.P., Silva, A.J., Pozzo-Miller, L. & Elgersma, Y. 2007. Kinase activity is not required for alphaCaMKII-dependent presynaptic plasticity at CA3-CA1 synapses. *Nature neuroscience*, 10(9): 1125–1127.

Holbro, N., Grunditz, A. & Oertner, T.G. 2009. Differential distribution of endoplasmic

reticulum controls metabotropic signaling and plasticity at hippocampal synapses. *Proceedings of the National Academy of Sciences of the United States of America*, 106(35): 15055–15060.

Holderith, N., Lorincz, A., Katona, G., Rózsa, B., Kulik, A., Watanabe, M. & Nusser, Z. 2012. Release probability of hippocampal glutamatergic terminals scales with the size of the active zone. *Nature neuroscience*, 15(7): 988–997.

Hopfield, J.J. 1982. Neural networks and physical systems with emergent collective computational abilities. *Proceedings of the National Academy of Sciences*, 79(8): 2554–2558.

Hopper, R.A. & Garthwaite, J. 2006. Tonic and phasic nitric oxide signals in hippocampal long-term potentiation. *The Journal of neuroscience*, 26(45): 11513–11521.

Hou, Q., Zhang, D., Jarzylo, L., Huganir, R.L. & Man, H.-Y. 2008. Homeostatic regulation of AMPA receptor expression at single hippocampal synapses. *Proceedings of the National Academy of Sciences of the United States of America*, 105(2): 775–780.

Huang, C.-C., Chan, S.H.H. & Hsu, K.-S. 2003. cGMP/protein kinase G-dependent potentiation of glutamatergic transmission induced by nitric oxide in immature rat rostral ventrolateral medulla neurons in vitro. *Molecular pharmacology*, 64(2): 521–532.

Huang, E.P. & Stevens, C.F. 1997. Estimating the distribution of synaptic reliabilities. *Journal of Neurophysiology*, 78(6): 2870–2880.

Huang, P.L., Dawson, T.M., Bredt, D.S., Snyder, S.H. & Fishman, M.C. 1993. Targeted disruption of the neuronal nitric oxide synthase gene. *Cell*, 75(7): 1273–1286.

Huang, Y., Man, H.-Y., Sekine-Aizawa, Y., Han, Y., Juluri, K., Luo, H., Cheah, J., Lowenstein, C., Huganir, R.L. & Snyder, S.H. 2005. S-nitrosylation of N-ethylmaleimide sensitive factor mediates surface expression of AMPA receptors. *Neuron*, 46(4): 533–540.

Huang, Y.Y. & Malenka, R.C. 1993. Examination of TEA-induced synaptic enhancement in area CA1 of the hippocampus: the role of voltage-dependent Ca2+ channels in the induction of LTP. *Journal of Neuroscience*, 13(2): 568–576.

Humpel, C. 2015. Organotypic brain slice cultures: A review. *Neuroscience*, 305: 86–98.

Hunt, D.L. & Castillo, P.E. 2012. Synaptic plasticity of NMDA receptors: mechanisms and functional implications. *Current Opinion in Neurobiology*, 22(3): 496–508.

Ibata, K., Sun, Q. & Turrigiano, G.G. 2008. Rapid synaptic scaling induced by changes in postsynaptic firing. *Neuron*, 57(6): 819–826.

Ignarro, L.J., Buga, G.M., Wood, K.S., Byrns, R.E. & Chaudhuri, G. 1987. Endothelium-derived relaxing factor produced and released from artery and vein is nitric oxide. *Proceedings of the National Academy of Sciences*, 84(24): 9265–9269.

Isaacson, J.S. & Scanziani, M. 2011. How inhibition shapes cortical activity. *Neuron*, 72(2): 231–243.

Izumi, Y. & Zorumski, C.F. 1993. Nitric oxide and long-term synaptic depression in the rat hippocampus. *Neuroreport*, 4(9): 1131–1134.

Jaffrey, S.R., Erdjument-Bromage, H., Ferris, C.D., Tempst, P. & Snyder, S.H. 2001. Protein S-

nitrosylation: a physiological signal for neuronal nitric oxide. *Nature cell biology*, 3(2): 193–197.

Jakawich, S.K., Nasser, H.B., Strong, M.J., McCartney, A.J., Perez, A.S., Rakesh, N., Carruthers, C.J.L. & Sutton, M.A. 2010. Local presynaptic activity gates homeostatic changes in presynaptic function driven by dendritic BDNF synthesis. *Neuron*, 68(6): 1143–1158.

Jiang, L.H., Gawler, D.J., Hodson, N., Milligan, C.J., Pearson, H.A., Porter, V. & Wray, D. 2000. Regulation of cloned cardiac L-type calcium channels by cGMP-dependent protein kinase. *The Journal of biological chemistry*, 275(9): 6135–6143.

Johnston, D., Magee, J.C., Colbert, C.M. & Cristie, B.R. 1996. Active properties of neuronal dendrites. *Annual Review of Neuroscience*, 19(1): 165–186.

Johnstone, V.P.A. & Raymond, C.R. 2011. A protein synthesis and nitric oxide-dependent presynaptic enhancement in persistent forms of long-term potentiation. *Learning & memory (Cold Spring Harbor, N.Y.)*, 18(10): 625–633.

Ju, W., Morishita, W., Tsui, J., Gaietta, G., Deerinck, T.J., Adams, S.R., Garner, C.C., Tsien, R.Y., Ellisman, M.H. & Malenka, R.C. 2004. Activity-dependent regulation of dendritic synthesis and trafficking of AMPA receptors. *Nature neuroscience*, 7(3): 244–253.

Kamiya, H., Ozawa, S. & Manabe, T. 2002. Kainate receptor-dependent short-term plasticity of presynaptic Ca2+ influx at the hippocampal mossy fiber synapses. *The Journal of neuroscience* , 22(21): 9237–9243.

Kang, M.-G., Guo, Y. & Huganir, R.L. 2009. AMPA receptor and GEF-H1/Lfc complex regulates dendritic spine development through RhoA signaling cascade. *Proceedings of the National Academy of Sciences of the United States of America*, 106(9): 3549–3554.

Kang-Park, M.-H., Wilson, W.A., Kuhn, C.M., Moore, S.D. & Swartzwelder, H.S. 2007. Differential sensitivity of GABA A receptor-mediated IPSCs to cannabinoids in hippocampal slices from adolescent and adult rats. *Journal of Neurophysiology*, 98(3): 1223–1230.

Kano, M., Ohno-Shosaku, T., Hashimotodani, Y., Uchigashima, M. & Watanabe, M. 2009. Endocannabinoid-mediated control of synaptic transmission. *Physiological reviews*, 89(1): 309–380.

Kastellakis, G., Cai, D.J., Mednick, S.C., Silva, A.J. & Poirazi, P. 2015. Synaptic clustering within dendrites: An emerging theory of memory formation. *Progress in Neurobiology*, 126: 19–35.

Kato, K. & Zorumski, C.F. 1993. Nitric oxide inhibitors facilitate the induction of hippocampal long-term potentiation by modulating NMDA responses. *Journal of Neurophysiology*, 70(3): 1260–1263.

Katz, B. & Miledi, R. 1965. THE EFFECT OF CALCIUM ON ACETYLCHOLINE RELEASE FROM MOTOR NERVE TERMINALS. *Proceedings of the Royal Society of London. Series B, Biological sciences*, 161(985): 496–503.

Katz, Y., Menon, V., Nicholson, D.A., Geinisman, Y., Kath, W.L. & Spruston, N. 2009. Synapse distribution suggests a two-stage model of dendritic integration in CA1 pyramidal neurons. *Neuron*, 63(2): 171–177.

Kim, J. & Alger, B.E. 2001. Random response fluctuations lead to spurious paired-pulse facilitation. *The Journal of neuroscience*, 21(24): 9608–9618.

Kleindienst, T., Winnubst, J., Roth-Alpermann, C., Bonhoeffer, T. & Lohmann, C. 2011. Activity-dependent clustering of functional synaptic inputs on developing hippocampal dendrites. *Neuron*, 72(6): 1012–1024.

Klyachko, V.A. & Stevens, C.F. 2006. Excitatory and feed-forward inhibitory hippocampal synapses work synergistically as an adaptive filter of natural spike trains. l. Segev, ed. *PLoS biology*, 4(7): e207.

Klyachko, V.A., Ahern, G.P. & Jackson, M.B. 2001. cGMP-mediated facilitation in nerve terminals by enhancement of the spike afterhyperpolarization. *Neuron*, 31(6): 1015–1025.

Ko, G.Y. & Kelly, P.T. 1999. Nitric oxide acts as a postsynaptic signaling molecule in calcium/calmodulin-induced synaptic potentiation in hippocampal CA1 pyramidal neurons. *The Journal of neuroscience*, 19(16): 6784–6794.

Koester, H.J. & Johnston, D. 2005. Target Cell-Dependent Normalization of Transmitter Release at Neocortical Synapses. *Science*, 308(5723): 863–866.

Konnerth, A., Dreessen, J. & Augustine, G.J. 1992. Brief dendritic calcium signals initiate long-lasting synaptic depression in cerebellar Purkinje cells. *Proceedings of the National Academy of Sciences*, 89(15): 7051–7055.

König, P., Engel, A.K. & Singer, W. 1996. Integrator or coincidence detector? The role of the cortical neuron revisited. *Trends in Neurosciences*, 19(4): 130–137.

Kullmann, D.M. 2012. The Mother of All Battles 20 years on: is LTP expressed pre- or postsynaptically? *The Journal of physiology*, 590(10): 2213–2216.

Kullmann, D.M., Perkel, D.J., Manabe, T. & Nicoll, R.A. 1992. Ca2+ entry via postsynaptic voltage-sensitive Ca2+ channels can transiently potentiate excitatory synaptic transmission in the hippocampus. *Neuron*, 9(6): 1175–1183.

Kunz, P.A., Roberts, A.C. & Philpot, B.D. 2013. Presynaptic NMDA receptor mechanisms for enhancing spontaneous neurotransmitter release. *The Journal of neuroscience*, 33(18): 7762–7769.

Kurz, J.E., Moore, B.J., Henderson, S.C., Campbell, J.N. & Churn, S.B. 2008. A cellular mechanism for dendritic spine loss in the pilocarpine model of status epilepticus. *Epilepsia*, 49(10): 1696–1710.

Lacinová, L. & Hofmann, F. 2005. Ca2+- and voltage-dependent inactivation of the expressed L-type Cav1.2 calcium channel. *Archives of biochemistry and biophysics*, 437(1): 42–50.

Lafourcade, C.A. & Alger, B.E. 2008. Distinctions among GABAA and GABAB responses revealed by calcium channel antagonists, cannabinoids, opioids, and synaptic plasticity in rat hippocampus. *Psychopharmacology*, 198(4): 539–549.

Lai, K.-O. & Ip, N.Y. 2013. Structural plasticity of dendritic spines: the underlying mechanisms and its dysregulation in brain disorders. *Biochimica et biophysica acta*, 1832(12): 2257–2263.

Lancaster, J.R. 1994. Simulation of the diffusion and reaction of endogenously produced

nitric oxide. *Proceedings of the National Academy of Sciences*, 91(17): 8137–8141.

Larkum, M.E. & Nevian, T. 2008. Synaptic clustering by dendritic signalling mechanisms. *Current Opinion in Neurobiology*, 18(3): 321–331.

Lau, C.G. & Murthy, V.N. 2012. Activity-dependent regulation of inhibition via GAD67. *The Journal of neuroscience*, 32(25): 8521–8531.

Laughlin, S.B., de Ruyter van Steveninck, R.R. & Anderson, J.C. 1998. The metabolic cost of neural information. *Nature neuroscience*, 1(1): 36–41.

Lauri, S.E., Bortolotto, Z.A., Bleakman, D., Ornstein, P.L., Lodge, D., Isaac, J.T. & Collingridge, G.L. 2001. A critical role of a facilitatory presynaptic kainate receptor in mossy fiber LTP. *Neuron*, 32(4): 697–709.

Leal, G., Afonso, P.M., Salazar, I.L. & Duarte, C.B. 2015. Regulation of hippocampal synaptic plasticity by BDNF. *Brain research*, 1621: 82–101.

Lee, A., Scheuer, T. & Catterall, W.A. 2000. Ca2+/calmodulin-dependent facilitation and inactivation of P/Q-type Ca2+ channels. *Journal of Neuroscience*, 20(18): 6830–6838.

Lee, C.M., Stoelzel, C., Chistiakova, M. & Volgushev, M. 2012. Heterosynaptic plasticity induced by intracellular tetanization in layer 2/3 pyramidal neurons in rat auditory cortex. *The Journal of physiology*, 590(10): 2253–2271.

Lee, K.J., Park, I.S., Kim, H., Greenough, W.T., Pak, D.T.S. & Rhyu, I.J. 2013. Motor skill training induces coordinated strengthening and weakening between neighboring synapses. *The Journal of neuroscience*, 33(23): 9794–9799.

Lee, S.-J.R., Escobedo-Lozoya, Y., Szatmari, E.M. & Yasuda, R. 2009. Activation of CaMKII in single dendritic spines during long-term potentiation. *Nature*, 458(7236): 299–304.

Letellier, M., Levet, F., Thoumine, O. & Goda, Y. 2019. Differential role of pre- and postsynaptic neurons in the activity-dependent control of synaptic strengths across dendrites. A. Bacci, ed. *PLoS biology*, 17(6): e2006223.

Letellier, M., Park, Y.K., Chater, T.E., Chipman, P.H., Gautam, S.G., Oshima-Takago, T. & Goda, Y. 2016. Astrocytes regulate heterogeneity of presynaptic strengths in hippocampal networks. *Proceedings of the National Academy of Sciences of the United States of America*, 113(19): E2685–94.

Levy, W.B. & Baxter, R.A. 1996. Energy Efficient Neural Codes. *Neural computation*, 8(3): 531–543.

Li, L., Stefan, M.I. & Le Novère, N. 2012. Calcium input frequency, duration and amplitude differentially modulate the relative activation of calcineurin and CaMKII. Z.-P. Feng, ed. *PloS one*, 7(9): e43810.

Liaw, J.S. & Berger, T.W. 1996. Dynamic synapse: a new concept of neural representation and computation. *Hippocampus*, 6(6): 591–600.

Liaw, J.S. & Berger, T.W. 1999. Dynamic synapse: Harnessing the computing power of synaptic dynamics. *Neurocomputing*, 26-27: 199–206.

Liley, A.W. & North, K.A. 1953. An electrical investigation of effects of repetitive stimulation on mammalian neuromuscular junction. *Journal of Neurophysiology*, 16(5): 509–527.

Lin, L.H., Taktakishvili, O. & Talman, W.T. 2007. Identification and localization of cell types that express endothelial and neuronal nitric oxide synthase in the rat nucleus tractus solitarii. *Brain research*, 1171: 42–51.

Lin, P.-Y., Kavalali, E.T. & Monteggia, L.M. 2018. Genetic Dissection of Presynaptic and Postsynaptic BDNF-TrkB Signaling in Synaptic Efficacy of CA3-CA1 Synapses. *Cell reports*, 24(6): 1550–1561.

Linkert, M., Rueden, C.T., Allan, C., Burel, J.-M., Moore, W., Patterson, A., Loranger, B., Moore, J., Neves, C., MacDonald, D., Tarkowska, A., Sticco, C., Hill, E., Rossner, M., Eliceiri, K.W. & Swedlow, J.R. 2010. Metadata matters: access to image data in the real world. *The Journal of cell biology*, 189(5): 777–782.

Linsker, R. 1992. Local Synaptic Learning Rules Suffice to Maximize Mutual Information in a Linear Network. *Neural computation*, 4(5): 691–702.

Linsker, R. 1988. Self-organization in a perceptual network. *Computer*, 21(3): 105–117.

Liu, G. 2004. Local structural balance and functional interaction of excitatory and inhibitory synapses in hippocampal dendrites. *Nature neuroscience*, 7(4): 373–379.

Liu, G. & Tsien, R.W. 1995. Properties of synaptic transmission at single hippocampal synaptic boutons. *Nature*, 375(6530): 404–408.

Liu, G., Choi, S. & Tsien, R.W. 1999. Variability of neurotransmitter concentration and nonsaturation of postsynaptic AMPA receptors at synapses in hippocampal cultures and slices. *Neuron*, 22(2): 395–409.

Liu, J.P., Sim, A.T. & Robinson, P.J. 1994. Calcineurin inhibition of dynamin I GTPase activity coupled to nerve terminal depolarization. *Science*, 265(5174): 970–973.

Llinás, R., Steinberg, I.Z. & Walton, K. 1981. Relationship between presynaptic calcium current and postsynaptic potential in squid giant synapse. *Biophysical journal*, 33(3): 323–351.

Lo, Y.J. & Poo, M.M. 1991. Activity-dependent synaptic competition in vitro: heterosynaptic suppression of developing synapses. *Science*, 254(5034): 1019–1022.

Losonczy, A. & Magee, J.C. 2006. Integrative properties of radial oblique dendrites in hippocampal CA1 pyramidal neurons. *Neuron*, 50(2): 291–307.

Lu, B. 2003. BDNF and activity-dependent synaptic modulation. *Learning & memory (Cold Spring Harbor, N.Y.)*, 10(2): 86–98.

Lu, B., Nagappan, G. & Lu, Y. 2014. BDNF and synaptic plasticity, cognitive function, and dysfunction. *Handbook of experimental pharmacology*, 220(Suppl 5): 223–250.

Lu, F.-M. & Hawkins, R.D. 2006. Presynaptic and postsynaptic Ca(2+) and CamKII contribute to long-term potentiation at synapses between individual CA3 neurons. *Proceedings of the National Academy of Sciences*, 103(11): 4264–4269.

Luo, D. & Vincent, S.R. 1994. Metalloporphyrins inhibit nitric oxide-dependent cGMP formation in vivo. *European journal of pharmacology*, 267(3): 263–267.

Luo, F. & Südhof, T.C. 2017. Synaptotagmin-7-Mediated Asynchronous Release Boosts High-Fidelity Synchronous Transmission at a Central Synapse. *Neuron*, 94(4): 826–839.e3.

Lüscher, C. & Malenka, R.C. 2012. NMDA Receptor-Dependent Long-Term Potentiation and Long-Term Depression (LTP/LTD). *Cold Spring Harbor perspectives in biology*, 4(6).

Lynch, G.S., Dunwiddie, T. & Gribkoff, V. 1977. Heterosynaptic depression: a postsynaptic correlate of long-term potentiation. *Nature*, 266(5604): 737–739.

Ma, X., Sayed, N., Beuve, A. & van den Akker, F. 2007. NO and CO differentially activate soluble guanylyl cyclase via a heme pivot-bend mechanism. *The EMBO journal*, 26(2): 578–588.

Maass, W. & Zador, A.M. 1999. Dynamic stochastic synapses as computational units. *Neural computation*, 11(4): 903–917.

Magby, J.P., Bi, C., Chen, Z.-Y., Lee, F.S. & Plummer, M.R. 2006. Single-cell characterization of retrograde signaling by brain-derived neurotrophic factor. *The Journal of neuroscience*, 26(52): 13531–13536.

Magee, J.C. & Cook, E.P. 2000. Somatic EPSP amplitude is independent of synapse location in hippocampal pyramidal neurons. *Nature neuroscience*, 3(9): 895–903.

Mainen, Z.F., Malinow, R. & Svoboda, K. 1999. Synaptic calcium transients in single spines indicate that NMDA receptors are not saturated. *Nature*, 399(6732): 151–155.

Makino, H. & Malinow, R. 2011. Compartmentalized versus global synaptic plasticity on dendrites controlled by experience. *Neuron*, 72(6): 1001–1011.

Malen, P.L. & Chapman, P.F. 1997. Nitric oxide facilitates long-term potentiation, but not long-term depression. *Journal of Neuroscience*, 17(7): 2645–2651.

Malenka, R.C. & Bear, M.F. 2004. LTP and LTD: an embarrassment of riches. *Neuron*, 44(1): 5–21.

Malinow, R. & Tsien, R.W. 1990. Presynaptic enhancement shown by whole-cell recordings of long-term potentiation in hippocampal slices. *Nature*, 346(6280): 177–180.

Mallart, A. & Martin, A.R. 1968. The relation between quantum content and facilitation at the neuromuscular junction of the frog. *The Journal of physiology*, 196(3): 593–604.

Mallart, A. & Martin, A.R. 1967. Two components of facilitation at the neuromuscular junction of the frog. *The Journal of physiology*, 191(1): 19P–20P.

Malleret, G., Haditsch, U., Genoux, D., Jones, M.W., Bliss, T.V., Vanhoose, A.M., Weitlauf, C., Kandel, E.R., Winder, D.G. & Mansuy, I.M. 2001. Inducible and reversible enhancement of learning, memory, and long-term potentiation by genetic inhibition of calcineurin. *Cell*, 104(5): 675–686.

Manabe, T., Wyllie, D.J., Perkel, D.J. & Nicoll, R.A. 1993. Modulation of synaptic transmission and long-term potentiation: effects on paired pulse facilitation and EPSC variance in the CA1 region of the hippocampus. *Journal of Neurophysiology*, 70(4): 1451–1459.

Markram, H. & Tsodyks, M. 1996. Redistribution of synaptic efficacy between neocortical pyramidal neurons. *Nature*, 382(6594): 807–810.

Markram, H., Wang, Y. & Tsodyks, M. 1998. Differential signaling via the same axon of neocortical pyramidal neurons. *Proceedings of the National Academy of Sciences of*

the United States of America, 95(9): 5323–5328.

Martin, A.R. 1966. Quantal Nature of Synaptic Transmission. *Physiological reviews,* 46(1): 51–66.

Marvin, J.S., Borghuis, B.G., Tian, L., Cichon, J., Harnett, M.T., Akerboom, J., Gordus, A., Renninger, S.L., Chen, T.-W., Bargmann, C.I., Orger, M.B., Schreiter, E.R., Demb, J.B., Gan, W.-B., Hires, S.A. & Looger, L.L. 2013. An optimized fluorescent probe for visualizing glutamate neurotransmission. *Nature methods*, 10(2): 162–170.

Maschi, D. & Klyachko, V.A. 2017. Spatiotemporal Regulation of Synaptic Vesicle Fusion Sites in Central Synapses. *Neuron*, 94(1): 65–73.e3.

Matsumoto, T., Rauskolb, S., Polack, M., Klose, J., Kolbeck, R., Korte, M. & Barde, Y.-A. 2008. Biosynthesis and processing of endogenous BDNF: CNS neurons store and secrete BDNF, not pro-BDNF. *Nature neuroscience*, 11(2): 131–133.

Matsuzaki, M., Ellis-Davies, G.C., Nemoto, T., Miyashita, Y., Iino, M. & Kasai, H. 2001. Dendritic spine geometry is critical for AMPA receptor expression in hippocampal CA1 pyramidal neurons. *Nature neuroscience*, 4(11): 1086–1092.

Matsuzaki, M., Honkura, N., Ellis-Davies, G.C.R. & Kasai, H. 2004. Structural basis of long-term potentiation in single dendritic spines. *Nature*, 429(6993): 761–766.

Matveev, V., Zucker, R.S. & Sherman, A. 2004. Facilitation through buffer saturation: constraints on endogenous buffering properties. *Biophysical journal*, 86(5): 2691–2709.

McGuinness, L., Taylor, C., Taylor, R.D.T., Yau, C., Langenhan, T., Hart, M.L., Christian, H., Tynan, P.W., Donnelly, P. & Emptage, N.J. 2010. Presynaptic NMDARs in the hippocampus facilitate transmitter release at theta frequency. *Neuron*, 68(6): 1109–1127.

Megías, M., Emri, Z., Freund, T.F. & Gulyás, A.I. 2001. Total number and distribution of inhibitory and excitatory synapses on hippocampal CA1 pyramidal cells. *Neuroscience*, 102(3): 527–540.

Mel, B.W. 1992. The Clusteron: Toward a Simple Abstraction for a Complex Neuron. In *Advances in Neural Information Processing Systems 4*. Advances in Neural Information Processing Systems, San Mateo, CA: Morgan Kaufmann: 35-42.

Mellentin, C., Møller, M. & Jahnsen, H. 2006. Properties of long-term synaptic plasticity and metaplasticity in organotypic slice cultures of rat hippocampus. *Experimental brain research*, 170(4): 522–531.

Menon, V., Musial, T.F., Liu, A., Katz, Y., Kath, W.L., Spruston, N. & Nicholson, D.A. 2013. Balanced synaptic impact via distance-dependent synapse distribution and complementary expression of AMPARs and NMDARs in hippocampal dendrites. *Neuron*, 80(6): 1451–1463.

Meyer, D., Bonhoeffer, T. & Scheuss, V. 2014. Balance and stability of synaptic structures during synaptic plasticity. *Neuron*, 82(2): 430–443.

Micheva, K.D., Holz, R.W. & Smith, S.J. 2001. Regulation of presynaptic phosphatidylinositol 4,5-biphosphate by neuronal activity. *The Journal of cell biology*, 154(2): 355–368.

Miesenböck, G., De Angelis, D.A. & Rothman, J.E. 1998. Visualizing secretion and synaptic transmission with pH-sensitive green fluorescent proteins. *Nature*, 394(6689): 192–195.

Miki, N., Kawabe, Y. & Kuriyama, K. 1977. Activation of cerebral guanylate cyclase by nitric oxide. *Biochemical and biophysical research communications*, 75(4): 851–856.

Miki, T., Kaufmann, W.A., Malagon, G., Gomez, L., Tabuchi, K., Watanabe, M., Shigemoto, R. & Marty, A. 2017. Numbers of presynaptic Ca2+ channel clusters match those of functionally defined vesicular docking sites in single central synapses. *Proceedings of the National Academy of Sciences of the United States of America*, 114(26): E5246–E5255.

Miller, K.D. & MacKay, D.J. 1994. The Role of Constraints in Hebbian Learning. *Neural computation*, 6(1): 100–126.

Milstein, A.D., Bloss, E.B., Apostolides, P.F., Vaidya, S.P., Dilly, G.A., Zemelman, B.V. & Magee, J.C. 2015. Inhibitory Gating of Input Comparison in the CA1 Microcircuit. *Neuron*, 87(6): 1274–1289.

Min, R. & Nevian, T. 2012. Astrocyte signaling controls spike timing-dependent depression at neocortical synapses. *Nature neuroscience*, 15(5): 746–753.

Moore, E.F. & Shannon, C.E. 1956. Reliable circuits using less reliable relays. *Journal of the Franklin Institute*, 262(3): 191–208.

Mothet, J.P., Le Bail, M. & Billard, J.M. 2015. Time and space profiling of NMDA receptor co-agonist functions. *Journal of neurochemistry*, 135(2): 210–225.

Mowla, S.J., Pareek, S., Farhadi, H.F., Petrecca, K., Fawcett, J.P., Seidah, N.G., Morris, S.J., Sossin, W.S. & Murphy, R.A. 1999. Differential sorting of nerve growth factor and brain-derived neurotrophic factor in hippocampal neurons. *Journal of Neuroscience*, 19(6): 2069–2080.

Muller, D., Buchs, P.A. & Stoppini, L. 1993. Time course of synaptic development in hippocampal organotypic cultures. *Brain research. Developmental brain research*, 71(1): 93–100.

Murakoshi, H., Wang, H. & Yasuda, R. 2011. Local, persistent activation of Rho GTPases during plasticity of single dendritic spines. *Nature*, 472(7341): 100–104.

Murthy, K.S. & Zhou, H. 2003. Selective phosphorylation of the IP3R-I in vivo by cGMP-dependent protein kinase in smooth muscle. *American journal of physiology. Gastrointestinal and liver physiology*, 284(2): G221–30.

Murthy, V.N., Sejnowski, T.J. & Stevens, C.F. 1997. Heterogeneous release properties of visualized individual hippocampal synapses. *Neuron*, 18(4): 599–612.

Musleh, W.Y., Shahi, K. & Baudry, M. 1993. Further studies concerning the role of nitric oxide in LTP induction and maintenance. *Synapse (New York, N.Y.)*, 13(4): 370–375.

Naber, P.A., Lopes da Silva, F.H. & Witter, M.P. 2001. Reciprocal connections between the entorhinal cortex and hippocampal fields CA1 and the subiculum are in register with the projections from CA1 to the subiculum. *Hippocampus*, 11(2): 99–104.

Nakahata, Y. & Yasuda, R. 2018. Plasticity of Spine Structure: Local Signaling, Translation and Cytoskeletal Reorganization. *Frontiers in synaptic neuroscience*, 10: 29.

Nakamura, Y., Harada, H., Kamasawa, N., Matsui, K., Rothman, J.S., Shigemoto, R., Silver, R.A., DiGregorio, D.A. & Takahashi, T. 2015. Nanoscale distribution of presynaptic Ca(2+) channels and its impact on vesicular release during development. *Neuron*, 85(1): 145–158.

Namiki, S., Sakamoto, H., Iinuma, S., Iino, M. & Hirose, K. 2007. Optical glutamate sensor for spatiotemporal analysis of synaptic transmission. *The European journal of neuroscience*, 25(8): 2249–2259.

Natschläger, T., Maass, W. & Zador, A. 2001. Efficient temporal processing with biologically realistic dynamic synapses. *Network: Computation in Neural Systems*, 12(1): 75–87.

Neher, E. & Sakaba, T. 2001. Combining deconvolution and noise analysis for the estimation of transmitter release rates at the calyx of held. *The Journal of neuroscience*, 21(2): 444–461.

Neitz, A., Mergia, E., Eysel, U.T., Koesling, D. & Mittmann, T. 2011. Presynaptic nitric oxide/cGMP facilitates glutamate release via hyperpolarization-activated cyclic nucleotide-gated channels in the hippocampus. *The European journal of neuroscience*, 33(9): 1611–1621.

Nevian, T., Larkum, M.E., Polsky, A. & Schiller, J. 2007. Properties of basal dendrites of layer 5 pyramidal neurons: a direct patch-clamp recording study. *Nature neuroscience*, 10(2): 206–214.

Ngo-Anh, T.J., Bloodgood, B.L., Lin, M., Sabatini, B.L., Maylie, J. & Adelman, J.P. 2005. SK channels and NMDA receptors form a Ca2+-mediated feedback loop in dendritic spines. *Nature neuroscience*, 8(5): 642–649.

Nichols, R.A., Sihra, T.S., Czernik, A.J., Nairn, A.C. & Greengard, P. 1990. Calcium/calmodulin-dependent protein kinase II increases glutamate and noradrenaline release from synaptosomes. *Nature*, 343(6259): 647–651.

Nikonenko, I., Jourdain, P. & Muller, D. 2003. Presynaptic remodeling contributes to activity-dependent synaptogenesis. *The Journal of neuroscience*, 23(24): 8498–8505.

Nikonenko, I., Nikonenko, A., Mendez, P., Michurina, T.V., Enikolopov, G. & Muller, D. 2013. Nitric oxide mediates local activity-dependent excitatory synapse development. *Proceedings of the National Academy of Sciences of the United States of America*, 110(44): E4142–51.

Ninan, I. & Arancio, O. 2004. Presynaptic CaMKII is necessary for synaptic plasticity in cultured hippocampal neurons. *Neuron*, 42(1): 129–141.

Nishiyama, J. & Yasuda, R. 2015. Biochemical Computation for Spine Structural Plasticity. *Neuron*, 87(1): 63–75.

Nowak, L., Bregestovski, P., Ascher, P., Herbet, A. & Prochiantz, A. 1984. Magnesium gates glutamate-activated channels in mouse central neurones. *Nature*, 307(5950): 462–465.

O'Dell, T.J., Hawkins, R.D., Kandel, E.R. & Arancio, O. 1991. Tests of the roles of two diffusible substances in long-term potentiation: evidence for nitric oxide as a possible early retrograde messenger. *Proceedings of the National Academy of Sciences*, 88(24): 11285–11289.

O'Dell, T.J., Huang, P.L., Dawson, T.M., Dinerman, J.L., Snyder, S.H., Kandel, E.R. & Fishman, M.C. 1994. Endothelial NOS and the blockade of LTP by NOS inhibitors in mice lacking neuronal NOS. *Science*, 265(5171): 542–546.

Oertner, T.G., Sabatini, B.L., Nimchinsky, E.A. & Svoboda, K. 2002. Facilitation at single synapses probed with optical quantal analysis. *Nature neuroscience*, 5(7): 657–664.

Oh, W.C., Parajuli, L.K. & Zito, K. 2015. Heterosynaptic structural plasticity on local dendritic segments of hippocampal CA1 neurons. *Cell reports*, 10(2): 162–169.

Oja, E. 1982. A simplified neuron model as a principal component analyzer. *Journal of mathematical biology*, 15(3): 267–273.

Oliveira, A.F. & Yasuda, R. 2014. Neurofibromin is the major ras inactivator in dendritic spines. *The Journal of neuroscience*, 34(3): 776–783.

Ouimet, C.C., McGuinness, T.L. & Greengard, P. 1984. Immunocytochemical localization of calcium/calmodulin-dependent protein kinase II in rat brain. *Proceedings of the National Academy of Sciences*, 81(17): 5604–5608.

Padamsey, Z. & Emptage, N. 2014. Two sides to long-term potentiation: a view towards reconciliation. *Philosophical Transactions of the Royal Society B: Biological Sciences*, 369(1633): 20130154.

Padamsey, Z., McGuinness, L., Bardo, S.J., Reinhart, M., Tong, R., Hedegaard, A., Hart, M.L. & Emptage, N.J. 2017b. Activity-Dependent Exocytosis of Lysosomes Regulates the Structural Plasticity of Dendritic Spines. *Neuron*, 93(1): 132–146.

Padamsey, Z., Tong, R. & Emptage, N. 2017a. Glutamate is required for depression but not potentiation of long-term presynaptic function. *eLife*, 6: 839.

Padamsey, Z., Tong, R. & Emptage, N. 2019. Optical Quantal Analysis Using Ca2+ Indicators: A Robust Method for Assessing Transmitter Release Probability at Excitatory Synapses by Imaging Single Glutamate Release Events. *Frontiers in synaptic neuroscience*, 11: 5.

Palmer, R.M., Ferrige, A.G. & Moncada, S. 1987. Nitric oxide release accounts for the biological activity of endothelium-derived relaxing factor. *Nature*, 327(6122): 524–526.

Pang, P.T., Teng, H.K., Zaitsev, E., Woo, N.T., Sakata, K., Zhen, S., Teng, K.K., Yung, W.-H., Hempstead, B.L. & Lu, B. 2004. Cleavage of proBDNF by tPA/plasmin is essential for long-term hippocampal plasticity. *Science*, 306(5695): 487–491.

Park, H., Li, Y. & Tsien, R.W. 2012. Influence of synaptic vesicle position on release probability and exocytotic fusion mode. *Science*, 335(6074): 1362–1366.

Peixoto, R.T., Kunz, P.A., Kwon, H., Mabb, A.M., Sabatini, B.L., Philpot, B.D. & Ehlers, M.D. 2012. Transsynaptic signaling by activity-dependent cleavage of neuroligin-1. *Neuron*, 76(2): 396–409.

Pelkey, K.A., Askalan, R., Paul, S., Kalia, L.V., Nguyen, T.H., Pitcher, G.M., Salter, M.W. & Lombroso, P.J. 2002. Tyrosine phosphatase STEP is a tonic brake on induction of long-term potentiation. *Neuron*, 34(1): 127–138.

Penny, C.J. & Gold, M.G. 2018. Mechanisms for localising calcineurin and CaMKII in dendritic spines. *Cellular signalling*, 49: 46–58.

Pfeiffer, S., Leopold, E., Hemmens, B., Schmidt, K., Werner, E.R. & Mayer, B. 1997. Interference of carboxy-PTIO with nitric oxide- and peroxynitrite-mediated reactions. *Free radical biology & medicine*, 22(5): 787–794.

Philippides, A., Husbands, P. & O'Shea, M. 2000. Four-dimensional neuronal signaling by nitric oxide: a computational analysis. *The Journal of neuroscience*, 20(3): 1199–1207.

Pinheiro, P.S. & Mulle, C. 2008. Presynaptic glutamate receptors: physiological functions and mechanisms of action. *Nature reviews. Neuroscience*, 9(6): 423–436.

Pockett, S., Brookes, N.H. & Bindman, L.J. 1990. Long-term depression at synapses in slices of rat hippocampus can be induced by bursts of postsynaptic activity. *Experimental brain research*, 80(1): 196–200.

Poirazi, P. & Mel, B.W. 2001. Impact of active dendrites and structural plasticity on the memory capacity of neural tissue. *Neuron*, 29(3): 779–796.

Poirazi, P., Brannon, T. & Mel, B.W. 2003. Pyramidal neuron as two-layer neural network. *Neuron*, 37(6): 989–999.

Pool, R.R. & Mato, G. 2011. Spike-timing-dependent plasticity and reliability optimization: the role of neuron dynamics. *Neural computation*, 23(7): 1768–1789.

Poss, K.D., Thomas, M.J., Ebralidze, A.K., O'Dell, T.J. & Tonegawa, S. 1995. Hippocampal long-term potentiation is normal in heme oxygenase-2 mutant mice. *Neuron*, 15(4): 867–873.

Pouille, F. & Scanziani, M. 2004. Routing of spike series by dynamic circuits in the hippocampus. *Nature*, 429(6993): 717–723.

Qu, L., Akbergenova, Y., Hu, Y. & Schikorski, T. 2009. Synapse-to-synapse variation in mean synaptic vesicle size and its relationship with synaptic morphology and function. *The Journal of comparative neurology*, 514(4): 343–352.

Raastad, M., Storm, J.F. & Andersen, P. 1992. Putative Single Quantum and Single Fibre Excitatory Postsynaptic Currents Show Similar Amplitude Range and Variability in Rat Hippocampal Slices. *The European journal of neuroscience*, 4(1): 113–117.

Rabinowitch, I. & Segev, I. 2008. Two opposing plasticity mechanisms pulling a single synapse. *Trends in Neurosciences*, 31(8): 377–383.

Rall, W. 1959. Branching dendritic trees and motoneuron membrane resistivity. *Experimental neurology*, 1(5): 491–527.

Rameau, G.A., Chiu, L.-Y. & Ziff, E.B. 2004. Bidirectional regulation of neuronal nitric-oxide synthase phosphorylation at serine 847 by the N-methyl-D-aspartate receptor. *The Journal of biological chemistry*, 279(14): 14307–14314.

Rameau, G.A., Tukey, D.S., Garcin-Hosfield, E.D., Titcombe, R.F., Misra, C., Khatri, L., Getzoff, E.D. & Ziff, E.B. 2007. Biphasic coupling of neuronal nitric oxide synthase phosphorylation to the NMDA receptor regulates AMPA receptor trafficking and neuronal cell death. *The Journal of neuroscience*, 27(13): 3445–3455.

Rand, M.J. & Li, C.G. 1995. Nitric oxide as a neurotransmitter in peripheral nerves: nature of transmitter and mechanism of transmission. *Annual Review of Physiology*, 57(1): 659–682.

Rangaraju, V., Calloway, N. & Ryan, T.A. 2014. Activity-driven local ATP synthesis is required for synaptic function. *Cell*, 156(4): 825–835.

Ratnayaka, A., Marra, V., Bush, D., Burden, J.J., Branco, T. & Staras, K. 2012. Recruitment of resting vesicles into recycling pools supports NMDA receptor-dependent synaptic potentiation in cultured hippocampal neurons. *The Journal of physiology*, 590(7): 1585–1597.

Regehr, W.G. 2012. Short-term presynaptic plasticity. *Cold Spring Harbor perspectives in biology*, 4(7): a005702.

Remy, S. & Spruston, N. 2007. Dendritic spikes induce single-burst long-term potentiation. *Proceedings of the National Academy of Sciences*, 104(43): 17192–17197.

Rex, C.S., Chen, L.Y., Sharma, A., Liu, J., Babayan, A.H., Gall, C.M. & Lynch, G. 2009. Different Rho GTPase-dependent signaling pathways initiate sequential steps in the consolidation of long-term potentiation. *The Journal of cell biology*, 186(1): 85–97.

Reyes-Harde, M., Potter, B.V., Galione, A. & Stanton, P.K. 1999. Induction of hippocampal LTD requires nitric-oxide-stimulated PKG activity and Ca2+ release from cyclic ADP-ribose-sensitive stores. *Journal of Neurophysiology*, 82(3): 1569–1576.

Roberts, W.M. 1993. Spatial calcium buffering in saccular hair cells. *Nature*, 363(6424): 74–76.

Rodrigo, J., Springall, D.R., Uttenthal, O., Bentura, M.L., Abadia-Molina, F., Riveros-Moreno, V., Martínez-Murillo, R., Polak, J.M. & Moncada, S. 1994. Localization of nitric oxide synthase in the adult rat brain. *Philosophical transactions of the Royal Society of London. Series B, Biological sciences*, 345(1312): 175–221.

Rodríguez-Moreno, A., González-Rueda, A., Banerjee, A., Upton, A.L., Craig, M.T. & Paulsen, O. 2013. Presynaptic self-depression at developing neocortical synapses. *Neuron*, 77(1): 35–42.

Romano, D.R., Pharris, M.C., Patel, N.M. & Kinzer-Ursem, T.L. 2017. Competitive tuning: Competition's role in setting the frequency-dependence of Ca2+-dependent proteins. J. J. Saucerman, ed. *PLoS computational biology*, 13(11): e1005820.

Royer, S., Zemelman, B.V., Losonczy, A., Kim, J., Chance, F., Magee, J.C. & Buzsáki, G. 2012. Control of timing, rate and bursts of hippocampal place cells by dendritic and somatic inhibition. *Nature neuroscience*, 15(5): 769–775.

Rozov, A., Burnashev, N., Sakmann, B. & Neher, E. 2001. Transmitter release modulation by intracellular Ca2+ buffers in facilitating and depressing nerve terminals of pyramidal cells in layer 2/3 of the rat neocortex indicates a target cell-specific difference in presynaptic calcium dynamics. *The Journal of physiology*, 531(Pt 3): 807–826.

Rusakov, D.A., Saitow, F., Lehre, K.P. & Konishi, S. 2005. Modulation of presynaptic Ca2+ entry by AMPA receptors at individual GABAergic synapses in the cerebellum. *The Journal of neuroscience*, 25(20): 4930–4940.

Ryan, T.A., Reuter, H., Wendland, B., Schweizer, F.E., Tsien, R.W. & Smith, S.J. 1993. The kinetics of synaptic vesicle recycling measured at single presynaptic boutons. *Neuron*, 11(4): 713–724.

Ryan, X.P., Alldritt, J., Svenningsson, P., Allen, P.B., Wu, G.-Y., Nairn, A.C. & Greengard, P.

2005. The Rho-specific GEF Lfc interacts with neurabin and spinophilin to regulate dendritic spine morphology. *Neuron*, 47(1): 85–100.

Sakamoto, H., Ariyoshi, T., Kimpara, N., Sugao, K., Taiko, I., Takikawa, K., Asanuma, D., Namiki, S. & Hirose, K. 2018. Synaptic weight set by Munc13-1 supramolecular assemblies. *Nature neuroscience*, 21(1): 41–49.

Sanderson, T.M., Bradley, C.A., Georgiou, J., Hong, Y.H., Ng, A.N., Lee, Y., Kim, H.-D., Kim, D., Amici, M., Son, G.H., Zhuo, M., Kim, K., Kaang, B.-K., Kim, S.J. & Collingridge, G.L. 2018. The Probability of Neurotransmitter Release Governs AMPA Receptor Trafficking via Activity-Dependent Regulation of mGluR1 Surface Expression. *Cell reports*, 25(13): 3631–3646.e3.

Sausbier, M., Schubert, R., Voigt, V., Hirneiss, C., Pfeifer, A., Korth, M., Kleppisch, T., Ruth, P. & Hofmann, F. 2000. Mechanisms of NO/cGMP-dependent vasorelaxation. *Circulation research*, 87(9): 825–830.

Scanziani, M., Malenka, R.C. & Nicoll, R.A. 1996. Role of intercellular interactions in heterosynaptic long-term depression. *Nature*, 380(6573): 446–450.

Schikorski, T. & Stevens, C.F. 1997. Quantitative ultrastructural analysis of hippocampal excitatory synapses. *Journal of Neuroscience*, 17(15): 5858–5867.

Schindelin, J., Arganda-Carreras, I., Frise, E., Kaynig, V., Longair, M., Pietzsch, T., Preibisch, S., Rueden, C., Saalfeld, S., Schmid, B., Tinevez, J.-Y., White, D.J., Hartenstein, V., Eliceiri, K., Tomancak, P. & Cardona, A. 2012. Fiji: an open-source platform for biological-image analysis. *Nature methods*, 9(7): 676–682.

Schlossmann, J., Ammendola, A., Ashman, K., Zong, X., Huber, A., Neubauer, G., Wang, G.X., Allescher, H.D., Korth, M., Wilm, M., Hofmann, F. & Ruth, P. 2000. Regulation of intracellular calcium by a signalling complex of IRAG, IP3 receptor and cGMP kinase Ibeta. *Nature*, 404(6774): 197–201.

Schneider, C.A., Rasband, W.S. & Eliceiri, K.W. 2012. NIH Image to ImageJ: 25 years of image analysis. *Nature methods*, 9(7): 671–675.

Schreiber, S., Machens, C.K., Herz, A.V.M. & Laughlin, S.B. 2002. Energy-efficient coding with discrete stochastic events. *Neural computation*, 14(6): 1323–1346.

Schuman, E.M. & Madison, D.V. 1991. A requirement for the intercellular messenger nitric oxide in long-term potentiation. *Science*, 254(5037): 1503–1506.

Schuman, E.M. & Madison, D.V. 1994. Locally distributed synaptic potentiation in the hippocampus. *Science*, 263(5146): 532–536.

Schweighofer, N. & Ferriol, G. 2000. Diffusion of nitric oxide can facilitate cerebellar learning: A simulation study. *Proceedings of the National Academy of Sciences*, 97(19): 10661–10665.

Seidel, B., Stanarius, A. & Wolf, G. 1997. Differential expression of neuronal and endothelial nitric oxide synthase in blood vessels of the rat brain. *Neuroscience letters*, 239(2-3): 109–112.

Segal, M., Vlachos, A. & Korkotian, E. 2010. The spine apparatus, synaptopodin, and dendritic spine plasticity. The Neuroscientist : a review journal bringing neurobiology, neurology and psychiatry, 16(2): 125–131.

Serfass, L. & Burstyn, J.N. 1998. Effect of heme oxygenase inhibitors on soluble guanylyl cyclase activity. *Archives of biochemistry and biophysics*, 359(1): 8–16.

Shadlen, M.N. & Newsome, W.T. 1994. Noise, neural codes and cortical organization. *Current Opinion in Neurobiology*, 4(4): 569–579.

Shakiryanova, D., Morimoto, T., Zhou, C., Chouhan, A.K., Sigrist, S.J., Nose, A., Macleod, G.T., Deitcher, D.L. & Levitan, E.S. 2011. Differential control of presynaptic CaMKII activation and translocation to active zones. *The Journal of neuroscience*, 31(25): 9093–9100.

Shepherd, G.M. & Harris, K.M. 1998. Three-dimensional structure and composition of CA3-->CA1 axons in rat hippocampal slices: implications for presynaptic connectivity and compartmentalization. *Journal of Neuroscience*, 18(20): 8300–8310.

Shepherd, J.D. & Bear, M.F. 2011. New views of Arc, a master regulator of synaptic plasticity. *Nature neuroscience*, 14(3): 279–284.

Siegel, S.J., Brose, N., Janssen, W.G., Gasic, G.P., Jahn, R., Heinemann, S.F. & Morrison, J.H. 1994. Regional, cellular, and ultrastructural distribution of N-methyl-D-aspartate receptor subunit 1 in monkey hippocampus. *Proceedings of the National Academy of Sciences*, 91(2): 564–568.

Sjöström, P.J., Turrigiano, G.G. & Nelson, S.B. 2003. Neocortical LTD via coincident activation of presynaptic NMDA and cannabinoid receptors. *Neuron*, 39(4): 641–654.

Sjöström, P.J., Turrigiano, G.G. & Nelson, S.B. 2001. Rate, timing, and cooperativity jointly determine cortical synaptic plasticity. *Neuron*, 32(6): 1149–1164.

Smetters, D.K. & Zador, A. 1996. Synaptic transmission: Noisy synapses and noisy neurons. *Current biology : CB*, 6(10): 1217–1218.

Smith, M.A., Ellis-Davies, G.C.R. & Magee, J.C. 2003. Mechanism of the distance-dependent scaling of Schaffer collateral synapses in rat CA1 pyramidal neurons. *The Journal of physiology*, 548(Pt 1): 245–258.

Somogyi, P. & Klausberger, T. 2005. Defined types of cortical interneurone structure space and spike timing in the hippocampus. *The Journal of physiology*, 562(Pt 1): 9–26.

Sorra, K.E. & Harris, K.M. 1993. Occurrence and three-dimensional structure of multiple synapses between individual radiatum axons and their target pyramidal cells in hippocampal area CA1. *Journal of Neuroscience*, 13(9): 3736–3748.

Spacek, J. & Harris, K.M. 1997. Three-dimensional organization of smooth endoplasmic reticulum in hippocampal CA1 dendrites and dendritic spines of the immature and mature rat. *Journal of Neuroscience*, 17(1): 190–203.

Spruston, N. 2008. Pyramidal neurons: dendritic structure and synaptic integration. *Nature reviews. Neuroscience*, 9(3): 206–221.

Stanarius, A., Töpel, I., Schulz, S., Noack, H. & Wolf, G. 1997. Immunocytochemistry of endothelial nitric oxide synthase in the rat brain: a light and electron microscopical study using the tyramide signal amplification technique. *Acta Histochemica*, 99(4): 411–429.

Stanley, E.F. 1993. Single calcium channels and acetylcholine release at a presynaptic

nerve terminal. *Neuron*, 11(6): 1007–1011.

Stanley, E.F. 2016. The Nanophysiology of Fast Transmitter Release. *Trends in Neurosciences*, 39(3): 183–197.

Stanton, P.K. & Gage, A.T. 1996. Distinct synaptic loci of Ca2+/calmodulin-dependent protein kinase II necessary for long-term potentiation and depression. *Journal of Neurophysiology*, 76(3): 2097–2101.

Stanton, P.K., Heinemann, U. & Muller, W. 2001. FM1-43 imaging reveals cGMP-dependent long-term depression of presynaptic transmitter release. *The Journal of neuroscience,* 21(19): RC167.

Stanton, P.K., Winterer, J., Bailey, C.P., Kyrozis, A., Raginov, I., Laube, G., Veh, R.W., Nguyen, C.Q. & Müller, W. 2003. Long-term depression of presynaptic release from the readily releasable vesicle pool induced by NMDA receptor-dependent retrograde nitric oxide. *The Journal of neuroscience*, 23(13): 5936–5944.

Stanton, P.K., Winterer, J., Zhang, X.-L. & Müller, W. 2005. Imaging LTP of presynaptic release of FM1-43 from the rapidly recycling vesicle pool of Schaffer collateral-CA1 synapses in rat hippocampal slices. *The European journal of neuroscience*, 22(10): 2451–2461.

Stevens, C.F. 2003. Neurotransmitter release at central synapses. *Neuron*, 40(2): 381–388.

Stevens, C.F. & Wang, Y. 1995. Facilitation and depression at single central synapses. *Neuron*, 14(4): 795–802.

Stevens, C.F. & Wang, Y. 1993. Reversal of long-term potentiation by inhibitors of haem oxygenase. *Nature*, 364(6433): 147–149.

Stevens, C.F. & Wang, Y. 1994. Changes in reliability of synaptic function as a mechanism for plasticity. *Nature*, 371(6499): 704–707.

Stocca, G. & Vicini, S. 1998. Increased contribution of NR2A subunit to synaptic NMDA receptors in developing rat cortical neurons. *The Journal of physiology*, 507(1): 13–24.

Stratford, K.J., Tarczy-Hornoch, K., Martin, K.A., Bannister, N.J. & Jack, J.J. 1996. Excitatory synaptic inputs to spiny stellate cells in cat visual cortex. *Nature*, 382(6588): 258–261.

Stricker, C., Cowan, A.I., Field, A.C. & Redman, S.J. 1999. Analysis of NMDA-independent long-term potentiation induced at CA3-CA1 synapses in rat hippocampus in vitro. *The Journal of physiology*, 520 Pt 2(2): 513–525.

Sun, H.Y. & Dobrunz, L.E. 2006. Presynaptic kainate receptor activation is a novel mechanism for target cell-specific short-term facilitation at Schaffer collateral synapses. *The Journal of neuroscience*, 26(42): 10796–10807.

Sutton, M.A., Ito, H.T., Cressy, P., Kempf, C., Woo, J.C. & Schuman, E.M. 2006. Miniature neurotransmission stabilizes synaptic function via tonic suppression of local dendritic protein synthesis. *Cell*, 125(4): 785–799.

Sutton, M.A., Taylor, A.M., Ito, H.T., Pham, A. & Schuman, E.M. 2007. Postsynaptic decoding of neural activity: eEF2 as a biochemical sensor coupling miniature synaptic transmission to local protein synthesis. *Neuron*, 55(4): 648–661.

Südhof, T.C. 2013. Neurotransmitter release: the last millisecond in the life of a synaptic

vesicle. *Neuron*, 80(3): 675–690.

Südhof, T.C. 2002. Synaptotagmins: why so many? *The Journal of biological chemistry*, 277(10): 7629–7632.

Takago, H., Nakamura, Y. & Takahashi, T. 2005. G protein-dependent presynaptic inhibition mediated by AMPA receptors at the calyx of Held. *Proceedings of the National Academy of Sciences*, 102(20): 7368–7373.

Takahashi, H. & Magee, J.C. 2009. Pathway interactions and synaptic plasticity in the dendritic tuft regions of CA1 pyramidal neurons. *Neuron*, 62(1): 102–111.

Takahashi, K.A. & Castillo, P.E. 2006. The CB1 cannabinoid receptor mediates glutamatergic synaptic suppression in the hippocampus. *Neuroscience*, 139(3): 795–802.

Takahashi, N., Kitamura, K., Matsuo, N., Mayford, M., Kano, M., Matsuki, N. & Ikegaya, Y. 2012. Locally Synchronized Synaptic Inputs. *Science*, 335(6066): 348–353.

Takao, K., Okamoto, K.-I., Nakagawa, T., Neve, R.L., Nagai, T., Miyawaki, A., Hashikawa, T., Kobayashi, S. & Hayashi, Y. 2005. Visualization of synaptic Ca2+ /calmodulin-dependent protein kinase II activity in living neurons. *The Journal of neuroscience*, 25(12): 3107–3112.

Takasago, T., Imagawa, T., Furukawa, K., Ogurusu, T. & Shigekawa, M. 1991. Regulation of the cardiac ryanodine receptor by protein kinase-dependent phosphorylation. *Journal of biochemistry*, 109(1): 163–170.

Tamura, T., Hou, J., Reist, N.E. & Kidokoro, Y. 2007. Nerve-evoked synchronous release and high K+ -induced quantal events are regulated separately by synaptotagmin I at Drosophila neuromuscular junctions. *Journal of Neurophysiology*, 97(1): 540–549.

Tanaka, J.-I., Horiike, Y., Matsuzaki, M., Miyazaki, T., Ellis-Davies, G.C.R. & Kasai, H. 2008. Protein synthesis and neurotrophin-dependent structural plasticity of single dendritic spines. *Science*, 319(5870): 1683–1687.

Tang, A.-H., Chen, H., Li, T.P., Metzbower, S.R., MacGillavry, H.D. & Blanpied, T.A. 2016. A trans-synaptic nanocolumn aligns neurotransmitter release to receptors. *Nature*, 536(7615): 210–214.

Thies, R.E. 1965. NEUROMUSCULAR DEPRESSION AND THE APPARENT DEPLETION OF TRANSMITTER IN MAMMALIAN MUSCLE. *Journal of Neurophysiology*, 28(3): 427–442.

Thomson, A.M. 2003. Presynaptic Frequency- and Pattern-Dependent Filtering. *Journal of computational neuroscience*, 15(2): 159–202.

Thoreson, W.B., Rabl, K., Townes-Anderson, E. & Heidelberger, R. 2004. A highly Ca2+-sensitive pool of vesicles contributes to linearity at the rod photoreceptor ribbon synapse. *Neuron*, 42(4): 595–605.

Toda, N. & Herman, A.G. 2005. Gastrointestinal function regulation by nitrergic efferent nerves. *Pharmacological reviews*, 57(3): 315–338.

Toda, N. & Okamura, T. 2003. The pharmacology of nitric oxide in the peripheral nervous system of blood vessels. *Pharmacological reviews*, 55(2): 271–324.

Toyoizumi, T., Pfister, J.-P., Aihara, K. & Gerstner, W. 2005. Generalized Bienenstock-

Cooper-Munro rule for spiking neurons that maximizes information transmission. *Proceedings of the National Academy of Sciences*, 102(14): 5239–5244.

Toyoizumi, T., Pfister, J.-P., Aihara, K. & Gerstner, W. 2007. Optimality model of unsupervised spike-timing-dependent plasticity: synaptic memory and weight distribution. *Neural computation*, 19(3): 639–671.

Trussell, L.O., Zhang, S. & Raman, I.M. 1993. Desensitization of AMPA receptors upon multiquantal neurotransmitter release. *Neuron*, 10(6): 1185–1196.

Tsodyks, M., Pawelzik, K. & Markram, H. 1998. Neural networks with dynamic synapses. *Neural computation*, 10(4): 821–835.

Tsodyks, M.V. & Markram, H. 1997. The neural code between neocortical pyramidal neurons depends on neurotransmitter release probability. *Proceedings of the National Academy of Sciences of the United States of America*, 94(2): 719–723.

Turrigiano, G. 2012. Homeostatic synaptic plasticity: local and global mechanisms for stabilizing neuronal function. *Cold Spring Harbor perspectives in biology*, 4(1): a005736–a005736.

Turrigiano, G.G., Leslie, K.R., Desai, N.S., Rutherford, L.C. & Nelson, S.B. 1998. Activity-dependent scaling of quantal amplitude in neocortical neurons. *Nature*, 391(6670): 892–896.

Valtschanoff, J.G. & Weinberg, R.J. 2001. Laminar organization of the NMDA receptor complex within the postsynaptic density. *The Journal of neuroscience*, 21(4): 1211–1217.

van Groen, T. & Wyss, J.M. 1990. The connections of presubiculum and parasubiculum in the rat. *Brain research*, 518(1-2): 227–243.

Van Hook, M.J., Babai, N., Zurawski, Z., Yim, Y.Y., Hamm, H.E. & Thoreson, W.B. 2017. A Presynaptic Group III mGluR Recruits Gβγ/SNARE Interactions to Inhibit Synaptic Transmission by Cone Photoreceptors in the Vertebrate Retina. *The Journal of neuroscience*, 37(17): 4618–4634.

van Rossum, M.C., Bi, G.Q. & Turrigiano, G.G. 2000. Stable Hebbian learning from spike timing-dependent plasticity. *The Journal of neuroscience*, 20(23): 8812–8821.

van Strien, N.M., Cappaert, N.L.M. & Witter, M.P. 2009. The anatomy of memory: an interactive overview of the parahippocampal-hippocampal network. *Nature reviews. Neuroscience*, 10(4): 272–282.

Vincent, S.R. & Kimura, H. 1992. Histochemical mapping of nitric oxide synthase in the rat brain. *Neuroscience*, 46(4): 755–784.

Volgushev, M., Balaban, P., Chistiakova, M. & Eysel, U.T. 2000. Retrograde signalling with nitric oxide at neocortical synapses. *The European journal of neuroscience*, 12(12): 4255–4267.

Volgushev, M., Mittmann, T., Chistiakova, M., Balaban, P. & Eysel, U.T. 1999. Interaction between intracellular tetanization and pairing-induced long-term synaptic plasticity in the rat visual cortex. *Neuroscience*, 93(4): 1227–1232.

Volgushev, M., Voronin, L.L., Chistiakova, M. & Singer, W. 1994. Induction of LTP and LTD in visual cortex neurones by intracellular tetanization. *Neuroreport*, 5(16): 2069–

2072.

Volgushev, M., Voronin, L.L., Chistiakova, M. & Singer, W. 1997. Relations between long-term synaptic modifications and paired-pulse interactions in the rat neocortex. *The European journal of neuroscience*, 9(8): 1656–1665.

von der Malsburg, C. 1981. *The correlation theory of brain function.* Internal Report, Dept. Neurobiology, Max-Planck-Institute for Biophysical Chemistry: 81–82

Wadiche, J.I. & Jahr, C.E. 2001. Multivesicular release at climbing fiber-Purkinje cell synapses. *Neuron*, 32(2): 301–313.

Walaas, S.I., Gorelick, F.S. & Greengard, P. 1989. Presence of calcium/calmodulin-dependent protein kinase II in nerve terminals of rat brain. *Synapse (New York, N.Y.)*, 3(4): 356–362.

Walker, A.S., Neves, G., Grillo, F., Jackson, R.E., Rigby, M., O'Donnell, C., Lowe, A.S., Vizcay-Barrena, G., Fleck, R.A. & Burrone, J. 2017. Distance-dependent gradient in NMDAR-driven spine calcium signals along tapering dendrites. *Proceedings of the National Academy of Sciences of the United States of America*, 114(10): E1986–E1995.

Wang, Hong-Gang, Lu, F.-M., Jin, I., Udo, H., Kandel, E.R., de Vente, J., Walter, U., Lohmann, S.M., Hawkins, R.D. & Antonova, I. 2005a. Presynaptic and postsynaptic roles of NO, cGK, and RhoA in long-lasting potentiation and aggregation of synaptic proteins. *Neuron*, 45(3): 389–403.

Wang, Yan, Shibasaki, F. & Mizuno, K. 2005b. Calcium signal-induced cofilin dephosphorylation is mediated by Slingshot via calcineurin. *The Journal of biological chemistry*, 280(13): 12683–12689.

Wang, Zhao-Wen. 2008. Regulation of synaptic transmission by presynaptic CaMKII and BK channels. *Molecular neurobiology*, 38(2): 153–166.

Ward, B., McGuinness, L., Akerman, C.J., Fine, A., Bliss, T.V.P. & Emptage, N.J. 2006. State-dependent mechanisms of LTP expression revealed by optical quantal analysis. *Neuron*, 52(4): 649–661.

Watanabe, S., Rost, B.R., Camacho-Pérez, M., Davis, M.W., Söhl-Kielczynski, B., Rosenmund, C. & Jorgensen, E.M. 2013. Ultrafast endocytosis at mouse hippocampal synapses. *Nature*, 504(7479): 242–247.

Watt, A.J. & Desai, N.S. 2010. Homeostatic Plasticity and STDP: Keeping a Neuron's Cool in a Fluctuating World. *Frontiers in synaptic neuroscience*, 2: 5.

Waxham, M.N., Malenka, R.C., Kelly, P.T. & Mauk, M.D. 1993. Calcium/calmodulin-dependent protein kinase II regulates hippocampal synaptic transmission. *Brain research*, 609(1-2): 1–8.

White, G., Levy, W.B. & Steward, O. 1990. Spatial overlap between populations of synapses determines the extent of their associative interaction during the induction of long-term potentiation and depression. *Journal of Neurophysiology*, 64(4): 1186–1198.

Wiegert, J.S. & Oertner, T.G. 2013. Long-term depression triggers the selective elimination of weakly integrated synapses. *Proceedings of the National Academy of Sciences of the United States of America*, 110(47): E4510–9.

Williams, J.H., Li, Y.G., Nayak, A., Errington, M.L., Murphy, K.P. & Bliss, T.V. 1993. The suppression of long-term potentiation in rat hippocampus by inhibitors of nitric oxide synthase is temperature and age dependent. *Neuron*, 11(5): 877–884.

Willmott, N., Sethi, J.K., Walseth, T.F., Lee, H.C., White, A.M. & Galione, A. 1996. Nitric oxide-induced mobilization of intracellular calcium via the cyclic ADP-ribose signaling pathway. *The Journal of biological chemistry*, 271(7): 3699–3705.

Wilson, M. & McNaughton, B. 1993. Dynamics of the hippocampal ensemble code for space. *Science*, 261(5124): 1055–1058.

Wilson, N.R., Kang, J., Hueske, E.V., Leung, T., Varoqui, H., Murnick, J.G., Erickson, J.D. & Liu, G. 2005. Presynaptic regulation of quantal size by the vesicular glutamate transporter VGLUT1. *The Journal of neuroscience*, 25(26): 6221–6234.

Wilson, R.I. & Nicoll, R.A. 2001. Endogenous cannabinoids mediate retrograde signalling at hippocampal synapses. *Nature*, 410(6828): 588–592.

Wilson, R.I., Gödecke, A., Brown, R.E., Schrader, J. & Haas, H.L. 1999. Mice deficient in endothelial nitric oxide synthase exhibit a selective deficit in hippocampal long-term potentiation. *Neuroscience*, 90(4): 1157–1165.

Wittenberg, G.M. & Wang, S S H. 2006. Malleability of Spike-Timing-Dependent Plasticity at the CA3-CA1 Synapse. *The Journal of neuroscience*, 26(24): 6610–6617.

Wood, J. & Garthwaite, J. 1994. Models of the diffusional spread of nitric oxide: implications for neural nitric oxide signalling and its pharmacological properties. *Neuropharmacology*, 33(11): 1235–1244.

Woolley, C.S., Gould, E., Frankfurt, M. & McEwen, B.S. 1990. Naturally occurring fluctuation in dendritic spine density on adult hippocampal pyramidal neurons. *Journal of Neuroscience*, 10(12): 4035–4039.

Xu, J., Mashimo, T. & Südhof, T.C. 2007. Synaptotagmin-1, -2, and -9: Ca(2+) sensors for fast release that specify distinct presynaptic properties in subsets of neurons. *Neuron*, 54(4): 567–581.

Yang, L., Liu, G., Zakharov, S.I., Bellinger, A.M., Mongillo, M. & Marx, S.O. 2007. Protein kinase G phosphorylates Cav1.2 alpha1c and beta2 subunits. *Circulation research*, 101(5): 465–474.

Yang, S.N., Tang, Y.G. & Zucker, R.S. 1999. Selective induction of LTP and LTD by postsynaptic [Ca2+]i elevation. *Journal of Neurophysiology*, 81(2): 781–787.

Yasuda, H., Huang, Y. & Tsumoto, T. 2008. Regulation of excitability and plasticity by endocannabinoids and PKA in developing hippocampus. *Proceedings of the National Academy of Sciences of the United States of America*, 105(8): 3106–3111.

Yasumatsu, N., Matsuzaki, M., Miyazaki, T., Noguchi, J. & Kasai, H. 2008. Principles of long-term dynamics of dendritic spines. *The Journal of neuroscience*, 28(50): 13592–13608.

Yoshihara, M. & Littleton, J.T. 2002. Synaptotagmin I functions as a calcium sensor to synchronize neurotransmitter release. *Neuron*, 36(5): 897–908.

Zabel, U., Kleinschnitz, C., Oh, P., Nedvetsky, P., Smolenski, A., Müller, H., Kronich, P., Kugler, P., Walter, U., Schnitzer, J.E. & Schmidt, H.H.H.W. 2002. Calcium-dependent membrane association sensitizes soluble guanylyl cyclase to nitric oxide. *Nature cell*

biology, 4(4): 307–311.

Zador, A. 1998. Impact of Synaptic Unreliability on the Information Transmitted by Spiking Neurons. *Journal of Neurophysiology*, 79(3): 1219–1229.

Zakharenko, S.S., Patterson, S.L., Dragatsis, I., Zeitlin, S.O., Siegelbaum, S.A., Kandel, E.R. & Morozov, A. 2003. Presynaptic BDNF required for a presynaptic but not postsynaptic component of LTP at hippocampal CA1-CA3 synapses. *Neuron*, 39(6): 975–990.

Zakharenko, S.S., Zablow, L. & Siegelbaum, S.A. 2001. Visualization of changes in presynaptic function during long-term synaptic plasticity. *Nature neuroscience*, 4(7): 711–717.

Zeng, H., Chattarji, S., Barbarosie, M., Rondi-Reig, L., Philpot, B.D., Miyakawa, T., Bear, M.F. & Tonegawa, S. 2001. Forebrain-specific calcineurin knockout selectively impairs bidirectional synaptic plasticity and working/episodic-like memory. *Cell*, 107(5): 617–629.

Zenke, F. & Gerstner, W. 2017. Hebbian plasticity requires compensatory processes on multiple timescales. *Philosophical transactions of the Royal Society of London. Series B, Biological sciences*, 372(1715): 20160259.

Zenke, F., Agnes, E.J. & Gerstner, W. 2015. Diverse synaptic plasticity mechanisms orchestrated to form and retrieve memories in spiking neural networks. *Nature Communications*, 6(1): 6922.

Zenke, F., Hennequin, G. & Gerstner, W. 2013. Synaptic plasticity in neural networks needs homeostasis with a fast rate detector. A. Morrison, ed. *PLoS computational biology*, 9(11): e1003330.

Zhang, Q., Li, Y. & Tsien, R.W. 2009. The dynamic control of kiss-and-run and vesicular reuse probed with single nanoparticles. *Science*, 323(5920): 1448–1453.

Zhang, X.-L., Pöschel, B., Faul, C., Upreti, C., Stanton, P.K. & Mundel, P. 2013. Essential role for synaptopodin in dendritic spine plasticity of the developing hippocampus. *The Journal of neuroscience*, 33(30): 12510–12518.

Zhang, X.-L., Zhou, Z.-Y., Winterer, J., Müller, W. & Stanton, P.K. 2006. NMDA-dependent, but not group I metabotropic glutamate receptor-dependent, long-term depression at Schaffer collateral-CA1 synapses is associated with long-term reduction of release from the rapidly recycling presynaptic vesicle pool. *The Journal of neuroscience*, 26(40): 10270–10280.

Zhou, Q., Homma, K.J. & Poo, M.-M. 2004. Shrinkage of Dendritic Spines Associated with Long-Term Depression of Hippocampal Synapses. *Neuron*, 44(5): 749–757.

Zhu, P.J. & Lovinger, D.M. 2007. Persistent synaptic activity produces long-lasting enhancement of endocannabinoid modulation and alters long-term synaptic plasticity. *Journal of Neurophysiology*, 97(6): 4386–4389.

Zhuo, M., Laitinen, J.T., Li, X.C. & Hawkins, R.D. 1998. On the respective roles of nitric oxide and carbon monoxide in long-term potentiation in the hippocampus. *Learning & memory (Cold Spring Harbor, N.Y.)*, 5(6): 467–480.

Zhuo, M., Kandel, E.R. & Hawkins, R.D. 1994. Nitric oxide and cGMP can produce either synaptic depression or potentiation depending on the frequency of presynaptic stimulation in the hippocampus. *Neuroreport*, 5(9): 1033–1036.

Zhuo, M., Small, S.A., Kandel, E.R. & Hawkins, R.D. 1993. Nitric oxide and carbon monoxide produce activity-dependent long-term synaptic enhancement in hippocampus. *Science*, 260(5116): 1946–1950.

10. Appendix

Supplementary figures

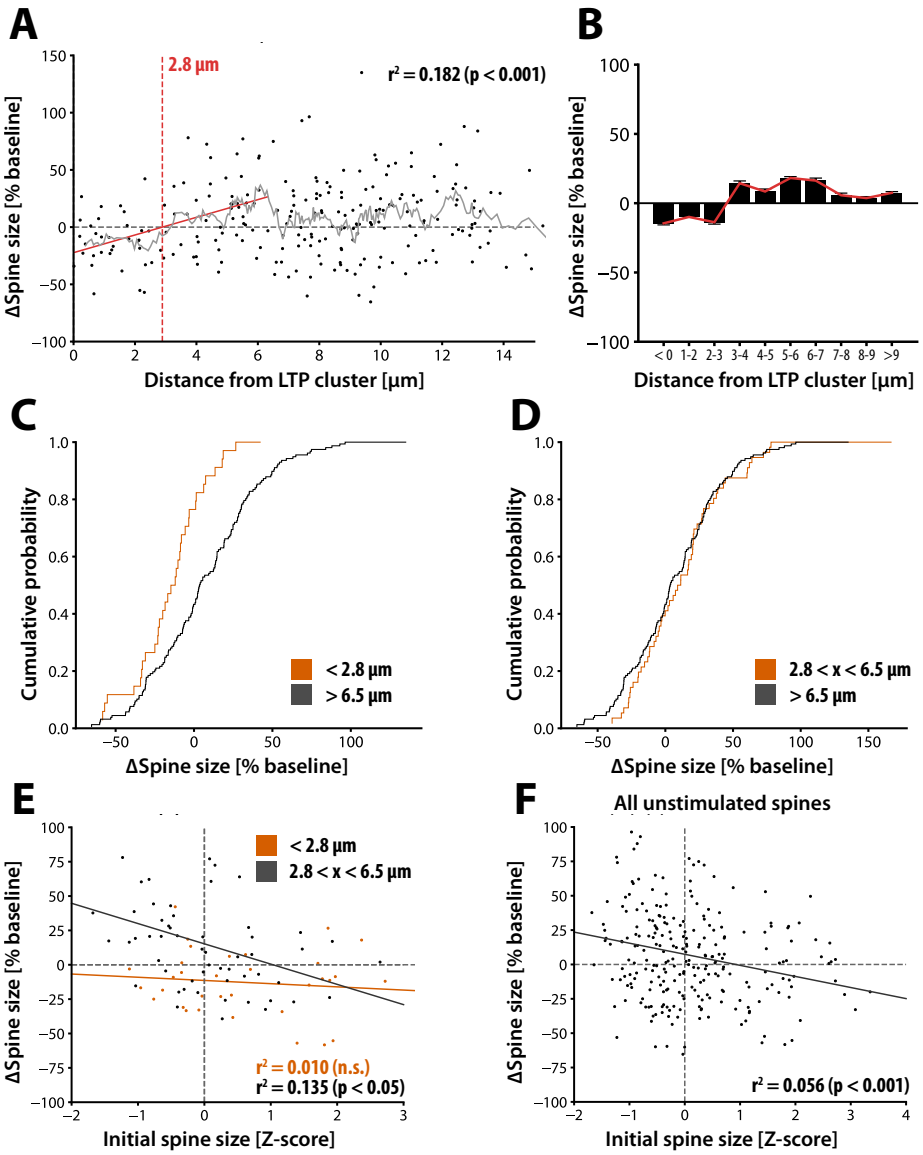

Suppl. Fig. 9.1: Analysis of heterosynaptic distance-dependent bi-directional spine size change for experiments in Chapter 6. (A) Distance and spine size change for all unstimulated spine analysed. The strongest correlation between distance and spine size change was found for spine located within 6.5 µm ($r = 0.427$, $p < 0.01$). The x-axis intercept is 2.8 µm and was used to group spines for further analysis. (B) Spine size changes grouped in 1 µm wide bins. Red line emphasises the mean spine size change. (C) Cumulative distribution of spine size change for proximal and distant spines. (D) Cumulative distribution of spine size change for spines 2.8-6.5 µm away and distant spines. (E,F) Spine size change in relation to initial spine size. A weak correlation was observed for more distant synapses.

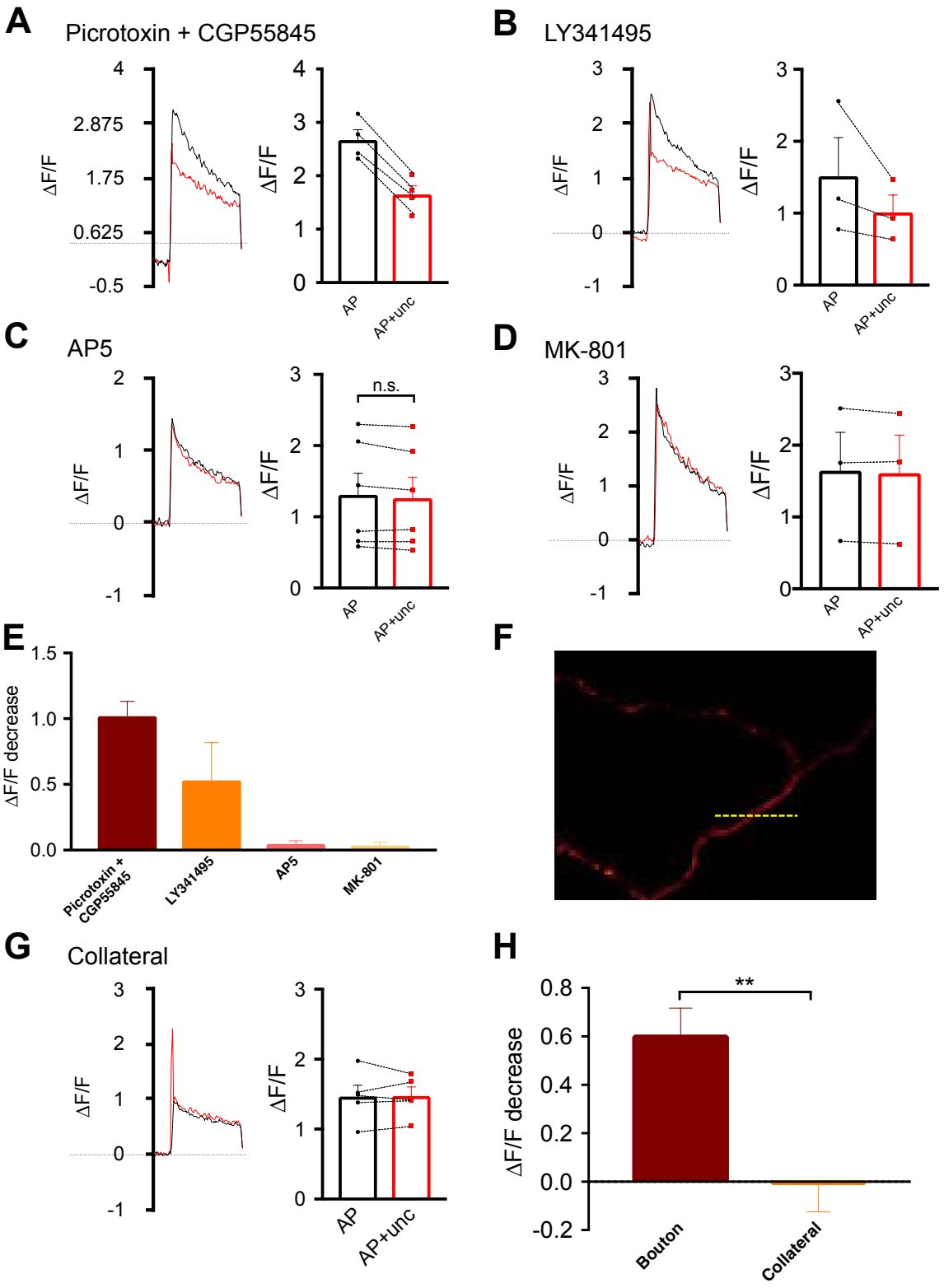

Suppl. Fig. 9.2: Figure 4 adapted from the internship report by Carla Schmidt with permission. "(A-D) Left: sample Ca2+ transients evoked by APs in CA3 boutons in the presence of several inhibitors. Controls = black traces, Uncaging experiments = red traces." *Cont'd on next page.*

Suppl. Fig. 9.2 cont'd "Every data point resembles an average of 10 line scans. Ca2+ transients were reduced by blockade of GABA receptors (A) and mGluR (B). No reduction could be detected under blockade of NMDA receptors (C and D). Right: average peak Ca2+ signal measured across conditions (n = 3–6 cells/condition). Error bars represent S.E.M. Significance was assessed where n > 5 (C) with Wilcoxon matched-pairs signed rank test. n.s. denotes no significant difference. (E) average ΔF/F decrease represents the difference in peak Ca2+ signal between control and uncaging experiments for every condition. Error bars represent S.E.M. (F) Enlarged image of an axon. Yellow dashed line indicates how line scans through the axon collateral were performed. (G) Left: sample Ca2+ transients evoked by APs in CA3 axon collaterals. Controls = black trace, Uncaging experiments = red trace. Every data point represents an average of 10 line scans. No photolysis induced decrease in signal could be detected in the collateral. Right: average peak Ca2+ signal for controls compared to uncaging experiments in the collateral (n = 5 cells). Error bars represent S.E.M. (H) average ΔF/F decrease resembles the difference in peak Ca2+ signal between control and uncaging experiments detected in boutons (red) and collaterals (orange). There was a significant reduction in Ca2+ transients in boutons compared to collaterals (n = 5 cells). Error bars represent S.E.M."

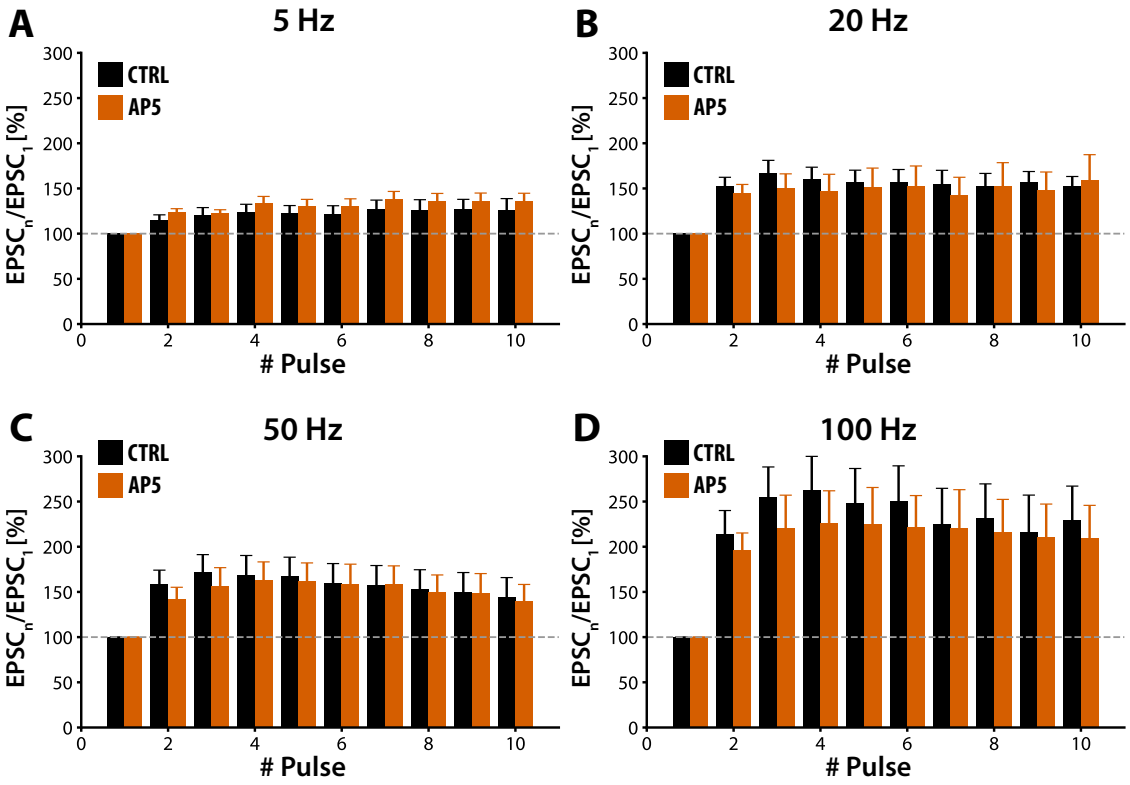

Suppl. Fig. 9.3: Presynaptic NMDARs do not affect short-term plasticity at lower frequencies. CA1 pyramidal neurones were stimulated with 10 AP at 5, 20, 50, or 100 Hz (A-D, respectively), with or without bath application of 50 µM AP5. These experiments were done in an unpaired manner. N = 10 cells (except 100 Hz, CTR: N = 9). No significant difference in the short-term behaviours was observed with the addition of AP5 (Mann-Whitney U test). Error bars represent SEM. Data was jointly collected with Carla Schmidt.

Details on statement of authorship

The work presented in this thesis is entirely my own work except for the experiments listed below.

Experiments in Chapter 6, figure 6.5 and figure 6.6, were done in collaboration with Carla Schmidt (Emptage lab). These experiments were designed and analysed by both, me and Carla Schmidt; Carla Schmidt collected the main set of experiments. Additional preliminary experiments in supplementary figure 2 and 3 were conducted partly or completely by Carla Schmidt and included with permission.

The intracellular MK-801 experiments in Chapter 6, figure 6.7, were kindly provided by Zahid Padamsey (formerly Emptage lab).